REFERENCE ONLY
DO NOT REMOVE

Array Communications in Wireless Sensor Networks

Georgios Elissaios

Thesis Submitted for the degree of
Doctor of Philosophy
and the
Diploma of Imperial College

July 2008

Imperial College London
Department of Electrical and Electronic Engineering
Communications and Array Processing

Abstract

The main objective of this study is to propose techniques that introduce the employment of Array Communications in Wireless Sensor Networks (WSNs). The aim is to develop an infrastructureless, reconfigurable, low-bandwidth, high-capacity and low latency WSN ensuring Low Probability of Intereception and having anti-jam and anti-interference capabilities. The proposed approach is based on the integration of advanced spatiotemporal array processing techniques both on a node-to-node and on a group of nodes-to-group of nodes level with wireless networks and results in a new type of network, the Arrayed Wireless Sensor Network (Arrayed-WSN).

Initially, the basic foundations of the Arrayed-WSN are going to be discussed in terms of network operation. The capabilities of the nodes are going to be described, together with the roles and modes that they can take in the network. Furthermore, the initial network discovery and Code Division Multiple Access (CDMA) code allocation is going to be studied. The Arrayed-WSN is described with the aid of a general operational scenario.

A very important property of the Arrayed-WSN is the ability of nodes to group together and form *Wireless Arrays*, communication entities that behave as traditional antenna arrays but with the links between the antenna elements and the array processing unit replaced by wireless communication links. An investigation of how such arrays are formed, with emphasis on the geometrical aspect of the problem and its impact on the system performance is presented next. This leads to a distributed algorithm for choosing the nodes to form a *Wireless Array*.

The design of the communication links employed in the Arrayed-WSN is presented next. A beamforming Multi-Carrier CDMA MIMO scheme is employed, designed to exploit the presence of antenna arrays at both ends of the communications channel. In this way, spatiotemporal signal processing at both the transmitter and receiver, the presence of many sub-carriers and the employment of CDMA provide many degrees of freedom, allowing for high interference cancellation capabilities which in the environment of a WSN is a highly desired property.

Finally the uncertainties present in an Arrayed-WSN are modelled and studied. Geometrical, electrical and synchronisation uncertainties are considered. Furtheromore uncertainties that are naturally related to any antenna array system are analysed in the case of the Arrayed-WSN. In particular, the ambiguities of the antenna arrays involved and a potential resolution method are examined.

Acknowledgements

I am grateful to many people for their practical and psychological assistance during the research that supports this thesis. Here is an acknowledgement of the most important ones:

Primarily I want to thank my supervisor Professor Athanassios Manikas for his trust, his patience and his enlightening guidance. He has been a true source of inspiration during my research.

Furthermore, I thank my colleagues Ms Cara Beck and Mr George Efstathopoulos for their technical input and assistance. I also have to express my appreciation to Mr Victor Li, Ms Ting Ting Zhang and Mr Farrukh Rashid for their help and our constructive and entairtening discussions.

For her invaluable support and encouragement during the compilation of this document I am grateful to Ms Phebe Vayanos.

Finally and most importantly I thank my parents and my brother for their support during all of my academic career. Your infinite confidence in my capabilities has given me the purposefullness needed to overcome the difficulties and complete this endeavour.

Contents

Abstract 2

Acknowledgements 3

Contents 4

List of Figures 6

List of Tables 9

List of Publications 10

List of Symbols 11

Notation 13

Acronyms 15

1 Introduction 17
- 1.1 Research Challenges . . . 17
- 1.2 WSN Related Research . . . 19
- 1.3 Multiple-Input Multiple-Output Communications . . . 23
- 1.4 MIMO in WSN . . . 28
- 1.5 Thesis Description . . . 31

2 Basic Framework of Arrayed-WSN 33
- 2.1 Arrayed-WSN Node Outline . . . 33
- 2.2 Network Operation . . . 38
  - 2.2.1 Network Discovery and Code Allocation . . . 38
  - 2.2.2 Defining *Wireless Arrays* . . . 42
  - 2.2.3 Node Roles and Modes . . . 43

3 *Wireless Array* Formation 48
- 3.1 Array Geometry and Array Manifold . . . 49
- 3.2 Performance Criteria . . . 56
  - 3.2.1 Detection and Resolution Thresholds . . . 56
  - 3.2.2 Accuracy and Ambiguities . . . 58
  - 3.2.3 Array Sensitivity . . . 61
- 3.3 Array Formation . . . 63
  - 3.3.1 Ambiguity / Accuracy Tradeoff . . . 65

3.3.2 Array Circularity and Sensitivity 67
3.4 Conclusion 70

4 Arrayed-WSN Communication Link Design 73
4.1 Beamforming MIMO Multicarrier DS-CDMA Transmitter 77
4.2 Channel Model 84
4.3 Spatiotemporal Multicarrier DS-CDMA Receiver 92
4.3.1 3D RAKE Receiver 98
4.3.2 MMSE Block Linear Receiver 99
4.4 Computer Simulation Studies 100
4.4.1 *Intra-Wireless Array* Link 100
4.4.2 *Inter-Wireless Array* Link 106
4.5 Conclusion 108

5 Analysing and Resolving Ambiguities in the Arrayed-WSN 110
5.1 Ambiguities in the Arrayed-WSN 111
5.2 Resolving Ambiguities in Arrayed-WSN 124
5.2.1 An Efficient Array Cooperative Method for Resolving Ambiguities 126
5.3 Conclusion 137

6 Modelling Uncertainties in the Arrayed-WSN 138
6.1 Uncertainties/Errors Relating to Node Self Orientation and Self Position Estimation 139
6.1.1 *Local Array* Modelling 139
6.1.2 Node and Global Coordinate Systems 139
6.1.3 Converting Between Different Node Coordinate Systems . 140
6.1.4 The i^{th} Node's *Local Array* in the GCS 141
6.1.5 Modelling Estimation Errors of the i^{th} Node's Rotation Matrix and Position Vector 142
6.2 Imperfect Clock Model 143
6.3 Uncertainties Relating to the Node's *Local Array* 146
6.3.1 Modelling Signals Received by the Node's *Local Array* . . 146
6.3.2 Modelling Electrical and Geometric Uncertainties 149
6.4 Uncertainties Relating to a *Wireless Array* of Nodes 155
6.4.1 Reconstructing Streams from Element Nodes 160
6.4.2 Geometrical Uncertainties in *Wireless Arrays* 161
6.4.3 Electrical Uncertainties in *Wireless Arrays* 162
6.5 Conclusion 165

7 Conclusions and Future work 167
7.1 Thesis Summary 167
7.2 List of contributions 170
7.3 Future work 171

References 175

List of Figures

1.1 An exemplatory multi-hop WSN 18
1.2 In contrast to SISO, the MIMO wireless channel has a vector input and output 24
1.3 A typical array pattern of a uniform linear array 26

2.1 Possible 3D-grid array geometries on a cubical node. a)6, b)8 and c) 24 element configurations 36
2.2 A conceptual outline of the AWSN node with the sensor bank, power module data and array processor and the local array 37
2.3 Low Duty Cycle Channel Listening 41
2.4 The beamforming *inter* and *intra*-wireless links with array patterns in light and dark blue respectively 44
2.5 The unified mode and role state diagram for an Arrayed-WSN node 47

3.1 An electromagnetic signal transmitted by a far-field source, traversing an antenna array 51
3.2 An array manifold curve with respect to single parametre of intrest p as embedded in the N-dimensional complex space 52
3.3 Representation of the array manifold with example θ and φ-curves 55
3.4 Example Wireless Array Geometries 58
3.5 Square Root Cramer-Rao Lower Bound For Arrays A and B of Fig. 3.4 59
3.6 Number of Ambiguous Generator Sets of Array A against θ_0 (top) and Total Length of Manifold Curve Corresponding to the ELA of Wireless Array A of Fig. 3.4 at θ_0 (bottom) 60
3.7 Relative Sensitivities of each element in Wireless Arrays A and B of Fig. 3.4 62
3.8 An Event Of Interest and the 5 Potential Controllers selected through the described algorithm 65
3.9 Number of Ambiguous Generator Sets Against Worst Case Smallest Achievable RMS Error 66
3.10 Overall Sensitivity against Normalised Achievable RMS Error Difference 68
3.11 Number of Ambiguous Generator Sets Against Array Aperture . . 70
3.12 The 5 proposed Wireless Arrays shown with the proposing potential controller and in relation to the EOI 71
3.13 The final selected Wireless Array 72
3.14 The three best proposed Wireless Arrays for each potential controller, 72

4.1 MC-DS-CDMA Beamforming Antenna Array Transmitter 78
4.2 Simplified transmitter outline 82
4.3 *Initial/intra* wireless link - a VIVO channel between two nodes . . 85
4.4 *Inter* wireless array link - a VIVO channel between two arrays . . 85
4.5 Multiple access *initial/intra* wireless link - a MIVO channel . . . 86
4.6 Multiple access *inter* wireless array link - A MIVO channel 86
4.7 *Initial* or *intra* wireless array links - VIVO channel modelling for the k^{th} subcarrier, where K_i is the number of multipaths from the i^{th} transmitter 87
4.8 *Inter* wireless array link - VIVO channel of a single user's single subcarrier 88
4.9 Multicarrier Vector Input Vector Output Channel Between Two Arrays 90
4.10 The *intra*-wireless array link in operation. the multi-beamforming controller shows the separate beamformers corresponding to each element node in different colours. 91
4.11 The receiver front-end, common for all receiver types considered . 92
4.12 Main blocks of a MC-DS-CDMA receiver 96
4.13 Simulated A-WSN Environment 101
4.14 Raytracing parameters for the Intra Wireless Array channel . . . 101
4.15 DOWNLINK *intra* wireless array - SNIR at the output of the receiver operating in in the presence of 4 interferers (plotted against the SNR_{in}) 102
4.16 DOWNLINK *intra* wireless array - SNIR at the output of the receiver at a fixed SNR_{in} = 10 dB (plotted against the number of external interferers) 103
4.17 UPLINK *intra* wireless array - SNIR at the output of the receiver operating in the presence of 4 interferers (plotted against the SNR_{in})104
4.18 UPLINK *intra* wireless array - SNIR at the output of the receiver at a fixed SNR_{in}=10 dB (plotted against the number of external interferers) 104
4.19 Raytracing parameters for the Inter Wireless Array channel 105
4.20 Environment for modelling the Inter Wireless Array channel showing the raytracing results 106
4.21 *Inter* wireless array - SNIR at the output of the receiver in the presence of 4 interfering wireless arrays (plotted against the SNR_{in}) 107
4.22 *Inter* wireless array - SNIR at the output of the receiver at a fixed SNR_{in}=10 dB (plotted against the number of active transmitting arrays) 108

5.1 The concept of the Equivalent Linear Array for $\theta_0 = 20°$ for a planar array 113
5.2 MUSIC spectrum for 3D grid array with the 1^{st} set of 5 sources present (Table 5.1). The 6 peaks clearly illustrate the ambiguous situation 117
5.3 MUSIC spectrum for 3D grid array with the 2^{nd} set of 5 sources present (Table 5.2). The 6 peaks clearly illustrate the ambiguous situation 118

5.4 MUSIC spectrum for 3D grid array with the 3^{rd} set of 5 directions present (Table 5.3). The 6 peaks clearly illustrate the ambiguous situation 119
5.5 The development of a 3D-grid array showing θ and ϕ-lines 120
5.6 The development of a 3D grid array zoomed in, with the three discrete ambiguous sets of directions (Tables 5.1, 5.2 and 5.3) . . . 121
5.7 MUSIC spectrum of 3D grid array for sources incoming from the same elevation. 123
5.8 Representation of the array manifold with example α and β-curves 124
5.9 WA_1 and WA_2 lie close together on a plane close to each other compared to the far-field sources 129
5.10 MUSIC spectrum for WA_1 with 4 sources present in the environment. The peak at $(\theta, \phi) = (185, 44.2)$ does not correspond to a real source 130
5.11 MUSIC spectrum after coordinate transformation for WA_2 with 4 sources present in the environment. In contrast with Figure 5.10, there is no peak at $(\theta, \phi) = (211°, 61.2°)$ 131
5.12 Two nodes with their Local Arrays, lying close together in the 3D space, in the presence of far field sources 134
5.13 MUSIC spectrum for LA_1 with 5 sources present in the environment. The peak at $(\theta, \phi) = (95°, 68°)$ does not correspond to a real source 135
5.14 MUSIC spectrum after coordinate transformation for LA_2 with 5 sources present in the environment. In contrast with Figure 5.13, there is no peak at $(\theta, \phi) = (95°, 68°)$ 136

6.1 The Euler Angles That Transform Between Global and Node Coordinate Systems 141
6.2 MUSIC spectrum using nodes local array with no uncertainties . . 151
6.3 MUSIC spectrum using nodes local array in the presence of electrical uncertainties 152
6.4 MUSIC spectrum using nodes local array in the presence of geometrical uncertainties 154
6.5 Wireless Array model showing both individual node and overall wireless array gain patterns 158
6.6 Affect of timing errors on the demodulation of QPSK using a wireless array 164

List of Tables

2.1 Advantages of Homogeneous and Heterogeneous WSNs 34
2.2 The merged sensor node roles and modes 46

3.1 Partitioning the levels of performance for the ambiguities/accuracy trade-off 66
3.2 The weight vector formation for various regions of performance . . 68
3.3 The complexity of the algorithm in the number of evaluations performed by all potential controller 69

5.1 First ambiguous set of directions of sources in the environment . . 116
5.2 Second set of ambiguous directions 116
5.3 Third set of ambiguous directions 116
5.4 A signal environment with sources of common elevation 123
5.5 An ambiguous signal environment for the first WA 128
5.6 An ambiguous signal environment for the first LA 133

List of Publications

- Efstathopoulos G., Elissaios G., Manikas A., "The effect of uncertainties on the performance of array systems", Proceedings of IEEE PIMRC 2007, September 2007.

- Elissaios G., Efstathopoulos G., Manikas A., "Analysis of 3D Array Systems", WSEAS Transactions on Communications, vol 5, pages 1619-1623, October 2006

- Georgios Elissaios and Athanassios Manikas, "*Array formation in Arrayed Wireless Sensor Networks*", HERMIS-mu-pi International Journal of Computer Mathematics and its Applications, vol.6, pp.122-134, March 2006

- Elissaios G. and Manikas A., "*Multi-Carrier CDMA MIMO in Arrayed Wireless Sensor Networks*", Proceedings of IEEE ISWCS2005 (Wireless Communication Systems), September 2005.

List of Main Symbols

M	number of users
N	number of antennas at the receiver
T_{cs}	bit or symbol duration
r_{cs}	bit or symbol rate
L	channel order for the frequency selective FIR channel
$a_i[m]$	m^{th} bit or symbol of the data symbol sequence of the i^{th} user
$\underline{s}_i[n]$	n^{th} block or frame of the i^{th} user
$s_i[q]$	q^{th} sample of the transmitted sequence of the i^{th} user
$p(t)$	pulse shaping waveform
T_s	duration between adjacent transmitted sequence samples
r_s	sampling rate of the transmitted sequence samples
$m_i(t)$	complex baseband transmitted signal of the i^{th} user
$y_i(t)$	up-converted passband transmitted signal of the i^{th} user
P_i	power of the transmitted signal
F_c	carrier frequency
ΔF	inter-subcarrier spacing
K_i	number of spatially distinct subchannels of the i^{th} user
$\underline{c}_{ij}(t)$	complex baseband vector CIR for the j^{th} subchannel, i^{th} user
$\underline{\tau}_{ij}$	path delay vector of the j^{th} spatial subchannel, i^{th} user
θ_{ij}	nominal direction of the j^{th} spatial subchannel of the i^{th} user
$\underline{S}_{ij}$	array manifold vector of the j^{th} spatial subchannel of the i^{th} user
$\underline{u}_{ij}$	direction cosine vector of the j^{th} spatial subchannel of the i^{th} user
k	k^{th} receive antenna
$\underline{\beta}_{ij}$	CIR of the j^{th} subchannel of the i^{th} user

$\beta_{ij}^{(l)}$	l^{th} component of the CIR of the j^{th} subchannel of the i^{th} user
$\underline{h}_i^k[n]$	CIR vector of i^{th} user at the k^{th} receiver antenna
$\underline{x}[n]$	received signal vector for n^{th} symbol
$\underline{n}_k[n]$	sampled AWGN noise vector at the k^{th} receiver antenna
$\underline{x}(t)$	the received complex baseband signal vector
$\underline{n}(t)$	complex white Gaussian Noise vector
$\mathbb{C}_{ij}[n]$	circulant CIR matrix for the j^{th} subchannel of the i^{th} user
$\mathbb{B}_{ij}[n]$	channel transfer function matrix of the j^{th} subchannel, i^{th} user
$\mathbb{G}$	array manifold metric
$\underline{d}_i[n]$	n^{th} decoded OFDM symbol vector of the i^{th} user
$\mathbb{W}_i[n]$	joint receiver matrix for the n^{th} symbol of the i^{th} user
$\mathbb{T}_i[n]$	channel transfer function matrix for the n^{th} symbol, i^{th} user
$\underline{g}_{il}[n]$	normalised transfer function of the i^{th} user, l^{th} frequency bin
$\underline{k}$	wavenumber vector

Notation

	Scalar
	Vector
	Matrix
$\mathcal{Z}$	Set of integers
$\mathcal{R}$	Field of real numbers
$\mathcal{C}$	Field of complex numbers
a, A	Scalar
$\underline{a}$, $\underline{A}$	Column Vector
$\mathbf{A}$, $\mathbb{A}$	Matrix
$\|A\|$	Absolute value
$\|\|\underline{A}\|\|$	Euclidian norm of vector
$\|\|\mathbb{A}\|\|$	Frobenius norm of matrix
$\underline{A}^b$	Element by element power
$\exp(\underline{A})$	Element by element exponential of vector $\underline{A}$
$A^{(i)}$	i^{th} element of the vector $\underline{A}$
$(\cdot)^*$	Complex conjugate
$(\cdot)^T$	Transpose
$(\cdot)^H$	Hermitian transpose
$\otimes$	Kronecker product
$\odot$	Hadamard product
$\oslash$	Hadamard division
$\mathbb{I}_N$	Identity matrix of $N \times N$ dimension
$\underline{0}_N$	Zero vector of N elements

$\underline{1}_N$	$N \times 1$ vector of all ones
$\mathbb{J}_N$	$N \times N$ downshifting matrix
$\text{row}_l(\mathbb{A})$	l^{th} row of $\mathbb{A}$
$\text{flip}\,(\cdot)$	Flips the square matrix in up/down direction across the middle
$\underline{\underline{\text{diag}}}(\underline{A})$	Diagonal matrix with the vector $\underline{A}$ as the leading diagonal
$\underline{\text{diag}}(\mathbb{A})$	Column vector with elements the diagonal of the matrix A
$\mathbb{P}_{\mathbb{A}}$	Matrix projection operator onto the range space of A
$\mathbb{P}_{\mathbb{A}}^{\perp}$	Complementary projection operator of the matrix A
$\underline{\text{eig}}_{\max}(\mathbb{A})$	eigenvector corresponding to the maximum eigenvalue of $\mathbb{A}$
$\text{col}_e(\mathbb{A})$	e^{th} column of $\mathbb{A}$
$\text{ele}_n(\underline{A})$	n^{th} element of $\underline{A}$
$\mathcal{L}\{\mathbb{A}\}$	Space spanned by columns of $\mathbb{A}$

Acronyms

AGS	Ambiguity Generator Set
AOA	Angle of Arrival
Arrayed-WSN	Arrayed-Wireless Sensor Network
AWGN	Additive White Gaussian Noise
BER	Bit Error Rate
CANDLA-DCSA	Network Discovery using *Local Array* and Dynamic Code Self-Alloca
CCS	Controller Coordinate System
CDMA	Code Division Multiple Access
CRB	Cramer - Rao Bound
DAA	Direct Augmentation Approach
DOA	Direction Of Arrival
DS	Direct Sequence
ELA	Equivalent Linear Array
EOI	Event Of Interest
GCS	Global Coordinate System
GEDIR	Geographical Distance Routing
ISI	Inter Symbol interference
ISM	Industrial, Scientific and Medical
LA	Local Array
LEACH	Low Energy Adaptive Clustering Hierarchy
LMAC	Lightwait Medium Access Control
MAC	Medium Access Control
MAI	Multiple Acces Interference
MARA	Manifold Ambiguity Resolution by Association
MEMS	Micro-Electro-Mechanical Systems

MC	Multi Carrier
MFR	Most Forward Routing
MIMO	Multiple Input Multiple Output
MMSE	Minimum Mean Square Error
MUSIC	Multipl Signal Classification
NCS	Node Coordinate System
PCSMAC	Power Controlled Sensor MAC
PN	Pseudo Noise
SIR	Signal to Interference Ratio
SIVO	Scalar Input Vector Output
SISO	Scalar Input Scalar Output
S-MAC	Sensor MAC
SMACS	Self-Organising MAC for Sensors
SNIR	Signal to Noise plus Interference Ratio
SPIN	Sensor Protocols for Information via Negotiation
ST	Spatio Temporal
STBC	Space Time Block Coding
STC	Space Time Coding
STAR	Spatio Temporal Array Receiver
TDL	Tapped Delay Line
TDMA	Time Division Multiple Access
TDOA	Time Difference of Arrival
TOA	Tima of Arrival
UBS	Uniform Basic Set
ULA	Uniform Linear Array
V-BLAST	Vertical-Bell Laboratories -Layered -Space-Time
VIVO	Vector In Vector Out
WA	Wireless Array

Chapter 1

Introduction

The efficient exploitation of the wireless radio spectrum and the development of new extensible applications are undeniably two of the strongest forces underlying modern telecommunication technology evolution. The ample computational power made available in the research community in the past years has allowed the better modelling of the wireless radio channel and has spawned diverse designs that take advantage of its different aspects.

Wireless networks of an increasing number of wireless nodes have been made possible, and extensive research has been performed in the area, fuelled by both the commercial and military applications entailed. This advance of wireless technology in combination with the progress in sensor fabrication has inevitably led to the conception of the enormous in population networks called Wireless Sensor Networks.

WSNs consist of large numbers of low-cost, energy-constrained, small multifunctional electronic devices called sensor nodes or simply nodes. Node designs may differ in various features but resemble in the sense that they are wireless communications enabled sensing devices capable of acquiring information about their physical environment and wirelessly conveying this information. The deployment of these nodes and their subsequent, automatic interconnection results in a typical WSN.

1.1 Research Challenges

Deployment of a WSN in a remote, hostile environment can maintain constant surveillance of the area through the node sensors. The WSN operates unattended, identifying events in the environment and providing various types of information (location, classification, duration etc.) about those events as illustrated in Figure

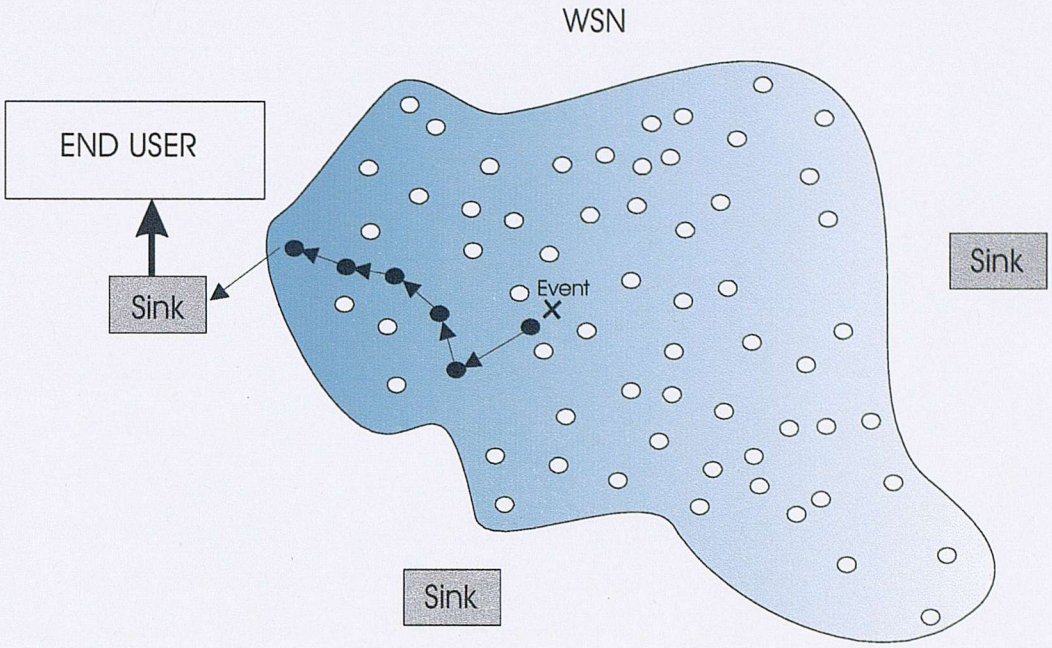


Figure 1.1: An exemplatory multi-hop WSN

1.1. WSNs are thus characterised by a minimum human supervision and rich information provision [1], [2].

The advances in hardware technology can allow the deployment of a large number of sensors with relatively advanced capabilities. The main issues that have to be considered when designing a sensor network span all design layers and include wireless communications design, network discovery, network control and routing and signal and information processing [3]. In addition the hardware and software platforms that underlie the construction of the nodes are a very important design factor and greatly affect the usability and lifetime of the network [4], [5]. Existing network design algorithms and protocols are applicable to a certain degree, but must be altered in order not only to tackle the unique in nature challenges that a WSN poses but also to exploit the many advantages offered.

One of the main advantages of a wireless sensor network is the expendability of the individual nodes that their great number provides. This is translated into a high system robustness to individual node failure. Another advantage is the large amount of data that are collected for a single event in the environment. An event will be typically sensed by a large number of nodes, a fact that will provide numerous different views of the same event. By combining the data collected from different viewpoints and extracting the most important information the network can provide higher quality of information about the event. It is clear that this

redundancy in information can also be used to gain a degree of confidence on each decision. This extended degree of accuracy that can be achieved is significant, especially when considering high-end applications.

Although the large number of nodes is the main advantage of a WSN, it also creates a number of obstacles for the operation of the network. The sheer amount of data collected for a single event needs to be managed in an efficient way. The transmission of the whole amount of raw data is preventive in terms of total energy consumption and information usability at the sink end. The raw data from different nodes have to be combined in an effective way, stripped from unimportant or irrelevant information and then routed to the sink. This process is commonly described as data or information fusion. Data fusion in a WSN is mainly obstructed by the lack of central control and central processing points within the network. Thus, a decentralised approach to data fusion that takes into account the special conditions of a WSN is needed [6].

In addition, the efficient organisation of such a large ad-hoc network with no specific backbone seems to require complicated communication protocols. Routing data, synchronising nodes for collision avoidance when communicating, effective node clustering and data fusion are issues that will potentially overcomplicate the operation of the network and impose heavy loads in terms of energy, memory and processing requirements on the small, inexpensive nodes. In fact, although most of the time the nodes of a WSN are not transmitting, large numbers of them will try to transmit information when events take place in the environment.

When tackling these problems a designer has to keep in mind the particular requirements involved. In specific, a sensor network's lifetime is very relevant and since all the nodes have a limited energy capacity, power consumption becomes a concern. Communication has to be limited as much as possible since it is usually the most power-consuming activity. Furthermore, the sensors, although relatively advanced, have a limited storage capacity and information processing capability. This implies that communication between nodes has to be very efficient and data flow through the network very fast and highly directive. For example a node will not be able to store long queues of packets waiting to be routed nor will it be able to hold and update tables containing the whole network topology.

1.2 WSN Related Research

A considerable amount of research and development has been performed in the area of WSNs by many research groups around the world, which, have developed

algorithms and platforms to be used in various realisations of WSNs. Various network configurations that correspond to different needs have been considered. Different characterisations can be given to sensor networks according to the nodes they are using, their structure and their use.

The first basic discrimination area where networks can be categorised corresponds to the types of nodes that are being used. A homogeneous network consists of only one type of nodes whereas a heterogeneous network can, for example, use simpler hardware nodes to perform simple tasks and more sophisticated ones for more complex tasks. Usually a non-homogeneous network implies a hierarchical network as well, where different levels of control are used through the network and nodes do not assume the same tasks and responsibilities (roles). In the most common example, a hierarchical network design will incorporate a large number of nodes assuming the most basic role of sensing and transmitting information relating to Event of Interest (EOI) while some others are also concerned with network organisation tasks while even fewer may even assume the role of a local base-station resulting in a pyramid shape network organisation. The difference here does not lie on the capabilities of the nodes themselves, but on the roles they assume. An autonomous network can perform self-configuration without external intervention. Sensor networks tend to be autonomous since their large scale and inaccessible is prohibiting human configuration. Continuous networks constantly monitor the environment and transmit the sensed data while on-demand networks answer to external queries. According to the connection of the network to its environment, two categories can be defined. A reactive network responds to changes to its environment that it recognises as events whereas a programmed network carries out tasks, such as sensing and data acquisition, according to a specific pre-programmed set of rules. Although this categorisation of WSNs is useful, it is a common occurrence that a WSN design utilises various characteristics of these categories thus defining a hybrid WSN.

Although the main concern of this study is not actual routing and MAC protocols but the incorporation of Array Processing in a WSN, a brief description of common solutions proposed in designs of WSNs is presented. This aims at clarifying the research background in the area and relate our proposed techniques to existing research. The main research in WSNs has at the past focused on medium access control (MAC), routing, localisation and energy conservation for maximising network lifetime [7], [8], [9].

Designing a MAC protocol appropriate to a WSN is a challenging problem mainly because of the scalability and synchronisation issues mentioned before.

Sensor-MAC (S-MAC) is an access protocol based on the IEEE 802.11 with various refinements mainly aiming at energy conservation [10]. Time is quantised into frames which in turn are divided into listen and sleep periods. Thus a duty cycle is implemented, during which a node will turn its transceiver off for the time that it is not needed and thus save energy. Latency is the main drawback of the S-MAC protocol. By using adaptive duty cycles another protocol, Timeout-MAC, is proposed as an extension to S-MAC so as to decrease latency on urgent applications. Adding a power control feature, is proposed as an advancement to S-MAC, aiming at furthermore increasing energy conservation by controlled transmissions [11].

A number of groups have proposed time division based MAC protocols which avoid constant hand-shaking overhead procedures and thus save time and energy. The Self-Organising Medium Access Control for Sensor Nets (SMACS) is based on a neighbour discovery phase upon which time schedules and links of different frequency bands are assigned to pairs of nodes. Thus two neighbouring nodes can effectively communicate between them and save energy by turning their transmitters and receivers on at pre-agreed upon times. This also eliminates the need of master nodes and network wide synchronisation [12]. Another time based protocol is the Lightweight Medium Access Protocol (LMAC). By letting nodes choose their own time slot and having a separate mechanism for tackling the rare case of two nodes selecting the same slot, LMAC can implement dynamic duty cycles chosen based upon local information. The result is that nodes are, simply and in the absence of global control, assigned appropriate sleeping patterns according to various useful parameters such as local traffic load [13].

Routing protocols designed for WSNs can be classified as normal network routing solutions and as location aided routing schemes. An early routing-MAC scheme designed for WSNs is LEACH (Low Energy Adaptive Clustering Hierarchy) in which non overlapping clusters form within the network. In each cluster, a cluster head node is elected and used to gather information from the rest of the nodes in the cluster, perform a degree of data fusion and forward the resulting information packets to directly to the sink. Clusterheads are periodically switched in each cluster so that energy depletion due to heavy workload is avoided. The LEACH protocol is simple and may increase lifetime, however, it involves basic assumptions such as connectivity of every node to the sink and neglects the trade-off of consumed energy in algorithm complexity and packet overhead and wireless transmission ranges [14]. Flooding like protocols designed specifically for WSNs also exist. The SPIN (Sensor Protocols for Information via Negotiation)

is a scheme where negotiation between nodes for useful information exchanges and resource awareness are utilised in order to tackle the traditional setbacks of a flooding routing protocol. Directed diffusion is another scheme particularly suitable to on-demand networks but also applicable to other types of WSN. According to this protocol the sink node broadcasts an interest which as it travels through the network sets up gradient characterised routes that can be used by the nodes for answering back. The data is also aggregated on route to the sink and the routes are periodically updated to accommodate a dynamic network topology [15].

Location based routing protocols are more demanding in terms of information, since they imply a general knowledge of the spatial positions of the nodes. Acquiring and sharing such information between nodes may be implemented in various ways, the simple of which is to equip every single node with a GPS receiver. However, this can increase the cost of manufacturing nodes, reduce node lifetime due to the incorporation of GPS hardware and constrain the applicability of the network to only those areas where GPS reception is guaranteed. Various localisation algorithms have been proposed that avoid the use of GPS. In most cases beacons with known positions transmit known messages, used by the nodes of the WSN to estimate their positions.

In such algorithms, there are two main aspects that define the operation of the scheme. The first part is the actual localisation of a node (for example using Angle of Arrival (AOA) or Time Difference of Arrival (TDOA) techniques) and the second part is the dissemination of the newly discovered location information in the network if such information has to be shared by more than one nodes. Some research groups have proposed algorithms that seamlessly combine these two stages. This is possible for example if the actual localising procedure involves naturally sharing node position information and using it for further node localisation or for iterative procedures aiming at increasing the accuracy of the estimated node positions. More generally, the research direction concerning localisation schemes in WSNs currently seems to be pointing to node collaboration and distributed localisation implementations aiming at making the procedure as autonomous as possible, in line with the WSN mentality [16].

Although location based routing requires at least a general knowledge of some of the node positions it seems more appropriate to WSN design, especially when taking into account that information about the node locations may be valuable in other aspects of the network operation as well. An external query-type network for example may need to respond to the user about the location in addition to the

nature of sensed events, or provide information about the environment of specific parts of the network. Furthermore, such routing protocols may be particularly applicable to WSNs since they can be more scalable and energy efficient. One of the most simple such protocols is the Most Forward within Radius (MFR) protocol [17]. In this case, the node with the most progress towards the destination node within a predefined radius is chosen to relay messages. This does not necessitate a pre-defined route to be set up for the messages and thus saves a lot of energy and processing in terms of overhead and constant renewal of route tables. The main advantage of geographic routing is that nodes only need local information of close neighbours. This implies a simpler design and energy conservation in renewing the information needed. The avoidance of large scale flooding is also of great importance, especially in dense networks. A family of simplistic algorithms that clearly demonstrate these advantages is greedy forwarding. In this case information about only direct neighbours (1-hop) is needed and a node will forward a message to the neighbour closer to the end destination. A good example is the GEDIR (Geographical Distance Routing) algorithm, which also tackles the problem of loops inherently present to greedy forwarding algorithms. An overview of geographic routing algorithms can be found in [18].

It is clear that the MAC and routing problems in WSN, although still remaining open problems, have already been extensively researched worldwide. In this study we follow a different direction making the incorporation of array processing into the WSN design our main concern. The aim is to use such advanced communication techniques to improve the wireless communications and employ highly cooperative techniques to lay the foundation for any properly designed geographically aided routing scheme to operate. Furthermore, by highly increasing the interference rejection capabilities of the network we aim at creating a platform on which very light MAC protocols can operate.

1.3 Multiple-Input Multiple-Output Communications

Wireless communications have been limited for some time to the traditional employment of a single antenna at the transmitter and receiver. In contrast to this Single-Input Single-Output (SISO) scheme, Multiple-Input Multiple-Output (MIMO) communications are based on the employment of more than one antennas, either at the receiver, the transmitter or on both sides of the wireless channel, see Figure 1.2. Since the wireless channel is a function of both space

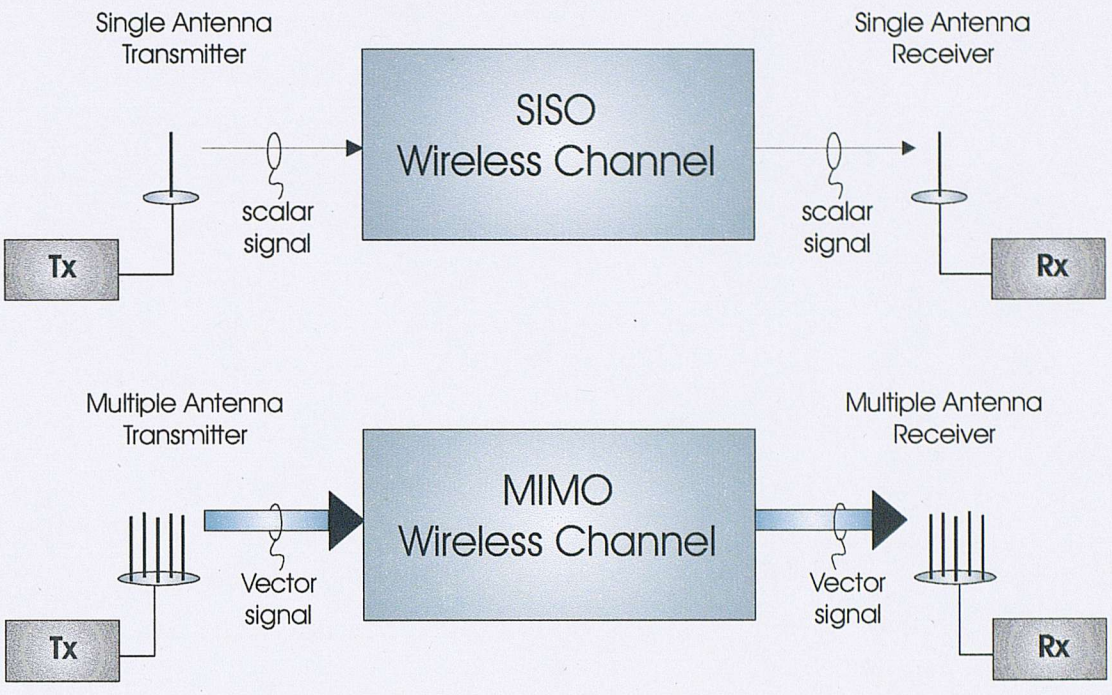


Figure 1.2: In contrast to SISO, the MIMO wireless channel has a vector input and output

and time, MIMO communications are considered as a way to increase the capacity of a system by exploitation of the spatiotemporal domain [19]. Building a MIMO system and implementing the necessary signal processing algorithms costs in hardware and processing power. Thus, implementations of antenna arrays up to date have been restricted to larger base-stations while smaller scale mobile devices were limited to single antenna designs. However, the advances in hardware technology and the passing from Micro-Electro-Mechanical Systems to Nano-Electro-Mechanical Systems predefine an era where microstrip antennas and powerful microprocessors can provide the necessary processing power and hardware in very small packages. It is thus expected that employing multiple antennas in smaller, mobile devices will be a common practice in the future, particularly suitable to applications where exploitation of the available bandwidth is more crucial. The constant drive to higher carrier frequencies also works in favour of multiple antenna implementations, which can be made smaller as the wavelength of the associated electromagnetic signals decreases. One ordinary method of exploiting the multiple receiving antennas has been to select the highest Signal-to-Noise Ratio (SNR) yielding antenna at any time, thus increasing the link reliability (selection diversity combining) [20],[21]. However this method is strictly not a MIMO technique. A slightly more complicated procedure is to phase shift the received signals from each antenna and then add the synchronised

signals together to yield a higher SNR (Equal Gain Combining). An extension to this is to apply a scaling weight on each antenna element output according to the corresponding signal power and subsequently add the antenna outputs as before (Maximum Ratio Combining) in order to achieve even better performance. This increase in performance is based on the assumption that signals impinging on different antennas have experienced radio channels which are independent to a degree associated to the actual antenna separation. This translates into a greatly reduced probability of all antennas facing a highly degraded signal due to channel fading at the same time, i.e. spatial diversity is exploited.

A more advanced MIMO scheme, still based on the uncorrelated channels assumption, lies on the combination of spatial diversity exploitation techniques with channel coding schemes. This results into novel coding methods, performed both in time and space simultaneously. Such Space-Time Coding (STC) schemes have been shown to exhibit greatly superior performance to SISO and primitive MIMO systems. A well known example of STC is the Space Time Block Coding Alamouti scheme [22].

A very efficient MIMO scheme of a different nature called Bell Labs Layered Space-Time (BLAST), has been under development in Bell Laboratories for a few years. In BLAST the transmitting stream is broken into a number of parallel streams, each transmitted by a different antenna. Thus, the transmission rate increases, under perfect circumstances, proportionally to the number of transmitting antennas. At the other end, each receiving antenna will receive a superposition of all the transmitted streams and their delayed versions that arrive from multipath scattering. However, (and again under the above assumption of channel independence) the received signals will be slightly different due to the different spatial positions of the receiving and transmitting antennas. This independent fading, is used to separate the different transmitted signals and remove them in a descending order of received power from the total received signal, until all streams have been decoded. The BLAST protocol thus uses the traditionally degrading effect of multipath to its advantage to achieve a performance unattainable by SISO systems especially in heavily scattered environments.

Another advanced technique for exploiting the spatial domain of the radio channel is the use of multiple antennas placed at pre-defined positions and thus forming an antenna array of known geometry. A single radio wave traversing an antenna array will change in amplitude and phase according to the carrier frequency. Each element of the array will thus receive a phase shifted waveform. Directly summing the shifted waveforms will produce a reception pattern varying

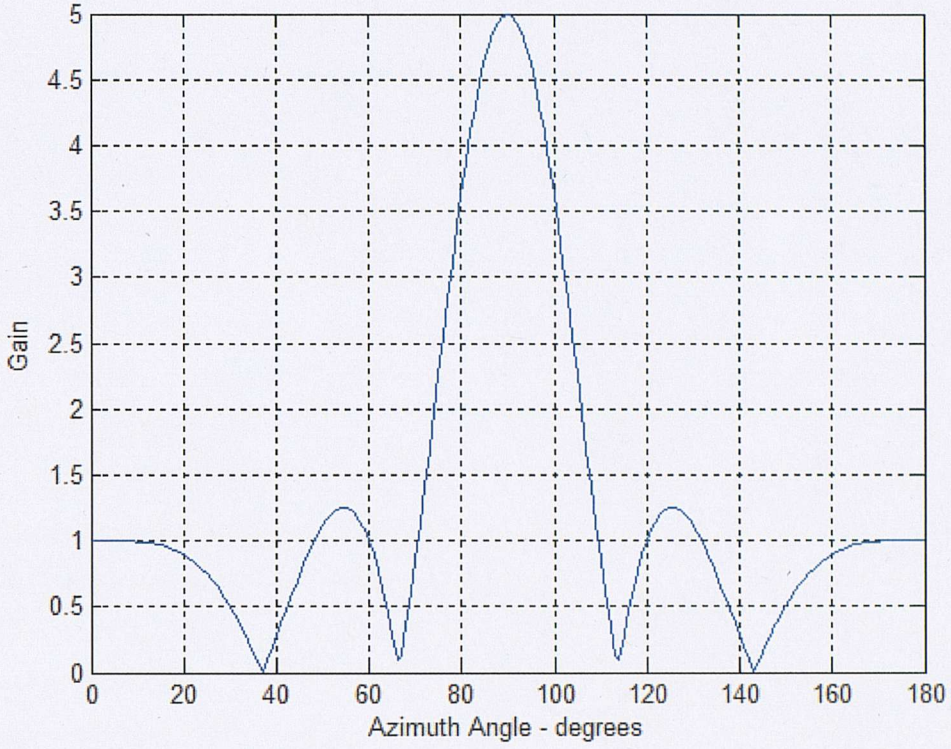


Figure 1.3: A typical array pattern of a uniform linear array

in amplitude in accordance to the direction of arrival of the impinging radio wave. This pattern can be viewed as the gain pattern of the antenna array to different directions as illustrated in Figure 1.3, and the same holds for transmitting arrays too (radiation pattern). Directions of high gain indicate constructive combination of the received phase-shifted waveforms while low-gain corresponds to destructive combination. It is clear that the array pattern depends only on the geometry of the array and the carrier frequency of the signal.

A widely used technique applicable to antenna arrays is beamforming. The simplest beamformers essentially apply a phase shift (complex weight of unity magnitude) on each antenna element (phased arrays) before adding the waveforms and passing the result to the signal processing receiver. In this way the gain pattern of the array can be "steered" onto the desired direction, maximising the gain for a desired signal [23]. By adjusting a beamformer's weights according to the varying channel parameters an adaptive beamformer can be formed, operating as a spatial filter before the normal temporal filtering takes place. Spatial filtering can alter and shift the pattern of an antenna array, maximising the receiving gain at desired directions and putting nulls at directions of unwanted interference and thus maximising the Signal-to-Noise-Plus-Interference

Ratio (SNIR) Wiener-Hopf beamformers. This type of beamformer may couple spatial diversity exploitation with temporal multipath diversity (RAKE receiver for recombination of multipaths with co-channel interference rejection) [23] to optimise the SNIR. However, Wiener-Hopf receivers have limitations, mainly lying on the limited spatial resolution exhibited especially at lower SNR. This means that interfering sources impinging from directions similar to the desired source multipaths, will not be cancelled, but will pass through, with degrading effects to the receiver's performance. Superresolution beamforming techniques have thus been devised to tackle this problem [24]. These beamformers, although more complex in implementation, can provide an asymptotically infinite resolution of incoming signals. These beamformers are based on more complex mathematical techniques in order to separate the noise, desired and unwanted signal subspaces, and are very useful for high end applications.

The fact that multipath can be used in the advantage of the communications system is not unique to spatial processing techniques. In fact, a serious restraint of spatial processing is that the degrees of freedom, i.e. the number of separate multipaths that can be accommodated, is limited by the number of antennas employed. With the advent of Code Division Multiple Access (CDMA) systems, temporal processing extended from channel equalisation and interference rejection techniques, to temporal multipath recombination. This technique is epitomised by the RAKE receiver originally introduced in [25], where a "rake" is used to recombine the received signals, with each finger corresponding to a separate multipath. CDMA systems can achieve higher data rates and are very resistant to co-channel interference. Once again, the previously destructive effects of multipath are turned around to the advantage of the receiver to exploit diversity. In this case however, more degrees of freedom are provided, theoretically limited by only the length of the CDMA codes used. The limitation lies in the fact that, in order to constructively exploit multipath, the paths must be temporally resolvable, i.e. must be separated in time by an interval dependent on the CDMA chip time period.

The natural extension of the above technologies comes in the combination of MIMO and CDMA systems. By using an antenna array on the front-end of a CDMA receiver the temporal and spatial processing techniques described can be effectively coupled. This leads to the joint spatiotemporal reception of signals, whose benefits include a greatly increased number of degrees of freedom but also to the effective lift of the temporal or spatial resolvability limitation. This is because paths only need to either be resolvable in time or space, which greatly

reduces the probability of two paths being unresolvable. A simpler space-time receiver based on the RAKE CDMA receiver is the 2D RAKE (an antenna array RAKE CDMA receiver) [26]. In this case, two-dimensional fingers extend to space and time in order to separate multipaths and thus avoid the traditional RAKE limitations. Space-time receivers can operate in heavy interfering environments, with no need of training sequences and are considered to be at the cutting edge of the communication systems because of their excellent characteristics and potential to fully exploit both space and time diversity simultaneously. Subspace receivers that operate jointly in space and time have also been proposed, showing that it is possible to accomodate a very large number of users-multipaths with great accuracy, under environments of low SNIR.

The advance in communication systems seems to favour MIMO systems and justifiably so. MIMO systems have been shown to exhibit desirable characteristics and increased system capacity combined with the potential to allow wireless communications under heavy interfering environments. The inclusion of MIMO communications to emerging technologies such as WSNs is thus a natural step. In the next section we discuss the first attempts to include MIMO schemes in WSNs and potential performance evaluations of such systems.

1.4 MIMO in WSN

By using multiple nodes to transmit and receive information in cooperation within the WSN we aim at exploiting a number of advantages that such Multiple-Input Multiple-Output techniques offer. A number of studies have been performed examining the potential performance of a MIMO communications system when applied to WSN. In [27], the authors investigate the effects of using MIMO communications on the energy expenditure of the transmission and reception schemes. The discussion is based on Alamouti code based MIMO communications on a single node but also on the analysis of node cooperation for wireless communications. The main disadvantage concerning MIMO in terms of necessary power lies on the fact that MIMO systems employ more complicated circuitry and operations and in the case of node cooperation an amount of energy overhead is also involved. The authors show that MIMO systems are still superior in this aspect (energy conservation), as long as the range of the wireless transmissions is not too small. By allowing an optimised constellation size this superiority extends to even smaller communication distances. However, the advantage offered by the interference rejection capabilities is not factored in. In [28], the energy performance of MIMO

systems in co-channel interfering environments is compared to SISO under the framework of WSNs. In fact, this is a much more suitable comparison since a WSN is a heavy-interference environment. Again the MIMO systems are shown to perform distinctively better except for small transmission distances with the average required energy per bit being the same for distances of around 15 metres but the difference increasing to a full order of magnitude at around 60 metres. The results further favour MIMO systems when transmissions are simulated over more heavily fading channels.

Although MIMO transmissions may have great potential in terms of energy saving and channel capacity increase, an important downside that should not be neglected is how the same communications essential for the node cooperation itself may increase the actual amount of interference present. This is not a concern for multiple antenna equipped nodes, but it is important for any node cooperative schemes. In [29], the authors examine the trade-off between the interference and the sum network capacity. By taking into account a different number of nodes used, and varying transmission distances they attempt to provide general design guidelines for the incorporation of node cooperating MIMO techniques in WSNs. Furthermore, in [30], the authors analyse a Space Time Block Coding (STBC) node-cooperative transmission scheme based on Alamouti codes to evaluate energy efficiency. The study is performed under the LEACH protocol, discussed in Section 1.2, and concludes that on top of the traditional advantages that MIMO schemes offer, energy savings may also be achieved if the trade-off between processing energy and transmission energy requirements is carefully studied. A similar study on STBC but on a more routing oriented approach is performed in [31], illustrating how better link quality may be achieved by the employment of a MIMO cooperative scheme. In [32], the authors propose a virtual MIMO system based on the V-BLAST (Vertical-Bell Laboratories -Layered -Space-Time) architecture discussed in the previous section. Their study introduces a very important trade-off between latency and energy efficiency in a WSN using MIMO schemes. This can prove a useful design parameter for constellation optimisation for networks with very tight energy constraints.

Further research into MIMO and WSNs by the authors of [33]and [34], indicates that the incorporation of such a communication system not only improves network cohesion but also reduces the average mean path length to destination. By using Monte Carlo simulations for various network configurations and densities, it has been shown that MIMO enabled WSNs are more well-connected, resulting in bigger clusters of interconnected nodes, thus providing a more effi-

cient platform for message exchange and a more useful network in general. Furthermore, the mean path length which closely relates to the energy expended in forwarding messages is on average shorter in MIMO WSNs. The improvement ranges on a variety of densities but is more significant on moderately dense WSNs.

It is clear that employing MIMO in WSNs is a direction that many researchers are currently pursuing, mainly in the sense of exploiting spatial diversity in a wireless channel. However, a very promising area of MIMO communications that aims at fully exploiting the spatial dimension of the wireless channel, namely the Array Processing field has not yet been so extensively explored in terms of its potential usefulness to the WSNs operation. The so-far limited effort includes nevertheless some attempts worth mentioning. The authors of [35] for example, analyse the beamforming capabilities of randomly formed arrays in a WSN. By using a stochastic approach, they conclude that a good degree of directionality and sidelobe performance can be achieved, as long as issues of synchronisation, calibration and sharing transmit information are resolved. In contrast to the random arrays of [35], in [36] the authors propose a method for actually selecting which nodes are suitable to participate in a *Wireless Array* (WA). Their goal is to minimise the perimeter of the resulting array in the same time as satisfying a diversity distance constraint. They achieve energy savings by using a neural network approach for the selection of close by nodes and by using a different communication channel for the internal array communications so as to minimise overhead. Yet another example that illustrates the various benefits of using array communications in WSNs is [37]. The paper presents ways of achieving secrecy implemented in the physical level, by using inherent and implanted ambiguities in the internal transmissions of a WSN. By employing beamforming transmissions they design a communication scheme where several degrees of secrecy can be achieved. This approach may be particularly appropriate for military application where maximum security is a highly desirably characteristic.

Following this introduction to WSNs, we have glimpsed at how research into the area varies from traditional network organisation, routing and MAC to advanced physical layer fields. The research into MIMO communications in the context of WSNs is of particular importance to this thesis, since the end goal is to use such advanced techniques for the improvement of WSN operation. The ultimate goal is to develop techniques for an infrastructureless, reconfigurable, low-bandwidth, high-capacity and low latency Wireless Sensor Network ensuring Low Probability of Interception and having anti-jam and anti-interference capabilities. The approach will be based on the employment of advanced spa-

tiotemporal array processing techniques on two levels. The nodes of the proposed WSN will be equipped with fully capable antenna array communication modules. Furthermore nodes will be allowed to group together to form *Wireless Arrays* operating as autonomous entities, resulting in a new type of network, the Arrayed Wireless Sensor Network (Arrayed-WSN).

1.5 Thesis Description

Initially (Chapter 2), the basic foundations of the Arrayed-WSN are going to be discussed. Firstly, the capabilities of the nodes are going to be described, together with the roles and modes that they can take in the network. Initial network organisation with a neighbour discovery and CDMA code allocation scheme is presented. A general operation scenario illustrating the Arrayed-WSN operation is discussed.

A very important property of the WSN is the ability of nodes to group together and form *Wireless Arrays*. These are communication entities that behave as traditional antenna arrays but with the links between the antenna elements and the array processing unit replaced by wireless communication links. An investigation of how such an array may be formed will be also studied in Chapter 3, with emphasis on the geometrical aspect of the problem and its impact on the system performance. This leads to a novel distributed algorithm for choosing the nodes to form a *Wireless Array*. The algorithm employs a compound measure to evaluate the suitability of the resulting *Wireless Array* based on the impact of the geometry to various areas of array performance.

The design of the various communication links employed in the WSN is presented next, in Chapter 4. A beamforming Multi-Carrier CDMA MIMO scheme will be employed, designed to exploit the presence of antenna arrays at both ends of the communications channel. In this way, spatiotemporal signal processing at both the transmitter and receiver, the presence of many sub-carriers and the employment of CDMA, provide many degrees of freedom. These extra degrees of freedom allow for high interference cancellation capabilities which in the environment of a Wireless Senor Network is a highly desired property.

In Chapters 5 and 6, various uncertainties involved in the Arrayed-WSN are modelled and analysed. Since information about the nodes and their position is collected a posteriori, it is expected that estimation errors will be present. Geometrical and electrical uncertainties relating to the antenna arrays employed in the Arrayed-WSN are analysed. Furthermore, the uncertainties that are natu-

rally related to any antenna array system namely the ambiguities are presented in the case of the Arrayed-WSN. In particular, the ambiguities of the antenna arrays involved in the Arrayed-WSN are examined and a way of resolving by using minimal communications is proposed. Furthermore, an analysis of the full network operation is performed via computer simulation studies.

Finally, in Chapter 7, we summarise the study, provide a brief list of the thesis contributions and discuss potential future directions for the extension of the research presented herein.

Chapter 2

Basic Framework of Arrayed-WSN

In this chapter the basic smallest individual entity of the Arrayed-WSN, the node, is described. A main characteristic of the proposed Arrayed-WSN is that individual nodes are equipped with complete antenna arrays (*Local Array,* LA). This allows for comprehensive joint spatiotemporal communication techniques to be applied to node-to-node communications. Furthermore, nodes can form groups (*Wireless Array*) that operate under the direction of a controller node. These are antenna arrays, incorporating node cooperation, in which each node takes the role of a single antenna element while the array processing is performed on the *Wireless Array* controller node. The *Wireless Array* is described together with its general operation principles in Section 2.2.2.

These two types of antenna arrays (*Local* and *Wireless Arrays*) will form the basic building blocks of the Arrayed-WSN. Based on these, a general operative scenario of the Arrayed-WSN will be outlined. This will finally lead to the description of the three distinct necessary communication links and the node modes and roles employed in the Arrayed-WSN.

2.1 Arrayed-WSN Node Outline

The Arrayed-WSN is a homogeneous network, meaning that all nodes are based on the same hardware platform, irrespective of what role they may take once the network is deployed. This is advantageous in the sense that node fabrication is easier and that the network is more robust because it does not depend on a few sophisticated nodes to perform advanced operations as is commonly the case with heterogeneous networks. Thus, node failure does not severely affect the network

Homogenous Network	Heterogeneous Network
Power dissipation can be shared out among all the sensor nodes by dynamically changing roles	More nodes can be deployed for the same total cost (although the cost associated with designing and setting up different production runs may offset this)
More robust to deliberate attempts to disrupt/destroy the network	Existence of more sophisticated nodes simplifies network design
All nodes can take on any of the roles outlined	Natural hierarchical structure
More robust to node failure	
Node fabrication simplified	

Table 2.1: Advantages of Homogeneous and Heterogeneous WSNs

operation, in the sense that node responsibilities can be easily assumed by other nodes upon node failure. On the other hand, it means that all algorithms and schemes designed must be executable by all nodes and cannot assume a natural hierarchy or a backbone of advanced nodes. An outline of some of the arguments leading to the choice of a homogeneous approach is presented in Table 2.1

As mentioned above, individual Arrayed-WSN nodes are equipped with *Local Arrays*. Recent advancements in microstrip antenna technology have made it possible to fabricate antenna arrays with elements confined closely in space [38]. This allows an antenna array to be placed on each individual node (denoted as the local antenna array) which greatly increases the capabilities of the network.

The antenna array has, as mentioned before, advantages in the design of the receiver. As most of the communications of the node are actually directed to specific destinations (except for broadcast messages), using omnidirectional antennas would waste most of the energy in directions that are not useful. Being able to steer the transmission/reception towards a desired direction is thus a very efficient approach. This can be easily provided by an antenna array. Furthermore transmitting only in one direction greatly reduces the amount of multipath and interference being introduced in the channel. For example, a node using directed transmissions will not interfere with other nearby nodes that are simultaneously accessing the channel even if the same frequency band is used. Steering the transmissions has another practical use when it comes to military applications. The probability of transmission interception is greatly reduced when the transmission direction is restricted. A potential jammer will also have to use higher powered transmissions to overcome the directionality of the transmitter/receiver.

Further advantages are offered by the employment of *Local Arrays*, in the area of channel access. The proposed communication scheme for the Arrayed-WSN

is based on MIMO CDMA techniques because of the great advantages that such techniques offer in the area of channel multi-access, interference rejection and possible power savings as discussed in the previous chapter. Since the chosen scheme is based on CDMA, more than one node will transmit at the same frequency at the same time. This means that a receiver will have to isolate the desired node's transmission from the received signal whilst suppressing the unwanted Multiple Access Interference (MAI) from other nodes. The ability to use advanced space-time techniques in both the transmitter and the receiver increases by equipping the node with an antenna array. Jointly using the space and time dimensions in spread-spectrum systems has been shown to exhibit superior performance over conventional (disjoint) techniques [39].

Including a local antenna array on a node presents various challenges. For instance, due to the size of the node the antennas have to be compact and closely spaced leading to the use of a microstrip antenna array. Microstrip antenna arrays have been given extensive research attention due to their small size and ease in fabrication. Although this type of arrays usually poses limitations on the achievable bandwidth, techniques have been developed to compensate and attain higher bandwidths [40].

A very important feature to consider when designing an array of N antennas is the geometry of the array, i.e. the spatial position of the antenna array elements. This is denoted by the matrix $\mathbf{r}$ with columns the Cartesian coordinates of the antenna array elements. The geometry of the array determines the shape of the "array manifold" which is a geometrical object embedded in the N-dimensional complex space. This object is of great importance to array processing and is going to be discussed in the next chapter. For the moment it is sufficient to say that the array manifold is the locus of all array response vectors and is a useful means of analysing the array properties. A very desirable geometry due to its differential geometric manifold properties is the 3D-grid array. A 3D-grid array of N antenna elements is one for which the element locations conform to:

$$\mathbf{r}\mathbf{r}^T = \rho\mathbb{I}^3, \ \rho \in \mathbb{R} \tag{2.1}$$

where $\mathbf{r} = \left[\underline{r}_1, \ \underline{r}_2, \ \ldots, \ \underline{r}_i, \ \ldots \ \underline{r}_N\right]$ with $\underline{r}_i$ the 3×1 real vector of Cartesian coordinates of the i^{th} antenna and ρ a constant real number.

3-D grid arrays of N elements have a spherical array manifold embedded in an N-dimensional complex space with their manifold metric being a diagonal matrix. Thus the manifold of these arrays is "developable" in the sense that they can be mapped onto a plane without distortion. These properties have an effect

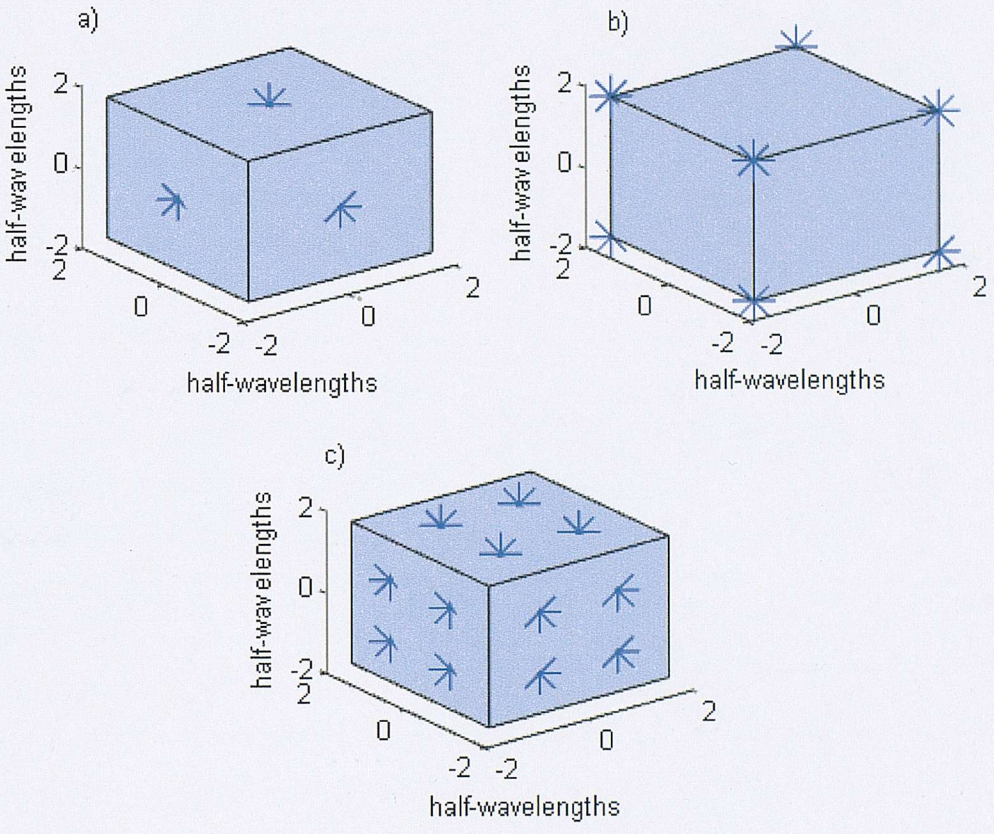


Figure 2.1: Possible 3D-grid array geometries on a cubical node. a)6, b)8 and c) 24 element configurations

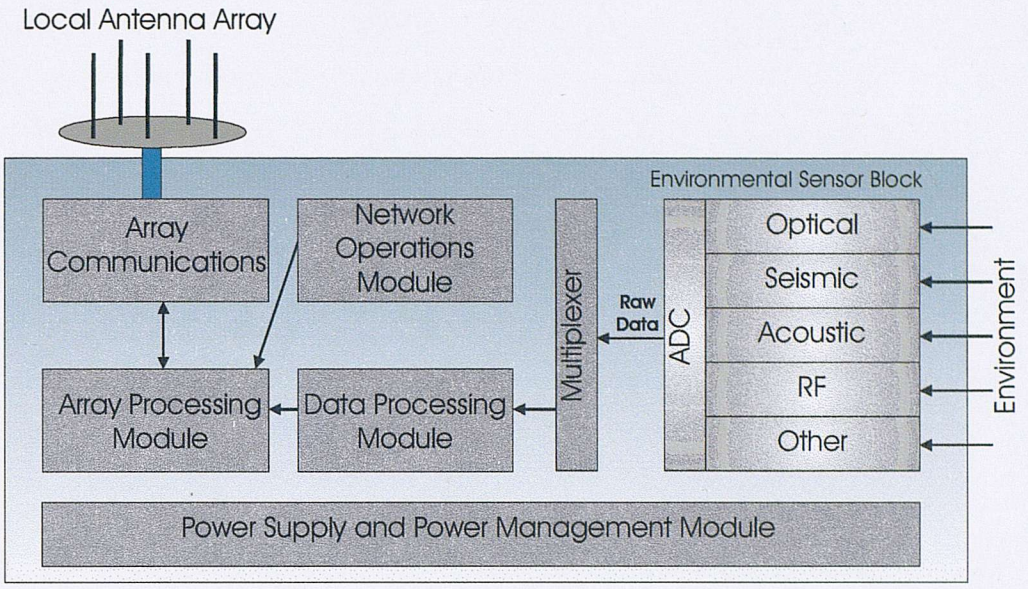


Figure 2.2: A conceptual outline of the AWSN node with the sensor bank, power module data and array processor and the local array

on the differential geometry of the manifold and greatly simplify the analysis of the constructed array system [41].

Due to its desirable characteristics the 3D-grid array geometry is adopted for the *Local Array* in the Arrayed-WSN, but without any loss of generality. By assuming a cubical node physical shape, one antenna can be placed on each face in order to form a 3D-grid array where $N = 6$ or one at each vertex resulting to $N = 8$. The number of antenna elements is chosen as such, due to the 3D-grid array constraint. The next number of antenna elements that can form a 3D-grid array on a cube is twenty four elements which although may imply more degrees of freedom, also implies an increased computational requirement for the energy-constrained node. Example node 3D-grid *Local Arrays* are illustrated in Figure 2.1.

Note that since microstrip antenna arrays are used, a greater number of antennas that are actually simultaneously used can be placed on each node. This can allow for choosing which antenna elements are used each time. Furthermore it can compensate for potential antenna element failure. The case of more antenna elements than the ones being used is incorporated in the analysis of Chapter 6.

The main role of a node in a WSN is to sense the environment using a sensor or a combination of sensors, perform a degree of data processing and then communicate with other nodes with the final goal of forwarding information about the sensed data towards a sink, or a data extraction point. The node thus will usually comprise of a power module that will include a battery and in some cases

a power control unit, a bank of environmental sensors, a DSP module and a communications module. Network operations such as network setup, neighbour discovery, localisation, routing and protocol implementation may be performed in the communications module or on a separate processor. In addition to these, an Arrayed-WSN node will include an array processing module, that can perform the necessary processing needed by the more complicated communication scheme involved. Furthermore, the array processing module ensures the node can perform the implied duties as a *Wireless Array* element or even controller. A conceptual outline of the Arrayed-WSN node is illustrated in Figure 2.2

2.2 Network Operation

2.2.1 Network Discovery and Code Allocation

Like most WSNs, the Arrayed-WSN nodes are assumed to be deployed in a random manner in an inaccessible area. This means that upon deployment, nodes have no knowledge about their neighbours or their own positions. In order to form a cohesive network, the nodes must pass through a set-up phase. During network set-up, a neighbour discovery and a self-localisation phase are introduced. However, before these important steps can take place, a way for the nodes to effectively communicate needs to be established. As mentioned before and will be extensively discussed in Chapter 4, a CDMA based communication scheme was favoured for the Arrayed-WSN. Following such a scheme requires that each node is allocated a specific CDMA code that will allow it to access the channel. In an effort to combine a solution to this requirement with a neighbour discovery algorithm by exploiting the node *Local Array*, we now present an algorithm for Channel Access and Network Discovery using *Local Array* and Dynamic Code Self-Allocation (CANDLA-DCSA).

The Picoradio project at the Berkeley Wireless Research Centre uses a combination of CDMA and CSMA/CA and also incorporates a 'Wake-up radio' to allow the nodes to enter a sleep mode when not actively transmitting or receiving. The scheme uses a distributed algorithm using CSMA/CA over a common channel to assign roughly 30 CDMA codes over an almost unlimited number of nodes such that each node's assigned code is different from any of its two-hop neighbours [42]. Note that for this to be feasible, the maximum 2-hop degree of the network (i.e. the largest number of 2-hop neighbours) must be less than the number of codes available.

However, instead of CDMA codes being assigned by using an algorithm that requires nodes to exchange complex messages on a separate channel, the nodes proposed here sense the channel for a set period of time, which is denoted as the beaconing interval[1]. Then each node selects the conventional CDMA code associated with the lowest combined received power level. A code is selected at random if no signals from other nodes are detected within the beaconing interval.

Once a node has selected the CDMA code it periodically (once in a beaconing interval) transmits a short-duration omnidirectional beacon signal using this code - or more strictly a beacon packet containing at least the following information:

- Node ID
- Transmit power level (note: not used for range estimation)
- Number of beacon packets received in the last beaconing interval from other nodes that meet the given link quality requirements (that is, how well connected the node is to the network).
- Remaining battery power
- The transmitting nodes symbol index for the symbol at the start of the packet. The symbol index is simply a counter of the number of symbol periods elapsed since a node was activated as determined by that node's clock (Periodical reset can be used to prevent potential counter overflow).

It is this beacon packet that allows other nodes within range to select their code according to which code has the lowest combined received power from all nodes detected using this code.

Using this scheme it is possible that two or more nodes may choose the same code, in which case signals from these nodes may be separated using joint space time processing techniques. The term local co-code party will be used to denote the set of nodes using the same code as detected by a given node. Due to the asynchronous nature of this scheme most nodes choose their code at different times. However, if a number of nodes sense the channel over the same period of time and therefore choose their codes without knowledge of the other code assignments, a given code may become over-subscribed. To mitigate this problem each node monitors the power level associated with every local co-code party. If a node's own co-code party power level is greater than the next highest power

[1] (Note that in general, the times at which each node starts to sense the channel are not the same)

co-code party by a given threshold, a number (say k) nodes must change their codes. In order to coordinate this without sending messages, node(s) in the over subscribed co-code party compare their own node ID to the other node IDs in the same co-code party and the k nodes with the smallest node IDs perform the code self-allocation again.

If, after a given period of time transmitting a beacon at the default initial power level, a node has not received a beacon from a given number of nodes known as the required network degree, it increases its transmitting power level by a given (small) amount and indicates in the beacon packet that it has yet to be adequately connected to the network. Any node receiving this packet can use the transmit power level contained in the packet to adjust its own power level to establish contact with this node (provided this node's connectivity is not close to the maximum network degree). If the first node does not receive any response signal within a given period of time it increases its transmit power again – this process repeats until a node either receives another nodes beacon or the maximum transmit power level is reached. In the second case, the node ceases to transmit beacon pulses and infrequently (at a period determined at deployment) senses the channel for beacon packets from other nodes. Only when it detects another beacon packet it switches back into the above described mode and starts the code self-allocation and network discovery algorithm again.

Each node maintains a table of the IDs of nodes it has received a beacon packet from in the last beaconing interval. The received power level combined with the transmitted power level field in the beacon packets is used by each node to implement a self power control mechanism. This ensures that a given link quality with a given number of its neighbours (the required network degree) is maintained subject to transmit power constraints.

The receiver on each node incorporates a channel estimation algorithm that provides the direction and relative time of arrival of each multipath component corresponding to a given node. This information is not only used for demodulating this nodes data stream; it can also be used by the node for relative position estimation and for beamforming when transmitting messages back to that node.

This system has the advantage that absolutely no synchronisation (local or global) is required in order for nodes to establish communication links. Very little overhead is required, as the beaconing interval can be greatly increased after the initial network discovery phase is complete. In order to allow for changes in the topology of the network to be detected this particular network phase can be periodically repeated with small frequency. Furthermore, the size of the beacon

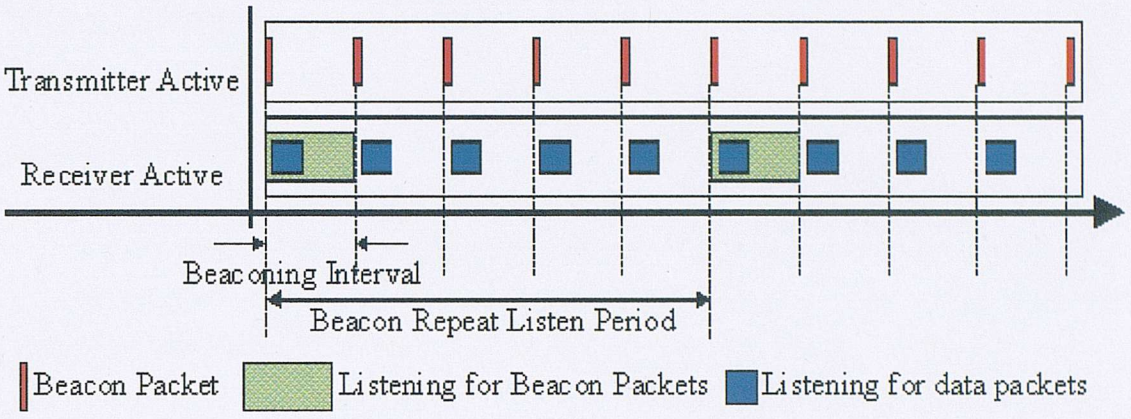


Figure 2.3: Low Duty Cycle Channel Listening

packet is small compared to the messages required in the Picoradio project (which contain code allocation tables for a node and its neighbours) while the use of the *Local Array* permits space-time processing of the received signals allowing code re-use [43].

Some sensor networks conserve energy by only listening to the medium for short (in general pre-arranged) periods of time. The above scheme can be easily extended to allow this type of scheduling at the expense of increased message latency by stating that packets intended for a given node should be transmitted in a given time window after reception of that nodes beacon packet. Of course each node must still occasionally listen for to the channel for an entire beaconing interval to ensure it has up to date information on which nodes are operating and which codes they are using. This lower duty cycle approach is illustrated in Figure 2.3.

The single node-to-single node communications such as the one described above, are performed via what is called in the Arrayed-WSN, the *initial*-wireless link. The *initial*-wireless link can also be used for the localisation procedure that takes place in an Arrayed-WSN. Many localisation procedures have been proposed for WSNs [16], however, especially applicable to the Arrayed-WSN are distributed localisation procedures that takes advantage of the node *Local Array* capabilities. The *initial*-wireless link is especially designed for node to node communications and is furthermore discussed in Chapter 4.

2.2.2 Defining *Wireless Arrays*

When an EOI takes place within the network, a number of nodes will simultaneously sense that event. In the Arrayed-WSN, at this point, a distributed algorithm, extensively discussed in Chapter 3 takes place, aiming at the formation of a *Wireless Array*. The *Wireless Array* is a collection of nodes with appropriate spatial positions, that operate as a unit with the aim of forming quality communication links with other *Wireless Arrays* (i.e. MIMO links). The main purpose of a *Wireless Array* is to transmit and relay the appropriate messages about the sensed event towards the sink.

A *Wireless Array* is comprised of a number of nodes N of which one is the *Wireless Array* controller, while the rest $N-1$ nodes are the *Wireless Array* element nodes. The controller node of the *Wireless Array* is responsible for the organisation of the array and the array signal processing involved with the wireless transmission and reception. The element nodes in turn, act as normal antenna array elements. In a sense a *Wireless Array* is very similar to a normal antenna array system of N elements, but with the traditionally wired links between the array elements and the array processing module replaced by separate wireless links. The advantages offered by *Wireless Arrays* are many and diverse. Since *Wireless Array* transmissions are essentially a node cooperation technique, the energy dissipated in transmission is actually shared between many nodes. Furthermore, because of the larger node separation, a *Wireless Array* has an aperture bigger than that of a *Local Array*. This results in higher performance gains in terms of directionality and asymptotic interference rejection capabilities.

It is clear, that two communication links are involved with the operation of a *Wireless Array*. Firstly, the *intra-Wireless Array* link corresponds to all the communications between the array controller and the element nodes. Received data that need to be processed by the controller are transmitted in the *intra*-wireless uplink, while data destined for transmission are transmitted in the *intra*-wireless downlink, i.e. from the controller to the elements. It has to be noted that the *intra*-wireless link is very similar to the *initial*-wireless link, since they both correspond to node-to-node communications.

After a *Wireless Array* is formed near an EOI, it will automatically send a request for the formation of another *Wireless Array*, in the direction of the closest sink. This request that includes the transmitting array's position will be sensed by a number of nodes which will estimate their distance to the transmitting array. In that way, another *Wireless Array* will be formed in an area within the confines of a predefined distance. This is a relay *Wireless Array*, aiming at forwarding

the received signals towards the sink. This procedure is repeated as many times as needed (hops) to reach the sink. It is clear therefore that a request for a *Wireless Array* formation can be categorised as an internal EOI, since it evokes the same response by the network, as a normal environmental EOI would. The communication between *Wireless Arrays* is performed via the third separate link present in the Arrayed-WSN, called the *inter-Wireless Array* link. The *inter-Wireless Array* link needs to be treated in a different manner than the other two links introduced so far, since it corresponds to *Wireless Array*-to-*Wireless Array* communications. Thus, in summary, there are three separate communication links:

- The *initial*-wireless link
- The *intra-Wireless Array* link
- The *inter-Wireless Array* link

  while details about their modelling and design of the three links are described in Chapter 4.

Figure 2.4 illustrates two *Wireless Arrays* communicating via the beamforming transmitter and receiver inter-wireless link. The *intra*-wireless link supporting the *Wireless Arrays* by allowing the *Wireless Array* nodes to communicate between them is also shown operating at the same time.

2.2.3 Node Roles and Modes

Next the various node roles and modes in the network are discussed. By considering various scenarios the aim is to define a complete table of modes for the Arrayed-WSN node. Typically sensor nodes in the Arrayed-WSN will have three basic operational modes, which are dependent on the application:

- Event driven: In this mode the sensor monitors the environment until a given stimulus is received. Once the event occurs the data processing unit activates the transceiver and signals that the event has occurred. Depending on the application, the sensor may then switch into another operating mode for a period of time or may return to its previous state.
- Periodic observation (sleeping mode): In this mode the sensor sleeps for a large proportion of the time, sampling the environment periodically. The samples are processed (to reduce the amount of raw data transmitted) and

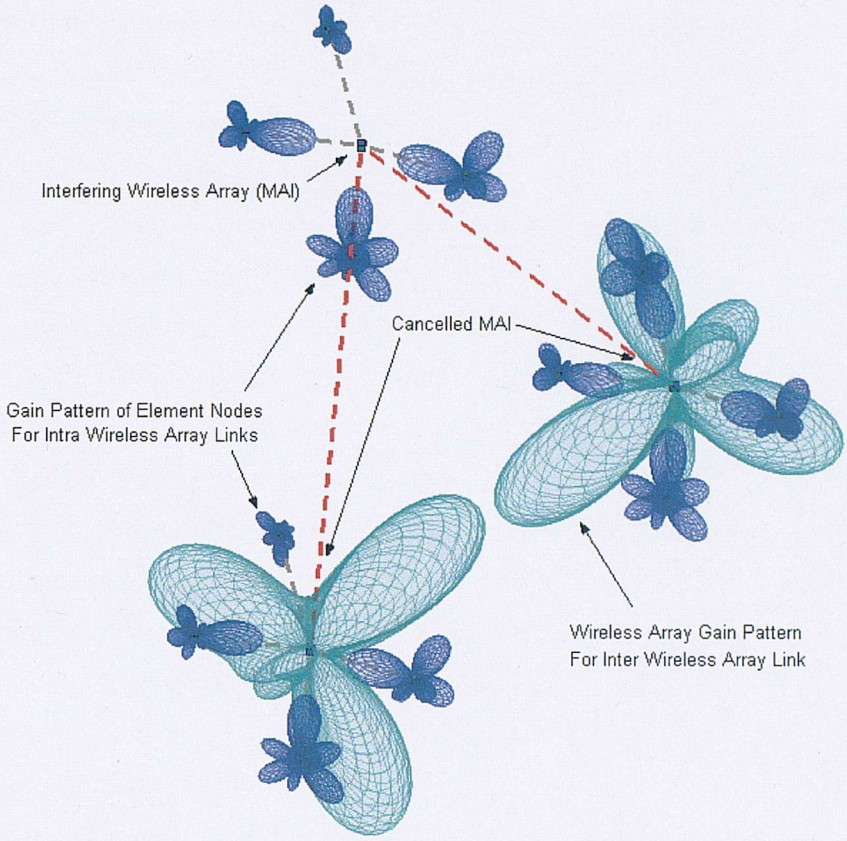


Figure 2.4: The beamforming *inter* and *intra*-wireless links with array patterns in light and dark blue respectively

stored for a given period of time either determined by the size of the data required to describe the observation and node storage capacity (if high latency is acceptable – this is done as turning the radio transceiver on and off too frequently wastes energy due to start up current drain [44]) or by the time taken for the MAC protocol to signal the intention to transmit (if low latency is required).

- Continuous: In this mode the sensor samples the environment continuously (at a sample rate dependent upon the type of sensor and the application). Some processing is then performed locally to reduce the amount of raw data transmitted. The processed (lossy compressed) data is stored for a period of time determined by the application and latency requirements before being passing to the radio transceiver for transmission.

- Emergency: If a sensor receives a stimulus that is extremely urgent other functions that the node is performing (such as acting as a controller node) can be overridden so that this crucial information can be transmitted with the shortest possible delay.

Furthermore, based on the network description so far, nodes may take upon three different roles in the Arrayed-WSN: individual node, *Wireless Array* node and *Wireless Array* controller.

As simple individual nodes, they firstly enter a set-up phase. When the sensor nodes are deployed, or when new nodes are introduced to the network, or when dormant nodes are activated, or for other significant changes to the network, new communication links will need to be established, the relative position of the node relative to other nodes in the immediate neighbourhood needs to be estimated in order to reduce the time taken to form arrays when a significant event occurs and to assist in routing messages through the network. During normal network operation, individual nodes will go through designated duty cycles. Through these cycles, nodes may be inactive in order to save energy, sensing the environment periodically for EOI or in full sensing mode if events have already been detected.

In the case of an important EOI being sensed, the node will go into an array formation mode. This will allow for the array formation algorithm to take over, resulting to the node possibly being selected for participation in a *Wireless Array.* In such a case the node may become either a simple *Wireless Array* element node or a *Wireless Array* controller. Depending on the status of the *Wireless Array* and the node role in it, various modules of the node may be activated or deactivated. In a transmitting *Wireless Array* for example, the nodes will continue to sense the environment while the transceiver is on and operating on both the *intra* and *inter*-wireless links. This allows the array to transmit information about the sensed event while still monitoring for further EOI. In a *Wireless Array* relay, nodes will typically have their transceivers on but will not have to sense the environment at the same time since the EOI has taken place in another area of the network.

As far as power modes are concerned, the following are possible for our sensor node:

- Fully Active: All subsystems of the node are functioning
- Standby: Various levels will be considered depending on the power levels of each subsystem. Consideration is given for which combinations make sense depending on the role of the node
- Inactive: All subsystems de-activated except a wake-up radio as in a PicoRadio node. The node periodically signals that it is still present and operational, then listens for the activation signal (very low duty cycle).

Mode	Role	Sensors	Data Processor	Array Processor
Deactivated	Dormant	Off	Inactive	Off
Inactive	Dormant	Off	Inactive	Off
Setup	Individual	Periodic	Periodic	Nominal
Standby	Individual	Periodic	Periodic	Off
Observe	Individual	Sense	Active	Off
Emergency	Individual	Sense	Active	High
Individual Relay	Individual	Periodic	Periodic	Nominal
ArrayForm	Choosing	Sense	Active	High
Array Element Active	Element	Sense	Active	Nominal
Array Controller Active	Controller	Sense	Active	High
Array Element Relay	Element	Off	Off	Nominal
Array Controller Relay	Controller	Off	Off	High

Table 2.2: The merged sensor node roles and modes

- Deactivated: This mode is entered when either the power falls below a certain threshold (preventing reliable operation) or another component of the node fails.

  by using the above discussion, we now move to the unification of the possible roles and modes of the sensor nodes. Table 2.2.3 shows our set of overall modes of our sensor node that encompasses all the features described above:

Furthermore, Figure 2.5 illustrates a mode state diagram with the inclusion of the various events that trigger the transition between modes.

In this chapter, the basic building block of the Arrayed-WSN, the *Local Array* equipped sensor node has been described. Based on the potential uses of the node in an Arrayed-WSN the roles and modes of the node have been unified into a comprehensive state diagram. Furthermore, the general operation of our network has been outlined and a code allocation scheme has been proposed that avoids complex message exchange between nodes, at the same time as combining neighbour discovery with node-to-node link establishment. In addition, the basic use of *Wireless Arrays* has been outlined, discussing how a potential directional routing protocol can take advantage of the directed transmissions offered. Through the discussion of the network and the *Wireless Array* operation, the three necessary distinct communication links of the Arrayed-WSN have been identified. In the next chapter, the formation of *Wireless Arrays* is studied, with emphasis given on the geometrical aspect of the problem, i.e. the selection of the nodes to comprise a *Wireless Array*.

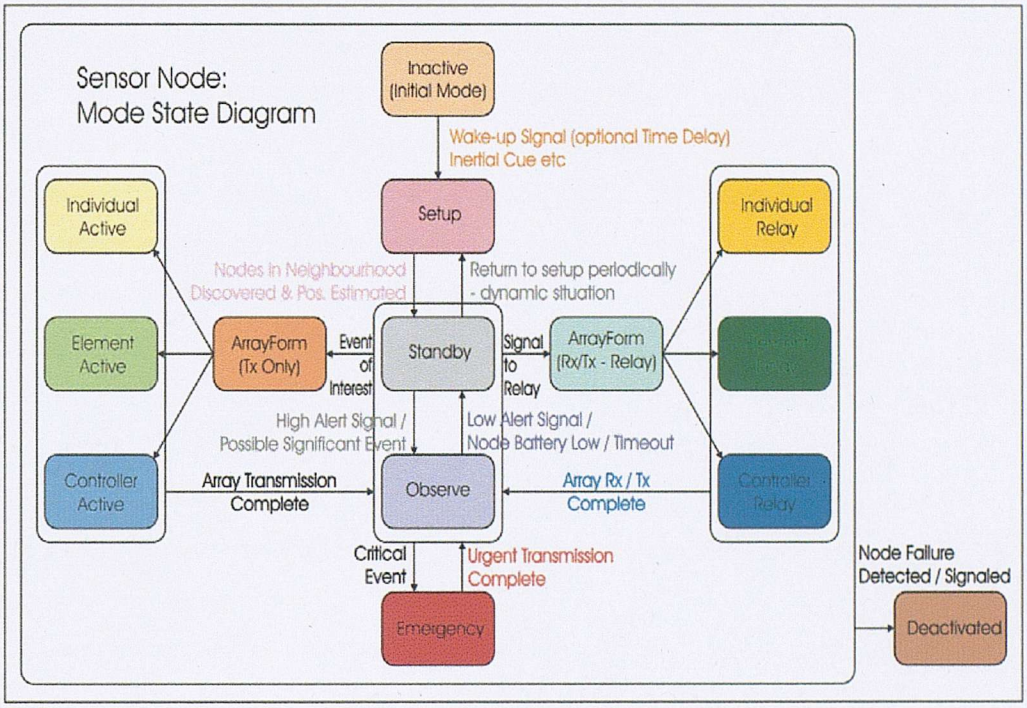


Figure 2.5: The unified mode and role state diagram for an Arrayed-WSN node

Chapter 3

Wireless Array Formation

As mentioned in the previous chapter, each node in the Arrayed-WSN is equipped with a microstrip antenna array (*Local Array*) and a number of nodes group together to form a *Wireless Array* in order to propagate information through the network. In this chapter, the rules that govern this formation (known as the array connectivity rules) are presented and the factors that affect the selection of nodes such as the number of ambiguities, the accuracy at which the positions of closely spaced sources can be estimated and the sensitivity to node location uncertainties are discussed. The proposed connectivity rules incorporate all these factors and allow the relative importance of each to be adjusted depending upon the intended application. The approach is illustrated using a few selected examples and the operation of the array connectivity rules is verified by means of computer simulation.

The positions of the nodes chosen to form the *Wireless Array* (i.e. the array geometry) affect several factors that collectively determine the performance of the Arrayed-WSN. One such factor is the best accuracy in the estimation to which two closely spaced sources can be resolved (the two emitter Cramer-Rao lower bound [45]). Another factor is the number of intrinsically uncertain scenarios possible in the estimation of signal environments for a specific array, i.e. the number of ambiguities related to the array. Furthermore, the sensitivity of the array to uncertainties in the node positions and also the energy required to maintain the operation of the *Wireless Array* are fields of concern. These factors depend on the concept of the *array manifold* which is introduced in Section 3.1 and are examined in Section 3.2.

Once deployed the positions of the nodes remain fixed, resulting to a constant network topology (except for when additional nodes are deployed to replace worn out/damaged nodes), hence the problem of selecting a set of nodes according to

a "performance" criterion is essentially combinatorial in nature. Section 3.3 of this chapter focuses on the array connectivity rules for array formation and the proposed method allows the relative importance of each factor to be adjusted to suit the intended use of the *Wireless Array*. Finally, conclusions are discussed in Section 3.4.

3.1 Array Geometry and Array Manifold

The manifold vector is a very important concept in Array Processing. In order to analyse the array manifold, we need to firstly describe it as a concept relating to an antenna array. For this purpose, consider an array of elements, where the locations of the elements are given by

$$\mathbf{r} = \left[\underline{r}_x,\ \underline{r}_y,\ \underline{r}_z\right]^T = \left[\ \underline{r}_1,\ \ldots,\ \underline{r}_k,\ \ldots,\ \underline{r}_N\ \right] \in \mathcal{R}^{3\times N} \tag{3.1}$$

where $\underline{r}_x, \underline{r}_y, \underline{r}_z$ are column vectors containing the positions of the elements respectively (in units of half wavelengths) and as a result the matrix $\mathbf{r}$ describes the array geometry. Note that the spatial position of the k^{th} array element is thus given by $\underline{r}_k = \left[r_{x_k},\ r_{y_k},\ r_{z_k},\right]^T \in \mathcal{R}^{3\times 1}$. The origin of the 3-dimensional Cartesian system in which the array element positions are expressed is called the array reference point. Note that, for reasons of practicality, but without any loss of generality, the array reference point is usually (and unless otherwise stated) taken to be at the array centroid. The array centroid is the geometrical centre of the array, i.e. if the array centroid and the array reference point coincide then

$$\underline{r}_x^T \underline{1}_N = \underline{r}_y^T \underline{1}_N = \underline{r}_z^T \underline{1}_N = 0 \tag{3.2}$$

As a wave propagates through an antenna array, it will meet the antenna array elements at different times due to their different spatial locations. Between these times, the carrier signal will have varied in phase, and as a result each array element will sense a phased version of the same signal. The essence of the array manifold vector is to represent the phase difference, of an impinging wave, between the locations of the corresponding array element and the array reference point. It is clear that the phase of each antenna will primarily depend on the position of the antenna and the direction of the signal.

As an example, consider an antenna array with geometry as given by Eq. 3.1. Furthermore, assume a far-field impinging carrier modulated signal wave. The far-field assumption implies that the wave transversing the array has almost zero curvature, i.e. it can be approximated by a planar wave. In order for this to

hold, the aperture of the array, i.e. the distance between the two most remote antenna elements expressed in signal wavelengths, must be small with respect to the distance between the signal source and array reference point. The impinging signal at the array reference point can be expressed by

$$y_{rp}(t) = m(t)\exp(j2\pi F_c t) \tag{3.3}$$

Then, and as illustrated in Figure 3.1, the time difference between the instants where the wave traverses the k^{th} sensor and the reference point, assuming free space electromagnetic propagation, is given by $\tau_k = \frac{l_k}{c}$. Thus the signal at the k^{th} element is expressed by $y_k(t) = m(t-\tau_k)\exp(j2\pi F_c(t-\tau_k))$. For reasonably small antenna separations it is logical to assume that the message signal remains almost constant for the time taken by the signal to traverse the array and thus $m(t-\tau_k) \approx m(t)$. The fact that we neglect any changes in the message signal, while considering phase changes in the carrier, implies that the bandwidth, B, of the message is a lot smaller than the carrier frequency F_c, i.e. $B \ll F_c$, a reasonable assumption for most systems.

It is clear from Figure 3.1, that the length l_k is, in the general case, the projection of the vector $\underline{r}_k$ onto the unit vector in the direction of the signal, i.e. $l_k = \underline{r}_k^T\underline{u}$ and thus $\tau_k = \frac{\underline{r}_k^T\underline{u}}{c}$. Then the signal at the k^{th} sensor can be expressed by

$$\begin{aligned} y_k(t) &= m(t)\exp(j2\pi F_c(t - \frac{\underline{r}_k^T\underline{u}}{c})) \\ &= m(t)\exp(-j2\pi F_c\frac{\underline{r}_k^T\underline{u}}{c})\exp(j2\pi F_c t) \end{aligned} \tag{3.4}$$

which, if the array geometry is expressed in terms of carrier frequency half wavelengths ($\frac{\lambda}{2}$), can be simplified to

$$y_k(t) = m(t)\exp(-j\underline{r}_k^T\underline{k})\exp(j2\pi F_c t) \tag{3.5}$$

where, $\underline{k} = \pi\underline{u}$ is the wavenumber vector in the direction of the signal source.The corresponding baseband, down-converted signal can thus be expressed by

$$x_k(t) = m(t)\exp(-j\underline{r}_k^T\underline{k}) \tag{3.6}$$

Grouping together all the element baseband signals results to

$$\underline{x}(t) = \begin{bmatrix} \exp(-j\underline{r}_1^T\underline{k}) \\ \vdots \\ \exp(-j\underline{r}_k^T\underline{k}) \\ \vdots \\ \exp(-j\underline{r}_N^T\underline{k}) \end{bmatrix} m(t) = \exp(-j\mathbf{r}^T\underline{k})m(t) = \underline{S}m(t) \in C^{Nx1} \tag{3.7}$$

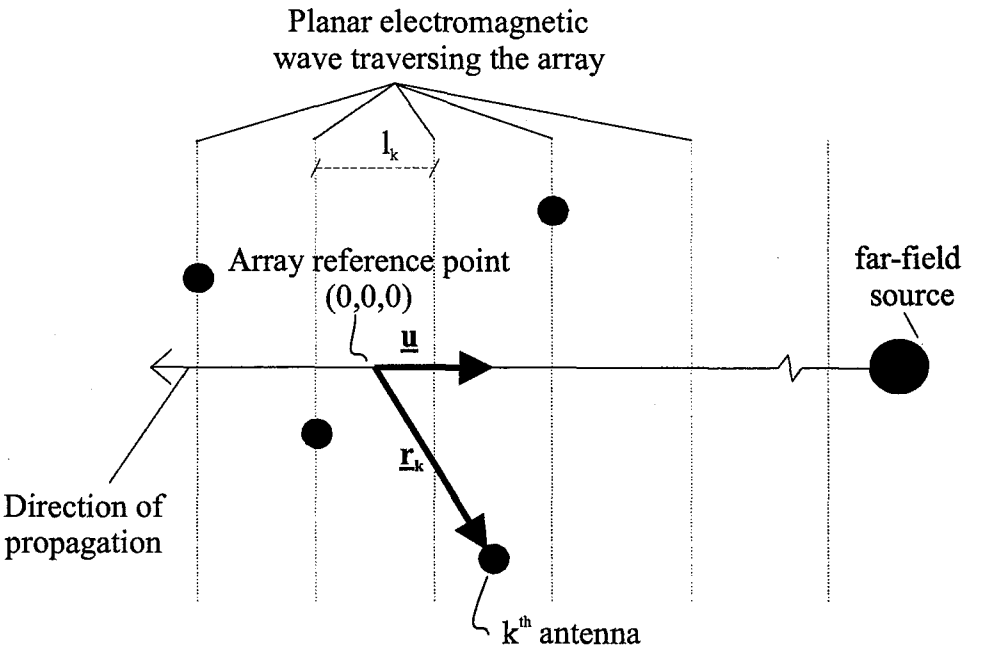


Figure 3.1: An electromagnetic signal transmitted by a far-field source, traversing an antenna array

where

$$\underline{S} = \exp(-j\mathbf{r}^T\underline{k}) \in \mathcal{C}^{Nx1} \tag{3.8}$$

is the array manifold vector vector corresponding to the specific source direction. Notice that it is very simple to incorporate directional antenna elements into this expression. In the same manner, for a number of transmitting sources in the environment and with the inclusion of noise, the above expression transforms to

$$\underline{x}(t) = \sum_i \underline{S}_i m_i(t) + \underline{n}(t) \tag{3.9}$$

where i denotes the i^{th} user and each element of $\underline{n}(t)$ is the baseband noise corresponding to each antenna element.

The essence of the array manifold vector is that it maps the array geometry and the signal characteristics (in the above case the direction of the incoming signal) to an N-dimensional complex subspace. This is a very important concept in various array processing applications such as subspace type receivers and superresolution techniques. With knowledge of the array geometry we can trace the locus of the varying array manifold vector for all possible values of the incoming signal parameters. This results to a geometrical object embedded in the N-dimensional complex space called the array manifold. For example, in the Multiple Signal Classification (MUSIC) algorithm, the array manifold is searched via a projection to the received signal space, to estimate the signal subspace. The

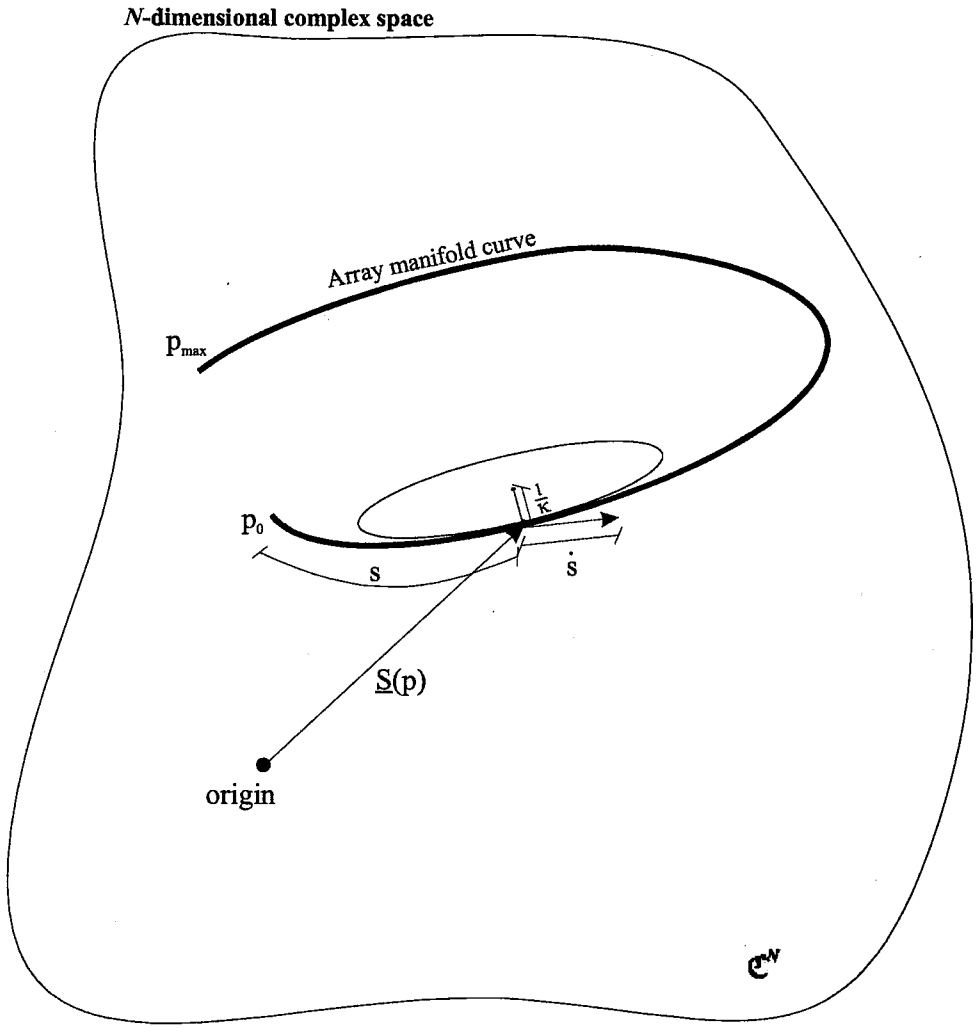


Figure 3.2: An array manifold curve with respect to single parametre of intrest p as embedded in the N-dimensional complex space

signal subspace is the space spanned by the array manifold vectors that correspond to the signal sources currently present in the environment. Note that the array manifold can be a function of various signal parameters of interest, but the incoming directions of azimuth and elevation are the most common.

As an example of a manifold, consider that a single parameter p is used to describe the direction of an impinging wave. Then the locations of the array elements (given by $\mathbf{r}$) define a mapping from p to the response of the array given by the manifold vector

$$p \xrightarrow{\mathbf{r}} \underline{S}(p) \in \mathcal{C}^N, p \in \Omega_p \subset \mathcal{R} \tag{3.10}$$

The locus of the array response vectors $\forall p$ in the range Ω_p describes a curve in an dimensional complex vector space known as the array manifold curve, illustrated in Figure 3.2. Several key properties of this curve will be used in this study, and

are listed below

- The arc length s at a point p is a measure of the distance traversed on the manifold curve

$$s(p) \triangleq \int_{p_0}^{p} \left\| \frac{d\underline{S}(p)}{dp} \right\| dp = \int_{p_0}^{p} \left\| \dot{\underline{S}}(p) \right\| dp \tag{3.11}$$

- The rate of change of arc length at a point p is similar to the instantaneous speed

$$\dot{s}(p) \triangleq \frac{ds}{dp} = \left\| \dot{\underline{S}}(p) \right\| \tag{3.12}$$

- The principal, or first curvature of the manifold curve at a point

$$k_1(s) \triangleq \left\| \underline{S}''(s) \right\| \tag{3.13}$$

(where dot indicates differentiation with respect to p and prime indicates differentiation with respect to s)

In the most common case, the parameter of interest p is chosen to be the incoming signal azimuth angle θ. In this case (for elevation $\phi = 0$), the aforementioned vector $\underline{u}$, which denotes the incoming signal direction is given by $\underline{u} = \begin{bmatrix} \cos\theta, & \sin\theta, & 0 \end{bmatrix}^T$. Furthermore, note that it is easy to incorporate the electrical characteristics of the antenna element, by assigning a complex gain function $g(\theta)$ dependent on the incoming signal azimuth angle to each antenna element. In such a case, the array manifold vector is given by $\underline{S} = \underline{g}(\theta) \odot \exp(-j\mathbf{r}^T\underline{k})$ where $\underline{g}(\theta) = \begin{bmatrix} g_1(\theta), & \ldots, & g_k(\theta), & \ldots, & g_N(\theta) \end{bmatrix}^T$.

In the above case, the array manifold consisted of a single curve embedded on the N-dimensional complex space. However, there are cases where more than one signal parameters may be of interest. Consider that the impinging wave is described by two such parameters (p, q). In this case the mapping is as follows:

$$(p, q) \xrightarrow{\mathbf{r}} \underline{S}(p, q) \in \mathcal{C}^{N \times 1} \tag{3.14}$$

And the locus of $\underline{S}(p, q) \forall (p, q)$, over Ω_p and Ω_q respectively, is now a surface embedded in an N-dimensional complex vector space known as the array manifold surface.

If the two parameters under consideration are the azimuth (θ), and elevation (φ) angles, then the array manifold vector is given by

$$\underline{S}(\theta, \varphi) = \underline{g}(\theta, \varphi) \odot \exp\left(-j\mathbf{r}^T\underline{k}(\theta, \varphi)\right) \in \mathcal{C}^{N \times 1} \tag{3.15}$$

or for omnidirectional elements

$$\underline{S}(\theta,\varphi) = \exp\left(-j\mathbf{r}^T\underline{k}(\theta,\varphi)\right) \in \mathcal{C}^{N\times 1} \tag{3.16}$$

where $\underline{k}(\theta,\varphi) = \pi\left[\cos\theta\cos\varphi, \sin\theta\cos\varphi, \sin\varphi\right]^T$ is the wavenumber vector that expresses the direction of the incoming signal. Choosing the azimuth and elevation angles as the signal parameters of interest is very useful in applications such as spatial filtering and localisation, since they completely describe the incoming signal direction in the 3D space. Although this can be described in many ways, the parametrisation in terms of (θ,φ) is commonly used because of its intuitive nature. It is clear from Eq. 3.16, that the array manifold vector is an N dimensional vector, where N is the number of antenna elements in the array, and that as θ and φ varies it traces a two dimensional complex surface embedded in the N dimensional complex space as illustrated in Figure 3.3. The manifold surface $\mathcal{M}$ is then defined by

$$\mathcal{M} = \left\{\underline{S}(\theta,\varphi) \in \mathcal{C}^N, \forall(\theta,\varphi) : (\theta,\varphi) \in \Omega_{(\theta,\varphi)}\right\} \tag{3.17}$$

where $\Omega_{(\theta,\varphi)}$ is the set of all possible pairs of incoming angles.

Another way to view the array manifold surface is as a family of curves. If one of the parameters is kept constant, e.g. $\theta = \theta_0$, and the other parameter, φ, is varied, then the manifold vector traces a curve embedded on the manifold surface. Thus, the manifold surface can be seen as a family of curves of constant θ's (φ-curves) or as a family of curves of constant φ's (θ-curves) (see Figure 3.3)

$$\mathcal{M} = \left\{\mathcal{A}_{\theta|\varphi_0}, \forall\varphi_0 : \varphi_0 \in \Omega_\varphi\right\} = \left\{\mathcal{A}_{\varphi|\theta_0}, \forall\theta_0 : \theta_0 \in \Omega_\theta\right\} \tag{3.18}$$

where

$$\mathcal{A}_{p|q_0} = \left\{\underline{S}(p,q_o) \in \mathcal{C}^N, \forall p : p \in \Omega_p, q_0 = const.\right\}, p \text{ or } q = \theta \text{ or } \varphi \tag{3.19}$$

It is clear therefore that when two sources are assumed to be on the same azimuth and varying elevation and vice versa, i.e. $p = \varphi$ or θ respectively, then the two sources manifold vectors belong to the same φ or θ curve respectively and their relation can be analysed by examining that specific curve alone. For example, in the case of a planar array ($\underline{r}_z = \underline{0}_N$) with omnidirectional elements and the directions of an impinging wave parameterised in terms of azimuth and elevation, then the manifold surface is shaped in the form of a conoid and lies on a hypersphere of radius $\sqrt{N}$ embedded in $\mathcal{C}^N$. By fixing $\theta = \theta_0$ the array response vector can be written as

$$\underline{S}(\theta_0,\varphi) = \exp(-j\pi\underline{r}(\theta_0)\cos\varphi) \tag{3.20}$$

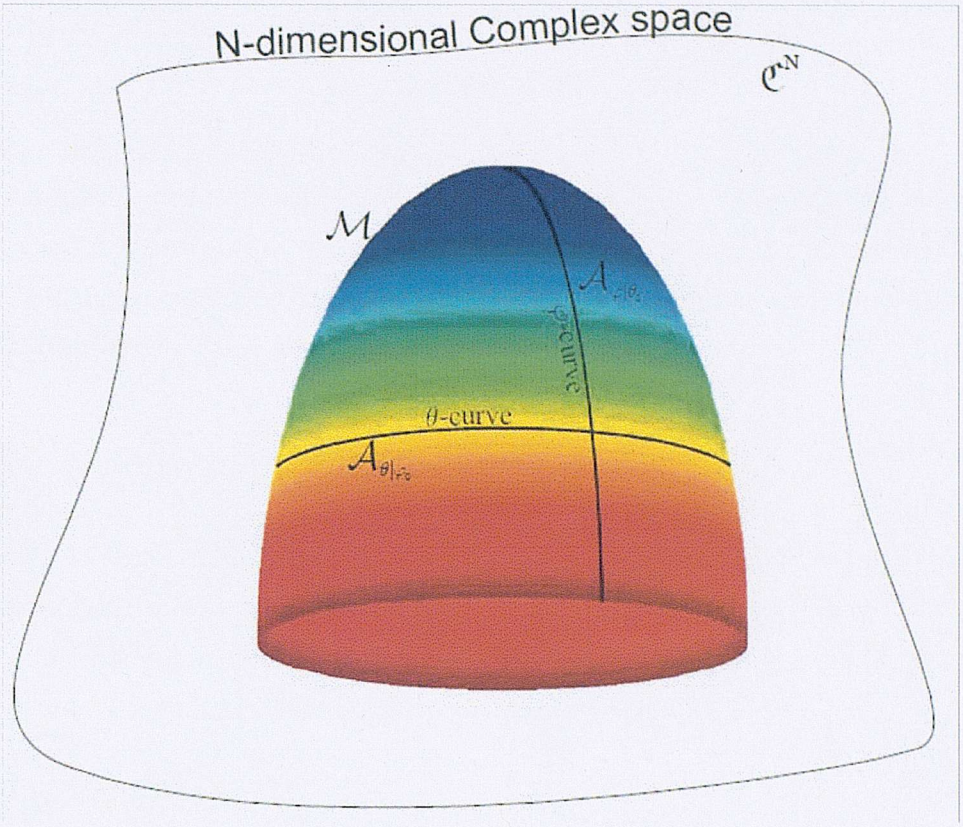


Figure 3.3: Representation of the array manifold with example θ and φ-curves

where $\underline{r}(\theta_0)$ denotes the Equivalent Linear Array (or ELA) and contains the sensor positions in half wavelengths according to

$$\underline{r}(\theta_0) = \underline{r}_x \cos\theta_0 + \underline{r}_y \sin\theta_0 \tag{3.21}$$

In this case Eq. 3.20 is equivalent to Eq. 3.8 for this case. The locus of $S(\theta_0, \varphi)\forall\varphi \in (-\frac{\pi}{2}, \frac{\pi}{2})$ defines a φ-curve as the one shown in Figure 3.3 which is known as a hyperhelix. The hyperhelix is a curve which has useful analytical properties and can be fully characterised using its length and curvatures. Furthermore, the curvatures are constant and the principal curvature is given by

$$\kappa_1 = \left\|\widetilde{\underline{r}}^2\right\| \tag{3.22}$$

where $\widetilde{\underline{r}} = \frac{\underline{r}}{\|\underline{r}\|}$.

In order to study the properties of the manifold surface there are a large number of complex parameters that can be examined. In this chapter we restrict our attention to the manifold metric $\mathbb{G}$ (and its determinant). The manifold metric can provide the means to measure distances and angles between lines on non-Euclidean surfaces and is defined as

$$\mathbb{G} = \begin{bmatrix} g_{pp} & g_{pq} \\ g_{qp} & g_{qq} \end{bmatrix} \tag{3.23}$$

where

$$g_{pq} = \underline{k}_p^T \mathbf{r}\mathbf{r}^T \underline{k}_q \tag{3.24}$$

and $\underline{k}_p = \frac{\partial}{\partial p}\underline{k}(p,q) = \pi \frac{\partial}{\partial p}\underline{u}(p,q)$.

Using the above definitions the discussion will be focused on the various criteria used to construct a distributed array formation algorithm. This will effectively be the implementation of the selection of the nodes that will participate in a *Wireless Array* when an EOI is detected.

3.2 Performance Criteria

In order to select nodes to form arrays in an Arrayed-WSN some method should be developed to rank different combination of nodes according to a performance criterion. A number of criteria may be used to assess an array geometry, the most important of which are listed below:

- Detection threshold
- Resolution threshold
- Accuracy in direction finding
- Number of Ambiguous Generator Sets (defined in [41])
- Sensitivity to uncertainties in the array element positions.

The first four are implicitly related to the total length of the manifold curve l_m which is defined by Eq. 3.11 with the integration taken over the whole range of the parameter p and the last is related to the manifold metric $\mathbb{G}$ of the manifold surface.

3.2.1 Detection and Resolution Thresholds

The detection capabilities of an array can be quantified using the detection threshold, which refers to the minimum separation Δp_d of two sources in the parameter of interest space Ω_p about an average parameter value p for a fixed SNR, number of observations L (or snapshots) and a given ratio between the powers of the two sources in order for the number of sources to be estimated as two and not one. Because of the importance of spatial processing in the Arrayed-WSN, the signal parameters of interest are the direction of arrival parameters of the signals. The expression for the detection threshold of an array of omnidirectional elements for

two sources with received powers P_1 and P_2 and average direction p is given by [41]

$$\Delta p_d = \sqrt{\frac{1}{2(C \times SNR \times L)}} \left(1 + \sqrt{\frac{P_1}{P_2}}\right) \frac{1}{\dot{s}(p)} \tag{3.25}$$

Where C is the efficiency of the array processing algorithm, $0 < C \leqslant 1$, SNR is the signal to noise ratio and L is the number of observations or snapshots of the environment available. For reasons of generality, it can be assumed that $C = 1$, thus providing a lower bound on the required minimum separation.

Another very important characteristic of the utilised arrays is their resolution capability [41]. The resolution capability of an array refers to the ability of an array to resolve (i.e. estimate the signal parameters) two sources that are closely located in space. The direction of arrival of a signal in 3D space is defined by the two angles of azimuth θ and elevation φ that the impinging signal makes with the x-axis and the x-y plane respectively. The resolution of an array varies with the angle of incidence, i.e. it is not a single value but rather a function of all the possible incoming directions. Resolution is usually expressed as a threshold in terms of the minimum angle at a specific direction, $\Delta p_r(\theta, \varphi)$ where $p = \theta$ or φ, that must exist between two signals so that the transmitting sources can be resolved i.e. to obtain two distinct spikes or peaks in the spectrum, The expression providing the resolution threshold is

$$\Delta p_r = \sqrt[4]{\frac{2}{(C \times SNR \times L)\left(\widehat{\kappa}_1^2(p) - \frac{1}{N}\right)}} \left(1 + \sqrt[4]{\frac{P_1}{P_2}}\right) \frac{1}{\dot{s}(p)} \tag{3.26}$$

where $\widehat{\kappa}_1^2(p)$ is a function of the first curvature of the manifold at the point p. For example if $p = \varphi$ then $\widehat{\kappa}_1(\varphi) = \sqrt{\kappa_1(\varphi) - \left|\text{sum}(\underline{\widetilde{r}}^3)\right|^2}$

In a hypothetical scenario where an infinite number of data (snapshots) from the two closely located sources were available at the array, the sources would be resolved irrespective of how small the angle between them was. It is clear therefore that the resolution threshold exists because of finite observation errors. It is thus preferable to express the resolution threshold as the minimum number of snapshots, $L_{\min}$, that are needed in order to resolve two sources that are separated by an angle Δp for a given SNR and a given array. In other words, the resolution of the array in terms of the minimum number of snapshots that are needed to resolve two sources separated by an angle Δp is a function of the incidence angle (θ, φ), the SNR, the power ratio between the two sources and the array manifold shape at (θ, φ). Analysing the resolution threshold of possible *Wireless Array* geometries will not only give an estimate of the potential performance of the Arrayed-WSN but can also instruct as to which combination of nodes should form

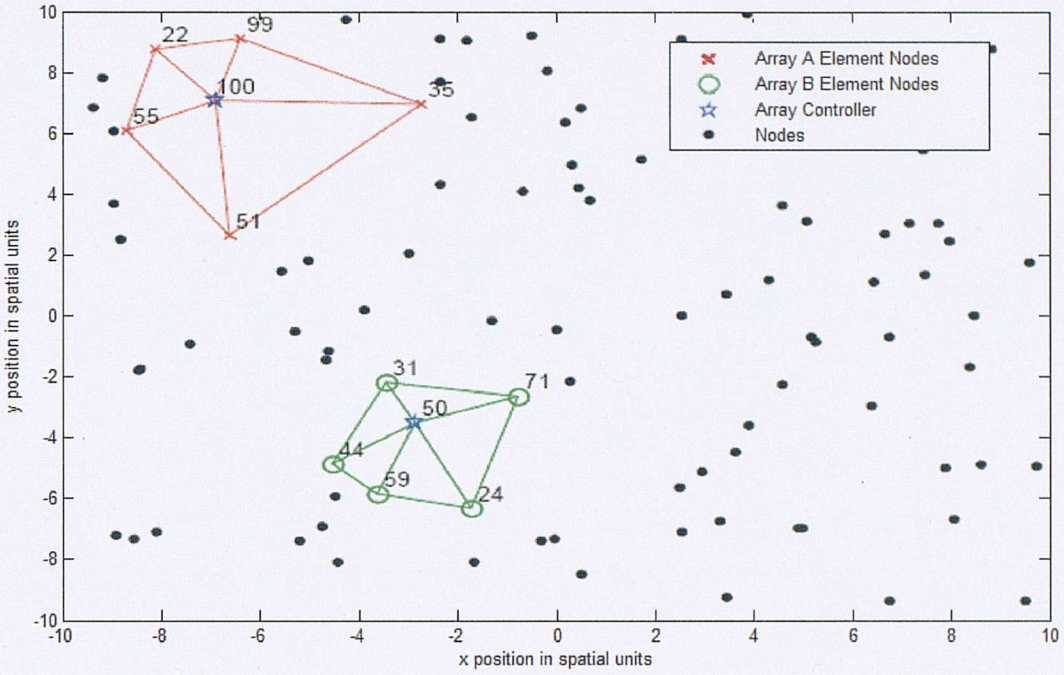


Figure 3.4: Example Wireless Array Geometries

a *Wireless Array*. Although the geometry of the *Local Array* is fixed on a node, the geometry of a *Wireless Array* is elected between many possible combinations of nodes. Choosing an appropriate geometry influences the shape of the manifold and thus the resolution threshold of the array.

3.2.2 Accuracy and Ambiguities

The accuracy of the array is defined as the lower bound on the estimation error on the signal parameter estimation of a source in the presence of another near-by source. For two sources, the best achievable accuracy or smallest variance for an unbiased estimator of the first sources position can be expressed using the two emitter Cramer-Rao lower bound (CRB) as shown below [46]

$$CRB[p_1] = \frac{1}{SNR \times L} \frac{2}{\left(\Delta p \times \dot{s}(p)\right)^2 \dot{s}^2(p_1) \left(\kappa_1^2(p) - \frac{1}{N}\right)} \tag{3.27}$$

where smaller values of the CRB indicate better accuracy and Δp is the separation of the two sources. The array geometry is implicitly involved in calculating the detection and resolution thresholds and the CRB through the rate of change of the arc length $\dot{s}(p)$ and the principal curvature $\kappa_1(p)$. Figure 3.4 shows two array geometries formed from nodes in a Arrayed-WSN in which the array at the top left of this figure (*Wireless Array* A) has a larger aperture (i.e. a larger maximum distance between elements) than the array in the middle of the figure (*Wireless*

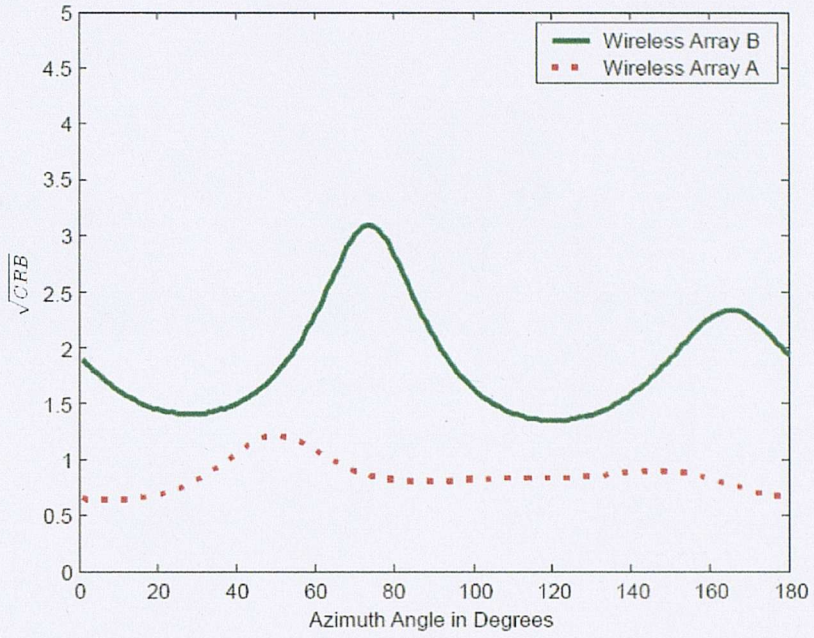


Figure 3.5: Square Root Cramer-Rao Lower Bound For Arrays A and B of Fig. 3.4

Array B). Assuming that one antenna element on the *Local Array* on each node is used to form the *Wireless Arrays* and one spatial unit is equal to one half wavelength, then for equal power sources separated by 2°, with an $SNR = 10$ and $L = 100$ snapshots, the square root of the CRB of the example *Wireless Arrays* is represented by Figure 3.5. This clearly illustrates that *Wireless Array* A has a better accuracy than *Wireless Array* B for all possible azimuth angles of arrival Ambiguities

Ambiguities occur when two or more signal environments cannot be distinguished between them by an antenna array. For example a linear array ($r_y = 0, r_z = 0$) cannot distinguish between a wave impinging at azimuth θ_0 or a wave impinging at $\theta_0 + 180^{\circ}$. This type of ambiguity is known as a trivial ambiguity and occurs because the manifold vector for one direction can be expressed as a scalar multiple of the manifold vector for another direction. Non trivial ambiguities occur when there exists a set of signals with direction of arrival angles that are associated with the same array response as a different set of signal arrival angles. Even if a single ambiguous situation exists then it can be proven that there is in fact an infinite number of ambiguous sets of directions associated with a single Ambiguous Generator Set (AGS) [41]. This implies that an Ambiguous Generator Set, as the name suggests, generates an infinite number of ambiguous sets of directions. However the number of Ambiguous Generator Sets is finite (although may be very large) and can be determined from the array geometry. It

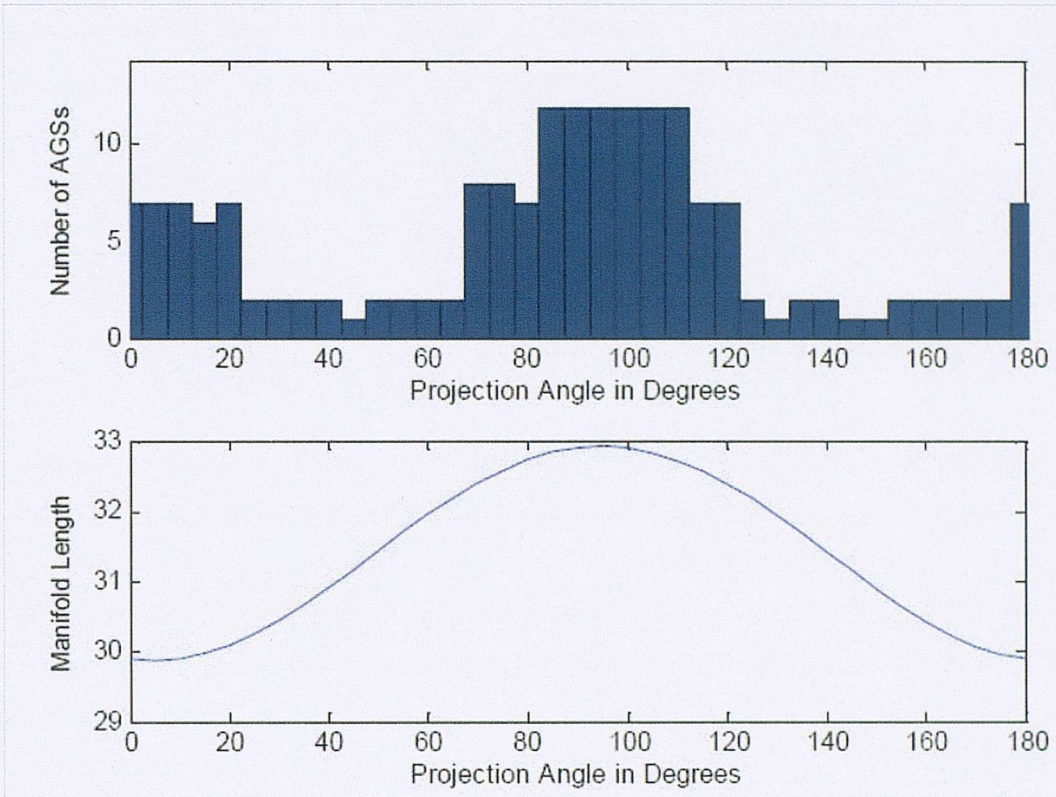


Figure 3.6: Number of Ambiguous Generator Sets of Array A against θ_0 (top) and Total Length of Manifold Curve Corresponding to the ELA of Wireless Array A of Fig. 3.4 at θ_0 (bottom)

is clearly desirable to choose array geometries with as few Ambiguous Generator Sets as possible. The number of Ambiguous Generator Sets corresponding to the equivalent linear array for all possible projection angles $0° < \theta_0 < 180°$ for the planar *Wireless Array* A is shown in Figure 3.6 whereas *Wireless Array* B does not possess any Ambiguous Generator Sets.

The above figures illustrate the fact that arrays with a larger aperture will have a higher accuracy (i.e. a lower CRB) although its geometry will effect the difference between the best and the worst case CRB. A larger array aperture will also result in better detection and resolution performance however the array will be prone to a greater number of ambiguities. In addition the energy required to maintain the *intra*-wireless communication links increases in proportion to the distance of the element nodes to the controller to the power of the path loss exponent which lies between 2 for free space to 4 for transmission above a reflecting surface such as the ground. This energy translates into the lifetime of the array (i.e. the amount of time for which an array can operate given a specific amount of energy at each node) and small variations in the inter-node

separation will have a large impact on the array's lifetime. In order to minimise the intra-array communication energy requirement it is proposed to locate the array controller as close as possible to the array centroid. It is clear that a number of trade-offs exist, hence, in order to formulate a strategy for selecting an array of N nodes from those available, a combination of the above criteria must be used.

3.2.3 Array Sensitivity

The last criterion to be considered in this study is the sensitivity to uncertainties in the array element positions. Since the individual node locations are not known a priori but rather are estimated via the localisation procedure, they are prone to estimation errors. These uncertainties will affect the operation of the resulting *Wireless Array*. However, different array geometries vary as to their performance sensitivity

The sensitivity could be measured with respect to some application specific performance measure such as the CRB. However in [47] an approach based purely on the differential geometry of the array manifold is presented. This work introduced the concept of sensor importance which is measured using the relative sensitivity of a criterion $\xi(p, q, \mathbf{r})$ to perturbations in the array element locations. This criterion describes the area of an infinitesimal region on the manifold surface and acts as a tool for detecting the changing shape of this surface as the element positions are changed.

First the relative sensitivity for a planar array as defined in [47] is given by

$$\left[D^{\xi}_{\underline{r}_x},\ D^{\xi}_{\underline{r}_y},\ \underline{0}_N\right]^T = \begin{bmatrix} \frac{\|\underline{r}_y\|^2 \underline{r}_x^T \odot \underline{r}_x^T - (\underline{r}_x^T \underline{r}_y)\underline{r}_y^T \odot \underline{r}_x^T}{\|\underline{r}_x\|^2 \|\underline{r}_y\|^2 - (\underline{r}_x^T \underline{r}_y)^2} \\ \\ \frac{\|\underline{r}_x\|^2 \underline{r}_y^T \odot \underline{r}_y^T - (\underline{r}_x^T \underline{r}_y)\underline{r}_x^T \odot \underline{r}_y^T}{\|\underline{r}_x\|^2 \|\underline{r}_y\|^2 - (\underline{r}_x^T \underline{r}_y)^2} \\ \\ \underline{0}_N^T \end{bmatrix} \tag{3.28}$$

Using this matrix, the effect of perturbations in the element locations on the manifold surface can be evaluated with the use of only the array geometry. In fact an overall array sensitivity factor

$$\zeta = E\left\{\left(\frac{\Delta\xi}{\xi}\right)^2\right\} \tag{3.29}$$

which is a measure of the array geometry's robustness to position uncertainties is defined. The expectation operator E{.} is taken over the position location errors

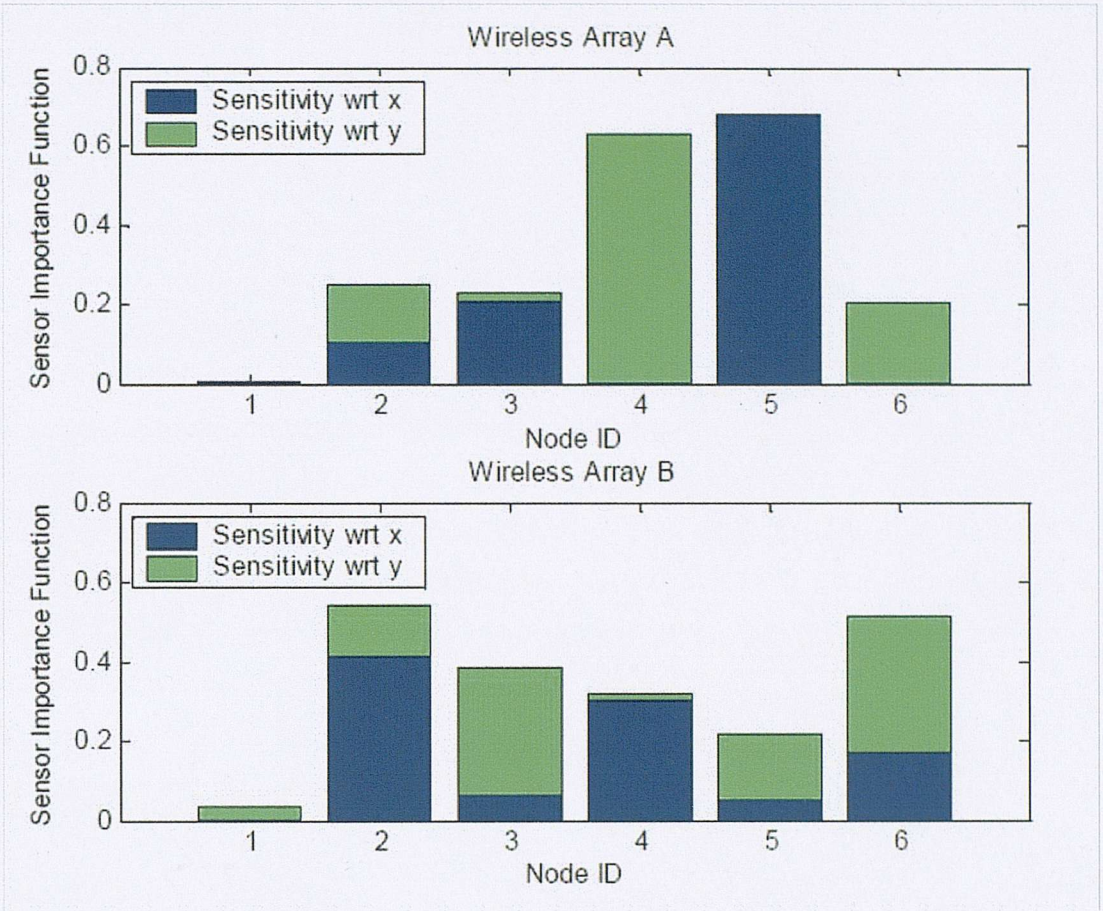


Figure 3.7: Relative Sensitivities of each element in Wireless Arrays A and B of Fig. 3.4

which are assumed to be uniformly distributed about the nominal locations. If the radius of this distribution for each element is assumed to be a proportion μ of the distance of the element from the array centroid then the overall array sensitivity for a planar array can be shown to be given by

$$\zeta = \frac{\mu^2}{2}\left[D_{\underline{r}_x}^{\xi\ T}\,\underline{\underline{\mathrm{diag}}}(\underline{\rho}_N \oslash \underline{r}_x)D_{\underline{r}_x}^{\xi} + D_{\underline{r}_y}^{\xi\ T}\,\underline{\underline{\mathrm{diag}}}(\underline{\rho}_N \oslash \underline{r}_y)D_{\underline{r}_y}^{\xi}\right] \tag{3.30}$$

In an Arrayed-WSN it is more reasonable to assume that the distribution of the location errors are the same for all elements, since they are primarily introduced by the localisation procedure. Then $\rho = \underline{1}_N$ and μ equals the radius of the location error distribution in half wavelengths.

Figure 3.7 shows the relative sensitivities for the two *Wireless Arrays* of Figure 3.4 calculated using Eq. 3.28. The overall sensitivities for the two arrays for $\mu = 0.1$ are $\zeta_1 = 4.03$ and $\zeta_1 = 8.82$. Clearly which array is less sensitive to location errors is dependent on how these location errors are distributed and this will depend on the localisation and calibration procedures employed. Although not considered in this study, another important property of an Arrayed-WSN

array is its robustness to element failure [48]. In contrast to the array sensitivity, the array robustness mainly refers to the state of an array element node rather than to its position. Complete failure of an array element node is a trivial case since it is relatively easy to detect and manage. However, partial failure of the node can cause degradation of the array performance if undetected.

In conclusion, it is clear that the array geometry is a very important factor in determining the performance of the system. In the case of an Arrayed-WSN the nodes containing the array elements cannot be positioned in exact a-priori known locations but are randomly distributed in space, having fixed positions once the network is deployed. Thus, the array design is associated with the selection of a number of nodes (according to a criterion) based on their estimated locations. This selection process must take into account the various trade-offs that exist in order to find the golden section between the various factors and is the topic of the next section.

3.3 Array Formation

The nodes forming the Arrayed-WSN are deployed randomly within a field of interest as described in Chapter 2. Immediately following deployment, each node has no knowledge of the locations and number of neighbouring nodes. The initial, start-up, phase of the network is designed to allow nodes to acquire this information. The start-up phase can be split into network discovery, clusterisation and localisation. The first task to be performed is network discovery. Network discovery is a process designed to provide information to each node about its neighbours. In an Arrayed-WSN the discovery is achieved through the completely decentralised and message exchange minimisation-oriented CANDLA-DCSA algorithm as described in Chapter 2. Although the network discovery algorithm provides rough estimates of the distances of a node to its neighbours, these estimates are not accurate enough for the purpose of forming *Wireless Arrays*. Thus, the information provided by network discovery has to be coupled with the information collected by the localisation procedure, building in this way a complete detailed map of the whole network. This map will contain all the node IDs, their positions, energies, etc. Note that each node only needs a small part of this "network map" describing its close neighbourhood. This dramatically reduces the number of messages that need to be exchanged and the amount of information that needs to be stored at each node, thus resulting in energy consumption and node complexity reduction. This could be easily implemented by clusterisation or

by only discovering nodes up to a maximum hop count. The problem of clusterisation is a well researched problem, [49], [50], and an existing technique will be sufficient for the purposes of this research. Although many algorithms have been considered, e.g. fuzzy-c-means clustering, a decentralised approach will eventually be used. The clustering for example could be done through random election of clusterheads and self-assignment of each node to its closest clusterhead. Each clusterhead together with the nodes assigned to it then becomes an independent cluster.

In order to form *Wireless Arrays* the positions of the nodes must be precisely known. Acquiring accurate information about the position of the nodes in space is achieved through the localisation process. The localisation process could involve a multistage estimation of the nodes' positions, with each stage producing more accurate positions.

When an event of interest is detected by the nodes in the neighbourhood, an array is formed close to it. The first step is to select a number of nodes, K, to potentially play the role of the array controller. Given a specific number of potential controllers the nodes within a predefined distance to the event of interest broadcast their intention (their proposal) of becoming controllers. The broadcast message also contains the estimated distance of the proposing node to the event of interest. The whole process of selecting potential controllers takes place over a small predetermined length of time, T_0. When a node intending to become a controller receives a broadcast from another node, it compares the distance of the broadcasting node to its own distance from the event of interest. If within the predetermined time T_0 a node applying to be a controller receives K broadcasts from nodes closer to the event of interest, it withdraws its own proposal and does not become a potential controller. This procedure ensures that after time T_0 the K closest nodes to the event of interest are the potential controllers. Figure 3.8 illustrates an event of interest taking place within a node neighbourhood in an Arrayed-WSN cluster. The potential controllers are also shown for $K = 5$. Throughout this chapter, we are going to use this example Arrayed-WSN and EOI, to discuss the *Wireless Array* formation procedure and focus on the trade-offs involved.Once the potential controllers are selected the procedure to select the nodes that will comprise the *Wireless Array* begins. Each controller creates a list containing all the N_L nodes in its neighbourhood according to their closeness to itself. By neighbouring nodes it is meant the nodes within a specific distance from the controller. That distance can be set to determine the maximum aperture that any formed *Wireless Array* can have.

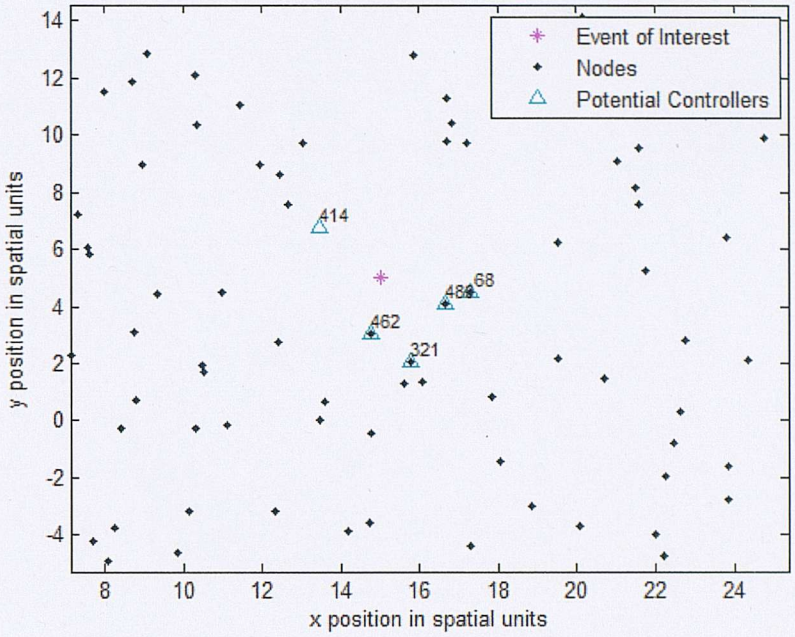


Figure 3.8: An Event Of Interest and the 5 Potential Controllers selected through the described algorithm

A potential controller will examine all possible combinations of all $N-1$ nodes out of the list and rate each array according to weighted function of the performance criteria outlined in the previous section. This will result to a *Wireless Array* of N nodes including the controller itself. The best array out of these combinations will become the potential controller's proposed array. After each potential controller has selected its proposed array, it broadcasts the proposed array's evaluation. The potential controller that proposes the better performing array takes on the responsibility of organising and forming it.

3.3.1 Ambiguity / Accuracy Tradeoff

Figure 3.9 shows two of the performance criteria, the number of Ambiguous Generator Sets $A_{\max}$ (or more specifically the largest number of AGS over all $0° < \theta_0 < 180°$) against the square root of the maximum Cramer-Rao bound for all θ_0 (evaluated for equal power sources separated by 5° with a $SNR = 10$ and $L = 100$ snapshots). Each point on this plane represents a different *Wireless Array* using a different combination of nodes. Combinations evaluated by the potential controllers of Figure 3.8 have been given different symbols to highlight the distribution of the points.

This figure shows that the best accuracy is achieved by arrays with a greater

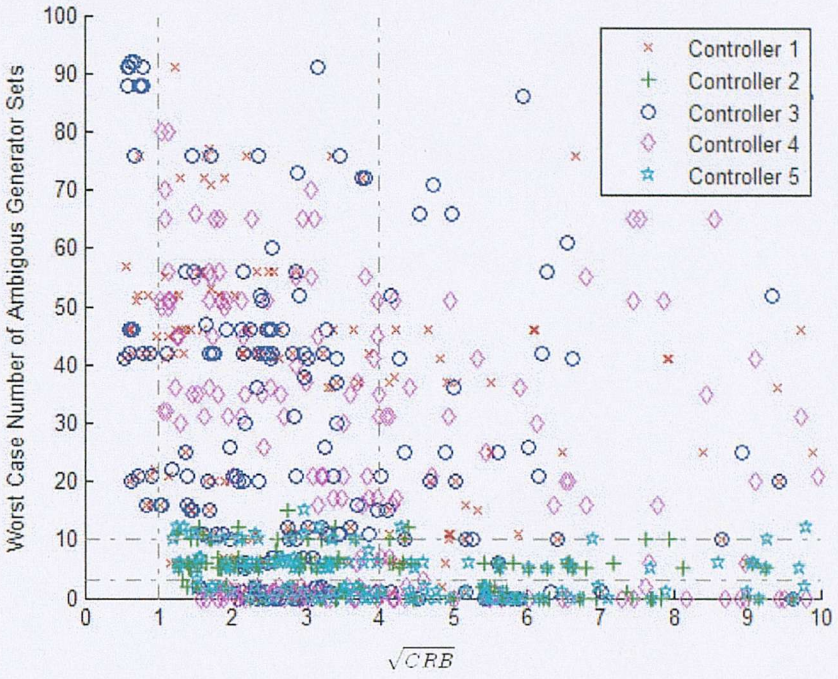


Figure 3.9: Number of Ambiguous Generator Sets Against Worst Case Smallest Achievable RMS Error

	Performance Levels		
	Good	Acceptable	Poor
Worst case number of AGS $A_{\max}$	$0-3$	$4-10$	$11+$
Worst case Smallest RMS Error $\sigma_{\max}$	$\leqslant 1°$	$> 1°, < 4°$	$> 4°$

Table 3.1: Partitioning the levels of performance for the ambiguities/accuracy trade-off

number of ambiguities. However, it is possible to choose sets of nodes that provide a reasonable accuracy and yet only possess a few AGS. In order to trade off accuracy and the number of AGS, Figure 3.9 has been partitioned into regions representing different levels of performance or acceptability (good, acceptable and poor) for each criterion. The thresholds for each criterion are dependent on the application and Table 3.1 shows the values that have been chosen in this case for the purposes of illustration.

Note that although 4° may seem small, over 30 m this represents a source separation of just over 2 meters whereas 1° equates to just over $52cm$ which is still an appreciable error if the intended application was direction finding or channel estimation based on direction finding. This emphasises the point that different threshold levels should be applied depending on the application.

It has to be noted that obtained results in the context of node selection for array formation are very similar for the detection, resolution and accuracy criteria.

this allows for a single one of them to be chosen without any loss of generality. This reduces the complexity of the algorithm, but does not affect the resulting selected nodes. Out of the three, the accuracy measure has been selected due to its relevance to the performance of the Arrayed-WSN arrays.

3.3.2 Array Circularity and Sensitivity

In addition to the worst case smallest achievable RMS error $\sigma_{\max}$, another criterion based on the Cramer-Rao lower bound can be defined. This is the normalised achievable RMS error difference or $\Delta\widehat{\sigma}$ which is given by

$$\Delta\widehat{\sigma} = \frac{\max\limits_{p}\left\{\sqrt{CRB[p]}\right\} - \min\limits_{p}\left\{\sqrt{CRB[p]}\right\}}{\max\limits_{p}\left\{\sqrt{CRB[p]}\right\}} \tag{3.31}$$

Due to the fact that circular arrays approach a performance independent of direction (i.e. constant performance for all azimuth angles, thus $\Delta\widehat{\sigma} \simeq 0$), minimising $\Delta\widehat{\sigma}$ is equivalent to choosing a set of nodes that produces an array which is as close to circular as possible.

This criterion, along with the overall array sensitivity given in Eq 3.30 is plotted in Figure 3.10 where $\Delta\widehat{\sigma} = 0$ indicates a circular array and $\Delta\widehat{\sigma} = 1$ indicates a linear structure. This shows that as the arrays become more linear the array becomes more sensitive to uncertainties in the node positions. However more importantly, the vast number of evaluated arrays have a small overall sensitivity. Thus combinations of nodes in the neighbourhood of the EOI as illustrated in Figure 3.8 can be found which provide a sensitivity close to the minimum whilst providing a reasonably consistent performance over all directions of arrival. The above four performance measures, that is ambiguities, accuracy, circularity and sensitivity, are combined into a single compound measure using a weighted cost function. The weight that is applied to each measure is dependent upon which region the array's performance resides for each criterion. This can be expressed using the following equation

$$\Xi = \underline{w}^T \underline{\mathcal{Y}} \tag{3.32}$$

where

$$\underline{w} = \begin{bmatrix} w_1(A_{\max}) \\ w_2(\sigma_{\max}) \\ w_3(\Delta\widehat{\sigma}) \\ w_4(\zeta) \end{bmatrix}, \underline{\mathcal{Y}} = \begin{bmatrix} \widehat{\mathcal{N}}(A_{\max}, 100) \\ \widehat{\mathcal{N}}(\sigma_{\max}, \pi/18) \\ \Delta\widehat{\sigma} \\ \widehat{\mathcal{N}}(\zeta, 0.02) \end{bmatrix} \text{ and } \widehat{\mathcal{N}}(x,y) = \begin{cases} 1 & x > y \\ x/y & x \leqslant y \end{cases} \tag{3.33}$$

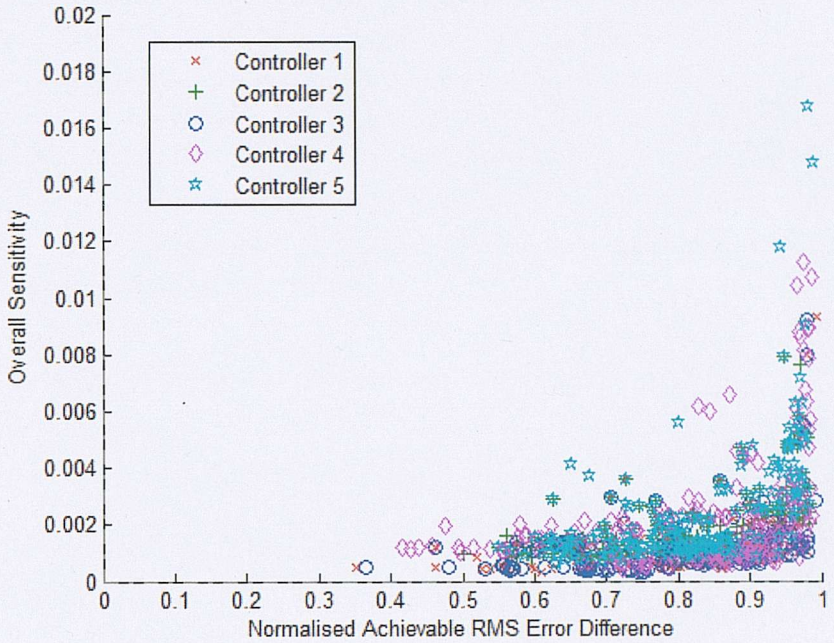


Figure 3.10: Overall Sensitivity against Normalised Achievable RMS Error Difference

	Cost function weight		
	Good	Acceptable	Poor
Worst case number of AGS	$w_1 = 1$	$w_1 = 10$	$w_1 = 100$
Worst Case smallest RMS error	$w_2 = 0.3$	$w_2 = 3$	$w_2 = 30$
Normalised RMS difference	$w_3 = 1$		
Overall array sensitivity	$w_4 = 1$		

Table 3.2: The weight vector formation for various regions of performance

Note that in the above formulation, $w_i(x)$ indicates that w_i is a function of x. Also a normalised measure of the number of ambiguities, the worst case RMS error and the overall array sensitivity has been used such that $0 \leqslant \widehat{\mathcal{N}}(\cdot, y) \leqslant 1$ with y equal to $100, 10°$ and 0.02 respectively. This normalisation is done to ensure that the importance of each factor is determined solely by the weight vector $\underline{w}$.

The functions contained in the weight vector $\underline{w}$ can be defined for the various performance regions by Table 3.2 The values selected in Table 3.2 are determined by the application with the ratio between pairs of weights indicating how much performance with respect to one criterion can be traded off for another. For example, if $A_{\max}$ and $\sigma_{\max}$ are both considered to be "Good" then 3 ambiguities is equivalent to 1 degree of accuracy whereas if $A_{\max}$ is only "Acceptable" then the cost function will allow a tenth of a degree of accuracy to be traded off against 3 AGS.

Potential Controllers K	Nodes in List N_L	Array Size N	Evaluated Arrays
5	6	5	75
5	10	5	1050
5	14	5	5005
5	18	5	15,300
5	20	5	48,450

Table 3.3: The complexity of the algorithm in the number of evaluations performed by all potential controller

The final node selection process can therefore be written as

$$\Xi_{selectedArray} = \min_{\mathcal{E}\subset\mathcal{P}_k,k} \left\{\underline{w}^T\underline{\mathcal{Y}}\right\}, 1 < k < K \tag{3.34}$$

where $\mathcal{E}$ is any set of $(N-1)$ element nodes chosen from the set $\mathcal{P}_k$ of N_L nodes for each controller k. The computational complexity of the above approach is proportional to K times the number of combinations of N_L objects in sets $N-1$ which increases rapidly as more nodes are included in the list of neighbouring nodes. Table 3.3 shows how many arrays have to be considered for various values of K and N_L given a *Wireless Array* size of $N = 5$. The most computationally intensive performance criterion to evaluate is the number of ambiguous generator sets, as a complex procedure has to be performed for all values of θ_0 (with a step size of no more than a few degrees to avoid "missing" ambiguities). However, if the computational complexity really needs to be reduced, and as Figure 3.11 illustrates, then only the arrays with "Good" or "Acceptable" performance in terms of the number of AGS may be allowed. In this case, only those arrays with an aperture less than a few half wavelengths need to be evaluated, as for bigger apertures, the number of AGS is greatly increased. By using the parameters $k = 5, N_L = 15, N = 5$ and simulating the *Wireless Array* formation algorithm in the example network and EOI of Figure 3.8, we arrive at the 5 proposed *Wireless Arrays*, one for each controller as shown in Figure 3.12. Figure 3.13 presents the final selected *Wireless Array* for the EOI shown in Figure 3.8. In addition the properties of the best *Wireless Array* for each potential controller are shown in Figure 3.14. Finally, as illustrated by Figure 3.14, the square root of the CRB for the selected *Wireless Array* is roughly 1.75° while the difference between the best and the worst achievable RMS error is roughly 0.7°.

Once the *Wireless Array* has been selected the nodes forming this array including the proposing controller pass into a *Wireless Array* set-up phase. This phase includes time synchronisation and location estimation improvement together with array calibration.

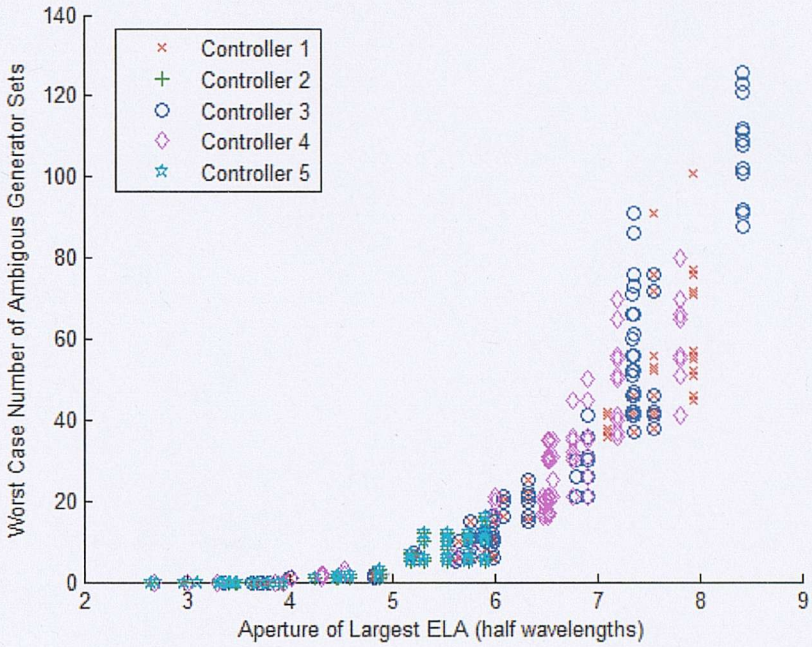


Figure 3.11: Number of Ambiguous Generator Sets Against Array Aperture

3.4 Conclusion

In this chapter a number of performance criteria for assessing different array geometries have been examined and it has been shown that the selection of a number of nodes to form a *Wireless Array* in an Arrayed-WSN is not a trivial problem but involves various trade-offs. A compound suitability measure has been proposed that combines a number of different performance factors including the number of Ambiguous Generator Sets, the accuracy at which the positions of two closely placed sources can be estimated and the sensitivity of the array to uncertainties in the locations of the nodes. The formulation allows the relative importance of each factor to be adjusted to suit the intended use of the *Wireless Array*. This compound measure, together with the decentralised approach to its evaluation form the array connectivity rules and the operation of these rules has been demonstrated by means of computer simulation.

In the next chapter we study the various communication links involved in the node-to-node and *Wireless Array*-to-*Wireless Array* communications, and propose a comprehensive design based on a novel channel modelling specifically applicable to the Arrayed-WSN.

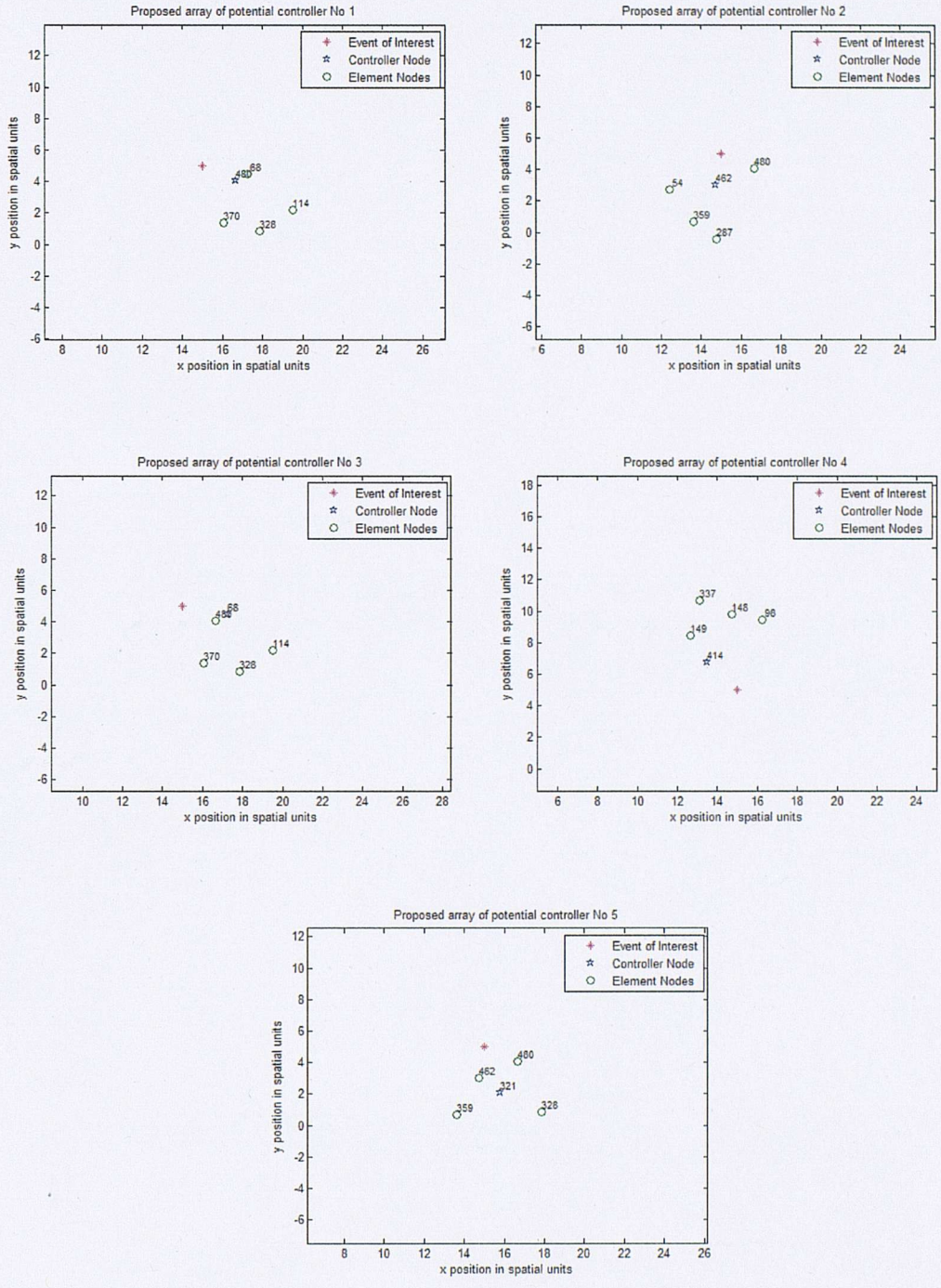


Figure 3.12: The 5 proposed Wireless Arrays shown with the proposing potential controller and in relation to the EOI

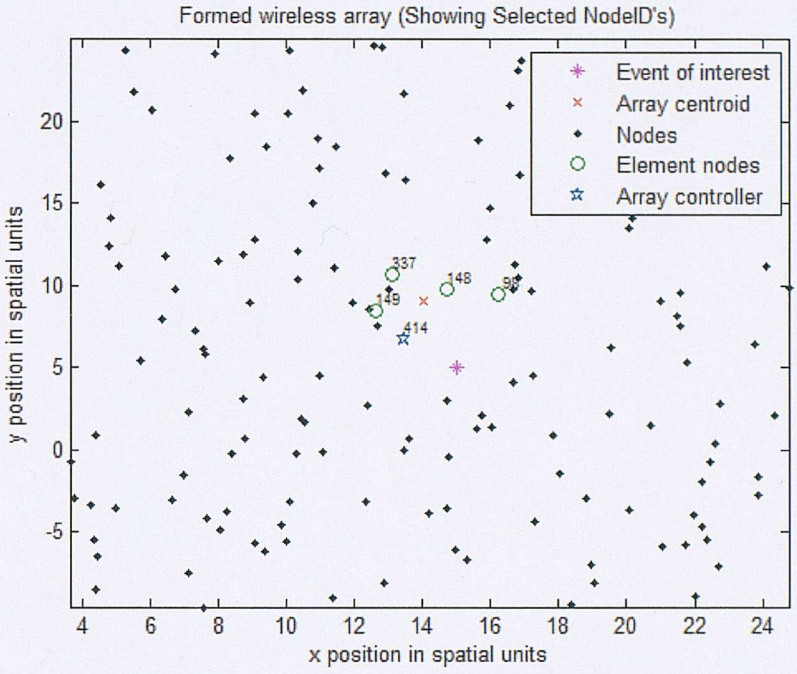


Figure 3.13: The final selected Wireless Array

Controller	Number of AGS	Worst Case RMS error	RMS error difference	Array sensitivity	Compound Measure
1	0	0.03643827	0.462852143	0.001223357	5.560688343
2	3	0.023181707	0.500375505	0.00097051	5.674846854
3	0	0.03643827	0.462852143	0.001223357	5.560688343
4	0	0.027670285	0.416516509	0.001214837	4.944491617
5	2	0.026633292	0.56501241	0.001076724	6.39709757

Figure 3.14: The three best proposed Wireless Arrays for each potential controller,

Chapter 4

Arrayed-WSN Communication Link Design

The reliable and efficient operation of the Arrayed-WSN is heavily dependent upon the performance of the *intra*-wireless link. It is this link that enables small groups of nodes to act as *Wireless Arrays* which in turn should allow information to be propagated through the network more effectively than in traditional WSNs (i.e. where messages propagate from node to adjacent node in a multi-hop fashion). The performance of the Arrayed-WSN as a whole is also dependent on the characteristics of the link between these *Wireless Arrays*, known as the *inter-Wireless Array* link. It is crucial therefore that detailed consideration be given to the design of these links and this is the principal purpose of this study.

The majority of the literature on transceiver design for wireless sensor networks has focused on energy requirements, for example: In [51] an ultra low power RF transceiver operating at 900 MHz and requiring only 1.3 mW in either transmit or receive mode is presented that operates up to a distance of 16 m at 20 kbps (-94 dBm sensitivity and -6 dBm transmit power). A two channel 40 kbps transceiver operating at 1.9 GHz was presented in [52] that employs MEMS radio frequency resonators instead of quartz crystals and only consumes 3.6 mW in receive mode and 8.5 mW in transmit mode (1.6 dBm transmit power at 17% efficiency). Also, in [53] Shih et al consider the power consumed by both the processor and the radio transceiver of a node. The transceiver model was used to compare binary and M-ary modulation schemes in terms of their energy efficiency and it was shown that for startup times in excess of 200 μs binary modulation schemes consume less power per transmitted bit than M-ary schemes.

As has been discussed in Chapter 1, MIMO techniques may offer potential energy savings to a WSN if careful routing and MAC is applied. Whilst energy

consumption is one of the most important factors in the design of wireless sensor networks, it is not the only concern. The abundance of the inexpensive, disposable nodes, together with the possibility of replenishment, makes the network capable of operating over long periods using nodes of short lifetime. This results in the performance of the network (e.g. measured by the Bit-Error Rate (BER), guaranteed message delivery within specified interval, capacity) becoming a very important factor. In this study the focus will be on the structure of both the transmitter and receiver in order to enhance the performance of both the *intra* and *inter-Wireless Array* links.

In a WSN, the density of the nodes will be such that even when a low transmit power is used, many nodes will receive transmitted signals. In addition, in an Arrayed-WSN many nodes will need to transmit at possibly the same time and therefore a wireless channel multi-access technique is required. The technique that will be presented in this chapter consists of a beamforming MIMO multicarrier DS-CDMA system. The beamforming refers to the fact that both receivers and transmitters in an Arrayed-WSN are equipped with antenna arrays and can therefore direct and control their transmitting and/or receiving capability.

This study is concerned with the design of the three individual wireless links involved in the Arrayed-WSN:

- the *initial* communication link
- the *intra-Wireless Array* communication link
- the *inter-Wireless Array* communication link.

The *initial* communication link is utilised for communication between individual nodes, up to the point where *Wireless Arrays* are formed. The *intra* and *inter*-wireless links are associated with the communications taking place between nodes in a *Wireless Array* and between *Wireless Arrays* respectively. The utility and necessity of these three links in the Arrayed-WSN was more extensively discussed in Chapter 2. The *intra*-wireless link is used for the internal communications of a *Wireless Array*, in other words, for the exchange of messages between the *Wireless Array* nodes and the controller. It was decided to employ a completely different link for the *Wireless Array* internal communications in order to limit the external interference and because the uninterrupted internal operation of the *Wireless Arrays* is crucial to the smooth operation of the network. The *inter-Wireless Array* link allows for the communication between *Wireless*

Arrays themselves. This link's main objective is to facilitate the flow of information through the network, possibly by employing a multi-hop array to array data forwarding.

As described previously, the Arrayed-WSN is characterised by its infrastructureless nature and the employment of a CDMA-type communications system. Note that an Arrayed-WSN environment is interference "rich" where due to the lack of infrastructure and synchronisation between the nodes, other schemes like TDMA are increasingly complicated. The excellent interference rejection capabilities together with the inherent protection against jamming or eavesdropping exhibited by an asynchronous CDMA scheme, render it most applicable to the Arrayed-WSN design.

The scheme that was actually selected for the design of the aforementioned links was a MultiCarrier Direct Sequence CDMA (MC-DS-CDMA) implementation. Although multicarrier implementations require more complex transceivers, since multiple carrier frequencies must be generated to modulate/demodulate the signal, and are less bandwidth efficient they offer many advantages. Firstly, multicarrier communication allows the extra degree of freedom of coding the signal in the frequency domain on top of the conventional spreading. This implies that more nodes can be accommodated for a given number of PN-codes. Another advantage is that the power of the transmitted signal is divided amongst subcarriers and thus less power is lost and less inter-symbol interference takes place at the receiver when the lower energy paths are ignored. Furthermore, because the bandwidth of the channel is subdivided, even channels with high frequency selectivity can be found to have flat fading subchannels. In fact, it has been shown in [54] that even some frequency selectivity in the subchannels can be exploited to increase the diversity gain. It is noted that the design and simulations that accompany this study were produced for short code CDMA (number of chips in the PN code equals the processing gain); the same model can be easily expanded to long code CDMA at the expense of extra complexity at the receiver.

The first two links (*initial* and *intra-Wireless Array*) defined above exist between individual nodes in the network whereas the third (*inter-Wireless Array*) involves a group of nodes operating as a whole. The accuracy at which the positions of the nodes can be estimated determines the maximum frequency (or minimum wavelength) at which this group of nodes can operate as a *Wireless Array*. This is because after the array element locations are estimated an array calibration method needs to be employed to compensate for geometrical (i.e. location errors), electrical uncertainties and mutual coupling effects. The maxi-

mum location error that can be accommodated clearly varies depending on the algorithm employed and the wavelength of the associated signals. In fact, smaller frequency signals require smaller accuracy in the location estimation due to the larger wavelengths involved. The *initial*-wireless link and the *intra-Wireless Array* link do not have this restriction and can therefore operate in a higher frequency band. This has the advantage of allowing a larger aperture in terms of half wavelengths for the *Local Array* which increases its directivity, direction finding capabilities, etc. Other factors to be taken into account when choosing the operating frequencies are given below:

- For frequencies below 1 GHz the antenna efficiency of the electrically small antennas required due to the small physical size of the sensor nodes is poor [55]

- The desire for worldwide operation without a license indicates the use of one of the Industrial, Scientific and Medical (ISM) bands. (Note: Another argument based on minimising the development cost of the network is presented in [55]). These requirements suggest 2.4 GHz for the *inter-Wireless Array* Link and either 5.8 GHz, 24 GHz, 61 GHz, 122 GHz or 244 GHz for the other links.

- Higher frequencies of operation require more costly components (specifically 60 GHz and above) and have larger current drains [55]. In addition atmospheric attenuation at the Earth's surface is over 1000 times greater at 60 GHz than at 5 GHz and approximately 50 times greater at 24 GHz [56] although this is less important because of the relatively short range required. This suggests either 5.8 GHz or 24 GHz for the first 2 links.

- Using a cubic sensor node of volume 10 cm^3 the maximum *Local Array* aperture is 5.97 half wavelengths at 24 GHz but only 1.44 half wavelengths at 5.8 GHz. (i.e. when there are array elements at the vertices of the node).

Based on the above it is proposed to use the 24GHz ISM band for the *initial* and *intra-Wireless Array* Links and the 2.4 GHz ISM band for the *inter-Wireless Array* Link. This has the additional benefit of allowing the 2.4 GHz carrier to be generated from the 24 GHz local oscillator.

After further consideration it was decided that the *initial* communication link should operate at a slightly different but adjacent frequency to the *intra-Wireless Array* link. This would greatly reduce the interference received by a node operating in one link due to neighbouring nodes transmitting on the other link.

This frequency separation would also allow a single node to communicate on both links simultaneously. This ability is particularly effective when it comes to the *intra-Wireless Array* link where a *Wireless Array* controller may need for example to communicate with the array nodes while it is simultaneously communicating with other nodes external to the *Wireless Array*. Furthermore the differentiation in frequency of the two links allows for the *Wireless Array* to be re-calibrated and re-configured through the *initial* link while operating uninterrupted.

The possible frequency bands for the three links are summarised as follows:

- 2.4 GHz Industrial Scientific and Medical band for the *inter*-wireless link
- 24 GHz ISM band for the *intra*-wireless link
- 24 GHz ISM band for the *initial* wireless link, at a different frequency channel to the *intra*-wireless link

In the following sections, transmitter, wireless channel and receiver structure and signal models will be presented jointly for the three links. Furthermore, the performance of each link will be discussed through computer simulations for an exemplary scenario, where the channel parameters are provided by ray-tracing software.

4.1 Beamforming MIMO Multicarrier DS-CDMA Transmitter

In this section the design of the node transmitter is illustrated and consideration is also given to how a number of such transmitters on different nodes in a *Wireless Array*, acting together, collectively form a *Wireless Array* transmitter to be used to propagate signals through the network (from *Wireless Array* to *Wireless Array*).

It has been decided to avoid using subarrays as it has been observed that different subarrays can see identical communication links. This observation is based on ray-tracing simulations of a network of 500 nodes randomly distributed in a 3D urban environment as described in more detail in Section 4.4.1.

Furthermore, the design is generalised to allow different transmit beamformers (i.e. different transmit weight vectors) for different subcarriers (see Eq 4.6 later on).

Message data to be transmitted on all three links (*initial*, *intra* and *inter*-wireless) are firstly source coded to reduce redundancy, possibly encrypted, and

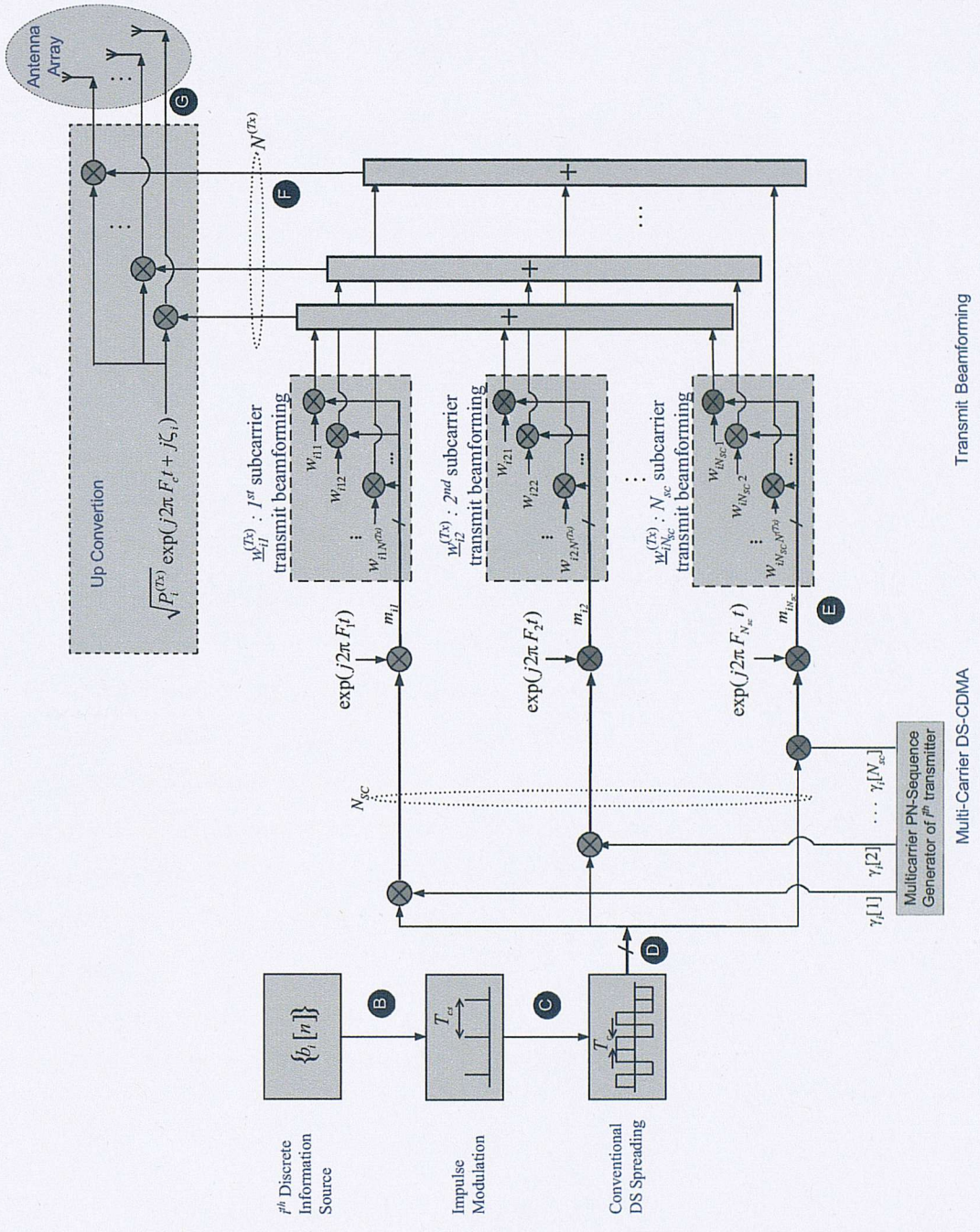


Figure 4.1: MC-DS-CDMA Beamforming Antenna Array Transmitter

then channel coded to intentionally reintroduce redundancy to allow forward error detection and correction at the receiver. The coded bit stream is then interleaved in order to reduce the effect of bursts of errors and to reduce or remove the correlation between adjacent bits. The resulting bit sequence for either a single node with NodeID i (in the case of the *initial* or *intra*-wireless links) or a *Wireless Array* in transmit mode with controller NodeID i is denoted by $\{b_i[n] = \pm 1, \forall n \in \mathcal{Z}\}$

For the purposes of simulation and analysis this bit stream is assumed to be a discrete information source with possibly different rates (r_b) for each type of link in which different symbols in the stream are completely decorrelated, that is $\mathcal{E}\{b_i[n]\, b_i[m]\} = \delta_{nm}$, where δ_{nm} is the Kronecker delta function defined as

$$\delta_{nm} \triangleq \begin{cases} 1 & n = m \\ 0 & n \neq m \end{cases}$$

Note that in general there will be some dependence between data symbols, however if an interleaver with a distance D is employed then the above assumption holds for $|n - m| < D$. Also symbol streams transmitted by different nodes will in general be uncorrelated, therefore $\mathcal{E}\{b_i[n]\, b_j[m]\} = \delta_{ij}\delta_{nm}$. However care needs to be taken in the *intra-Wireless Array* uplink (i.e. element nodes transmitting to a controller node) as the information that each element node transmits to the controller might be highly correlated. One possible solution to this is for the stream of each node to be XORed (exclusive OR'd) with a long sequence of ± 1's uniquely determined by its NodeID. This also has the benefit of implementing an additional level of encryption as the signal can then only be recovered by someone with knowledge of the NodeID and the mapping from NodeID to scrambling sequence.

Because of possibly differing data rates, the channel symbol rates for each link are denoted by r_{cs} with corresponding channel symbol periods T

$$r_{cs} = \frac{1}{T_{cs}} = \frac{r_b}{\log_2 \mathcal{M}} \tag{4.1}$$

where $\mathcal{M}$ is the number of channel symbols.

The structure of the proposed transmitter is shown in Figure 4.1. The sequence of channel symbols $\{b_i[n]\}$ at *point B* is impulse modulated and spread over a wider bandwidth using a PN-signal with period equal to the symbol period (short code CDMA). The DS-CDMA signal at *point D* is then multiplied by N_{sc} subcarriers, according to another PN-sequence, referred to as the multi-carrier spreading sequence and denoted by $\{\gamma_i[k] \in \pm 1,\ k \in 1, 2, ..., N_{sc}\}$. In

order to distinguish the elements of this sequence from the chips of the conventional direct sequence spreading sequence the term "flips" will be used for the γ_i's as this describes the effect of this PN-sequence on the signals modulating each subcarrier. The complex message signal at *point E* corresponding to the k^{th} subcarrier of the i^{th} transmitter is therefore given by

$$m_{ik}(t) = \gamma_i[k] \exp(j2\pi F_k t) \sum_{n=-\infty}^{+\infty} b_i[n]\, c_{PN_i}(t - nT_{cs}),\ nT_{cs} < t < (n+1)T_{cs} \tag{4.2}$$

where $c_{PN_i}(t)$ models one period of the PN-signal for the i^{th} transmitter on a particular link (as different links may be using different PN-codes). If the conventional direct PN-spreading sequence consisting of N_c chips is given by $\{\alpha_i[m] \in \mathcal{B},\ m \in 0, 1..., N_c - 1\}$ then $c_{PN_i}(t)$ can be written as

$$c_{PN_i}(t) = \frac{1}{\sqrt{N_c N_{sc}}} \sum_{m=0}^{N_c-1} \alpha_i[m]\, p_c(t - mT_c),\ mT_c < t < (m+1)T_c \tag{4.3}$$

where $p_c(t)$ denotes the chip pulse shaping waveform and T_c is the interval between chips. In this study it is assumed that $p_c(t)$ is a unit rectangular pulse with duration T_c. Note that the above assumes that the PN-sequence and symbol sequence have a common clock and the relationship $T_{cs} = N_c T_c$ holds.

In Eq. 4.2 $F_k = (k-1)\Delta f$ and Δf is the subcarrier separation chosen such that the signals are orthogonal over a chip duration, i.e. the following relationship holds

$$\Delta f = (an\ integer) \times \frac{1}{T_c} \tag{4.4}$$

The message signal for all subcarriers can then be expressed in a vector format *(point E)*, as shown by

$$\underline{m_i}(t) = \left[\underline{\gamma_i} \odot \underline{F}(t)\right] \sum_{n=-\infty}^{+\infty} b_i[n]\, c_{PN_i}(t - nT_{cs}) \in \mathcal{C}^{N_{sc}\times 1} \tag{4.5}$$

$$\text{where} \begin{cases} \underline{\gamma_i} = \left[\gamma_i[1],\ \cdots,\ \gamma_i[k],\ \cdots,\ \gamma_i[N_{sc}]\right]^T \in \mathcal{C}^{N_{sc}\times 1} \\ \underline{F}(t) = \exp\left(j2\pi \left[F_1,\ F_2,\ \cdots,\ F_k\ \cdots,\ F_{N_{sc}}\right]^T t\right) \in \mathcal{C}^{N_{sc}\times 1} \end{cases}$$

Following Figure 4.1, a scalar weight is applied to each subcarrier modulated signal and the weighted subcarrier modulated signals are then added at each

antenna. Thus the antenna array transmits $N^{(Tx)}$ signals, one per each antenna element.

As each node in an Arrayed-WSN is equipped with an antenna array, more than one antenna element can be used for transmission on the *initial* and *intra*-wireless communication links and *Wireless Arrays* can be used to transmit and receive on the *inter*-wireless communication link. Note that $N^{(Tx)}$ is the number of antenna elements available or chosen to be used for transmission. In the *initial* and *intra*-wireless links the number of array elements $N^{(Tx)}$ is the number of utilised elements on the node's *Local Array*. In the *inter*-*Wireless Array* link $N^{(Tx)}$ is the number of nodes comprising the *Wireless Array*. Note that an optimisation of $N^{(Tx)}$ for specific deployment areas and different operational scenarios may be performed.

A much simpler, but equivalent structure for the transmitter is illustrated in Figure 4.2. This model utilises a transmit beamforming weight matrix $\mathbb{W}_i^{(Tx)}$ which has the weight vectors for each subcarrier as columns:

$$\mathbb{W}_i^{(Tx)} = \left[\underline{w}_{i1}^{(Tx)}, \ \cdots, \ \underline{w}_{ik}^{(Tx)}, \ \cdots, \ \underline{w}_{iN_{sc}}^{(Tx)}\right] \in \mathcal{C}^{N^{(Tx)} \times N_{sc}} \tag{4.6}$$

Using the weight matrix, the signals can be weighted and added by a simple matrix multiplication resulting in the baseband signal to be transmitted at *point F*. The signals are then up-converted and transmitted by the antenna array.

The signal due to the k^{th} subcarrier of the i^{th} transmitter $\underline{y}_{ik}(t)$ can be expressed as

$$\underline{y}_{ik}(t) = \sqrt{P_i^{(Tx)}} \exp\left(j\left(2\pi F_c t + \zeta_i\right)\right) \underline{w}_{ik}^{(Tx)} m_{ik}(t) \in \mathcal{C}^{N^{(Tx)} \times 1} \tag{4.7}$$

where $P^{(Tx)}$ is the transmitted power, F_c is the carrier frequency and ζ_i is the i^{th} transmitter's local oscillator random phase $\zeta_i \in [0, 2\pi)$. However since the focus is on the baseband signal, omitting the carrier reduces the above equation to:

$$\underline{y}_{ik}(t) = \sqrt{P_i^{(Tx)}} \exp\left(j\zeta_i\right) \underline{w}_{ik}^{(Tx)} m_{ik}(t) \in \mathcal{C}^{N^{(Tx)} \times 1} \tag{4.8}$$

Based on the above equation the overall transmitted signal-vector (i^{th} Transmitter) can be expressed as follows:

$$\begin{aligned} \underline{y}_i(t) &= \sum_{k=1}^{N_{sc}} \underline{y}_{ik}(t) \in \mathcal{C}^{N^{(Tx)} \times 1} \\ \underline{y}_i(t) &= \sqrt{P_i^{(Tx)}} \exp\left(j\zeta_i\right) \mathbb{W}_i^{(Tx)} \underline{m}_i(t) \in \mathcal{C}^{N^{(Tx)} \times 1} \end{aligned} \tag{4.9}$$

The choice of the transmit weights is partly determined by the link type (*initial*, *intra* or *inter*-wireless) and how the link is being used at any point in time. For

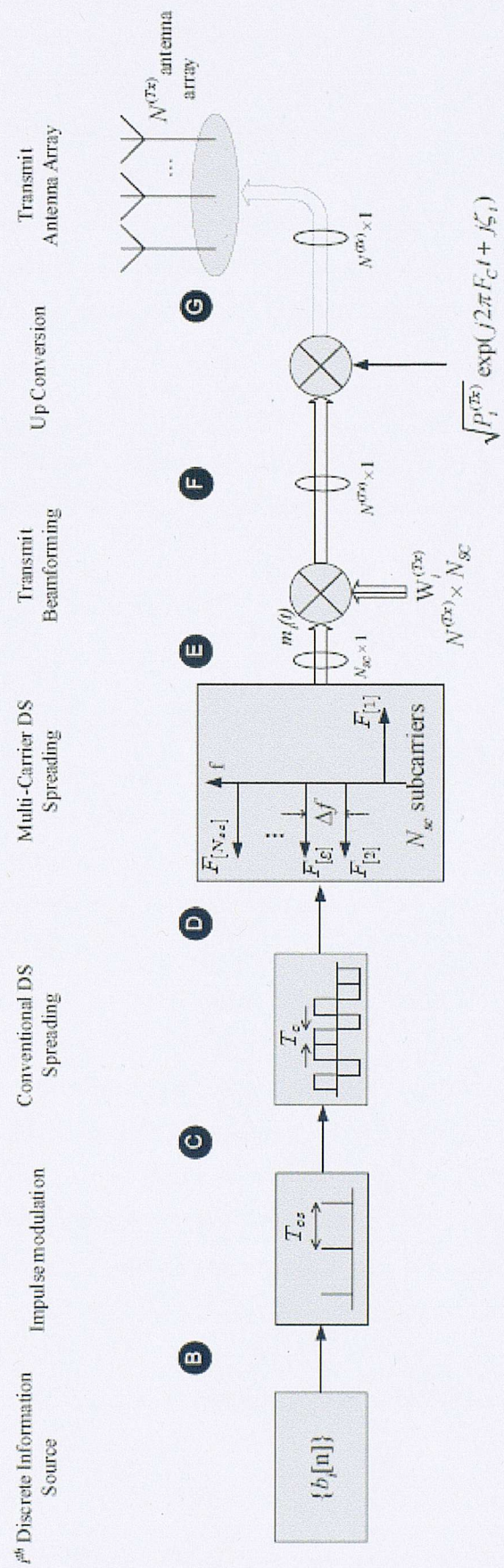


Figure 4.2: Simplified transmitter outline

the *initial* link, messages may either be intended for a particular node or are intended to be received by all the neighbouring nodes (broadcast messages) as was the case in the CANDLA algorithm presented in Chapter 2.

Two examples that can be used to construct a weight vector are now presented. The first weight construction consists of steering the transmitting array to the direction of the desired receiver. Messages intended for a particular receiver from the i^{th} transmitter could be sent using a transmit weight matrix designed to steer a beam in the direction of the desired recipient, with columns given by

$$\underline{w}_{ik}^{(Tx)} = \underline{S}_{des,ik}^{(Tx)} \in \mathcal{C}^{N^{(Tx)} \times 1} \tag{4.10}$$

where $\underline{S}_{des,ik}^{(Tx)}$ is the array transmit manifold vector for the desired path (i.e. in the direction of the desired receiver) of the i^{th} transmitter for the k^{th} subcarrier:

$$\underline{S}_{des}^{(Tx)} = \exp\left(-j\frac{2\pi(F_c + F_k)}{c}\left[\underline{r}_x,\ \underline{r}_y,\ \underline{r}_z\right]\underline{u}\left(\theta_{des}, \varphi_{des}\right)\right) \in \mathcal{C}^{N^{(Tx)} \times 1} \tag{4.11}$$

where $\underline{u}(\theta, \varphi) = \left[\cos\theta\cos\varphi,\ \sin\theta\cos\varphi,\ \sin\varphi\right]$ is a unity norm vector and $\left[\underline{r}_x,\ \underline{r}_y,\ \underline{r}_z\right]$ denotes the x, y, z coordinates of the antenna array elements.

Also note that it has been assumed that all the elements of the node's *Local Array* are omnidirectional elements, however Eq. 4.11 can easily be extended to cope with directional elements by using a complex vector which models the directional gain and phase response of each element of the array.

In order to simplify the operation of *Wireless Arrays*, nodes that have a direct Line of Sight path to the controller may only be allowed to become *Wireless Array* element nodes. This can be implemented as an additional connectivity rule to be incorporated into the node selection process described in Chapter 3, but is not a necessary requirement. However in such a case, the transmit beamformer for the *intra-Wireless Array* link can always be constructed according to Eq. 4.10.

The second and more sophisticated approach to the transmit weight construction process is to steer a main beam in the direction of the desired node and, at the same time, to control the array pattern placing nulls to core pre-specified directions. The weight matrix is then constructed with columns:

$$\underline{w}_{ik}^{(Tx)} = \mathbb{P}^{\perp}_{\mathbb{S}_{null,ik}^{(Tx)}}\, \underline{S}_{des,ik}^{(Tx)} \in \mathcal{C}^{N^{(Tx)} \times 1} \tag{4.12}$$

where $\mathbb{S}_{null,ik}^{(Tx)}$ has columns associated with the array manifold vectors in the pre-specified directions to be nulled, and $\mathbb{P}^{\perp}_{\mathbb{A}} = \mathbb{I}_N - \mathbb{A}\left(\mathbb{A}^H\mathbb{A}\right)^{-1}\mathbb{A}^H$ is the complement projection operator onto the subspace spanned by the columns of $\mathbb{A} \in \mathcal{C}^{N \times M}$.

It has to be noted that although only two techniques are presented here, many other approaches to the design of the transmit beamforming vector exist. For example, in [57], [58], solutions to maximising the SNR at the receiver, maximising a modified (pseudo) signal-to-noise plus interference ratio (P-SNIR) at the receiver and maximising the ratio transmission are presented.

4.2 Channel Model

The signals transmitted from each array element (whether it be an element of a node's *Local Array* or from a node in a *Wireless Array*) propagates through a wireless channel that is slightly different from a conventional mobile channel. Some key differences are summarised below:

- Nodes are on the whole stationary, this implies that time variations in the channel response are due mainly to the movement of scatterers (although not all the scatterers move).
- Nodes are low lying above either ground level or on rooftops with the proportion between the two groups being dependent upon the building density.
- The typical range of the links are smaller, although nodes have the ability to establish links of longer distances if necessary to form a connected network (*initial* and *intra-Wireless Array* links).

The range of the *inter-Wireless Array* link can be considerably larger than the *initial* and *intra*-wireless links, as the power of the nodes forming the *Wireless Array* is combined and focused towards a sink node (which will have the effect of creating another *Wireless Array* if it is required in order to forward the message to the sink as previously described in Chapter 2).

In a conventional communication scenario, a transmitter with a single antenna transmits the signal that reaches, via one or more paths, a receiver with a single antenna. The channel associated with this type of communication is referred to as a Scalar-Input Scalar-Output (SISO) channel, since both input and output signals are scalar (single) signals. Similarly, when the receiver is equipped with an antenna array, the channel is referred to as a Scalar-Input Vector Output (SIVO) channel, as the output of the channel is a signal-vector, one signal corresponding to each receiving antenna. In the *initial* or *intra*-wireless links, communication takes place between the Arrayed-WSN nodes, which are equipped with antenna arrays, resulting in a Vector-Input Vector-Output channel (VIVO) (see Figures



Figure 4.3: *Initial/intra* wireless link - a VIVO channel between two nodes

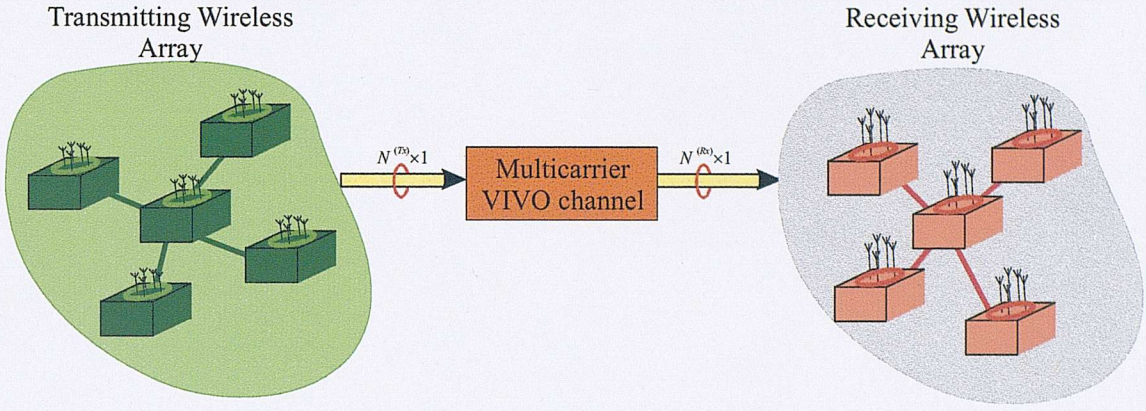


Figure 4.4: *Inter* wireless array link - a VIVO channel between two arrays

4.3, 4.4). In the case of the *inter-Wireless Array* link, many nodes cooperate and act as an antenna array (both at the transmitter and at the receiver) thus the channel remains a VIVO channel.

In contrast to that, when a receiving node (or for that matter, a receiving *Wireless Array*), is receiving the desired transmission of another node (*Wireless Array*) but also receives interference from other nodes (*Wireless Arrays*) that happen to operate at the vicinity, the channel has to be treated as a Matrix-Input Vector Output channel as depicted in Figures 4.5, 4.6.

In the *initial* and the *intra-Wireless Array* link the transmitting/receiving arrays are the *Local Array*s of the communicating nodes. This means that the antenna elements of the involved arrays are closely positioned in space, i.e. the arrays involved have small apertures. This implies that the signals leaving the transmitting elements experience a common fading towards all the receiving elements and the channel, for a single transmitter's (i^{th} transmitter) single subcarrier (k^{th} subcarrier) can be modelled following the outline presented in Figure 4.7.

In Figure 4.7, $S_{ijk}^{(Tx)}$ and $S_{ijk}^{(Rx)}$ are the transmitting and receiving array manifold vectors for the i^{th} transmitter's j^{th} path k^{th} subcarrier and β_{ijk} is the respective path coefficient that models the effect of path loss, random phase shift due to reflection and Doppler phase shift due to the possible motion of scatterers to all subcarriers.

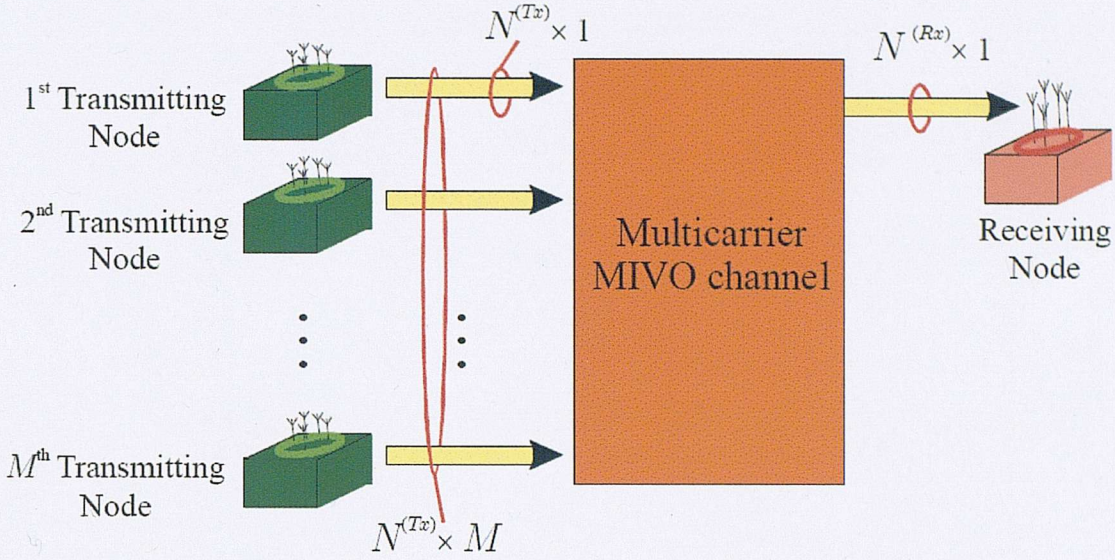


Figure 4.5: Multiple access *initial/intra* wireless link - a MIVO channel

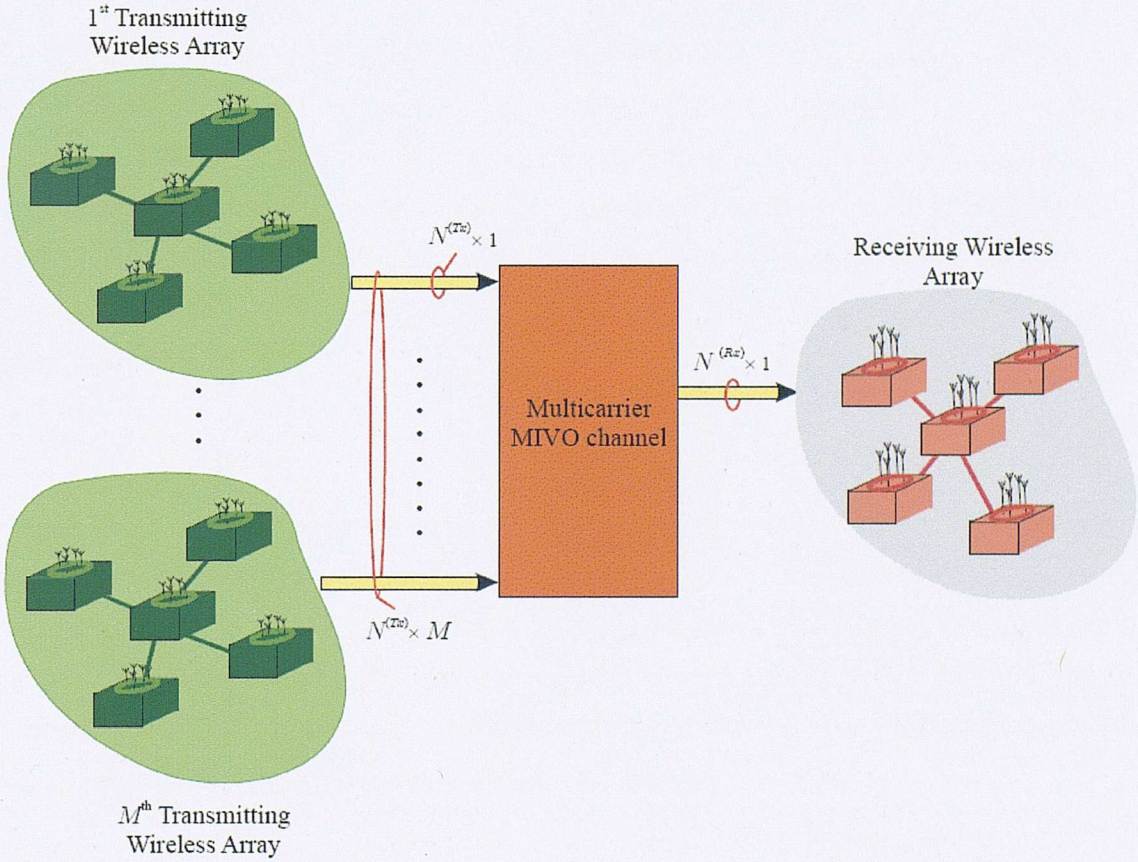


Figure 4.6: Multiple access *inter* wireless array link - A MIVO channel

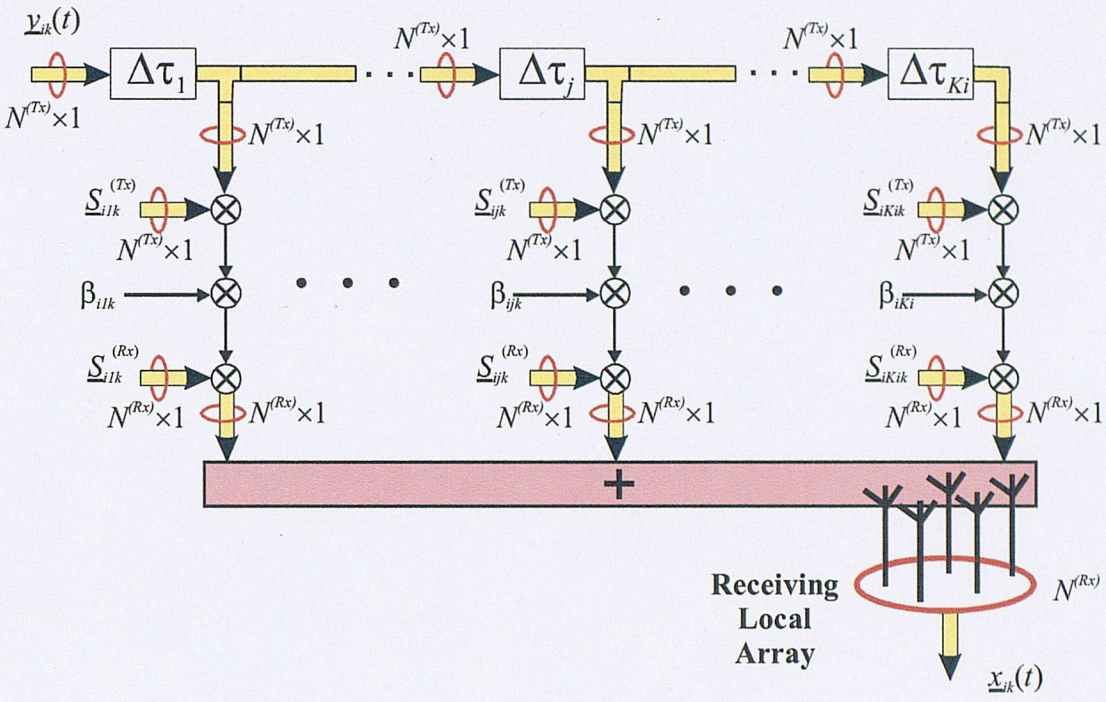


Figure 4.7: *Initial* or *intra* wireless array links - VIVO channel modelling for the k^{th} subcarrier, where K_i is the number of multipaths from the i^{th} transmitter

Although the model of Figure 4.7 is sufficient for the *initial* and *intra- Wireless Array* links, it needs to be expanded before it can be applied to the *inter- Wireless Array* link. That is because in this case, the communicating antenna arrays (i.e. the *Wireless Arrays*) have a large aperture and thus there is a different path coefficient corresponding to each pair of transmitting-receiving elements. In order to compensate for that, the path coefficient β_{ijk} has to be extended to a path coefficient matrix $\mathbb{B}_{ijk}$:

$$\mathbb{B}_{ijk} = \left[\underline{\beta}_{ijk}^{1}, \ \ldots, \ \underline{\beta}_{ijk}^{n}, \ \ldots, \ \underline{\beta}_{ijk}^{N^{(Tx)}} \right] \in \mathcal{C}^{N^{(Rx)} \times N^{(Tx)}} \tag{4.13}$$

where $\underline{\beta}_{ijk}^{n}$ is the vector containing the path coefficients from the n^{th} transmitting element to all receiving elements, for the j^{th} path and k^{th} subcarrier. Then the model follows Figure 4.8. It can be noted that the model of Figure 4.8 is a more general model than that of Figure 4.7, and in fact it encompasses the previous simpler case, if all the entries for each matrix $\mathbb{B}_{ijk}$ are the same. Thus from now on the model of Figure 4.8 is going to be considered.

$$\underline{x}_i(t) = \sum_{j=1}^{K_i} \sum_{k=1}^{N_{sc}} \underline{S}_{ijk}^{(Rx)} \odot \mathbb{B}_{ijk} \left(\underline{S}_{ijk}^{(Tx)} \odot \underline{y}_{ik}\left(t - \tau_{ij}\right) \right) \in \mathcal{C}^{N^{(Rx)} \times 1} \tag{4.14}$$

which can be written, using Eq. 4.8, as follows

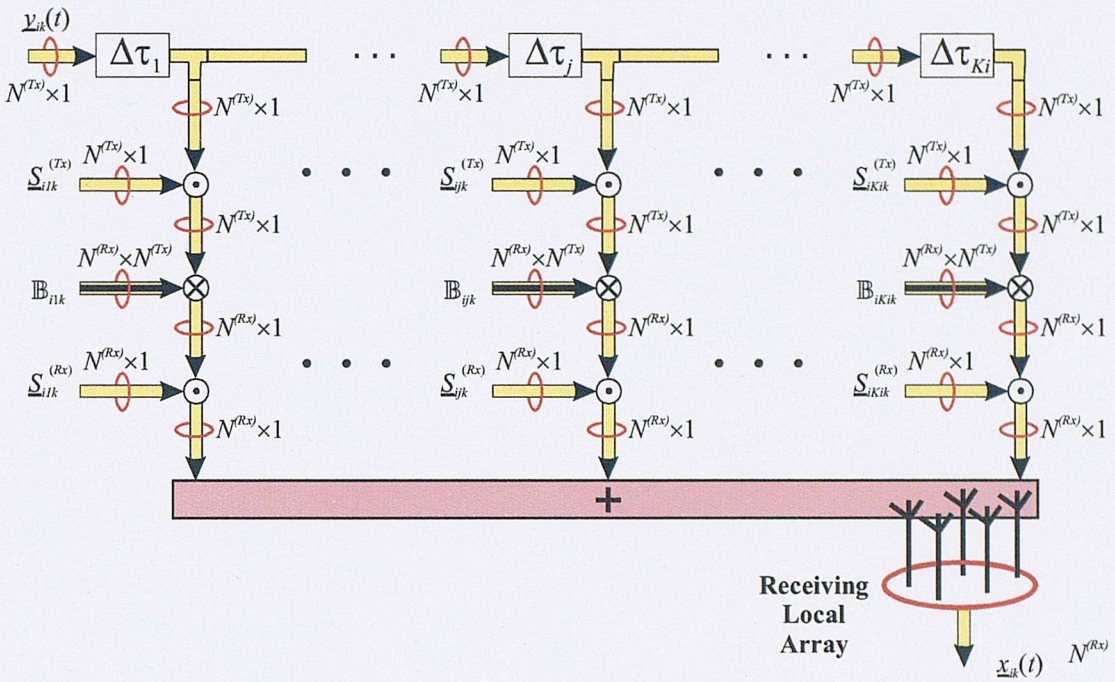


Figure 4.8: *Inter* wireless array link - VIVO channel of a single user's single subcarrier

$$\underline{x}_i(t) = \sum_{j=1}^{K_i} \sum_{k=1}^{N_{sc}} \underline{S}_{ijk}^{(Rx)} \odot \mathbb{B}_{ijk} \left(\underline{S}_{ijk}^{(Tx)} \odot \underline{w}_{ik} \right) m_{ik}\left(t - \tau_{ij}\right) \in \mathcal{C}^{N^{(Rx)} \times 1} \tag{4.15}$$

Note that Eq. 4.15 may be written as follows

$$\underline{x}_i(t) = \sum_{j=1}^{K_i} \sum_{k=1}^{N_{sc}} \left(\left(\underline{S}_{ijk}^{(Rx)} \underline{S}_{ijk}^{(Tx)^T} \right) \odot \mathbb{B}_{ijk} \right) \underline{w}_{ik} m_{ik}\left(t - \tau_{ij}\right) \in \mathcal{C}^{N^{(Rx)} \times 1} \tag{4.16}$$

Note that the factor $\sqrt{P_i^{(Tx)}} \exp\left(j\zeta_i\right)$, present in Eq. 4.8, has been absorbed into $\mathbb{B}$ for convenience. Furthermore, the parameters $\mathbb{B}$ and $\underline{S}$ could be extended to be time dependent, however, because nodes are stationary most of the multipaths will not vary with time.

The channel model presented above refers to each subcarrier separately. However, actual multicarrier expressions can furthermore simplify the channel model. The multicarrier array response (manifold) vector is defined

$$\underline{S}_{ij} = \exp\left(-j \frac{2\pi}{c} \underline{F} \otimes \left(\mathrm{r}_b \underline{u}\left(\theta_j, \varphi_j\right) \right) \right) \in \mathcal{C}^{N_{sc} N^{(Rx)} \times 1} \tag{4.17}$$

$$\text{where} \begin{cases} \underline{F} = \left[F_c + F_1, ..., F_c + F_k, ..., F_c + F_{N_{sc}} \right]^T \\ \underline{u}\left(\theta, \varphi\right) = \left[\cos\theta \cos\varphi, \quad \sin\theta \cos\varphi, \quad \sin\varphi \right]^T \end{cases}$$

and $\mathbf{r}_b = \left[\begin{array}{ccc} \underline{r}_x, & \underline{r}_y, & \underline{r}_z \end{array} \right]$ is the geometry of the receiver (b) array.

The multicarrier manifold vector contains the separate conventional array manifold vectors for all subcarriers, and follows the above approach of treating subcarriers separately. It has to be noted that when an array transmit vector is defined in general, the wave vector $\underline{u}(\theta, \varphi)$ has an outgoing direction in reference with the transmitting array, resulting in a manifold vector which is the complex conjugate of the corresponding receiving array response vector.

As mentioned above, Figures 4.7 and 4.8, model a single carrier (k) of the i^{th} transmitter. A more complete model would be one that included the effects of all subcarriers of a transmitter. In order to construct such a model, the multicarrier signal and manifold vectors, introduced by Eq. 4.8 and 4.17, are employed, in conjunction with an extended, multicarrier path coefficient matrix $\mathbb{B}_{MC,ij}$:

$$\mathbb{B}_{MC,ij} = \left[\begin{array}{ccccc} \mathbb{B}_{ij1} & 0 & 0 & \ldots & 0 \\ 0 & \ldots & & \ldots & \ldots \\ 0 & & \mathbb{B}_{ijk} & & 0 \\ \ldots & & & \ldots & 0 \\ 0 & \ldots & 0 & 0 & \mathbb{B}_{ijN_{sc}} \end{array} \right] \in \mathcal{C}^{N_{sc}N^{(Rx)} \times N_{sc}N^{(Tx)}} \tag{4.18}$$

Then the whole channel (i.e. for all subcarriers) of a single transmitter can be formulated as in Figure 4.9.

The respective complex baseband equivalent representation of the signals at the receiving array due to the signals from just the i^{th} transmitter (following Figure 4.9) can therefore be written as:

$$\underline{x}_i(t) = \left(\underline{1}_{N_{sc}}^T \otimes \mathbb{I}_{N^{(Rx)}}\right) \sum_{j=1}^{K_i} \underline{S}_{ij}^{Rx} \odot \mathbb{B}_{MC,ij} \left(\underline{S}_{ij}^{Tx} \odot \underline{y}_i(t - \tau_j)\right) \in \mathcal{C}^{N^{(Rx)} \times 1}$$

which is equivalent to:

$$\underline{x}_i(t) = \left(\underline{1}_{N_{sc}}^T \otimes \mathbb{I}_{N_u}\right) \sum_{j=1}^{K_i} \left(\left(\underline{S}_{ij}^{Rx} \; \underline{S}_{ij}^{Tx\,T}\right) \odot \mathbb{B}_{MC,ij}\right) \underline{y}_i(t - \tau_j) \in \mathcal{C}^{N^{(Rx)} \times 1} \tag{4.19}$$

The term $\left(\underline{1}_{N_{sc}}^T \otimes \mathbb{I}_{N^{(Rx)}}\right)$ has the effect of properly adding the different subcarriers to yield a signal vector in the dimensions of the receiver array.

This is not yet a complete model of the link as more than one node will transmit at the same time. In the case of the *intra-Wireless Array* uplink, all the element nodes transmit to the controller node and other nodes belonging to other *Wireless Arrays* will also access the medium giving a total of $M_{total} =$

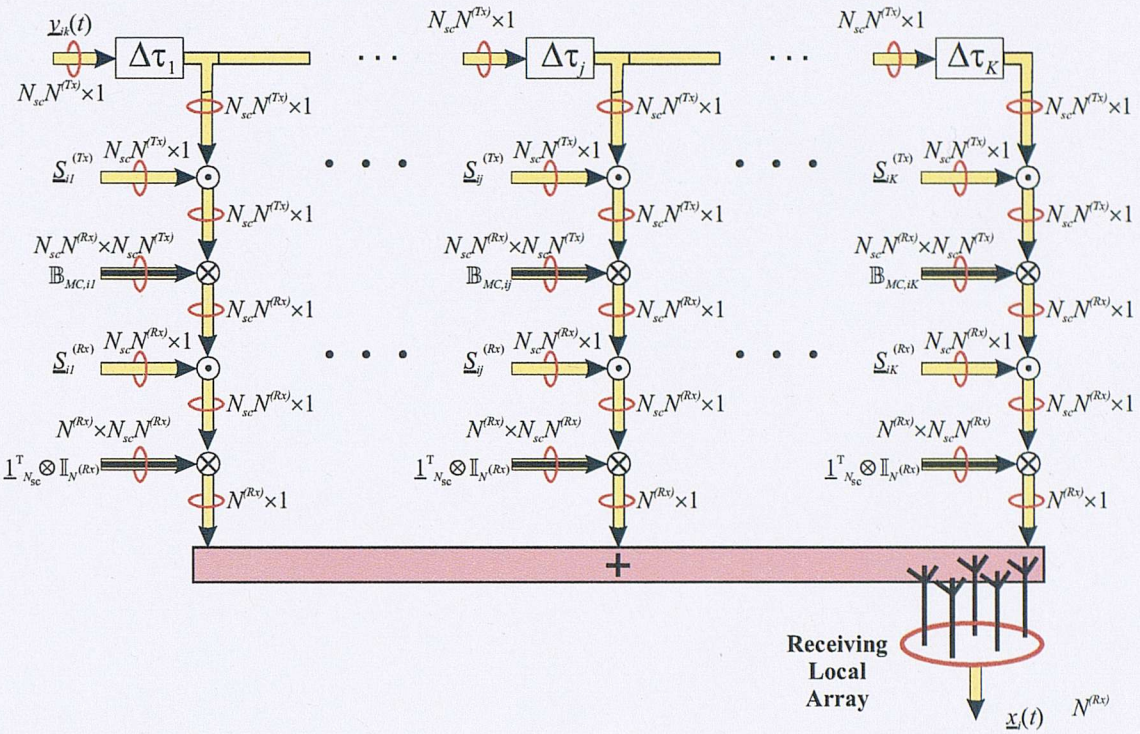


Figure 4.9: Multicarrier Vector Input Vector Output Channel Between Two Arrays

$4 + M_{int}$ effective users of the channel where M_{int} is the number of interfering nodes external to the considered *Wireless Array*. Conversely, in the case of the *intra-Wireless Array* downlink, the controller node can transmit the same signal to all the element nodes (with additional information unique to each node such as the delay and *Local Array* weights to apply to the signal before retransmitting on the *inter* array link being sent using the *initial* link), giving a total of $M_{total} = 1+M_{int}$ effective users. In the case of the *initial* or *inter-Wireless Array* links, the interferers M_{total} are other communicating nodes (or *Wireless Arrays* respectively) operating at the vicinity of the receiver. The multiuser receiver of the controller, using a separate beamformer for each element node is presented in Figure .

The total received signal at the receiver is the sum of the signals due to each of the M_{total} transmitting nodes through their respective VIVO channels in addition to background noise in the environment and thermal noise in the receiver. This is expressed by

$$\underline{x}(t) = \sum_{i=1}^{M} \underline{x}_i(t) + \underline{n}(t) \in \mathcal{C}^{N^{(Rx)} \times 1} \tag{4.20}$$

where $\underline{n}(t) \in \mathcal{C}^{N^{(Rx)} \times 1}$ is assumed to be complex white Gaussian noise.

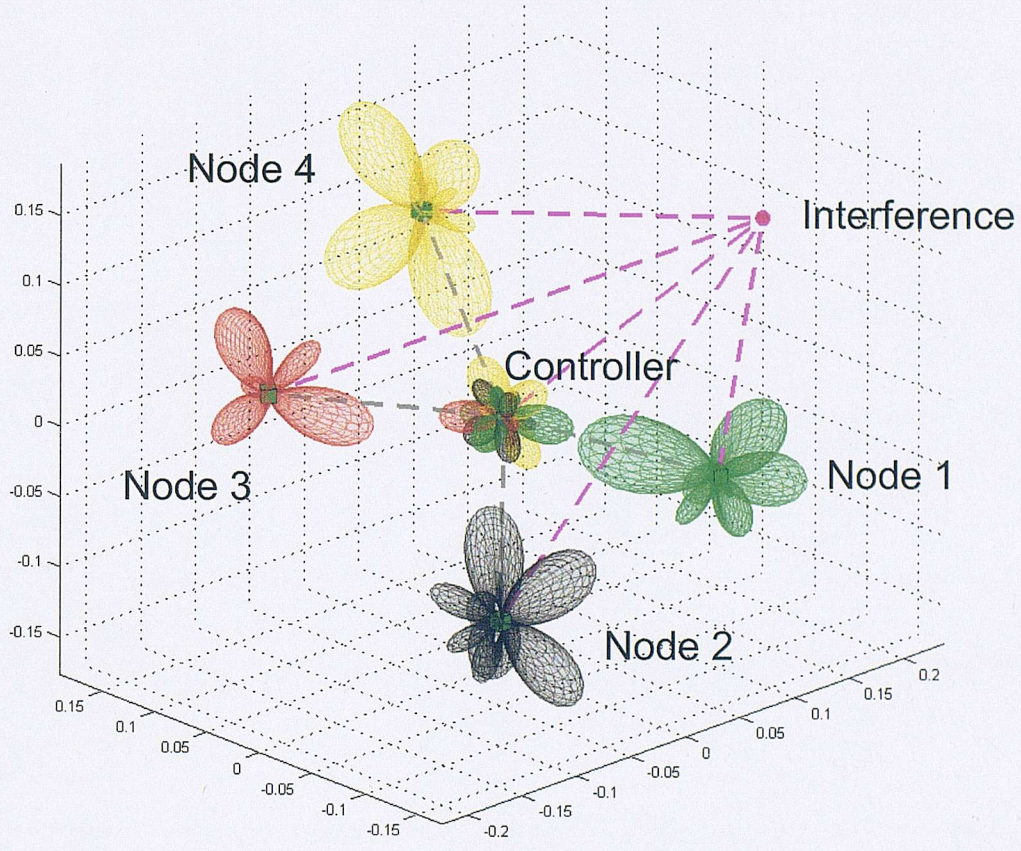


Figure 4.10: The *intra*-wireless array link in operation. the multi-beamforming controller shows the separate beamformers corresponding to each element node in different colours.

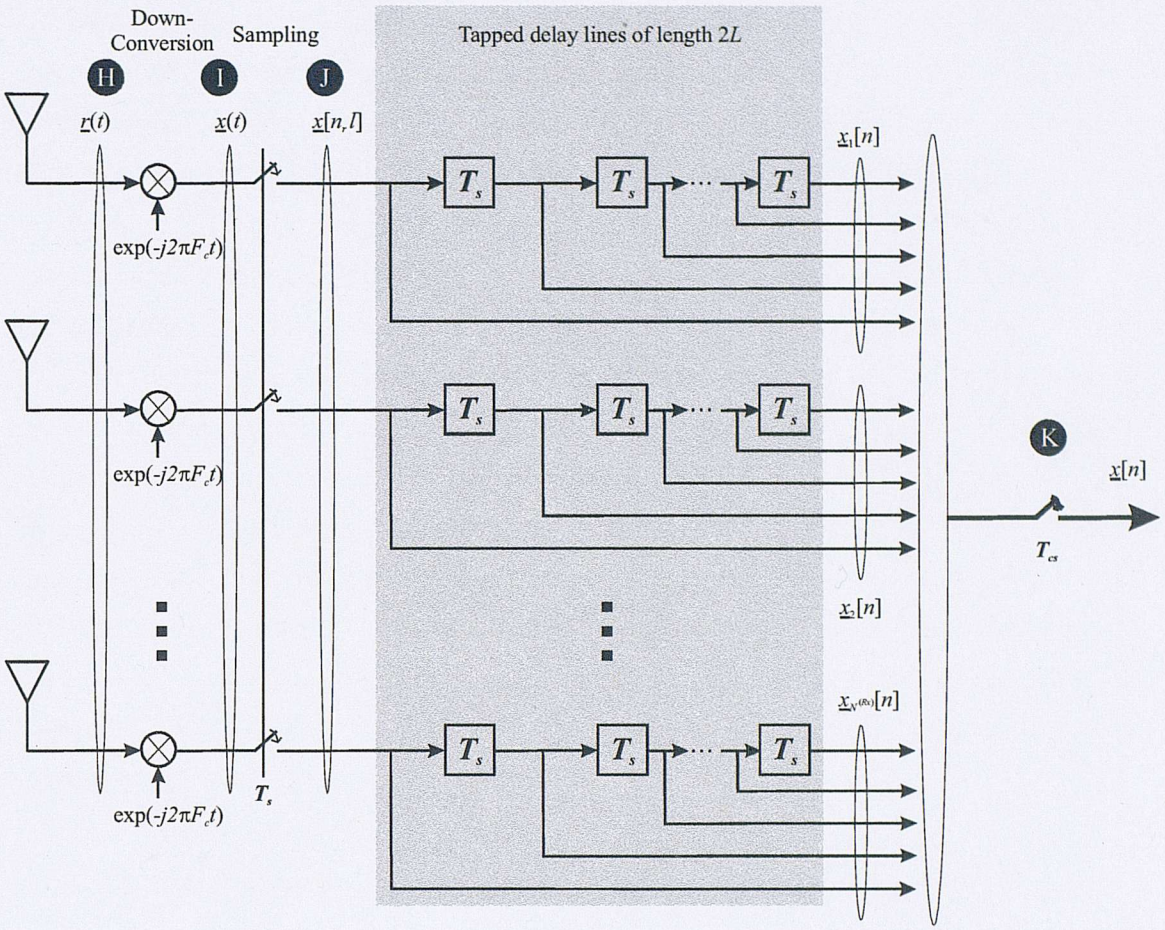


Figure 4.11: The receiver front-end, common for all receiver types considered

4.3 Spatiotemporal Multicarrier DS-CDMA Receiver

In order to ease the description of the multicarrier receiver, each link will not be addressed individually but instead the receiver is going to be studied jointly. As far as this link is concerned, a *Wireless Array* operating in receive or in transmit modes can be viewed as a conventional array whose array processor (the array processing unit of the *Wireless Array* controller) is connected to the array elements through wireless links. This implies that the only parameters that change between the two considered links (*intra* and *inter*-wireless) are the operating and the subcarrier frequencies, the number of antenna elements used and the array geometries involved. Furthermore when a *Wireless Array* is transmitting, it has the capability to use each transmitting element as a directional transmitter, but this also does not affect the design of the receiver.

Figure 4.11 depicts the outline of an MC-DS-CDMA receiver front-end. The signal is received by an array of $N^{(Rx)}$ elements and the carrier is removed *(point*

H). Then, each antenna's signal is sampled at a rate $\frac{1}{T_s}$ where $T_s = \frac{T_c}{qN_{sc}}$ and q is the oversampling factor *(point J)*. This produces $L = qN_{sc}N_c$ temporal samples per channel symbol. The sampling results in the quantisation of the delay τ_{ij} of the j^{th} path into an integer multiple l_{ij} also leaving a fractional part ρ_{ij}, i.e. $\tau_{ij} = (l_{ij} + \rho_{ij})T_s$. If the assumption that any path has a delay smaller than a symbol period is made then l_{ij} is constrained so that $l_{ij} \in \{0, 1, ..., L-1\}$. The fractional part ρ_{ij} introduces a phase shift $\exp(-j2\pi F_k \rho_{ij} T_s)$ to the signal of the i^{th} path, which is absorbed into the complex path coefficient $\mathbb{B}_{ijk}$. The front-end of the receiver incorporates a bank of $N^{(Rx)}$ tapped delay lines to compensate for the lack of synchronisation between transmitter and receiver. The tapped delay lines are of length $2L$ to ensure containment of a whole channel symbol at any time. The contents of the tapped delay lines are read at a rate of $\frac{1}{T_{cs}}$ and are concatenated to form the vector $\underline{x}[n]$ *(point K)*. This vector contains the contributions of all paths for the current symbol and further contributions from the previous and next data symbols. The following modelling is based on the work presented in [59].

The discrete received signal associated with the i^{th} transmitter can then be formed in accordance with Eq. 4.15:

$$\begin{aligned} \underline{x}_i[n] &= \sum_{j=1}^{K_i}\sum_{k=1}^{N_{sc}} \left(\left(\mathbb{B}_{ijk}\left(\underline{w}_{ik}^{(Tx)} \odot \underline{S}_{ijk}^{(Tx)}\right)\right) \odot \underline{S}_{ijk}^{(Rx)}\right) \otimes \qquad (4.21) \\ &\quad \left(\mathbb{J}^T\right)^L \mathbb{J}^{l_{ij}} \underline{\mathfrak{a}}_{ik}[l_{ij}]\, b_i[n-1] + \mathbb{J}^{l_{ij}} \underline{\mathfrak{a}}_{ik}[l_{ij}]\, b_i[n] + \mathbb{J}^L \mathbb{J}^{l_{ij}} \underline{\mathfrak{a}}_{ik}[l_{ij}]\, b_i[n+1] \\ &\in \mathcal{C}^{2LN^{(Rx)}\times 1} \qquad (4.22) \end{aligned}$$

where the vector $\underline{\mathfrak{a}}_{ik}$ includes the PN-sequence $\{\alpha_i[l]\}$of the i^{th} transmitter, takes into account the effect of the k^{th} subcarrier phase shift and is defined as follows:

$$\underline{\mathfrak{a}}_{ik}[\ell] = \frac{1}{\sqrt{N_c N_{sc}}}\gamma_i[k] \begin{bmatrix} \alpha_i[\lfloor 0 \rfloor] \exp(j2\pi F_k(-\ell)T_s) \\ \alpha_i\left[\left\lfloor \frac{1}{qN_{sc}} \right\rfloor\right] \exp(j2\pi F_k(1-\ell)T_s) \\ \vdots \\ \alpha_i\left[\left\lfloor \frac{L-1}{qN_{sc}} \right\rfloor\right] \exp(j2\pi F_k(L-1-\ell)T_s) \\ 0 \\ 0 \\ \vdots \\ 0 \end{bmatrix} \in \mathcal{C}^{2L\times 1} \qquad (4.23)$$

The pre-multiplication of the vector $\underline{\mathfrak{a}}_{ik}[\ell]$ with the $2L \times 2L$ matrix $\mathbb{J}^\ell$

$$\mathbb{J} = \begin{bmatrix} \underline{0}_{2L-1}^T & 0 \\ \mathbb{I}_{2L-1} & \underline{0}_{2L-1} \end{bmatrix} \qquad (4.24)$$

neatly implements a right (down) shift by ℓ elements accounting for the delay of the path.

Next, the MultiCarrier Spatiotemporal Array (MC-STAR) manifold vector will be defined, which is a function of the angle of reception, subcarrier, delay, and PN-sequences. In particular, the spatiotemporal array manifold vector incorporates the receiver's spatial array manifold vector for the j^{th} path and k^{th} subcarrier, $\underline{S}_{ijk}^{(Rx)}$, as well as the temporal vector $\mathbb{J}^{l_{ij}}\underline{\mathfrak{a}}_{ik}[l_{ij}]$, and is defined as follows:

$$\underline{\mathfrak{h}}_{ijk} = \underline{S}_{ijk}^{(Rx)} \otimes \mathbb{J}^{l_{ij}}\underline{\mathfrak{a}}_{ik}[l_{ij}] \in \mathcal{C}^{2LN^{(Rx)}\times 1} \tag{4.25}$$

Using the above definition in conjunction with the property

$$(\underline{a} \odot \underline{b}) \otimes \underline{c} = (\underline{a} \otimes \underline{c}) \odot (\underline{b} \otimes \underline{1}_c) \tag{4.26}$$

where c is the length of $\underline{c}$.

Eq.4.21 can be expressed as a function of the MC-STAR manifold vector of the i^{th} transmitter, j^{th} path, k^{th} subcarrier $\underline{\mathfrak{h}}_{ijk}$ as follows:

$$\underline{x}_i[n] = \sum_{j=1}^{K_i}\sum_{k=1}^{N_{sc}} \begin{pmatrix} \mathbb{J}_{prev}\left(\underline{\mathfrak{h}}_{ijk} \odot \mathbb{B}_{ijk}\left(\underline{w}_{ik}^{(Tx)} \odot \underline{S}_{ijk}^{(Tx)}\right) \otimes \underline{1}_{2L}\right) b_i[n-1] \\ + \left(\underline{\mathfrak{h}}_{ijk} \odot \mathbb{B}_{ijk}\left(\underline{w}_{ik}^{(Tx)} \odot \underline{S}_{ijk}^{(Tx)}\right) \otimes \underline{1}_{2L}\right) b_i[n] \\ \mathbb{J}_{next}\left(\underline{\mathfrak{h}}_{ijk} \odot \mathbb{B}_{ijk}\left(\underline{w}_{ik}^{(Tx)} \odot \underline{S}_{ijk}^{(Tx)}\right) \otimes \underline{1}_{2L}\right) b_i[n+1] \end{pmatrix} \tag{4.27}$$

where

$$\begin{aligned} \mathbb{J}_{prev} &= \left(\mathbb{I}_N \otimes \left(\mathbb{J}^T\right)^L\right) \in \mathcal{C}^{2LN^{(Rx)}\times 1} \\ \mathbb{J}_{next} &= \left(\mathbb{I}_N \otimes \mathbb{J}^L\right) \in \mathcal{C}^{2LN^{(Rx)}\times 1} \end{aligned}$$

A more compact form of expressing Eq. 4.27 is

$$\underline{x}_i[n] = \left[\, \mathbb{J}_{prev}\left(\mathbb{T}_i \odot \mathbb{H}_i\right)\underline{1}_{N_{sc}K_i},\ \left(\mathbb{T}_i \odot \mathbb{H}_i\right)\underline{1}_{N_{sc}K_i},\ \mathbb{J}_{next}\left(\mathbb{T}_i \odot \mathbb{H}_i\right)\underline{1}_{N_{sc}K_i}\right] \tag{4.28}$$

$$\begin{bmatrix} b_i[n-1] \\ b_i[n] \\ b_i[n+1] \end{bmatrix} \tag{4.29}$$

In the above expression the matrix $\mathbb{T}_i$ includes the i^{th} transmitter's manifold vectors and weights as well as the path coefficients for all subcarriers and paths. This matrix is defined as follows

$$\mathbb{T}_i = \left[\mathbb{T}_{i1},\ \mathbb{T}_{i2},\ \cdots,\ \mathbb{T}_{iK_i}\right] \in \mathcal{C}^{2LN^{(Rx)}\times N_{sc}K^{(i,b)}} \tag{4.30}$$

$$\text{where } \mathbb{T}_{ij} = \left[\, \mathbb{B}_{ij1}\left(\underline{w}_{i1}^{(Tx)} \odot \underline{S}_{ij1}^{(Tx)}\right) \otimes \underline{1}_{2L} \quad \mathbb{B}_{ij2}\left(\underline{w}_{i2}^{(Tx)} \odot \underline{S}_{ij2}^{(Tx)}\right) \otimes \underline{1}_{2L} \quad \cdots \quad \mathbb{B}_{ijN_{sc}}\left(\underline{w}_{iN_{sc}}^{(Tx)} \odot \underline{S}_{ijN_{sc}}^{(Tx)}\right) \otimes \underline{1}_{2L} \,\right] \tag{4.31}$$

In a similar fashion the matrix $\mathbb{H}_i$, can then be modelled in a very compact way as:

$$\begin{aligned} \mathbb{H}_i &= \left[\mathbb{H}_{i1},\ \mathbb{H}_{i2},\ \cdots,\ \mathbb{H}_{iK(i,b)}\right] \in \mathcal{C}^{2LN^{(Rx)}\times N_{sc}K_i} \\ \text{where } \mathbb{H}_{ij} &= \left[\underline{\mathfrak{h}}_{j1},\ \underline{\mathfrak{h}}_{j2},\ \cdots,\ \underline{\mathfrak{h}}_{jN_{sc}}\right] \in \mathcal{C}^{2LN^{(Rx)}\times N_{sc}} \end{aligned} \tag{4.32}$$

From now on the vector $(\mathbb{T}_i \odot \mathbb{H}_i)\,\underline{1}_{N_{sc}K_i}$ will be known as the composite channel vector $\underline{h}_i$ i.e.

$$\underline{h}_i \triangleq (\mathbb{T}_i \odot \mathbb{H}_i)\,\underline{1}_{N_{sc}K_i} \in \mathcal{C}^{2LN^{(Rx)}\times 1} \tag{4.33}$$

Note that the vector $\underline{1}_{N_{sc}K_i}$ implements the summation of all paths, all subcarriers.

Using the above definitions the overall signal vector $\underline{x}[n] \in \mathcal{C}^{2LN^{(Rx)}\times 1}$ due to M transmitters at *point K* can be expressed as

$$\underline{x}[n] = \sum_{i=1}^{M} \underline{x}_i[n] + \underline{\mathrm{n}}[n] \tag{4.34}$$

$$= \sum_{i=1}^{M} \left[\ \mathbb{J}_{prev}\underline{h}_i,\ \ \underline{h}_i,\ \ \mathbb{J}_{next}\underline{h}_i\ \right] \begin{bmatrix} b_i[n-1] \\ b_i[n] \\ b_i[n+1] \end{bmatrix} + \underline{\mathrm{n}}[n] \tag{4.35}$$

or, more compactly:

$$\underline{x}[n] = \mathbb{H}\underline{b}[n] + \underline{\mathrm{n}}[n] \tag{4.36}$$

where

$$\mathbb{H} = \left[\ \mathbb{J}_{prev}\overline{\mathbb{H}},\ \ \overline{\mathbb{H}},\ \ \mathbb{J}_{next}\overline{\mathbb{H}}\ \right] \tag{4.37}$$

$$\overline{\mathbb{H}}[n] = \left[\ \underline{h}_1,\ \ \underline{h}_2,\ \ \ldots,\ \ \underline{h}_M\ \right] \tag{4.38}$$

$$\underline{b}[n] = \left[\ \underline{b}'[n-1]^T,\ \ \underline{b}'[n]^T,\ \ \underline{b}'[n+1]^T\ \right]^T \tag{4.39}$$

$$\underline{b}'[n] = \left[\ b_1[n],\ \ b_2[n],\ \ \ldots,\ \ b_M[n]\ \right] \tag{4.40}$$

The vector $\underline{x}[n]$ is fed (see Figure 4.12) into the array processor which in turn can calculate a weight matrix

$$\mathbb{W}^{(Rx)} = \left[\underline{w}_1^{(Rx)},\ \ \underline{w}_2^{(Rx)},\ \ \ldots,\ \ \underline{w}_M^{(Rx)}\right] \in \mathcal{C}^{2LN^{(Rx)}\times M} \tag{4.41}$$

Each column of $\mathbb{W}^{(Rx)}$, by operating on $\underline{x}[n]$, will result in a decision variable $d_i[n]$- one decision variable per transmitter. Based on the $M \times 1$ decision variable vector $\underline{d}[n]$ i.e.

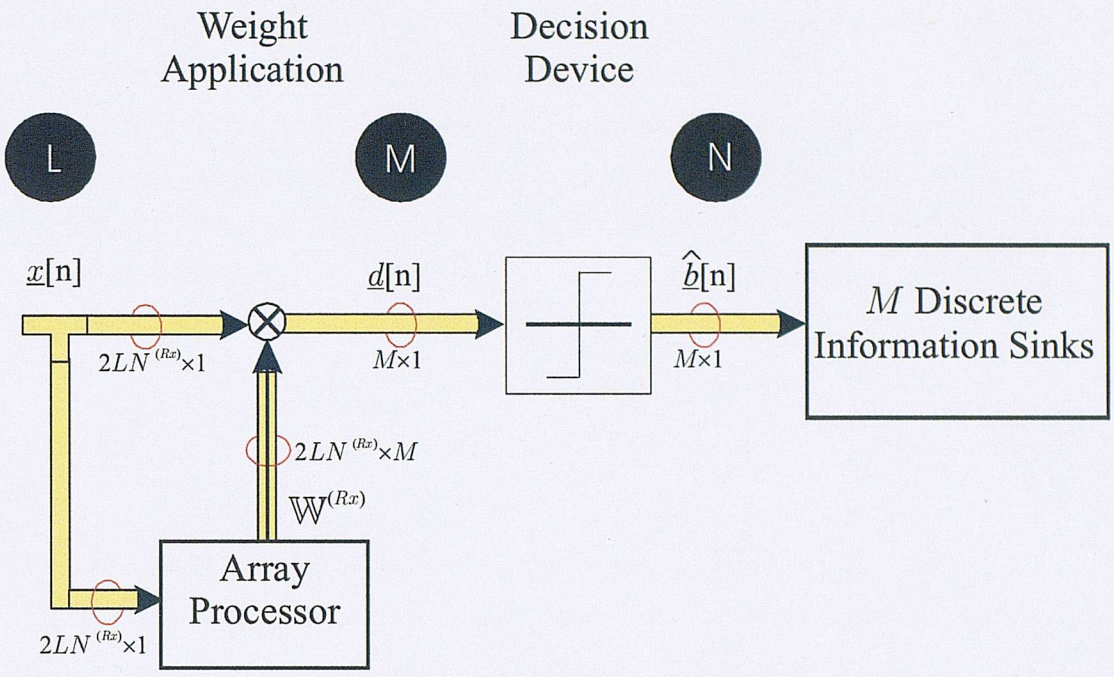


Figure 4.12: Main blocks of a MC-DS-CDMA receiver

$$\underline{d}[n] = \mathbb{W}^{(Rx)\,H}\,\underline{x}[n] \tag{4.42}$$

the data-symbol vector $\underline{b}[n]$ will be detected at the output of the decision-device, where its i^{th} element being the data-symbol of the i^{th} transmitter.

The way the array processor determines the appropriate weights for a specific transmitter reception defines the type of the receiver processor and will be discussed in the next sections. For the *inter-Wireless Array* link and the *intra-Wireless Array* downlink, it is usually the case that only one transmitter needs to be received while in the *intra-Wireless Array* uplink (and in later reference in the *initial* link), it may be necessary to receive and process signals from many transmitters at the same time. The RAKE receiver is a single-transmitter receiver in the sense that it needs channel information only about the received transmitter treating the other transmitters as additive white Gaussian noise. The other two receivers considered in this study, are multiuser receivers, they need complete channel information in order to operate. It must be noted that due to the above mentioned requirements in the *intra-Wireless Array* link, multiuser receivers are more suitable to the Arrayed-WSN. In the following, the desired transmitter is *transmitter* 1.

In order to construct the reception weights, the composite channel vector of at least the desired transmitter must be estimated. The following part of this section presents a way to estimate the channel composite vector of transmitter i.

Using the second order statistics of the vector $\underline{x}[n]$ and specifically by the eigenvalue decomposition of the covariance matrix $\mathbb{R}_{xx} \triangleq \mathcal{E}\{\underline{x}[n]\underline{x}^H[n]\}$ the signal subspace basis can be formed. This is a matrix $\mathbb{E}_s$ with the $3M_{total}$ signal eigenvectors as columns (three eigenvectors per transmitter, corresponding to the current, previous and next symbols contributions). The composite channel vector of the 1^{st} transmitter (desired), belongs to the space spanned by the columns of $\mathbb{E}_s$, that is:

$$\underline{h}_1 \in \mathcal{L}\{\mathbb{E}_s\} \tag{4.43}$$

or equivalently:

$$\mathbb{P}_s\underline{h}_1 = \underline{h}_1 \tag{4.44}$$

where $\mathbb{P}_s$ is the projection matrix to the signal subspace i.e. $\mathbb{P}_s = \mathbb{E}_s\mathbb{E}_s^H$.

However, it can be proved that $\underline{h}_1$ also belongs to the subspace spanned by the columns of the code matrix $\mathbb{C}_1$. The matrix $\mathbb{C}_1$ is formed by concatenating the submatrices $\mathbb{C}_{1k}[\ell]$ defined as

$$\mathbb{C}_{1k}[\ell] = \mathbb{I}_N \otimes \left(\mathbb{J}^\ell \underline{a}_{1k}[\ell]\right) \tag{4.45}$$

for $k = 0, 1, ..., N_{sc} - 1$, $\ell = 0, 1, ..., L - 1$. This implies that

$$\underline{h}_1 \in \mathcal{L}\{\mathbb{C}_1\} \tag{4.46}$$

or equivalently

$$\mathbb{P}_{\mathbb{C}_1}\underline{h}_1 = \underline{h}_1$$

Since the code matrix does not have full column rank, the projection matrix $\mathbb{P}_{\mathbb{C}}$ is

$$\mathbb{P}_{\mathbb{C}_1} = \mathbb{C}_1 \left(\mathbb{C}_1^H\mathbb{C}_1\right)^{\#} \mathbb{C}_1^H \tag{4.47}$$

It is important to point out that not only both spaces $\mathcal{L}\{\mathbb{E}_s\}$ and $\mathcal{L}\{\mathbb{C}_1\}$ contain the desired transmitter channel vector $\underline{h}_1$, but also their intersection uniquely defines the subspace spanned by $\underline{h}_1$. That is

$$\mathcal{L}\{\underline{h}_1\} = \mathcal{L}\{\mathbb{C}_1\} \cap \mathcal{L}\{\mathbb{E}_s\} \tag{4.48}$$

One approach that can yield the intersection of these two spaces is the alternate projection algorithm which will provide a scaled version of the desired vector $\underline{h}_1$. It can be proven that this approach is equivalent to estimating the eigenvector that corresponds to the largest eigenvalue of the matrix $\mathbb{P}_s\mathbb{P}_{\mathbb{C}_1}$ that is

$$\underline{h}_1 = \underline{eig}_{\max}(\mathbb{P}_s\mathbb{P}_{\mathbb{C}_1})$$

4.3.1 3D RAKE Receiver

The RAKE [60] receiver is the simplest receiver considered here. Its operation is based on the constructive combination of all the received paths of the desired transmitter. The receiver considered here is a 3D receiver in the sense that it combines the paths along the temporal, spatial and multicarrier dimensions. The RAKE constructed weight vector maximises the SNR at the output of the receiver.

In order to construct the 3D RAKE weight vector, the composite channel vector of the desired transmitter (which reflects all the effects of the radio channel to the data stream) is needed. In order to estimate this vector, the aforementioned subspace approach can be employed.

The weight vector for the 3D RAKE receiver can be formed by the following:

$$\underline{w}_1^{(Rx)} = \widehat{\underline{h}}_1 \tag{4.49}$$

where $\widehat{\underline{h}}_1$ is the estimated composite channel vector of the desired user. The RAKE receiver will provide maximisation of the SNR at the receiver output but will not effectively suppress interferences. Since an Arrayed-WSN is a heavy interference environment, the RAKE receiver may not provide the best implementation for the design of the communication link. Next a superresolution receiver with high interference suppression capabilities is discussed.

In order to receive multiple users at the same time a weight matrix needs to be constructed by

$$\mathbb{W}^{(Rx)} = \left[\underline{w}_1^{(Rx)}, \ \ldots, \ \underline{w}_i^{(Rx)}, \ \ldots, \ \underline{w}_M^{(Rx)} \right] \tag{4.50}$$

4.3.1.1 Linear Block Receiver for Complete (asymptotically) Interference Cancellation

In order to form a more advanced receiver, estimation of the channel vectors for all users is needed. In this way the interference due to other channel accessors (MAI) and the inter-symbol interference (ISI) due to the desired transmitter's later and earlier symbols can be asymptotically completely cancelled while all the paths of the desired transmitter current symbol are constructively combined. This can be done by projecting the RAKE weight vector to a subspace orthogonal to the interference subspace [54].

If all the estimated composite channel vectors $\widehat{\underline{h}}_i$ are estimated by using the procedure described in the previous section, the interference subspace of the de-

sired user, $\mathcal{L}\{\widehat{\mathbb{H}}_{1,int}\}$, can be modelled by defining

$$\widehat{\mathbb{H}}_{1,int} = \left[\mathbb{J}_{prev}\widehat{\mathbb{H}},\ \overline{\mathbb{H}}_1,\ \mathbb{J}_{next}\widehat{\mathbb{H}} \right] \tag{4.51}$$

where

$$\widehat{\mathbb{H}} = \left[\underline{\widehat{h}}_1, \underline{\widehat{h}}_2, ..., \underline{\widehat{h}}_M\right] \in \mathcal{C}^{2LN^{(Rx)}\times M} \tag{4.52}$$

contains the estimated composite channel vectors of all the transmitters and

$$\overline{\mathbb{H}}_1 = \left[\underline{\widehat{h}}_2, \underline{\widehat{h}}_3, ..., \underline{\widehat{h}}_M\right] \in \mathcal{C}^{2LN^{(Rx)}\times M-1} \tag{4.53}$$

contains the estimated composite channel vectors of only the interfering transmitters.

The projection to a subspace orthogonal to this subspace can be implemented by the orthogonal projection matrix $\mathbb{P}^{\perp}_{\widehat{\mathbb{H}}_{int}}$:

$$\mathbb{P}^{\perp}_{\widehat{\mathbb{H}}_{1,int}} = \mathbb{I}_{2NL} - \widehat{\mathbb{H}}_{1,int}\left(\widehat{\mathbb{H}}_{1,int}{}^{H}\widehat{\mathbb{H}}_{1,int}\right)^{-1}\widehat{\mathbb{H}}_{1,int}{}^{H} \tag{4.54}$$

and the appropriate weight of the receiver is given by

$$\underline{w}_1^{(Rx)} = \mathbb{P}^{\perp}_{\widehat{\mathbb{H}}_{1,int}}\underline{\widehat{h}}_1 \tag{4.55}$$

This receiver is optimal according to the Signal to Interference Ratio (SIR) criterion which is a more appropriate measure for the signal environment described by the Arrayed-WSN specifications. In order to receive more than one transmitter simultaneously, a weight matrix $\mathbb{W}^{(Rx)}$ needs to be constructed as in Eq. 4.50 i.e. $\mathbb{W}^{(Rx)} = \left[\ \underline{w}_1^{(Rx)},\ ...,\ \underline{w}_i^{(Rx)},\ ...,\ \underline{w}_M^{(Rx)}\ \right]$.

4.3.2 MMSE Block Linear Receiver

A minimum mean square error (MMSE) receiver [61] is a more complex implementation that maximises the SNIR at the output. A multiuser implementation of the MMSE receiver is going to be discussed in this section; by constructing an appropriate weight matrix, all the transmitters signals can be received in one step [59].

The weight matrix that satisfies the MMSE criterion is given by

$$\mathbb{W}^{(Rx)} = \arg\min_{\mathbb{W}^{(Rx)}} \mathcal{E}\left\{\left\|\underline{b}[n] - \mathbb{W}^{(Rx)\,H}\,\underline{x}[n]\right\|^2\right\} \tag{4.56}$$

which using the signal model can be found by

$$\mathbb{W}^{(Rx)} = \mathbb{R}_{xx}^{-1}\widehat{\mathbb{H}} \in \mathcal{C}^{2LN^{(Rx)}\times M} \tag{4.57}$$

With $\widehat{\mathbb{H}}$ as defined in Eq. 4.52. Substituting for $\mathbb{R}_{xx}$, and assuming completely uncorrelated symbols between accessors and white noise gives:

$$\mathbb{W}^{(Rx)}=\widehat{\mathbb{H}}\left(\widehat{\mathbb{H}}^{H}\widehat{\mathbb{H}}+\sigma^{2}\mathbb{I}_{M}\right)^{-1} \in \mathcal{C}^{2LN^{(Rx)}\times M} \tag{4.58}$$

where σ^2 represents the noise power. The next chapter discusses the computer simulation results that present the performance of the described receiver designs, when applied to different Arrayed-WSN communication links, in juxtaposition.

4.4 Computer Simulation Studies

The three receivers discussed in the previous section were implemented and their performance for the *inter* and *intra*-wireless links was simulated in a computer generated environment. The environment consisted of stationary city objects (as buildings) and a large number of randomly placed scatterers. The radio channel characteristics for any two given nodes were generated by a ray-tracing program. This provided the angles of transmitted and received radio waves, the fading coefficients and the delays for all paths between any two nodes in the network. These characteristics were assumed constant throughout the simulations which implies that only stationary scatterers were considered. Although scatterers in real environments may include motion, that motion is expected to be slow compared to the symbol rate, so that most dominant paths do not change significantly within many channel symbol periods and Doppler effects can be completely ignored. The *Local Array* on each node was taken to consist of 6 elements, forming a 3D grid array as described in Section 2.1. The number of subcarriers was $N_{sc} = 4$ and the PN-codes used were of length 15.

4.4.1 *Intra-Wireless Array* Link

The channel fading and multipath parameters mentioned before were generated using MATLAB interfaced to a ray-tracing tool (Radiowave Propagation Simulator - RPS v5.1.4). A basic urban environment was simulated using the sample 3D building database provided with RPS, augmented by 100 randomly placed blocks to act as additional scatterers within the region of interest. Five hundred nodes were then created within a 100 m by 100 m region of this environment with (x,y) positions identical to those used in the example of the previous chapter apart from a scaling factor and a translation. However, the height of each node was adjusted based on the terrain such that nodes rest on rooftops and not inside buildings. Then for each node, a transmitter and receiver were created in the

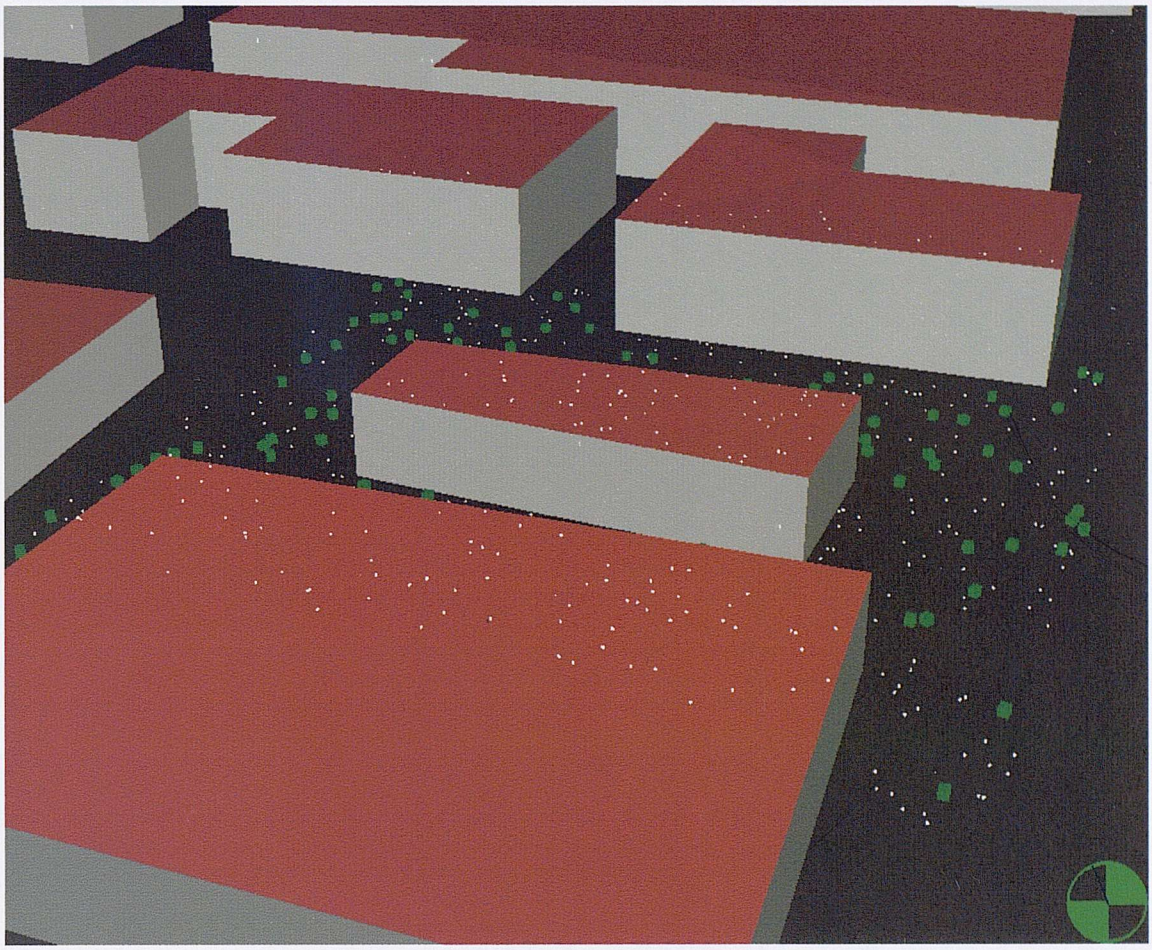


Figure 4.13: Simulated A-WSN Environment

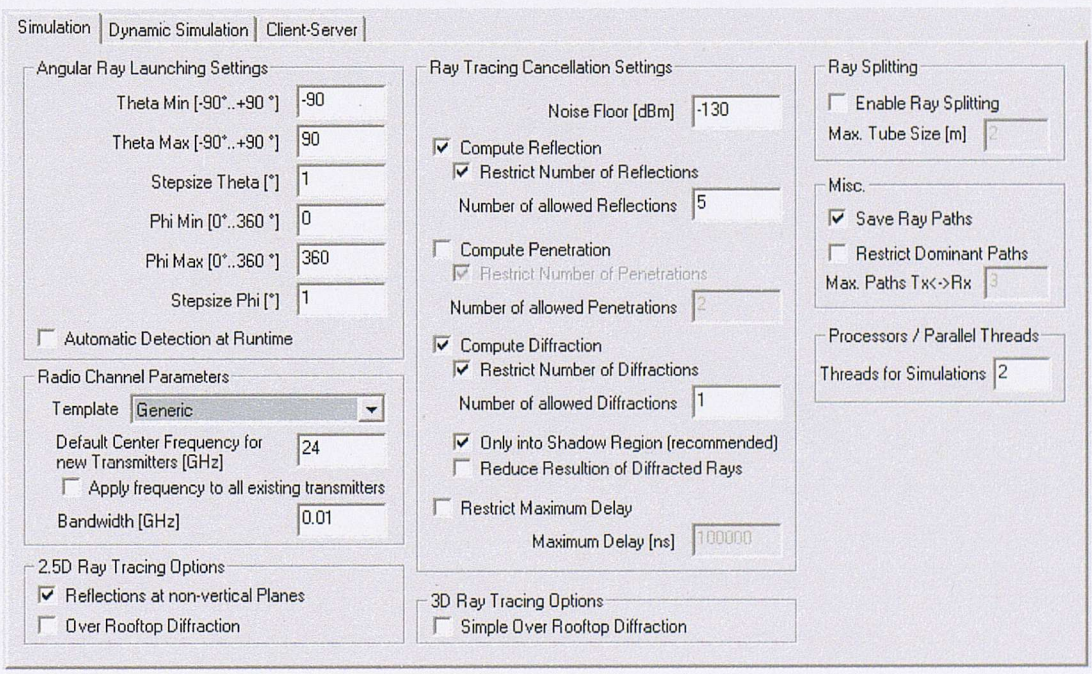


Figure 4.14: Raytracing parameters for the Intra Wireless Array channel

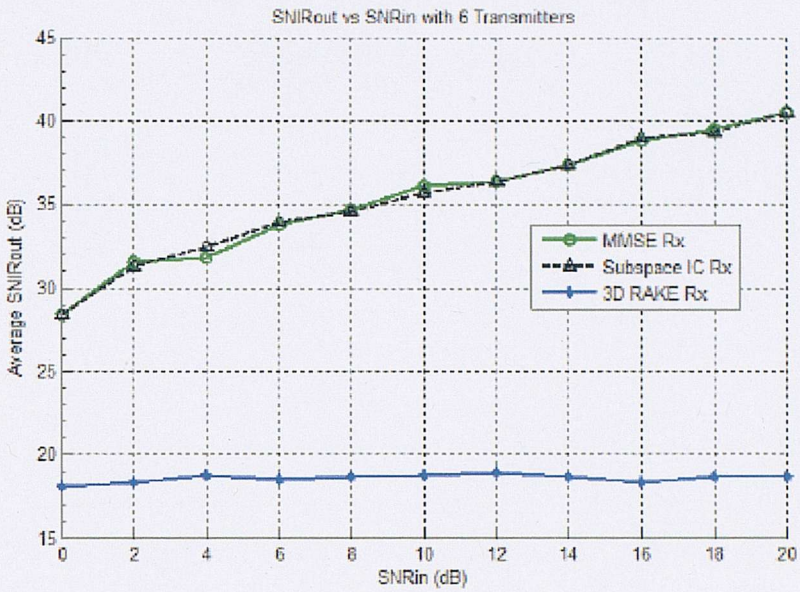


Figure 4.15: DOWNLINK *intra* wireless array - SNIR at the output of the receiver operating in in the presence of 4 interferers (plotted against the SNR_{in})

simulator and their antenna type were set to isotropic. A visualisation of this environment is shown by Figure 4.13, where cyan cubes represent the nodes and green cubes are the additional scatterers.

The ray-tracing parameters were then set as shown in Figure 4.14 and full 3D ray-tracing was performed at 24GHz. Note that RPS uses "Theta" for elevation and "Phi" for azimuth which is the opposite to the notation used elsewhere in this study. In addition, the bandwidth parameter is only used for additional analysis and doesn't impact the results of the simulation.

For each transmitting/receiving node pair the corresponding multipath parameters were then exported from the ray-tracer into MATLAB in order to be used in the simulations described later in this chapter.

The *intra-Wireless Array* link was simulated for both uplink and downlink cases for the same *Wireless Array*. When a *Wireless Array* is operating, its internal communications may be disrupted by another *Wireless Array* operating near-by or by an intentional jammer. As a representative example, the following parameters were chosen. The symbol period, $T_{cs} \approx 4\ \mu s$, was chosen so that the maximum delay for any path in the network was still smaller than a whole symbol period. Using a PN-code of length 15 and no oversampling at the receiver resulted in chip rate $T_c \approx 300\ ns$ and a sampling rate $T_s \approx 70\ ns$ and the carrier frequency was set to 24 GHz. The nodes to form the *Wireless Array* to be tested

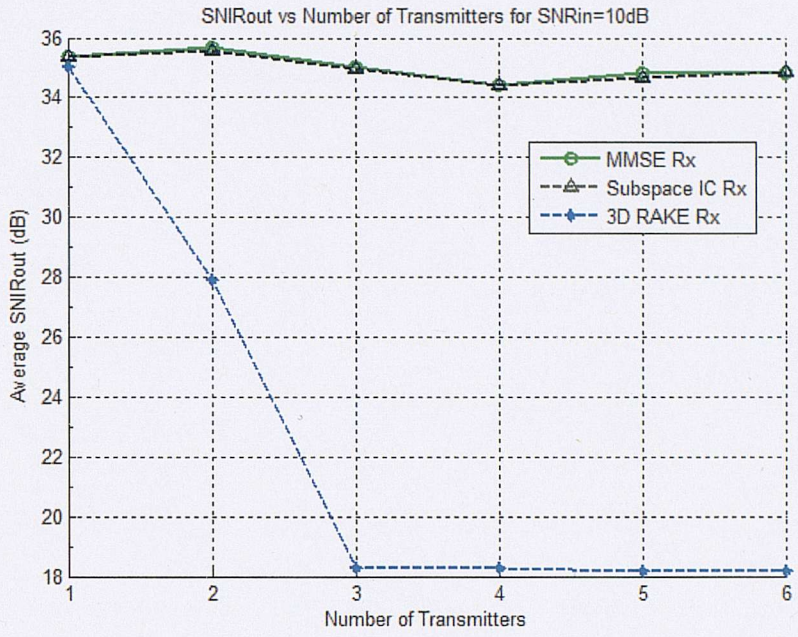


Figure 4.16: DOWNLINK *intra* wireless array - SNIR at the output of the receiver at a fixed $SNR_{in} = 10$ dB (plotted against the number of external interferers)

were chosen by using the selection algorithm of Chapter 3. Any interferers were assumed to transmit with the same power as the desired transmitter.

The downlink part of this link is the case where the *Wireless Array* controller is transmitting to one or more *Wireless Array* nodes. This means that there is only one transmitter within the *Wireless Array* and all interfering sources are external. Figures 4.15 and 4.16 present results for the simulations of the downlink of the *intra-Wireless Array* operation.

When a constant number of 4 external interferers (interfering nodes not belonging to the *Wireless Array*) were considered and the SNR at the input of the receiver was varied from 0 dB to 20 dB the RAKE receiver was observed to yield a constant low performance as far as the output SNIR is concerned. This is because the RAKE receiver does not have the capability to cancel any interfering sources, unlike the other two receivers considered. Indeed as Figure 4.15 illustrates the RAKE receiver produces a constant SNIR of about 10 dB while the other two receivers have similar performance starting approximately 16 dB above the RAKE and rising with increasing input SNR.

When the number of external interferers was varied while the input SNR was kept constant (10 dB) the SNIR at the output was constant and similar for the MMSE and super-resolution receiver. The RAKE receiver under-performed the other two by a large margin except for the case when no interferers were

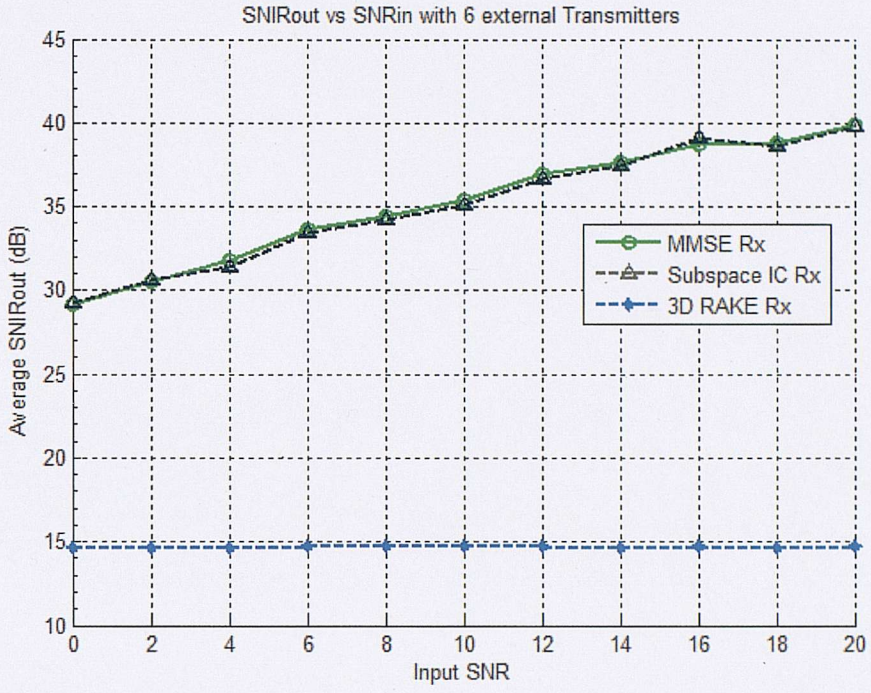


Figure 4.17: UPLINK *intra* wireless array - SNIR at the output of the receiver operating in the presence of 4 interferers (plotted against the SNR_{in})

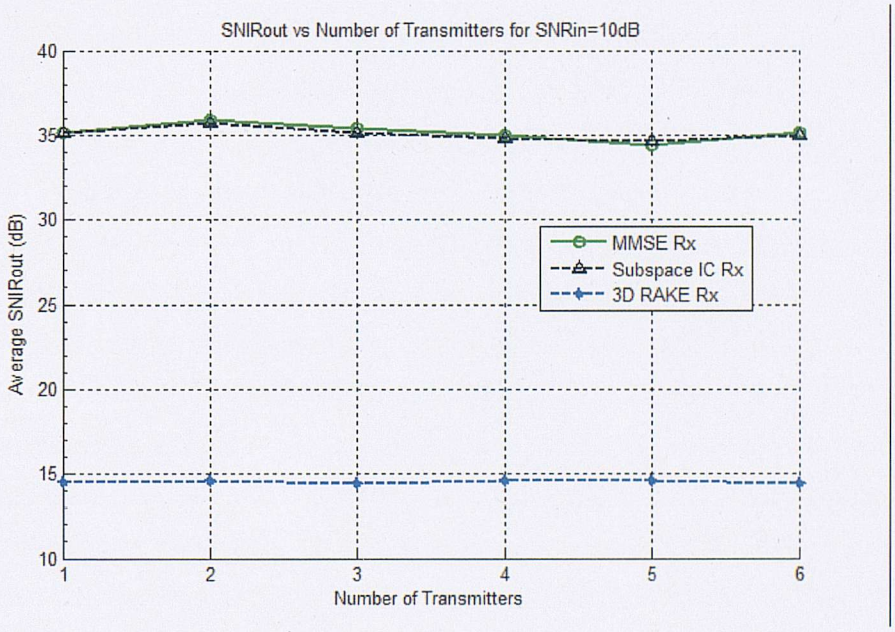


Figure 4.18: UPLINK *intra* wireless array - SNIR at the output of the receiver at a fixed SNR_{in}=10 dB (plotted against the number of external interferers)

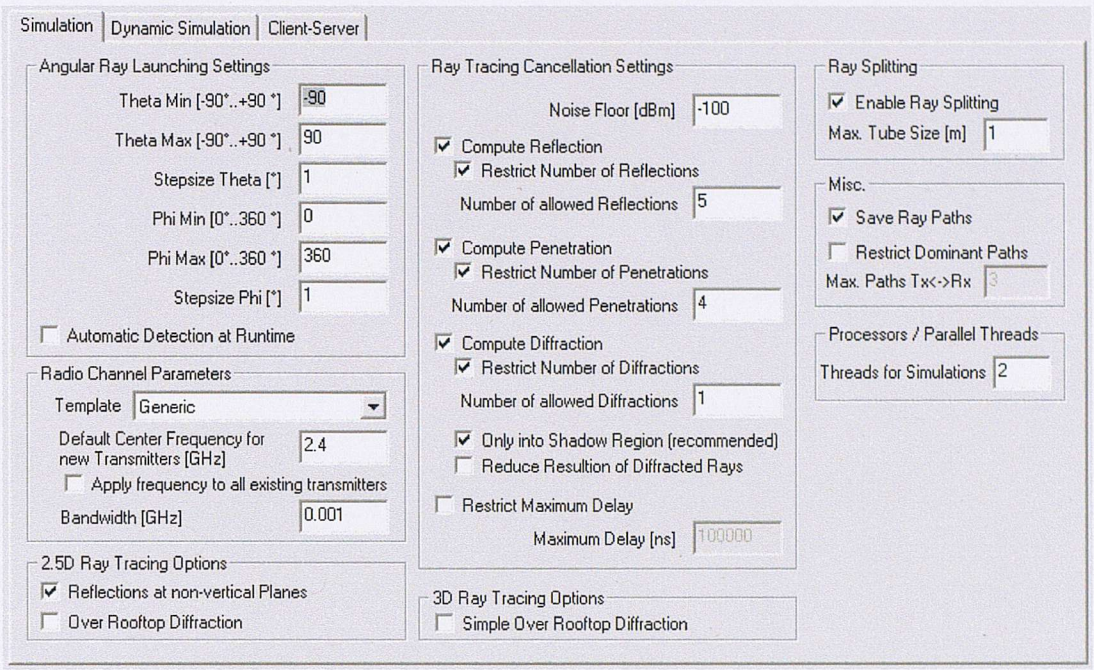


Figure 4.19: Raytracing parameters for the Inter Wireless Array channel

present, where the performances were comparable. This also exhibits the near-far resistance capabilities of the MMSE and the superresolution receiver in the presence of MAI. We have to note here that the performance of the MMSE multiuser receiver, although sub-optimal, is very close to the optimal bound.

The uplink part of this link is the case where the *Wireless Array* nodes transmit to the *Wireless Array* controller. If the focus is on the communication of a single array node to the controller, then the transmissions of the rest of the array nodes can be treated as interferences with known positions. The results of the simulations focusing on the reception of one of the *Wireless Array* nodes are presented in Figures 4.17 and 4.18. In the uplink case the interference is expected to be larger, because all the *Wireless Array* nodes are transmitting simultaneously to a common receiver, the controller. Figures 4.17 and 4.18 illustrate a similar performance as in the downlink case. However, in this case, the interferers in the communication link between an array node and the controller are the other array nodes plus the external interferences. In Figure 4.18 the RAKE receiver is under-performing the other receivers even when no external interferences are considered. This is because even when there are no external interferences, the performance of the receiver is still degraded by the internal interferers.

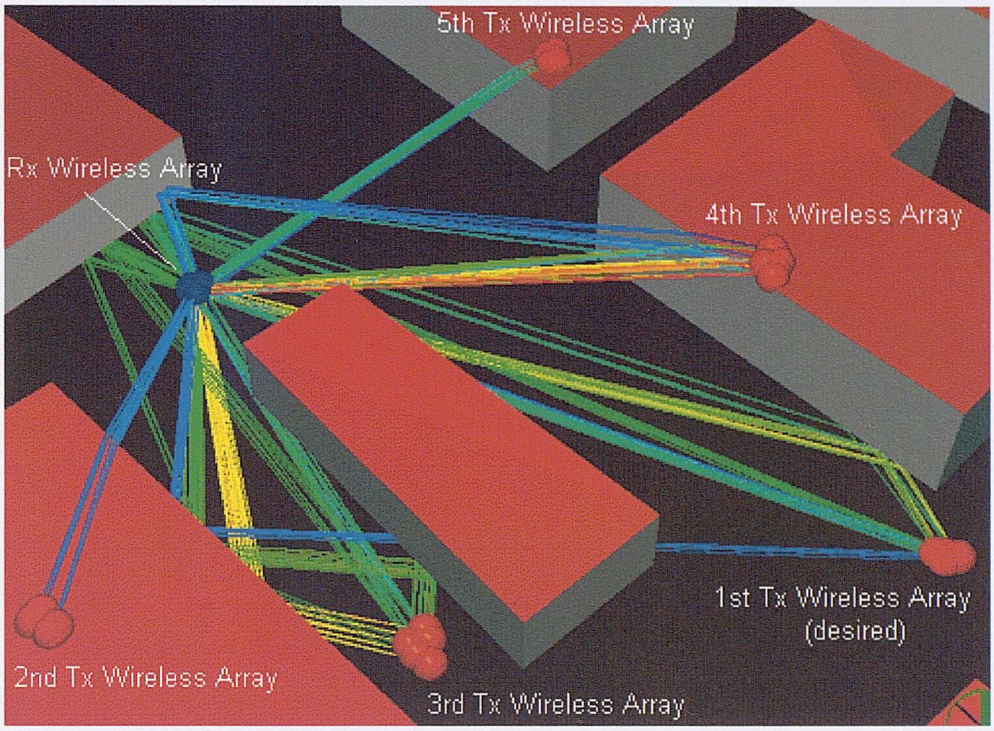


Figure 4.20: Environment for modelling the Inter Wireless Array channel showing the raytracing results

4.4.2 *Inter-Wireless Array* Link

The channel parameters for the *inter-Wireless Array* links were generated in the same manner as for the *intra*-wireless link. However, in order to ensure that the assumptions described above hold, a network of 1000 nodes with random positions within the same 100 m by 100 m region, as before, was generated. That is, a higher node density was used allowing formed *Wireless Arrays* to have smaller apertures. Also, in order to allow a more accurate simulation within a feasible time-frame only the nodes within a small number of *Wireless Arrays* were considered and no clutter was introduced. The 3D environment for this case is shown in Figure 4.20, where the transmitting *Wireless Array* is at the far right and the nodes forming the receiving *Wireless Array* are shown as blue spheres (middle left). Four additional *Wireless Arrays* were also included in order to model interfering transmissions.

The ray-tracing parameters used to generate the results for the *inter*-wireless links are shown in Figure 4.19. Notice that both penetrations and ray splitting have been enabled in this case in order to give a more accurate result over a longer range although the noise floor was raised to -100 dBm to disregard multipaths with negligible power. In addition, the frequency was set to 2.4GHz and full 3D ray-tracing was performed as before (in contrast to 2.5D ray-tracing which only

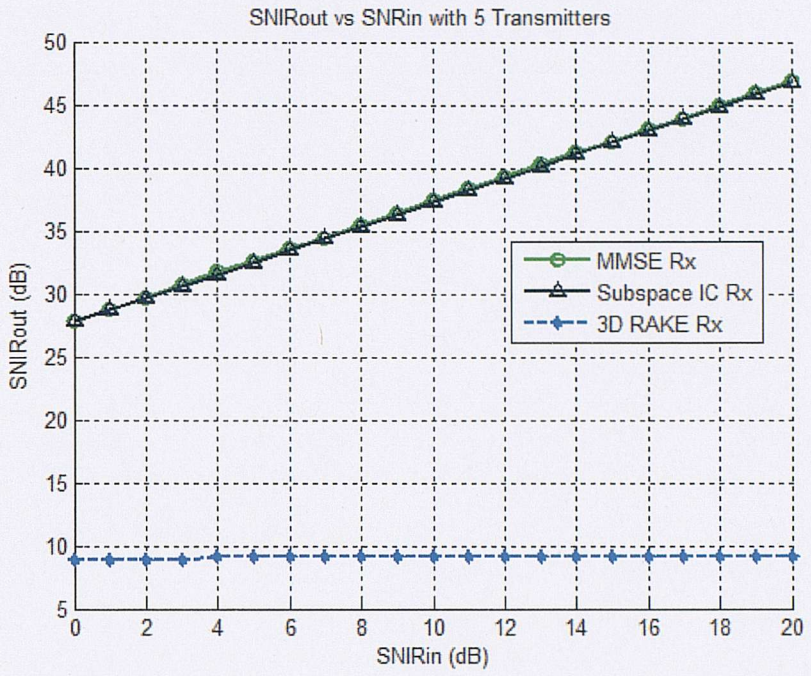


Figure 4.21: *Inter* wireless array - SNIR at the output of the receiver in the presence of 4 interfering wireless arrays (plotted against the SNR_{in})

launches rays over a limited range of angles).

The *inter-Wireless Array* link was simulated for communicating and interfering arrays also selected according to the algorithm of Chapter 3. When two arrays are communicating, interference may come from other arrays communicating in the vicinity or from intentional jammers.

In any case the interference was assumed to have unknown characteristics. Again, the symbol rate was chosen to provide symbol periods greater than the maximum delay in the network resulting in this particular example to $T_{cs} = 3\mu s, T_s \approx 70\ ns, T_c \approx 200\ ns$ with the carrier set to 2.4 GHz. Although the ray-tracing program provides radio channel parameters only for individual nodes, it was observed that these only change slightly between nodes in 2 *Wireless Arrays*. The results for the simulations of the *inter-Wireless Array* link present a similar picture to the *intra-Wireless Array* link. Again the RAKE receiver performs consistently lower than the other two considered receivers in terms of output SNR. The RAKE receiver only performs comparably when no interferences are considered. As far as the other two receivers are concerned they yielded the same results throughout the simulations.

The SNIR at the output of the receiver is plotted against the SNR at the input of the receiver for the *inter-Wireless Array* link, for 5 active transmitting

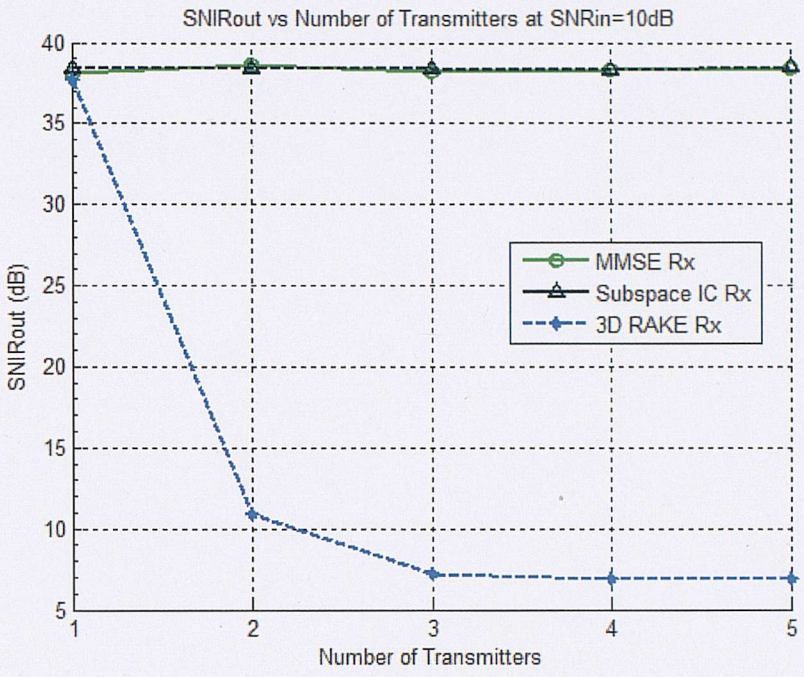


Figure 4.22: *Inter* wireless array - SNIR at the output of the receiver at a fixed SNR_{in}=10 dB (plotted against the number of active transmitting arrays)

arrays

4.5 Conclusion

In this study, the design of the Arrayed-WSN wireless communication links was finalised. The Arrayed-WSN is split according to the type of communication in three communication links: the *initial*, the *intra-Wireless Array* and the *inter-Wireless Array* link. These three links partition the design of the Arrayed-WSN in three different types of problems.

- The *initial* communication link is concerned with all the procedures that need to take place until *Wireless Arrays* are formed. This includes an *initial* network set-up, a potential node localisation procedure and a *Wireless Array* formation algorithm.

- The *intra*-wireless link is concerned with the internal operation of a *Wireless Array*. Synchronisation of nodes, *Wireless Array* control and processing as well as *Wireless Array* calibration are associated with this link.

- The *inter*-wireless link is used for the communication between two *Wireless Arrays*. Directly connected to this are the *Wireless Array* ambiguity space,

the *Wireless Array* relative geometries and the forwarding strategies to be followed.

Up to now, problems involved in all three domains were considered, based on the *initial* design of the communication links. However, in this chapter the communication links sere designed, perfecting the tools that are to be used to tackle any problem within the Arrayed-WSN. The motivation behind the choice of an MC-DS-CDMA approach was discussed and a comprehensive model of a transmitter - channel - receiver was presented.

During this study all three links were considered jointly since, from a communications point of view they experience similar channels. The main differences between the communication links are the operating frequencies and the geometries of the arrays involved. The latter factor has a great implication: when array elements are well separated in space (as in the *inter-Wireless Array* link), each transmitting element may experience a different fading to every receiving element. The model of the channel presented above incorporates this possibility by using a matrix of path coefficients for every channel path between two arrays, and thus allows the joint treatment of all three links.

Three different types of receivers were presented and simulated. The simulations were set-up to model the environment of an Arrayed-WSN as closely as possible. By using a combination of MATLAB and ray-tracing software the performance of the receivers was evaluated. The results suggest that the 3D-RAKE receiver is not suitable for an Arrayed-WSN due to the high-interference environment that such a network experiences. The other two receivers considered, namely the super-resolution and the MMSE receiver, exhibited much better performances in terms of SNIR_{out}. In fact these two receivers cannot be distinguished by their SNIR_{out} performance and thus in order to select one of the two their processing complexity may need to be considered.

Chapter 5

Analysing and Resolving Ambiguities in the Arrayed-WSN

In an array system it is important to be certain that some problems, based on array sensor measurements, have a unique solution. A potentially unresolvable situation might arise if two different sets of signals impinging on the array happen to provide identical responses at the array output. This is an 'abnormality' which is a direct consequence of the geometrical properties of the signal environment and the geometry of the array of sensors. In other words, the array is unable to distinguish, geometrically or otherwise, one set of signals from another. Such phenomena are commonly referred to as ambiguities and are a direct consequence of the behavior of the array manifold which is in turn dictated by the geometrical properties of the array. Thus the behavior of the array manifold, in particular its local geometry, plays an important role in handling ambiguities and also in defining the capabilities (e.g. the resolving power) of an array system. Therefore, it can be said that the manifold ambiguities are resolvable, at least for statistically independent sources.

Such ambiguous situations may arise when a nodes or *Wireless Arrays* operate in the Arrayed-WSN. In such cases, it is important to detect the ambiguous scenario and offer a resolution method. This process should take place in context to WSN concerns such as energy conservation and message exchange limitation. The challenge of this issue is to find an appropriate technique that can effectively remove ambiguities. The MUSIC algorithm, though is an effective approach to direction finding, fails to resolve ambiguity due to the fact that it is a subspace–based technique that primary assumes linear independence amongst the array manifold vectors.

In the next section, a modelling and analysis of the ambiguous space of ar-

rays involved in Arrayed-WSN is presented together with illustrative simulated examples. Several techniques available at the moment will be discussed and a novel method with cooperation of two arrays is proposed in Section 5.2. Finally, in Section 5.3 the chapter is concluded.

5.1 Ambiguities in the Arrayed-WSN

Let us consider a situation where M information sources are transmitting signals that arrive at an array of N sensors simultaneously at time t. The received signal vector $\underline{x}(t) = [x_1(t), \ldots, x_N(t)]^T$ can be modeled as before by

$$\underline{x}(t) = \mathbb{S}(\underline{p})\underline{m}(t) + \underline{n}(t) \tag{5.1}$$

where $\underline{m}(t)$ is a $M \times 1$ vector consisting of the narrow-band, common centre-frequency transmitted signals at the point of reference of the array system, $\underline{n}(t)$ is a $N \times 1$ vector of additive noise, and $\mathbb{S}(\underline{p})$ is an $N \times M$ matrix with columns the manifold vectors i.e.

$$\mathbb{S}(\underline{p}) = [\underline{S}(p_1), \underline{S}(p_2), \ldots, \underline{S}(p_M)] \tag{5.2}$$

An elementary abnormality is the case where two manifold vectors $\underline{S}(p_i), \underline{S}(p_j)$ corresponding to different signal parameters $p_i \neq p_j$, are colinear, i.e.

$$\underline{S}(p_i) = k\underline{S}(p_j) \tag{5.3}$$

In that case an "unresolvable" situation will occur. This is known as a *trivial* ambiguity. On the other hand, a *non–trivial* ambiguity occurs when a manifold vector can be written as a linear combination of two or more other manifold vectors, i.e.

$$\underline{S}(p_i) = k_1\underline{S}(p_1) + k_2\underline{S}(p_2) + \ldots + k_{i-1}\underline{S}(p_{i-1}) \tag{5.4}$$

It is clear that Eq. (5.3) is a special case of Eq. (5.4) and that the presence of an ambiguity reflects on the rank deficiency of the array manifold matrix $\mathbb{S}$, i.e. $\mathbf{rank}(\mathbb{S}(\underline{p})) = \rho < M$.

It was shown in [62] that, under the assumption of linearly independent manifold vectors, the maximum number of sources can be found in terms of number of sensors, number of sources, and rank of source correlation matrix. According to [63], subsequent research mainly focuses on either the performance analysis of specific arrays, or with the constructions of array structures free of ambiguities up to a certain rank. In [64] the fact that increasing the aperture of a circular

array will result in an increase of the risk of having trivial ambiguities is illustrated. In fact, since the aperture of an array directly influences the length of manifold curves, it is directly connected to the number of ambiguities present. In [65], [66], a class of *cross* arrays (the array configuration whose sensors all lie in two non–parallel straight lines) that are free up to rank k ambiguities, where $k \in \{1, 2, \ldots\}$ is introduced.

Approaching the same problem from a different perspective [63], represents ambiguous sets in the form of ambiguous generator set (AGS). The fundamental concept of AGS derived from the arc length rotation property presented in the papers is that for any ambiguous set of arc lengths $\underline{s} = [s_1, s_2, \ldots, s_c]^T$ with rank ρ, the increments of each arc length by $\triangle s$, i.e.

$$\underline{s}^* = [s_1 + \triangle s, s_2 + \triangle s, \ldots, s_c + \triangle s]^T \tag{5.5}$$

will also provide another ambiguous set of arc lengths with the same rank. Two general classes of ambiguous generator sets are identified based on how the manifold curve is partitioned, i.e. in uniform or non–uniform segments. This concept was extended to planar arrays in [67].

It is known that manifold ambiguity arises if the manifold matrix is rank deficient. However, a common misconception is the association of manifold ambiguity with nonidentifiability. In [68], [69], it is suggested that the presence of manifold ambiguities does not always imply nonidentifiability in obtaining the unique and consistent set of DOA's. Indeed, it is the statistical signal model that defines the identifiability condition for each given scenario. It has been proved that for the cases of partially and fully correlated sources, the manifold ambiguous condition leads to nonidentifiability. However, the conditions are different for independent Gaussian source cases. In fact, no nonidentifiable manifold ambiguous scenarios have been observed so far in the literature.

A manifold curve $\mathcal{A}$ is formed by the locus of points in the N dimensional space traced by the array manifold vector as the signal parameter p varies. This eventually maps the whole parameter space $\Omega_p \in \mathcal{R}^1$ to a curve embedded in the N-dimensional space $\mathcal{C}^N$ as described in Section 3.1.

A hyperhelical manifold curve is such a curve $\mathcal{A}$, which has a constant principal curvature. The hyperhelical curves are important because their properties can be expressed analytically [41] and they can be studied to yield a class of ambiguities. Hyperhelical manifold curves are principally a property of linear arrays. However it has been shown that they may also represent a manifold curve embedded on the manifold of planar arrays by using the concept of the ELA expressed in Eq. 3.21. In specific, it has been shown [41] that for a planar array, if the parameter

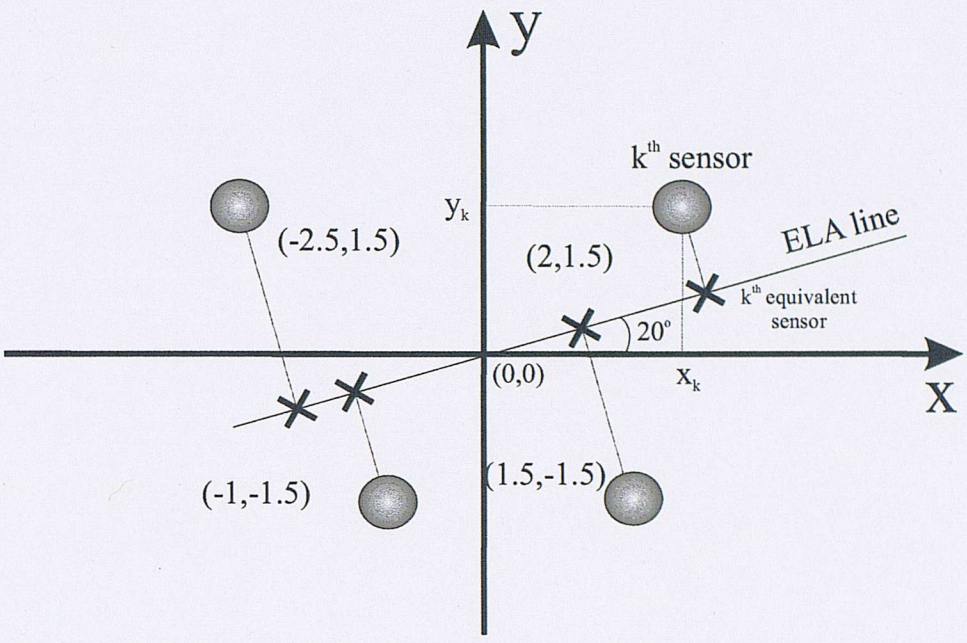


Figure 5.1: The concept of the Equivalent Linear Array for $\theta_0 = 20°$ for a planar array

of interest is chosen such that $p = \phi$, the manifold curve of the planar array is the same as the manifold curve of a specifically chosen linear array (the ELA). The ELA of a planar array with element positions at

$$\mathbf{r} = \begin{bmatrix} -2.5 & -1 & 1.5 & 2 \\ 1.5 & -1.5 & -1.5 & 1.5 \\ 0 & 0 & 0 & 0 \end{bmatrix}$$

is illustrated in Figure 5.1. Since the manifold curves of the two arrays are the same, the ambiguities on these curves will also coincide.

When estimating the parameters of interest p of signals using array sensor measurements, it is important to be certain that the problem has a unique solution. Otherwise, the array cannot distinguish between two (or more) different signal environments. For instance two different sets of signals impinging on the array can provide identical responses at the array output, i.e. the same measurements. In such a case any estimation algorithm may be unable to distinguish the true parameter values (e.g. directions) from the false ones. This is termed as the ambiguity problem:

It is the inability of an array of a given geometry to distinguish a set of parameter values

$$(p_1, p_2, ..., p_M) \text{ with } p_i \neq p_j \in \Omega_p \text{ for } i \neq j \tag{5.6}$$

from at least one of its subsets (or one subset from another). As mentioned before, array ambiguities can be classified as 'trivial' and 'non-trivial'. Trivial ambiguities are the simplest type of ambiguity and can be easily identified/detected. For instance it is impossible to distinguish whether a signal is impinging on a linear array from direction-of-arrival p_1 or from the direction $p_2 = 360° - p_1$, i.e. the mirror image of p_1 with respect to 180°. In this case $\underline{S}(p_1) = \underline{S}(p_2)$ and for this reason, in order to avoid this ambiguity problem, the parameter space in the case of linear arrays is confined to $\Omega_p = [0°, 180°)$. However, this is a special case of Eq. (5.3) for $k = 1$. Even if $k \neq 1$, and $\Omega_p = [0°, 180°)$ an array may present trivial ambiguities. Still, trivial ambiguities are easily dealt with, since they only involve two manifold vectors and can be detected by a simple search of the array manifold.

On the other hand, a 'non-trivial' ambiguity is more difficult both to detect and cope with. If there exists a set of values $p_1, p_2, ..., p_M \in \Omega p$ with $2 < M \leq N$ and $p_i \neq p_j$ for $i \neq j$ such that the resulting manifold vectors are linearly combined as in Eq. (5.4), then the set of parameters $(p_1, p_2, ..., p_M)$ and all its subsets of $M - 1$ elements are indistinguishable by the array. In such a case, the array will have identical responses for the sets of bearings $(p_1, p_2, ..., p_{M-1})$, $(p_2, p_3, ..., p_M)$, $(p_1, p_3, p_4, ..., p_M)$, etc. and the manifold matrix $\mathbb{A}$ with columns the manifold vectors will have a rank smaller than M.

This type of ambiguity is much more difficult to identify since, unlike a trivial ambiguity, it cannot be detected by a simple search of the manifold. However, a method for modelling a type of ambiguities in linear arrays has already been developed. The method is based on the fact that the array manifold curve of a linear array is of hyperhelical shape and involves partitioning the array manifold curve $\mathcal{A}$ into c equal segments according to the intersensor spacing of the array elements, to yield what is called a Uniform Basic Set (UBS). Firstly, $\mathcal{A}$ has to be parametrised according to the intrinsic parameter of the manifold arc length s. In this way, any point on the curve is represented by its distance from the beginning of the curve.

$$\mathcal{A} = \{\underline{S}(s) \in \mathcal{C}^N, \forall s : s \in [0, l_m]\}$$

where l_m is the total manifold curve length.

The problem of finding and modelling ambiguities is a lot more complex when it comes to three dimensional (3D) array geometries. For a general 3D array geometry the array manifold vector of Eq. 3.16 is used so as to encompass both azimuth and elevation angles. The geometry of such an array yields a manifold surface whose Gaussian curvature can be expressed as [41]

$$K_G(\theta,\phi) = \frac{1}{\sqrt{det(\mathbb{G})}}\frac{d}{d\phi}\left(\frac{\sqrt{det(\mathbb{G})}}{g_{\theta\theta}}\Gamma^{\phi}_{\theta\theta}\right) \tag{5.7}$$

which, in general, is not constant. In Eq. 5.7, $\Gamma^{\phi}_{\theta\theta}$ is the appropriate element of the Christoffel symbol matrix as discussed in [41]. A variable Gaussian curvature implies that the manifold surface of a 3D array is not developable and thus lacks many of the desirable characteristics that ease the analysis and modelling of the surface. For example, the concept of a "development" does not apply on the general case of 3D arrays. The concept of the "development" of a manifold surface is a very convenient way of illustrating the shape of the manifold surface, since it is the result of a distortionless mapping whose effect is that it translates the geodesic curvature of a curve in a higher dimensionality space, to the curvature of a curve in a two dimensional real plane. Since the manifold surface of an array is a structure that spans many complex dimensions, it is very difficult to visualise in its original space, so the development of an array manifold is a very useful tool. It is worth noting that all planar and linear array manifolds are developable.

There are, however, 3D array geometries that also possess manifolds of constant Gaussian curvature. Array geometries which have been identified to satisfy this condition are a special class of 3D arrays, known as 3D-grid arrays.

In 3D-grid arrays the N-dimensional vectors $\underline{r}_x$, $\underline{r}_y$ and $\underline{r}_z$ that form the array geometry matrix $\mathbf{r}$ are not only orthogonal but also have the same magnitude. Specifically, the manifold surface of a 3D-grid array of N omnidirectional sensors is spherical with radius $\pi\rho$ (and hence developable) embedded in an N-dimensional complex space. For example, the 6-element cube array with all sides equal to one half-wavelength is a 3D-grid array and has a spherical manifold with Gaussian curvature $(\rho\pi)^{-1}$. This implies that the array manifold of a 3D-grid array is isometric with a sphere of radius $\rho\pi$. The development of a 3D-grid array is illustrated in Figure 5.5.

In the sequel, let us consider the above described 3D-grid array which has elements positioned at

$$\mathbf{r} = \begin{bmatrix} 0 & 0 & 0 & 0 & -0.5 & 0.5 \\ 0 & 0 & -0.5 & 0.5 & 0 & 0 \\ -0.5 & 0.5 & 0 & 0 & 0 & 0 \end{bmatrix}^T \tag{5.8}$$

in an environment with five sources present at directions given by Table 5.1 in which the 3D grid array presents an ambiguity. Indeed, simulation results presented in Figure 5.2 clearly show that a MUSIC search for this 3D grid array

produces 6 distinct peaks, of which there are 5 peaks corresponding to the true directions of sources, while there is an extra peak at $(\theta, \varphi) = (169°, 84°)$.

θ	φ
212.1°	38°
132.8°	75.5°
166.7°	26.3°
226°	16.3°
209.1°	32.1°

Table 5.1: First ambiguous set of directions of sources in the environment

It is also straightforward to check that the matrix

$$\mathbb{S} = \Big[\underline{S}(226°, 16°), \ \underline{S}(209°, 32°), \ \underline{S}(169°, 84°), \\ \underline{S}(212°, 38°), \ \underline{S}(132°, 75°), \ \underline{S}(166°, 26°), \Big]$$

loses rank. This confirms that there is an ambiguity of rank 5 present.

The sets of directions displayed in Tables 5.2 and 5.3 are also ambiguous sets for this array. This fact is illustrated in Figures 5.3 and 5.4, where 6 distinct peaks are present at all 6 directions of the above sets, although only 5 of the sources were present in the simulation environment in each case.

θ	φ
250.9°	55°
146.7°	84.2°
175.3°	69.5°
172.7°	46.2°
93.5°	43.8°
230°	58.5°

Table 5.2: Second set of ambiguous directions

θ	φ
338.4°	24.9°
151.2°	78.2°
208.8°	52.8°
269.7°	35°
99.3°	73°
220.6°	47.3°

Table 5.3: Third set of ambiguous directions

The three ambiguous sets of directions are shown on the "development" of the above array in Figure 5.6. Note that in Figure 5.6, θ-curves are represented

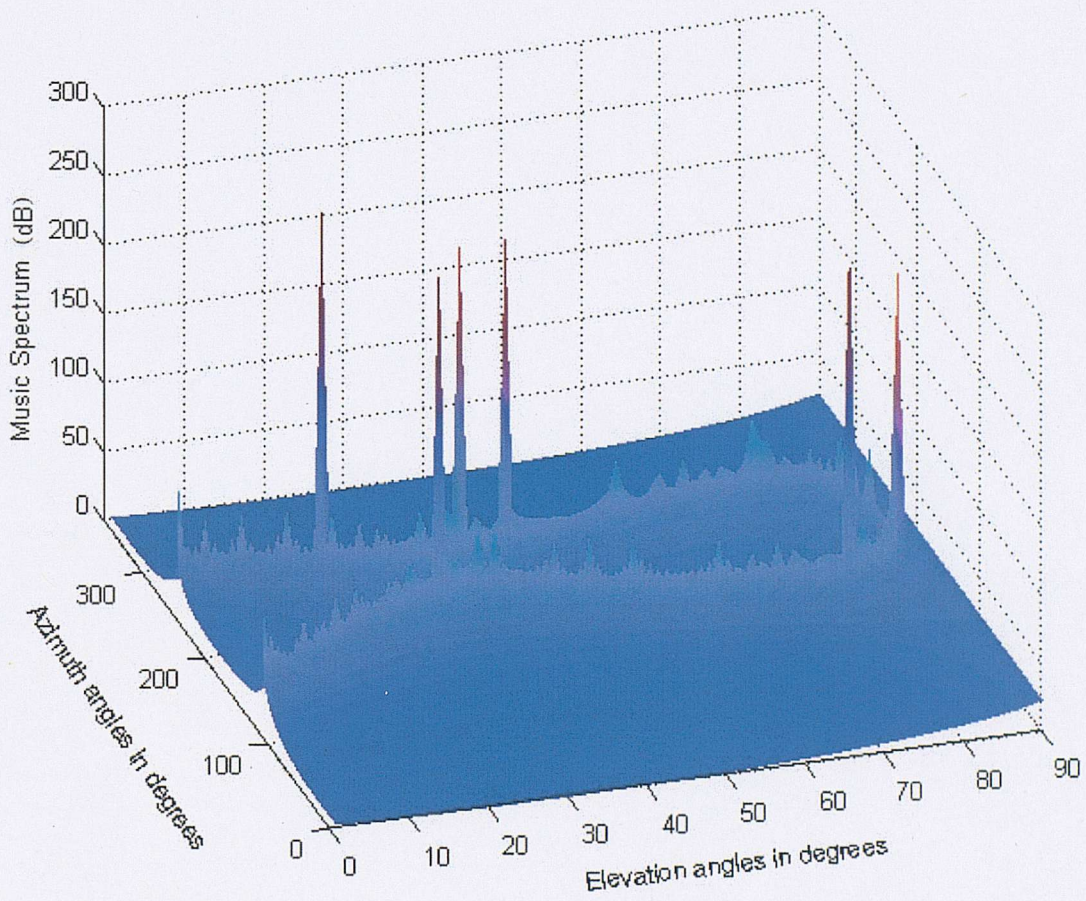


Figure 5.2: MUSIC spectrum for 3D grid array with the 1^{st} set of 5 sources present (Table 5.1). The 6 peaks clearly illustrate the ambiguous situation

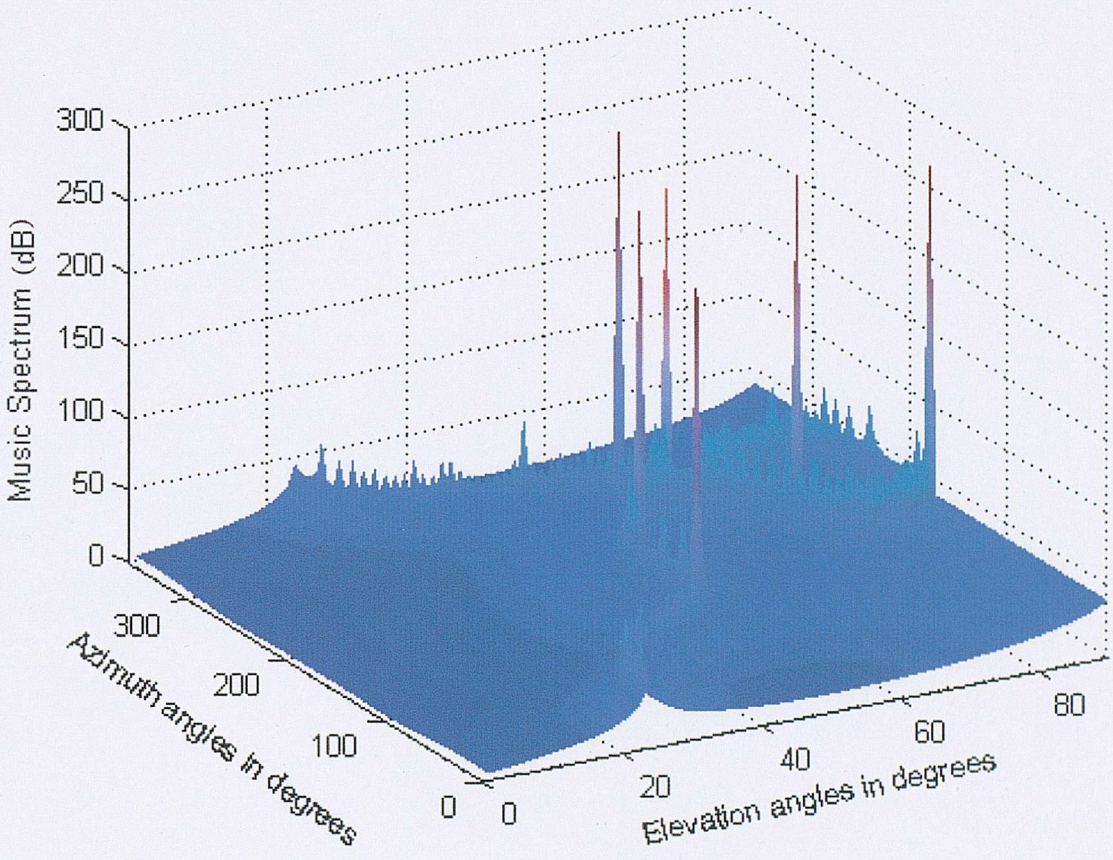


Figure 5.3: MUSIC spectrum for 3D grid array with the 2^{nd} set of 5 sources present (Table 5.2). The 6 peaks clearly illustrate the ambiguous situation

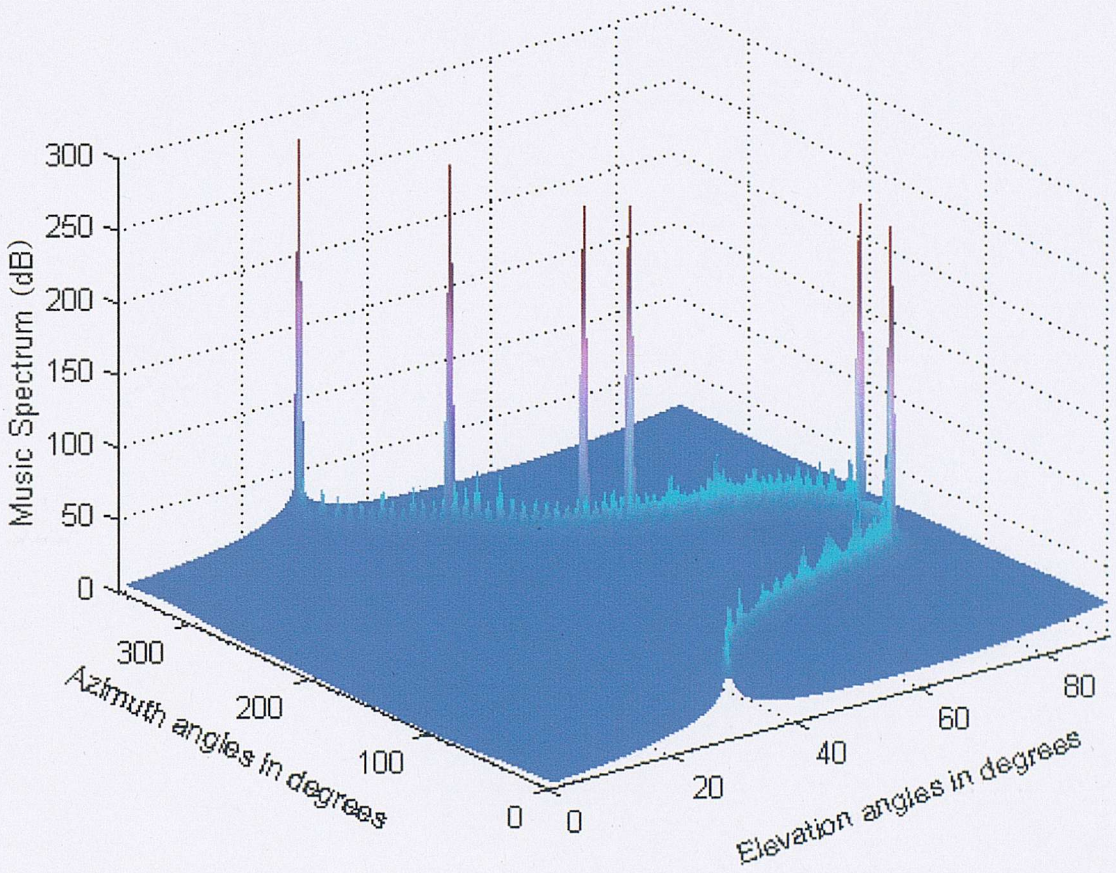


Figure 5.4: MUSIC spectrum for 3D grid array with the 3^{rd} set of 5 directions present (Table 5.3). The 6 peaks clearly illustrate the ambiguous situation

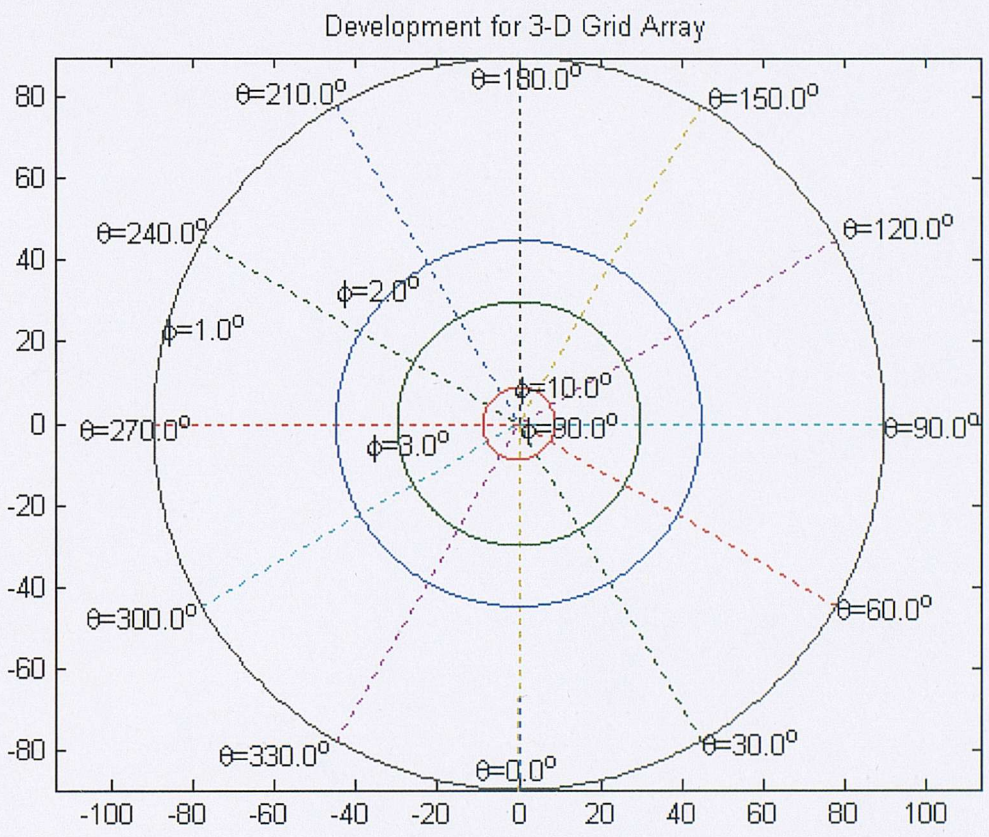


Figure 5.5: The development of a 3D-grid array showing θ and ϕ-lines

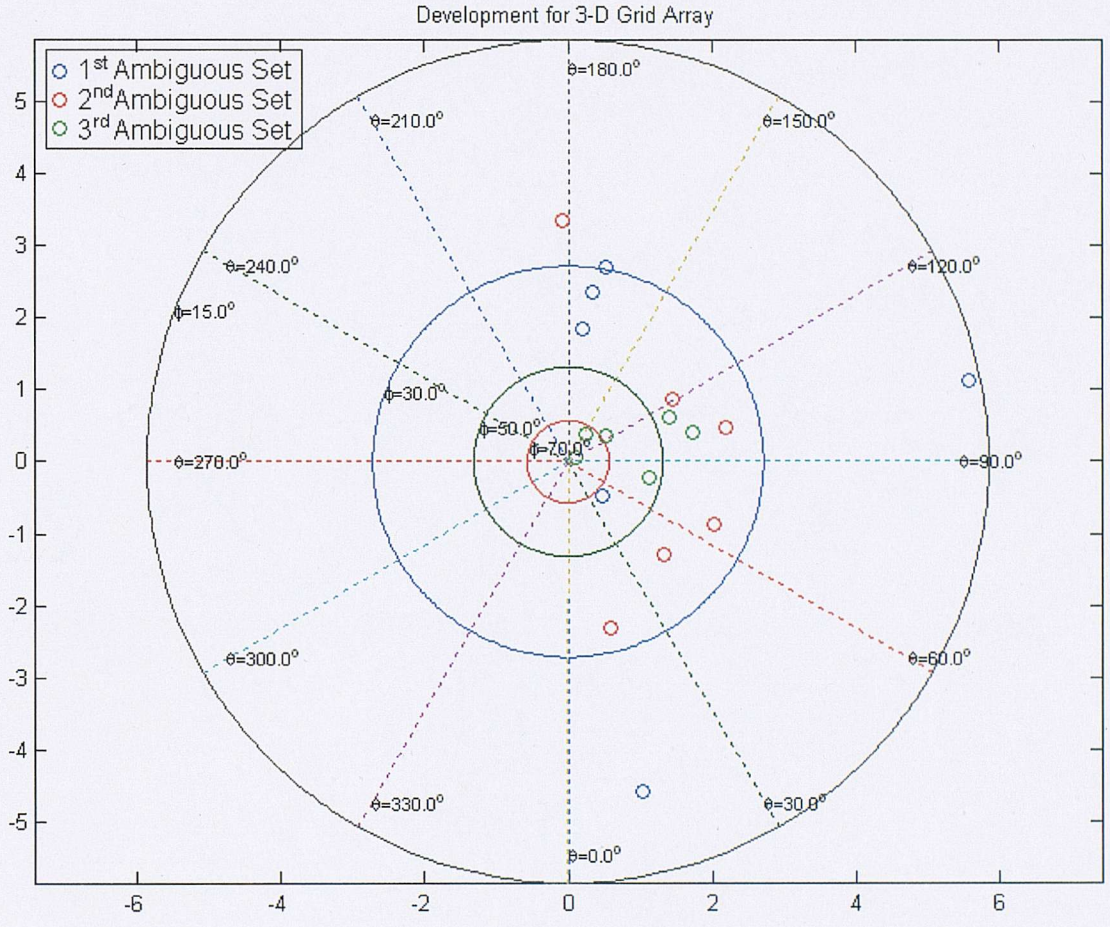


Figure 5.6: The development of a 3D grid array zoomed in, with the three discrete ambiguous sets of directions (Tables 5.1, 5.2 and 5.3)

by straight lines stretching out from 90° towards 0°. In fact, it can be shown that these lines are ambiguous for a 3D grid array and indeed for any 3D array which has two elements that are symmetric with respect to any plane parallel to the x-y plane. Indeed, assume an array of geometry $\mathbf{r} = \left[\underline{r}_x,\ \underline{r}_y,\ \underline{r}_z\right] = \left[\underline{r}_1,\ \underline{r}_2,\ \ldots,\ \underline{r}_N\right]^T = \begin{bmatrix} r_{x_1}, & r_{x_2}, & \ldots, & r_{x_N} \\ r_{y_1}, & r_{y_2}, & \ldots, & r_{y_N} \\ r_{z_1}, & r_{z_2}, & \ldots, & r_{z_N} \end{bmatrix}$ and assume without loss of generality that sensors $\underline{r}_1$ and $\underline{r}_2$ are symmetric with respect to any plane parallel to the x-y plane, i.e. $r_{x_1} = r_{x_2}$ and $r_{y_1} = r_{y_2}$. Then the manifold matrix $\mathbb{S}$ for $M = N$ sources of common elevation in the environment is given by $\mathbb{S} = \left[\underline{S}(\theta_1, \phi_0),\ \underline{S}(\theta_2, \phi_0),\ \ldots,\ \underline{S}(\theta_N, \phi_0)\right]$ $(\mathbb{S} \in C^{N \times N})$ and according to Eq (3.16) the first and second rows of the matrix read

$$\begin{bmatrix} \text{row}_1(\mathbb{S}) \\ \text{row}_2(\mathbb{S}) \end{bmatrix} = \begin{bmatrix} \exp(-j\pi \underline{r}_1^T \underline{k}_1), & \ldots, & \exp(-j\pi \underline{r}_1^T \underline{k}_N) \\ \exp(-j\pi \underline{r}_2^T \underline{k}_1), & \ldots, & \exp(-j\pi \underline{r}_2^T \underline{k}_N) \end{bmatrix}$$

where $k_i = \underline{k}(\theta_i, \phi_0) = \left[\cos\theta_i \cos\phi_0 \quad \sin\theta_i \cos\phi_0 \quad \sin\phi_0\right]^T$. Furthermore $\forall i$ we have

$$\begin{aligned} \exp(-j\pi \underline{r}_1^T \underline{k}_i) &= \exp(-j\pi(r_{x_1} \cos\theta_i \cos\phi_0 + r_{y_1} \sin\theta_i \cos\phi_0 + r_{z_1} \sin\phi_0)) \\ &= \exp(-j\pi(r_{x_1} \cos\theta_i \cos\phi_0 + r_{y_1} \sin\theta_i \cos\phi_0)) \exp(-j\pi(r_{z_1} \sin\phi_0) \\ &= \exp(-j\pi(r_{x_2} \cos\theta_i \cos\phi_0 + r_{y_2} \sin\theta_i \cos\phi_0 + r_{z_2} \sin\phi_0)) \cdot \\ &\quad \cdot \exp(-j\pi((r_{z_1} - r_{z_2}) \sin\phi_0) \\ &= c \exp(-j\pi(r_{x_2} \cos\theta_i \cos\phi_0 + r_{y_2} \sin\theta_i \cos\phi_0 + r_{z_2} \sin\phi_0)) \\ &= c \exp(-j\pi \underline{r}_2^T \underline{k}_i) \end{aligned}$$

which results to

$$\text{row}_1(\mathbb{S}) = c\, \text{row}_2(\mathbb{S})$$

where c is a complex constant (independent of θ) and thus $\mathbb{S}$ which is a square matrix loses rank $\forall\theta$. In fact, the matrix $\mathbb{S}$ will be of rank $N - K$ where K is the number of pairs of symmetric sensors with respect to any plane parallel to the x-y plane. The above results are illustrated in Figure 5.7, where the MUSIC spectrum for the array of Eq. (5.8) is plotted with the signal environment given by Table 5.4.

In fact, this finding can be furthermore generalised by using the same approach. If the wavenumber vectors of the sources present in the environment all lie on a single plane, then an ambiguity occurs if the array has elements symmetrical to that plane.It is clear that no successful estimation of the signal environment

θ	φ
10°	10°
20°	10°
30°	10°
40°	10°
50°	10°

Table 5.4: A signal environment with sources of common elevation

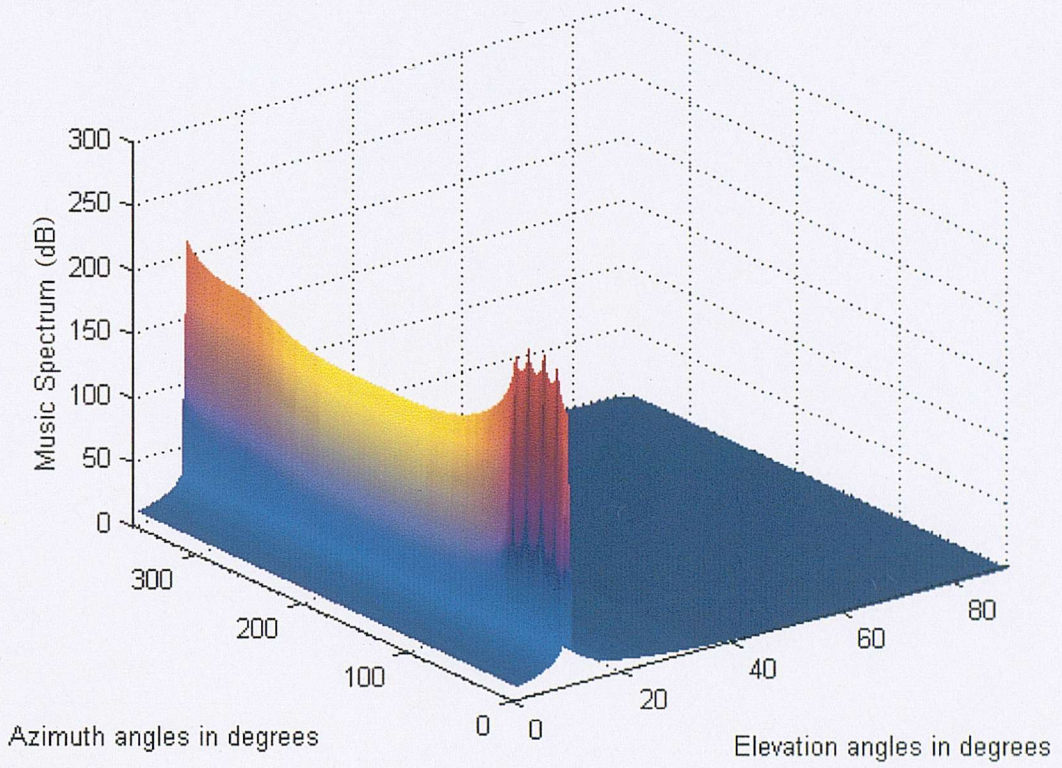


Figure 5.7: MUSIC spectrum of 3D grid array for sources incoming from the same elevation.

can be performed by the 3D-grid array in this case. It is also straightforward to extend the above findings, by using the same methodology, to α-curves (or β-curves). The α-curves (or β-curves) are manifold curves generated by the locus of the manifold with incoming angles that have a constant angle with the x-axis (y-axis) after the coordinate system has been rotated around the z-axis by an angle Θ_0. The array manifold surface with α and β-curves is illustrated in Figure 5.8. In order for an α-curve (β-curve) to be ambiguous, the array must include

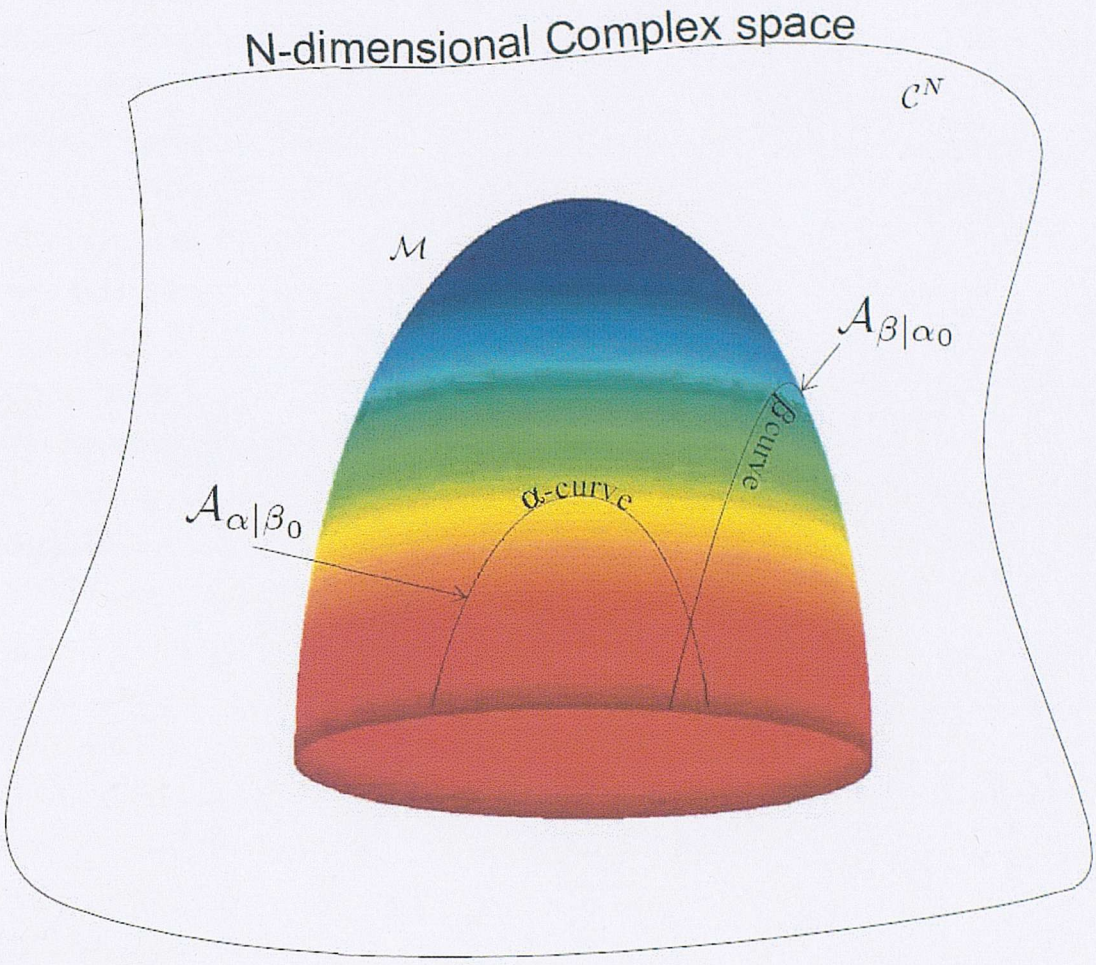


Figure 5.8: Representation of the array manifold with example α and β-curves

at least two sensors whose positions satisfy

$$\begin{aligned} \alpha - curve \quad &: \quad r_{z_1} = r_{z_2},\ r_{x_1}\cos(\Theta_0) + r_{y_1}\sin(\Theta_0) = && (5.9) \\ &= \quad r_{x_2}\cos(\Theta_0) + r_{y_2}\sin(\Theta_0) && (5.10) \\ \beta - curve \quad &: \quad r_{z_1} = r_{z_2},\ r_{x_1}\cos(\Theta_0 + 90°) + r_{y_1}\sin(\Theta_0 + 90°) = \\ &= \quad r_{x_2}\cos(\Theta_0 + 90°) + r_{y_2}\sin(\Theta_0 + 90°) \end{aligned}$$

In the next section a discussion on the work on resolving ambiguities is followed by various illustrative simulation results.

5.2 Resolving Ambiguities in Arrayed-WSN

As mentioned in the last section, the ambiguity problem in DOA estimation has usually been associated with manifold ambiguities, that is, with the rank of the

array manifold matrix. Actually, manifold ambiguities would occur in any linear array if the antenna array's aperture measured in half wavelengths is not less than the number of sensors in the array. In past decades, most researches to handle the ambiguity problem were mainly concerned with either the performance of specific arrays, or with the identification of array structures free of ambiguities up to a certain rank of ambiguity. Specifically, the subspace-type (MUSIC-type) methods have been used for DOA estimation popularly with simple linear arrays. While these methods fail to provide unambiguous DOA estimates for most practical array geometries, e.g. nonuniform linear or planar arrays, since they require the assumption of linear independence amongst the array manifold.

As complement of subspace-type methods, a couple of techniques have been proposed recently to resolve manifold ambiguity for uncorrelated sources. By combining the direct augmentation approach (DAA) and MUSIC method, unambiguous DOA estimates may be obtained for any number of sources up to and including the array aperture expressed in intersensor separation units [70]. Since the DAA-DOA estimates are significantly less accurate than the corresponding MUSIC estimates, which are asymptotically effective but ambiguous, it is proven that the final DOA estimates can be obtained by simply associating the accurate but ambiguous MUSIC estimates with the unambiguous but less accurate DAA estimates. This approach, called Manifold Ambiguity Resolution by Association (MARA) has been generalised further in the case of partially augmentable and noninteger-spaced arrays, and manifold ambiguity can be correctly resolved by a similar association method thanks to proper completion of the spatial covariance matrix [68].

In the conventional case that the number of sources is less than the number of sensors, a much more effective technique to resolve manifold ambiguities has also been proposed for the independent sources [69], [71]. This method seeks the best fit amongst the set of estimated spatial covariance lags and source powers for each of the MUSIC DOA estimates, including the ambiguous ones. For any identifiable source, the powers corresponding to the ambiguous DOA's tend to zero as the number of samples increases; meanwhile the DOA's associated with the greatest powers converge to the true DOA's. By adopting a computationally efficient linear programming routine, a diagonal fitting procedure is performed with an extremely high probability of correct identification in ambiguous scenarios. In fact, in many cases, the probability achieved by this method is even higher than the probability of obtaining normal DOA estimates by MUSIC. Although both of methods mentioned above have been examined to be statistically effective

to resolve manifold ambiguity of uncorrelated sources for arbitrary linear arrays, there is still space to develop a much more efficient and feasible method to improve the performance of ambiguities resolving.

Also, it is found that the manifold ambiguity could be resolved by polarisation, if the intersensor spacing is larger than half a wavelength [72]. By measuring three electric–field components and three magnetic–field components of the incident wave field, this method manages to find the correct vector sensor among those electromagnetic vector sensors with six co–located antennas. This technique, however, would result in large complexity and expenses of implementation. In the next section, we will propose a novel method to resolve manifold ambiguities in Arrayed-WSNs.

5.2.1 An Efficient Array Cooperative Method for Resolving Ambiguities

Resolving manifold ambiguities by cooperation of two arrays is a simple but efficient technique especially applicable to the Arrayed-WSN. As discussed in previously, in an Arrayed-WSN, the abundance of the simple nodes allows for great versatility and this can be exploited in resolving ambiguities as well.

The detection of an ambiguous situation is a procedure that can be performed by a single array, for example by merely comparing the dimensionality of the signal space with the number of sources detected. If the number of sources is greater, an ambiguity has occurred. When a WA or a LA on a node in an Arrayed-WSN detects an ambiguity, it can invoke the service of another WA or LA respectively in order to resolve the ambiguous situation. For example, assume that a WA with geometry given by $\mathbf{r}_1$ (WA_1) detects an ambiguous situation, i.e. although the dimensionality of the signal subspace is M, it detects M_{amb} sources, where $M_{amb} > M$. It will then try and find another already formed nearby WA (WA_2) or in the absence of a nearby *Wireless Array*, invoke the formation of one, via the procedure discussed in Chapter 3. It is a fair assumption that the same set of directions will not be ambiguous for WA_2 too, since the probability of such a situation occurring is very small (in any case, even if that particular set of directions is ambiguous for both arrays, the employment of a third WA can resolve the ambiguous situation.). The simplest way to resolve the ambiguity would be for WA_2 to run a complete MUSIC search and compare the detected directions with the ones detected by WA_1. However, this is not necessary and can be avoided since a complete search would be a waste of resources.

Let us assume that only two WA (WA_1 and WA_2) are needed for the resolution of the particular ambiguity. The corresponding received signals are denoted by $\underline{x}_1(t)$ and $\underline{x}_2(t)$. Since the set of directions is ambiguous for WA_1

$$\text{rank}(\mathbb{S}^{(1)}) = M$$

where $\mathbb{S}^{(1)}$ is the manifold matrix of WA_1

$$\mathbb{S}^{(1)} = \left[\underline{S}_1^{(1)}, \ ..., \ \underline{S}_i^{(1)}, \ ..., \ \underline{S}_M^{(1)}, \ ..., \ \underline{S}_{M_{amb}}^{(1)}\right] \tag{5.11}$$

where $\underline{S}_i^{(1)}$ denotes the manifold vector of WA_1 corresponding to the i^{th} source. The above means that by running a direction finding algorithm on $\underline{x}_1(t)$ (such as MUSIC), M_{amb} sources at angles $(\theta_i^{(1)}, \phi_i^{(1)})$, $i = 1, .., M_{amb}$ will be detected although only M sources are present. Since WA_1 cannot tell which of the detected sources are real, it will pass all the detected directions to WA_2.

First, WA_2 has to construct $\mathbb{S}^{(2)}$ so that it reflects all the M_{amb} directions detected by WA_1 so that

$$\mathbb{S}^{(2)} = \left[\underline{S}_1^{(2)}, \ ..., \ \underline{S}_i^{(2)}, \ ..., \ \underline{S}_M^{(2)}, \ ..., \ \underline{S}_{M_{amb}}^{(2)}\right] \tag{5.12}$$

where $\underline{S}_i^{(2)}$ denotes the manifold vector of WA_2 corresponding to the i^{th} source as it is seen by WA_2. Note that in general in an Arrayed-WSN the two WAs will have different coordinate systems so a specific source will appear at different (but interrelated) angles to the two arrays. Specifically, if the assumption that the two WAs are close to each other compared to the sources is made, then a translation between the two coordinate systems can be implied by

$$(\theta_i^{(2)}, \phi_i^{(2)}) = (\theta_i^{(1)} + \Theta, \phi_i^{(1)} + \Phi) \tag{5.13}$$

where (Θ, Φ) is the azimuth and elevation angles between the two coordinate systems.

By using the signal subspace deduced from the received signal $\underline{x}_2(t)$, according to Eq. (5.1), the projection operator to space orthogonal to the signal subspace $\mathbb{P}_s^{\perp}$ can be formed at WA_2. By simply projecting $\mathbb{S}^{(2)}$ to the signal subspace using

$$\mathbb{M} = \mathbb{P}_s^{\perp}\mathbb{S}^{(2)} \tag{5.14}$$

WA_2 can find which sources are not really present in the environment, merely by checking the non-zero columns of $\mathbb{M}$.

As an example (and without any loss of generality), consider two planar arrays with array geometries:

$$\mathbf{r}_{WA_1}=\begin{bmatrix} -2.5 & -2 & -2.5 & 2.5 & 2 & 2.5 \\ 1.5 & 0 & -1.5 & 1.5 & 0 & -1.5 \\ 0 & 0 & 0 & 0 & 0 & 0 \end{bmatrix}^T$$

$$\mathbf{r}_{WA_2}=\begin{bmatrix} -0.3873 & -3.0516 & -0.5119 & 2.8514 & 2.4081 & 1.2771 \\ 2.0874 & 0 & -0.6466 & 0.6053 & 0 & -2.4845 \\ 0 & 0 & 0 & 0 & 0 & 0 \end{bmatrix}^T$$

which lie on a plane as illustrated in Figure 5.9. It can be easily checked that the directions shown in Table 5.5 are an ambiguous set of rank 4 for WA_1.

θ	φ
5°	27.3°
5°	60.8°
5°	85.1°
185°	71.6°
185°	44.2°

Table 5.5: An ambiguous signal environment for the first WA

This is illustrated both by the fact that $\text{rank}(\mathbb{S}^{(1)}) = 4$ and by the fact that there are five distinct peaks in the music spectrum of Figure 5.10 although only the first 4 sources were included in the environment. Furthermore, by checking that $\text{rank}(\mathbb{S}^{(2)}) = 5$ and by inspecting Figure 5.11 it is clear that this set of directions is not ambiguous for WA_2. The two WAs have different azimuthial and elevation orientation expressed by $(\Theta, \Phi) = (36°, 17°)$. Thus, the sources, for example, incoming from $(5°, 27.3°)$ and $(5°, 85.1°)$ for WA_1, are impinging from directions $(41°, 44.3°)$ and $(221°, 77.9°)$ respectively for WA_2.Then, WA_1 will pass the directions corresponding to the five detected peaks to WA_2. The two arrays will also, via simple message exchange, determine the angles (Θ, Φ). In this way, WA_2 can form the matrix $\mathbb{S}^{(2)}$ which consists of manifold vectors of WA_2 for the five sources detected by WA_1.

$$\mathbb{S}^{(2)} = \begin{bmatrix} 0.84+0.53i & 0.95+0.30i & 0.99+0.05i & 0.97-0.20i & 0.89-0.44i \\ -0.59+0.80i & -0.05-0.99i & 0.68+0.73i & -0.99-0.12i & 0.84-0.53i \\ -0.01+0.99i & 0.64+0.76i & 0.98+0.15i & 0.84-0.53i & 0.29-0.95i \\ -0.22-0.97i & -0.27+0.96i & 0.71-0.70i & -0.96+0.26i & 0.97+0.23i \\ 0.91-0.40i & -0.86+0.50i & 0.79-0.60i & -0.72+0.69i & 0.63-0.76i \\ -0.98-0.19i & -0.04-0.99i & 0.95-0.28i & 0.50+0.86i & -0.72+0.69i \end{bmatrix}$$

In order to form the signal subspace an eigenvalue decomposition on the received signal covariance matrix $\mathbb{R}_{xx_2} = \mathcal{E}\{\underline{x}_2(t)\underline{x}_2^H(t)\}$ is necessary. If the matrix

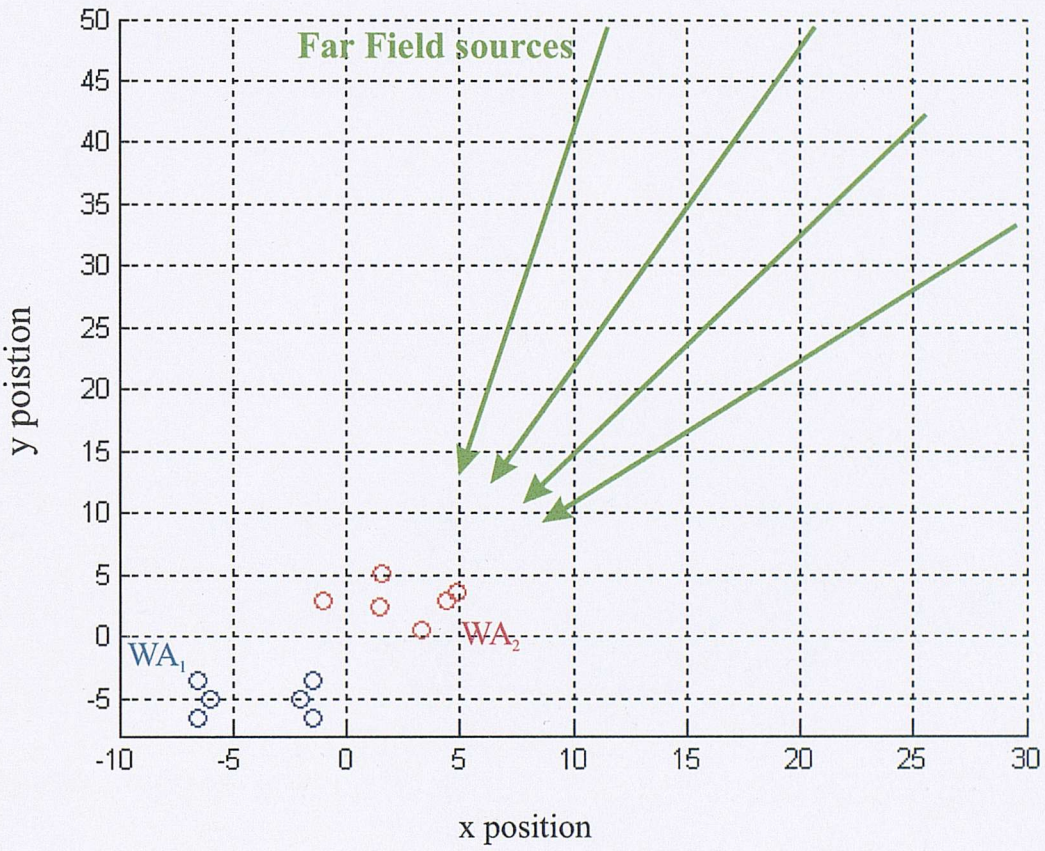


Figure 5.9: WA_1 and WA_2 lie close together on a plane close to each other compared to the far-field sources

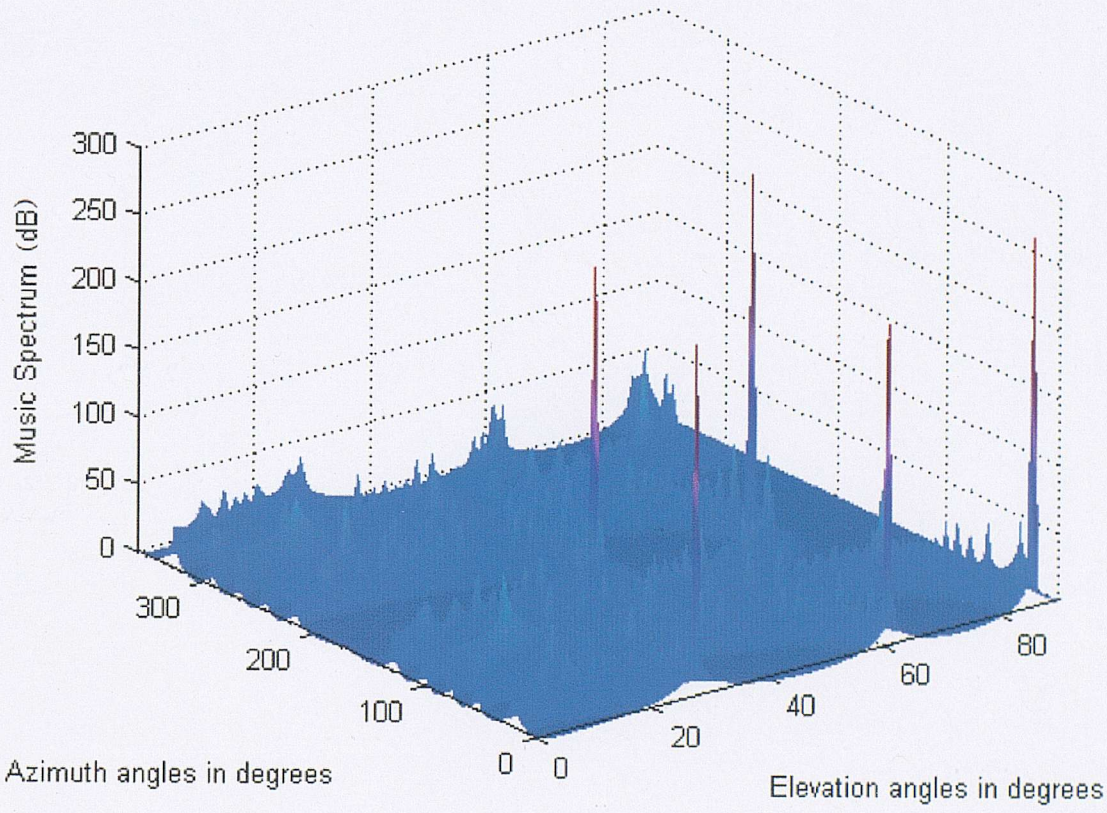


Figure 5.10: MUSIC spectrum for WA_1 with 4 sources present in the environment. The peak at $(\theta, \phi) = (185, 44.2)$ does not correspond to a real source

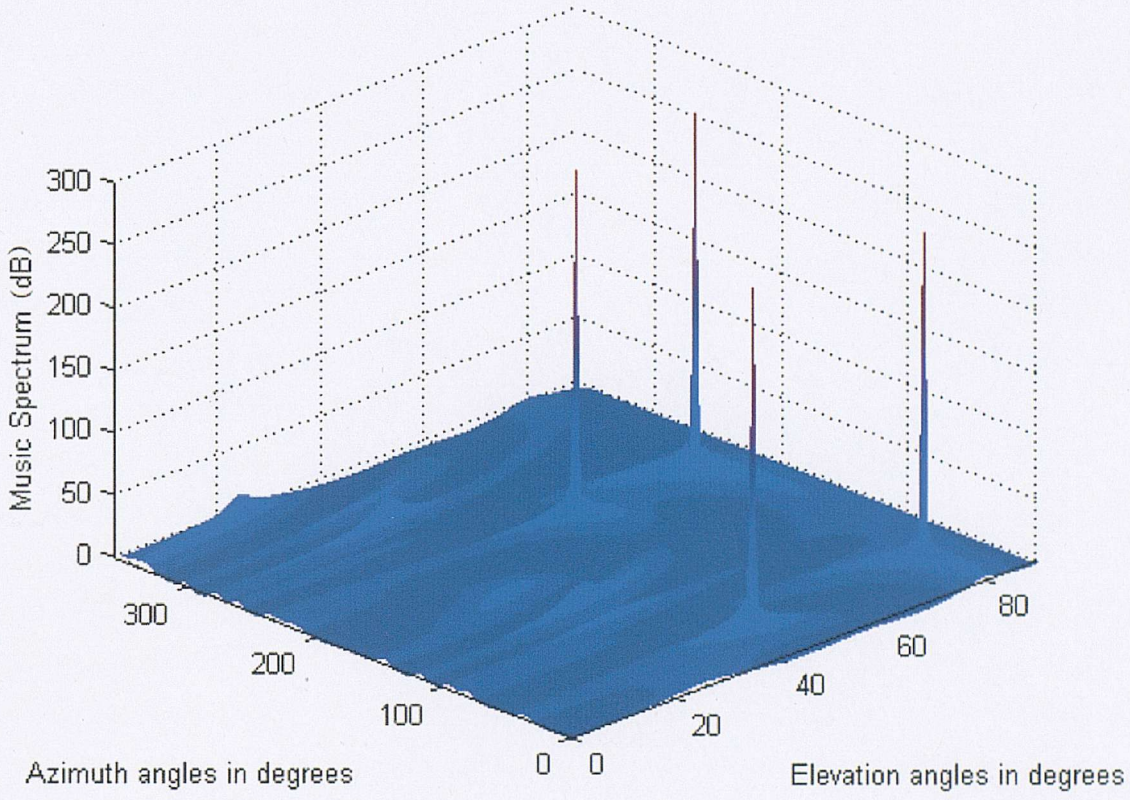


Figure 5.11: MUSIC spectrum after coordinate transformation for WA_2 with 4 sources present in the environment. In contrast with Figure 5.10, there is no peak at $(\theta, \phi) = (211°, 61.2°)$

$\mathbb{E} = \left[\underline{E}_1, \ ..., \ \underline{E}_M\right]$ with columns the M signal eigenvectors is constructed, the projector operator onto the space orthogonal to the signal subspace can be formed by

$$\mathbb{P}_s^{\perp} = \mathbb{I} - \mathbb{E}(\mathbb{E}^H\mathbb{E})^{-1}\mathbb{E}^H \tag{5.15}$$

Finally, the matrix $\mathbb{M} = \mathbb{P}_s^{\perp}\mathbb{S}^{(2)}$ can be calculated. In this case

$$\mathbb{M} = \begin{bmatrix} 0 & ... & 0 & 0.9000 + 0.2967i \\ 0 & ... & 0 & 0.2848 - 0.4976i \\ 0 & ... & 0 & -0.6760 - 0.5729i \\ 0 & ... & 0 & 0.1460 + 0.4542i \\ 0 & ... & 0 & 0.4541 - 0.3242i \\ 0 & ... & 0 & -0.2282 + 0.4041i \end{bmatrix}$$

which indicates that the last direction $(\theta, \phi) = (185°, 71.6°)$ (which corresponds to the last column of $\mathbb{M}$) does not represent a real source in the environment, but is an alias caused by the ambiguous situation. In conclusion it can be said that the zero columns of the matrix $\mathbb{M}$ correspond to real sources in the environment.

In contrast with the WAs in the Arrayed-WSN, the LA that are situated on the nodes, have standardised geometries. Although the presence of an ambiguity is solely dependent on the geometry of the array and signal environment, an ambiguous situation for one node will not in general be ambiguous for another one. This is because nodes are randomly scattered and thus have in general different orientation angles. Therefore, even if two nodes are closely located, which means that the sources in the environment will be impinging from the same angles on the two nodes according to a global coordinate system, the nodes' array geometries will be rotated and so the sources directions of arrival will differ in the nodes' local coordinate system. This means that the same procedure described above can in general be used for LAs too. In fact in the case of a *Local Array* ambiguity occurring, a node i can verify if indeed another node j in the vicinity is able to resolve the ambiguity with the proposed method, simply by comparing its own coordinate system to node's j coordinate system (more on local and global coordinate systems in the Arrayed-WSN in Chapter 6). If the coordinate systems differ in at least one angle the method will be guaranteed to work (that is except for the case of fully symmetrically deployed nodes).

As an example consider the two nodes of Figure 5.12, which for simplicity but without loss of generality have a difference in orientation only in the azimuth of their coordinate systems, i.e.$(\Theta, \Phi) = (33°, 0°)$. Figures 5.13 and 5.14 exhibit that while the set of directions (according to LA_1 coordinate system) of Table

θ	φ
113.7°	54.6°
102.2°	63.5°
95°	68°
45.3°	1°
106.8°	57.8°
186.9°	44.4°

Table 5.6: An ambiguous signal environment for the first LA

5.6 is ambiguous for LA_1, it is not ambiguous for LA_2 due to the rotation of the array geometry.

Thus, as in the previous case, LA_1 can resolve the ambiguous situation by employing the help of LA_2. In the case where the source at $(95°, 68°)$, is not present in the environment, although LA_1 will detect 6 sources, LA_2 will detect only 5. By forming the manifold matrix, associated with the estimated directions as follows

$$\mathbb{S}^{(2)} = \begin{bmatrix} 0.28+0.95i & 0.16+0.98i & 0.11+0.99i & 0.99+0.02i \\ 0.28-0.95i & 0.16-0.98i & 0.11-0.99i & 0.99-0.02i \\ 0.98+0.14i & 0.96+0.24i & 0.96+0.27i & 0.03+0.99i \\ 0.98-0.14i & 0.96-0.24i & 0.96-0.27i & 0.03-0.99i \\ 0.62+0.78i & 0.79+0.60i & 0.86+0.49i & 0.94+0.33i \\ 0.62-0.78i & 0.79-0.60i & 0.86-0.49i & 0.94-0.33i \end{bmatrix}$$
$$\begin{bmatrix} 0.23+0.97i & 0.45+0.89i \\ 0.23-0.97i & 0.45-0.89i \\ 0.97+0.23i & 0.53-0.84i \\ 0.97-0.23i & 0.53+0.84i \\ 0.69+0.71i & 0.88+0.47i \\ 0.69-0.71i & 0.88-0.47i \end{bmatrix}$$

and via Eq. (5.15) the matrix $\mathbb{M} = \mathbb{P}_s^{\perp}\mathbb{S}^{(2)}$ can be formed:

$$\mathbb{M} = \begin{bmatrix} 0 & 0 & 0.0087+0.0098i & 0 & 0 & 0 \\ 0 & 0 & 0.0087-0.0098i & 0 & 0 & 0 \\ 0 & 0 & 0.0012+0.0017i & 0 & 0 & 0 \\ 0 & 0 & 0.0012-0.0017i & 0 & 0 & 0 \\ 0 & 0 & -0.0075-0.0110i & 0 & 0 & 0 \\ 0 & 0 & -0.0075+0.0110 & 0 & 0 & 0 \end{bmatrix}$$

which shows that the direction $(\theta, \varphi) = (95°, 68°)$ (corresponding to the 3^{rd} column of $\mathbb{M}$) is indeed the ambiguous source.

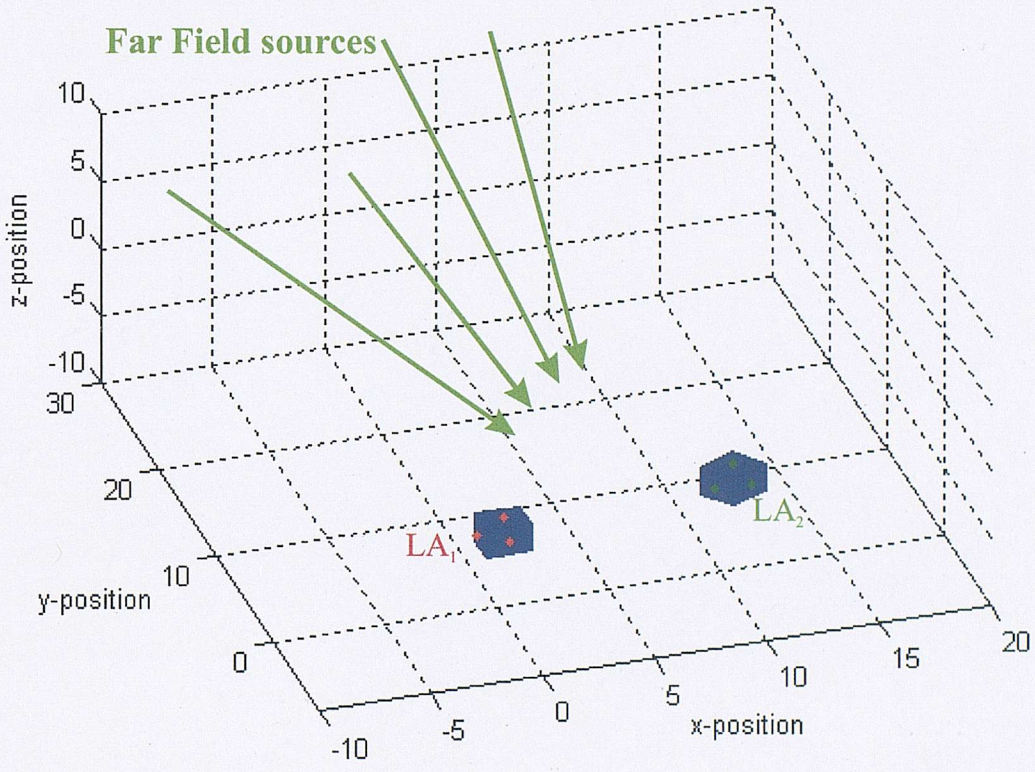


Figure 5.12: Two nodes with their Local Arrays, lying close together in the 3D space, in the presence of far field sources

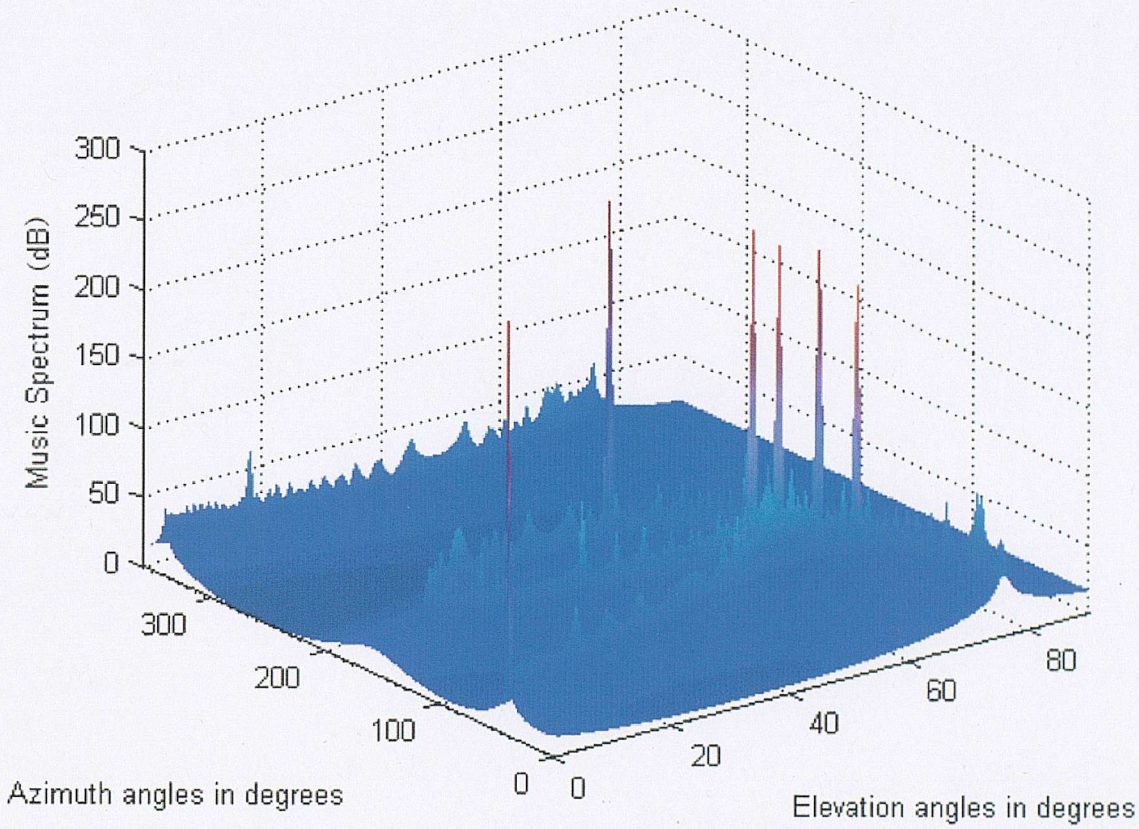


Figure 5.13: MUSIC spectrum for LA_1 with 5 sources present in the environment. The peak at $(\theta, \phi) = (95°, 68°)$ does not correspond to a real source

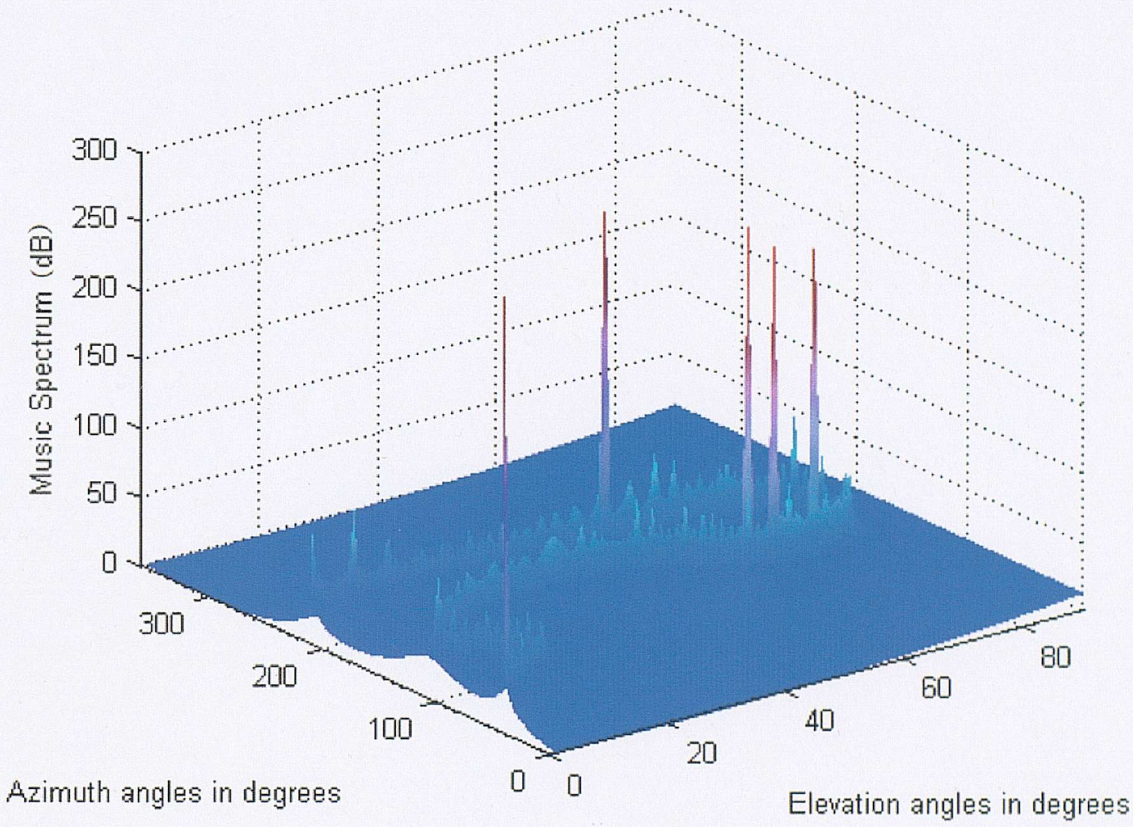


Figure 5.14: MUSIC spectrum after coordinate transformation for LA_2 with 5 sources present in the environment. In contrast with Figure 5.13, there is no peak at $(\theta, \phi) = (95°, 68°)$

5.3 Conclusion

In this study, certain types of ambiguities related to an Arrayed-WSN were discussed, analyzed and resolved. It has been shown that it is possible to model ambiguities in planar arrays by employing results applicable to linear arrays, and that 3D arrays possess classifiable ambiguities too. It has to be noted that ambiguities concerning 3D arrays, are a very difficult and extensive but exciting problem that is still under consideration and rigorous research.

Several techniques currently available for resolving manifold ambiguities for independent sources were discussed. As manifold ambiguities do not always lead to nonidentifiability, it has been shown that via a novel method, it is possible, under some straightforward assumptions, to employ two or more arrays in an Arrayed-WSN in order to obtain a unique set of DOA estimates even in an ambiguous situation. It is possible to extend this method to use sub-arrays of 3D, planar or linear arrays in order to resolve ambiguous situations.

Chapter 6

Modelling Uncertainties in the Arrayed-WSN

Because of the nature of a WSN, most of the information about the nodes condition and position is unknown when the network is deployed. The acquisition of any relevant information has to be done a posteriori. Keeping in mind the unknown environment, the energy efficiency pursuit and the constrained resources of a WSN, it is clear that any information acquired will contain a certain degree of uncertainty.

Considering the operation of the Arrayed-WSN, there are a number of uncertainty issues associated with the use of Local and *Wireless Arrays*. In order to mitigate the effect of any such uncertainties they have first to be identified, classified and modelled. Once the uncertainties are known they can be studied so that ways of avoiding them or counteracting their effects can be devised.

In this study various uncertainties/errors present in an Arrayed-WSN are identified and modelled. These uncertainties can be separated according to different aspects of the Arrayed-WSN approach, resulting in the following structure:

- Section 6.1 considers the uncertainties introduced due to incorrect estimation of a node's position and orientation, i.e. from the localisation procedure.
- The uncertainties due to the imperfect nature of the node's clocks in addition to synchronisation errors are presented in Section 6.2.
- All of the uncertainties/errors relating to the node's *Local Array* are described in Section 6.3.
- Finally in Section 6.4 the uncertainties connected to the operation of a *Wireless Array* are studied.

6.1 Uncertainties/Errors Relating to Node Self Orientation and Self Position Estimation

Before examining how the uncertainties/errors that arise from any orientation and position estimation technique may be modelled the following introduces some key definitions and notations required for Arrayed Wireless Sensor Networks.

6.1.1 *Local Array* Modelling

Let the positions of the antenna array elements on a general sensor node (in the node's own coordinate system with its origin at the center of the node) be denoted by the columns of $\mathbf{r}_{\mathrm{n}} = \begin{bmatrix} \underline{r}_1 & \cdots & \underline{r}_{N_{\mathrm{n}}} \end{bmatrix}$. The use of microstrip antenna arrays would allow for a large number of antenna elements to be placed on a node. In order to generalise the study, we consider a number N_{n} of available antenna elements on each node. In general, only a subset N_{L} of the available N_{n} elements on the nodes will be utilised at any one time, in order that an array of elements can be formed on the node having an array manifold conforming to certain design criteria. This *Local Array* at the i^{th} node is denoted by $\mathbf{r}_i \in \mathbb{R}^{3\times N_{\mathrm{L}}}$ and is given by the following expression:

$$\mathbf{r}_i = \mathbf{r}_{\mathrm{n}}\mathbb{Q}_i \tag{6.1}$$

where $\mathbb{Q}_i$ is a N_{n} by N_{L} selection matrix with each column containing a one in the row corresponding to a selected antenna element and zeros elsewhere. For example, a node equipped with $N_{\mathrm{n}} = 6$ antenna elements and for a *Local Array* formed from the 1^{st}, 2^{nd}, 4^{th} and 5^{th} elements, the corresponding selection matrix would be:

$$\mathbb{Q}_i = \begin{bmatrix} 1 & 0 & 0 & 0 \\ 0 & 1 & 0 & 0 \\ 0 & 0 & 0 & 0 \\ 0 & 0 & 1 & 0 \\ 0 & 0 & 0 & 1 \\ 0 & 0 & 0 & 0 \end{bmatrix} \tag{6.2}$$

6.1.2 Node and Global Coordinate Systems

The positions of the array elements represented by $\mathbf{r}_i$ remain relative to the i^{th} Node's Coordinate System which we denote as NCS_i. However due to the way in which they are distributed, nodes will not all land in the same relative orientation. In a 2D treatment of this problem only one rotation angle is required to model

this, however a full 3D treatment requires the consideration of all three (Euler) angles of rotation.

In order to simplify the treatment, let us define the Global Coordinate System (GCS) as the system of coordinates that will be used to describe the 3D environment in which the nodes are dispersed and also in which the estimated location of EOI are required from the sensor network. Note that the use of the word "Global" is not intended to imply a system of coordinates that cover the Globe but the region over which the nodes are deployed.

The transformation which maps points in the i^{th} Node's Coordinate System into the Global Coordinate System is given by:

$$\underline{\check{x}} = \mathbb{T}\left(\Omega_i, \iota_i, \omega_i\right) \underline{x}_i + \underline{\check{p}}_i \tag{6.3}$$

where $\underline{\check{p}}_i$ is a column vector containing the position of the center of the i^{th} node in the GCS and $(\Omega_i, \iota_i, \omega_i)$ are the Euler angles of the rotation. The orthogonal rotation matrix $\mathbb{T}_i = \mathbb{T}\left(\Omega_i, \iota_i, \omega_i\right)$ can be expressed in terms of these angles as shown below (Note: using the 'y' convention and the middle rotation is about the y-axis and with all rotations following a right handed screw convention):

$$\mathbb{T}\left(\Omega_i, \iota_i, \omega_i\right) = \begin{bmatrix} \cos\Omega_i & -\sin\Omega_i & 0 \\ \sin\Omega_i & \cos\Omega_i & 0 \\ 0 & 0 & 1 \end{bmatrix} \begin{bmatrix} \cos\iota_i & 0 & \sin\iota_i \\ 0 & 1 & 0 \\ -\sin\iota_i & 0 & \cos\iota_i \end{bmatrix} \begin{bmatrix} \cos\omega_i & -\sin\omega_i & 0 \\ \sin\omega_i & \cos\omega_i & 0 \\ 0 & 0 & 1 \end{bmatrix} \tag{6.4}$$

This relationship between the i^{th} Node's Coordinate System and the Global Coordinate System is illustrated in Figure 6.1. Similarly the transformation which maps points in the GCS to points in the NCS_i is clearly given by:

$$\underline{x} = \mathbb{T}\left(\Omega_i, \iota_i, \omega_i\right)^{-1} \left(\underline{\check{x}} - \underline{\check{p}}_i\right) \tag{6.5}$$

Note that although the rotation matrix is expressed in terms of three angles of rotation, nodes need not necessarily use them and the design of the algorithms can operate using just the elements of the rotation matrix (however more data will have to be transmitted if using an estimate of the rotation matrix rather than estimates of the angles of rotation).

6.1.3 Converting Between Different Node Coordinate Systems

By firstly considering the transformation between the i^{th} Node's Coordinate System and the GCS followed by a transformation from the GCS to the j^{th} Node's

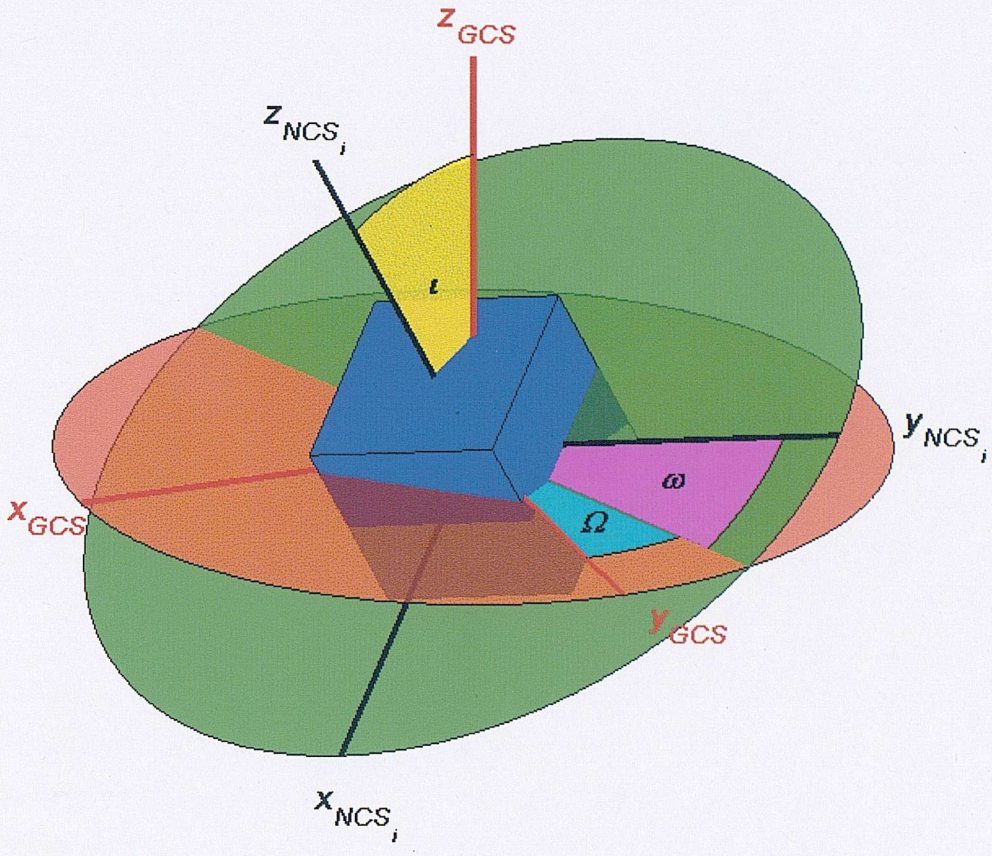


Figure 6.1: The Euler Angles That Transform Between Global and Node Coordinate Systems

Coordinate System the following expression is obtained for the transformation from NCS_i to NCS_j:

$$\underline{x}_j = \mathbb{T}_j^{-1}\left(\mathbb{T}_i\underline{x}_i + \underline{\check{p}}_i - \underline{\check{p}}_j\right) \tag{6.6}$$

If however one only needs to convert direction vectors from one coordinate system to another the node position vectors must be removed, i.e.

$$\underline{d}_j = \mathbb{T}_{j,i}\underline{d}_i \tag{6.7}$$

$$\text{where } \mathbb{T}_{j,i} = \mathbb{T}_j^{-1}\mathbb{T}_i \tag{6.8}$$

The same applies to the transformations in Equations (6.5) and (6.3) when applied to direction vectors.

6.1.4 The i^{th} Node's *Local Array* in the GCS

Applying the above to the *Local Array* on the i^{th} node gives the following expression for the locations of the elements of the *Local Array* in the GCS.

$$\check{\mathbf{r}}_i = \mathbb{T}\left(\Omega_i, \iota_i, \omega_i\right)\mathbf{r}_i + \underline{\check{p}}_i.\underline{1}_{N_L}^T \tag{6.9}$$

The matrix $\check{\mathbf{r}}_i$ will be used extensively in Section 6.3 to model the signals received at the *Local Array*.

6.1.5 Modelling Estimation Errors of the i^{th} Node's Rotation Matrix and Position Vector

In the above, the position and orientation of the node are known precisely, however nodes do not have access to this information and each node must (individually or collectively) estimate its orientation and position relative to other nodes and possibly absolute position and orientation if the network can communicate with other devices in the vicinity that are equipped with GPS. However, as mentioned previously, an Arrayed-WSN has no need for this to function correctly.

In any node self positioning and orientation algorithm one or more individual nodes, or nodes acting together, will form an estimate of the i^{th} node's orientation and position in the GCS. Note that strictly speaking, the estimates will eventually be translated into the coordinate system of the sink node or NCS_{sink}. However it is assumed, without any loss of generality, that NCS_{sink} corresponds to the GCS, (this can be done as the GCS is completely arbitrary).

The estimate of the i^{th} node's position vector is denoted by $\underline{\hat{\check{p}}}_i$ and $\left(\widehat{\Omega}_i, \widehat{\iota}_i, \widehat{\omega}_i\right)$ are the estimates of the Euler angles of rotation corresponding to the estimated rotation matrix $\widehat{\mathbb{T}}_i$. The error in the estimation of the i^{th} node's position vector can now be expressed straightforwardly as

$$\underline{\tilde{\check{p}}}_i = \underline{\hat{\check{p}}}_i - \underline{\check{p}}_i \tag{6.10}$$

and errors in the rotation matrix can be expressed as

$$\widetilde{\mathbb{T}}_i = \widehat{\mathbb{T}}_i - \mathbb{T}_i \tag{6.11}$$

Consider that node j has estimated its orientation relative to NCS_i, that is $\widehat{\mathbb{T}}_{j,i}$ has been calculated. If node i has been able to do the same relative to the sink node then the following estimate of the orientation of node j can be made

relative to the sink:

$$\begin{aligned}
\widehat{\mathbb{T}}_j &= \widehat{\mathbb{T}}_i \widehat{\mathbb{T}}_{j,i}^{-1} \qquad (6.12)\\
&= \left(\mathbb{T}_i + \widetilde{\mathbb{T}}_i\right) \times \left(\mathbb{T}_{j,i} + \widetilde{\mathbb{T}}_{j,i}\right)^{-1}\\
&= \mathbb{T}_i \left(\mathbb{T}_{j,i} + \widetilde{\mathbb{T}}_{j,i}\right)^{-1} + \widetilde{\mathbb{T}}_i \widehat{\mathbb{T}}_{j,i}^{-1}\\
&= \mathbb{T}_i \left(\mathbb{T}_{j,i}^{-1} - \left(\mathbb{T}_{j,i} + \widetilde{\mathbb{T}}_{j,i}\right)^{-1} \widetilde{\mathbb{T}}_{j,i} \mathbb{T}_{j,i}^{-1}\right) + \widetilde{\mathbb{T}}_i \widehat{\mathbb{T}}_{j,i}^{-1}\\
&= \mathbb{T}_i \left(\mathbb{T}_{j,i}^{-1} - \widehat{\mathbb{T}}_{j,i}^{-1} \widetilde{\mathbb{T}}_{j,i} \mathbb{T}_{j,i}^{-1}\right) + \widetilde{\mathbb{T}}_i \widehat{\mathbb{T}}_{j,i}^{-1}\\
&= \mathbb{T}_j - \mathbb{T}_i \widehat{\mathbb{T}}_{j,i}^{-1} \widetilde{\mathbb{T}}_{j,i} \mathbb{T}_{j,i}^{-1} + \widetilde{\mathbb{T}}_i \widehat{\mathbb{T}}_{j,i}^{-1}\\
&= \mathbb{T}_j + \widetilde{\mathbb{T}}_j \qquad (6.13)
\end{aligned}$$

where use has been made of the matrix identities

$$(\mathbb{A} + \mathbb{B})^{-1} = \mathbb{A}^{-1} \left(\mathbb{A}^{-1} + \mathbb{B}^{-1}\right)^{-1} \mathbb{B}^{-1} = \mathbb{A}^{-1} - \mathbb{A}^{-1} \left(\mathbb{A}^{-1} + \mathbb{B}^{-1}\right)^{-1} \mathbb{A}^{-1}$$

Hence $\widetilde{\mathbb{T}}_j$ is given by

$$\widetilde{\mathbb{T}}_j = \widetilde{\mathbb{T}}_i \widehat{\mathbb{T}}_{j,i}^{-1} - \mathbb{T}_i \widehat{\mathbb{T}}_{j,i}^{-1} \widetilde{\mathbb{T}}_{j,i} \mathbb{T}_{j,i}^{-1} \qquad (6.14)$$

Generalising the above to any number of intermediate nodes M gives the following iterative expression for the error in the j^{th} node's rotation matrix in terms of the errors in all the intermediate rotation matrices:

$$\widetilde{\mathbb{T}}_{n(m)} = \widetilde{\mathbb{T}}_{n(m-1)} \widehat{\mathbb{T}}_{n(m),n(m-1)}^{-1} + \mathbb{T}_{n(m-1)} \widehat{\mathbb{T}}_{n(m),n(m-1)}^{-1} \widetilde{\mathbb{T}}_{n(m),n(m-1)} \mathbb{T}_{n(m),n(m-1)}^{-1} \qquad (6.15)$$

$$\text{for } 1 \leq m \leq M+1 \text{ where } n(0) = sink \text{ and } n(M+1) = j$$

Finally a scalar measure of the errors $\widetilde{\mathbb{T}}_j$ can be provided by the Frobenius Norm of this real matrix

$$\left\|\widetilde{\mathbb{T}}_j\right\|_F = \sqrt{\mathrm{Tr}\left\{\widetilde{\mathbb{T}}_j \widetilde{\mathbb{T}}_j^T\right\}} \qquad (6.16)$$

6.2 Imperfect Clock Model

Many Wireless Sensor Network applications and protocols require nodes to maintain an accurate timebase in order to function correctly. For example:

- Many sensor network channel access algorithms require nodes to send messages at periodic intervals and any instability in the timebase could result in nodes sleeping when they should have the radio switched on to received messages [55].

- The temporal order in which events in the network occur may be important or even critical and any instability or incorrect synchronisation of clocks will result in messages being timestamped with incorrect values. In addition this information is required when performing *data or information fusion* as prior to the actual fusion a *registration* process needs to be performed, that is, messages that correspond to the same 'feature' or 'event' need to be identified [73].

- In an Arrayed Wireless Sensor Network, accurate and stable timing signals are required for the transmission of signals from a group of nodes acting as a *Wireless Array.*

In order to model uncertainties related to synchronisation issues between individual nodes, we first have to examine how a node's clock drifts. This will result in different nodes having different timebases, i.e. different conceptions about current time.

A mathematical model of the output of an oscillator which is used to derive the timebase of a node is given by

$$v(t) = A(t)\, p(\Phi(t)) \tag{6.17}$$

where $p(\Phi)$ is any periodic function with zero crossings at $p(n\pi) = 0, \forall n \in \mathcal{Z}$. As in [74], the effects of additive noise are included in the amplitude $A(t)$ and *total instantaneous phase* $\Phi(t)$, and we assume that $A(t) > 0 : \forall t$, so that this has no effect on the zero crossings of $v(t)$. The *instantaneous frequency* of the above signal is

$$f(t) \triangleq \frac{1}{2\pi} \frac{d\Phi(t)}{dt} \tag{6.18}$$

An ideal timing signal will have a constant $A(t)$ and $\Phi(t) = 2\pi f_{nom} t$, giving $f(t) = f_{nom}$, however in actual practical clocks a number of different deviations from this ideal behaviour are seen and these can be modelled by the following equation [75]

$$f(t) = f_0 + D_f\, f_{nom}\, t + \frac{1}{2\pi}\dot{\varphi}(t) \tag{6.19}$$

$$\text{where } f_0 = (f_{nom} + \Delta f) = \text{deterministic part of the } \textit{initial} \text{ frequency (i.e. at } t = 0) \tag{6.20}$$

In the above Δf is the *frequency offset* from the nominal value; D_f is the *linear fractional frequency drift* rate and models oscillator ageing effects and $\dot{\varphi}(t)/2\pi$

is the *random frequency deviation* which incorporates intrinsic *phase noise* (or *phase jitter*). Furthermore, the *time function* of a clock is defined as:

$$T(t) \triangleq \frac{\Phi(t)}{2\pi f_{nom}} \tag{6.21}$$

From Equations (6.18) and (6.21), the Time function of a node's clock can be calculated from the following integral:

$$T_{node}(t) = \frac{1}{f_{nom}} \int f(t)\, dt \tag{6.22}$$

Consider that a node's clock is synchronised or reset at the "ideal" time $t = T_{Synch}$ to the time value T_{SetTo} (and clock drift and ageing effects are measured relative to $t = 0$ when the nodes are assumed to be deployed). Therefore $T_{node}(T_{Synch}) = T_{SetTo}$. Substituting (6.19) into the above and integrating from T_{Synch} to the "current ideal time" $t = T_{Synch} + \tau$ gives:

$$\begin{aligned} T_{node}(t) - T_{SetTo} &= \int_{T_{Synch}}^{T_{Synch}+\tau} 1 + \frac{\Delta f}{f_{nom}} + D_f\, t + \frac{1}{2\pi f_{nom}} \dot{\varphi}(t)\, dt \\ &= \left[t + \frac{\Delta f}{f_{nom}} t + \frac{D_f}{2} t^2 + x_r(t) \right]_{T_{Synch}}^{T_{Synch}+\tau} \\ &= \tau + \frac{\Delta f}{f_{nom}} \tau + \frac{D_f}{2} \tau^2 + D_f T_{Synch} \tau + t_{Jitter}(t) \end{aligned} \tag{6.23}$$

where the timing jitter $t_{Jitter}(t)$ is defined as:

$$t_{Jitter}(t) \triangleq x_r(t) - x_r(T_{Synch}) = \int_{T_{Synch}}^{t} y_r(t)\, dt \tag{6.24}$$

then $T_{node}(t)$ can be written as

$$T_{node}(t) = (1 + \alpha_{Clock})(t - T_{Synch}) + \beta_{Clock}\left(t^2 - T_{Synch}^2\right) + T_{SetTo} + t_{Jitter}(t) \tag{6.25}$$

where

$$\alpha_{Clock} = \frac{\Delta f}{f_{nom}}, \beta_{Clock} = \frac{D_f}{2} \tag{6.26}$$

Using the above, the following model for the non-ideal nature of the node's clocks can be derived assuming that the i^{th} node's clock is synchronised or reset at $t = T_{Synch,i}$ to the value $T_{SetTo,i}$:

$$T_i(t) = (1 + \alpha_{Clock,i})(t - T_{Synch,i}) + \beta_{Clock,i}\left(t^2 - T_{Synch,i}^2\right) + T_{SetTo,i} + t_{Jitter,i}(t) \tag{6.27}$$

where $\alpha_{Clock,i}$ is the i^{th} node's 1^{st} order timing accuracy coefficient and is determined by the frequency offset of the oscillator and $\beta_{Clock,i}$ is the i^{th} node's 2^{nd} order timing accuracy coefficient and is determined by the fractional drift rate of the oscillator.

6.3 Uncertainties Relating to the Node's *Local Array*

The use of an array of antennas on each node brings many benefits such as the ability for a single node to perform direction of arrival estimation and cancellation of interfering signals based on their spatial signatures. However, it also introduces a number of uncertainties that are present in most, if not all, antenna array systems. These are:

- Geometrical errors/uncertainties related to the positions of the array elements.
- Electrical errors/uncertainties related to the gain and phase response of each antenna element.
- Uncertainties/Errors introduced by antenna element failure.

In this section, all of the above are considered and models for each are presented which are applicable to both the *initial* and the *intra-Wireless Array* links.

6.3.1 Modelling Signals Received by the Node's *Local Array*

The vector complex baseband representation of the signal received at the i^{th} node's *Local Array* due to *just the direct path* of a complex baseband signal $m_j(t)$ originating at a position $\underline{\check{r}}_j$ (relative to the Global Coordinate System as indicated) can be shown to be given by:

$$\underline{x}_{ij}(t) = \underline{S}_{ij}\, m_{ij}(t) \in \mathcal{C}^{N_L \times 1} \tag{6.28}$$

$$\text{in which } m_{ij}(t) = \frac{\kappa_{ij}}{(\rho_{ij})^{\eta}} m_j(t - \tau_{ij}),\ \tau_{ij} \triangleq \frac{\rho_{ij}}{v_{ph}} \text{ and } \rho_{ij} \triangleq \left\| \underline{\check{p}}_i - \underline{\check{r}}_j \right\|$$

where $\underline{S}_{ij}$ is the manifold vector, ρ_{ij} is the distance from the source to the center of the node, $m_{ij}(t)$ is the signal received at the reference point which in this case is defined to be the center of the node, κ_{ij}, η model attenuation and transmission effects (such as free space path loss) and it has been assumed that the bandwidth of the signal $m_j(t)$ is small compared to the phase velocity v_{ph} over the aperture D of the array.

If the distance between the i^{th} node and the j^{th} source ρ_{ij} satisfies:

$$\rho_{ij} > \frac{2D^2}{\lambda} \tag{6.29}$$

where λ is the wavelength associated with the carrier, then the signals can be considered to be plane waves and the array manifold vector can be expressed using Equation (6.30) or (6.34). Note that for a node with side length l_{n}, the aperture of the array can be considered to be given by $D = \sqrt{3}l_{\mathrm{n}}$ (which is the largest obtainable using antenna elements with negligible size and located at the corners of the node). Hence assuming a cubic node with volume 10 cm^3 and a carrier frequency of 24 GHz gives a plane wave boundary of $\rho_{ij} > 22.3\,\mathrm{cm}$ and requires that the bandwidth of the signal $m_j(t)$ to be much less than 8 GHz (which will clearly be easily satisfied for even high processing gains).

The array manifold vector assuming plane wave propagation is given in terms of the i^{th} node's *Local Array* $\mathbf{r}_i$ and position of the source (both relative to the i^{th} Node's Coordinate System) by the following expressions (adapted from [76]):

$$\underline{S}_{ij} = \underline{g}_{ij} \odot \exp\left(-j\mathbf{r}_i{}^T \underline{k}_{ij}\right) \in \mathcal{C}^{N_{\mathrm{L}} \times 1} \tag{6.30}$$

$$\underline{k}_{ij} = \frac{2\pi}{\lambda} \frac{\underline{r}_{ij}}{\left\|\underline{r}_{ij}\right\|} = \underline{k}\left(\theta_{ij}, \varphi_{ij}\right) \tag{6.31}$$

$$\underline{r}_{ij} = \mathbb{T}_i^{-1}\left(\check{\underline{r}}_j - \check{\underline{p}}_i\right) \tag{6.32}$$

where $\underline{g}_{ij}$ models the gain and phase response of each of the array elements (which will be examined in more detail in the following subsection) and $\underline{k}_{ij}$ is the wavenumber vector pointing from the center of the i^{th} node to the j^{th} source expressed using the wavenumber vector function $\underline{k}(\theta, \varphi)$ for an azimuth angle θ and elevation angle φ. The wavenumber vector function is defined as before by:

$$\underline{k}(\theta, \varphi) \triangleq \frac{2\pi}{\lambda}\left[\cos\theta\cos\varphi \quad \sin\theta\cos\varphi \quad \sin\varphi\right]^T \tag{6.33}$$

in which λ corresponds to any frequency used by the *initial* or *intra-Wireless Array* links in this section. Note however, that when this function is used in Section 6.4 the wavelength λ corresponds to any frequency used by the *intra-Wireless Array* link. Also note that because Multicarrier DS-CDMA may be used by the links, it may be necessary to compute a different array manifold vector for each subcarrier - if the total bandwidth of the modulated signal over the center carrier frequency is large enough to make a significant difference to the manifold vector.

The array manifold vector for plane wave propagation may also be expressed in terms of the Global Coordinate System by applying Equation (6.5) (both for position vectors in the case of $\mathbf{r}_i$ and for direction vectors in the case of $\underline{k}_{ij}$) to

give the following:

$$\begin{aligned}\underline{S}_{ij} &= \underline{g}_{ij} \odot \exp\left(-j\left(\mathbb{T}_i^{-1}\left(\check{\mathbf{r}}_i - \underline{\check{p}}_i \underline{1}_{N_L}^T\right)\right)^T \mathbb{T}_i^{-1} \underline{\check{k}}_j\right) \\ &= \underline{g}_{ij} \odot \exp\left(-j\left(\check{\mathbf{r}}_i - \underline{\check{p}}_i \underline{1}_{N_L}^T\right)^T \mathbb{T}_i \mathbb{T}_i^{-1} \underline{\check{k}}_j\right) \\ &= \underline{g}_{ij} \odot \exp\left(-j\check{\mathbf{r}}_i^T \underline{\check{k}}_j + j\underline{1}_{N_L}\left(\underline{\check{p}}_i^T \underline{\check{k}}_j\right)\right) \end{aligned} \tag{6.34}$$

where $\underline{\check{k}}_j = \underline{k}\left(\check{\theta}_j, \check{\varphi}_j\right) = (2\pi/\lambda)\,\underline{\check{r}}_j / \left\|\underline{\check{r}}_j\right\|$ and $\left(\check{\theta}_j, \check{\varphi}_j\right)$ are the azimuth and elevation of the j^{th} source relative to the GCS. Note that the additional term $\underline{\check{p}}_i^T \underline{\check{k}}_j$ in the above equation is required to shift the reference point of the array from the origin of the GCS to the center of the node so that the array reference point is the same as in Equation (6.30).

However if the distance ρ_{ij} satisfies:

$$\rho_{ij} < \frac{2D^2}{\lambda} \tag{6.35}$$

then the array manifold vector must be calculated using Equation (6.36) below (adapted from [77]):

$$\underline{S}_{ij} = \underline{g}_{ij} \odot \left(\rho_{ij}\underline{1}_{N_L} \oslash \underline{d}_{ij}\right)^{\eta} \exp\left(-j\frac{2\pi}{\lambda}\left(\rho_{ij}\,\underline{1}_{N_L} - \underline{d}_{ij}\right)\right) \tag{6.36}$$

$$\text{where } \text{ele}_n\left\{\underline{d}_{ij}\right\} = \sqrt{\left(\underline{\check{r}}_j - \text{col}_n\left\{\check{\mathbf{r}}_i\right\}\right)^T \left(\underline{\check{r}}_j - \text{col}_n\left\{\check{\mathbf{r}}_i\right\}\right)} \tag{6.37}$$

After some manipulation the distances from the j^{th} source to each of the array elements contained in $\underline{d}_{i,j}$ can be expressed in the following vector form:

$$\underline{d}_{ij} = \sqrt{\underline{1}_{N_L}\rho_j^2 + \text{diag}\left\{\check{\mathbf{r}}_i{}^T\check{\mathbf{r}}_i\right\} - 2\check{\mathbf{r}}_i{}^T\underline{\check{r}}_j} \tag{6.38}$$

$$= \sqrt{\underline{1}_{N_L}\rho_j^2 + \text{diag}\left\{\check{\mathbf{r}}_i{}^T\check{\mathbf{r}}_i\right\} - \frac{\rho_j\lambda}{\pi}\check{\mathbf{r}}_i{}^T\underline{k}\left(\check{\theta}_j, \check{\varphi}_j\right)} \tag{6.39}$$

where $\rho_j = \left\|\underline{\check{r}}_j\right\|$, i.e. the distance of the source from the origin of the GCS. Equations (6.37) to (6.39) are expressed using the both the sources position and the *Local Array* elements expressed in the Global Coordinate System. However it is also important to identify how $\underline{d}_{ij}$ can be expressed using vectors relative to the NCS_i which is addressed by the following:

$$\text{ele}_n\left\{\underline{d}_{ij}\right\} = \sqrt{\left(\underline{r}_{ij} - \text{col}_n\left\{\mathbf{r}_i\right\}\right)^T \left(\underline{r}_{ij} - \text{col}_n\left\{\mathbf{r}_i\right\}\right)} \tag{6.40}$$

and noting that $\rho_{ij} = \left\|\underline{r}_{ij}\right\|$, the above can be expressed in vector form as:

$$\underline{d}_{i,j} = \sqrt{\underline{1}_{N_L}\rho_{ij}^2 + \text{diag}\left\{\mathbf{r}_i{}^T\mathbf{r}_i\right\} - 2\mathbf{r}_i{}^T\underline{r}_{ij}} \tag{6.41}$$

$$= \sqrt{\underline{1}_{N_L}\rho_{ij}^2 + \text{diag}\left\{\mathbf{r}_i{}^T\mathbf{r}_i\right\} - \frac{\rho_{ij}\lambda}{\pi}\mathbf{r}_i{}^T\underline{k}\left(\theta_{ij}, \varphi_{ij}\right)} \tag{6.42}$$

Finally in the presence of M signal sources and noise, the i^{th} node's *Local Array* received signal is given by:

$$\underline{x}_i(t) = \sum_{j=1}^{M} \underline{S}_{ij}\, m_{ij}(t) + \underline{n}_i(t) \in C^{N_L \times 1} \tag{6.43}$$

where the elements of $\underline{n}_i(t)$ represents the thermal noise in addition to unmodelled interferences in the environment at each antenna element. The above equation can be written in a compact vector matrix form as:

$$\underline{x}_i(t) = \mathbb{S}_i \underline{m}_i(t) + \underline{n}_i(t) \tag{6.44}$$

$$\text{where} \begin{cases} \mathbb{S}_i = \left[\underline{S}_{i,1} \quad \cdots \quad \underline{S}_{i,M}\right] \\ \underline{m}_i(t) = \left[m_{i,1}(t) \quad \cdots \quad m_{i,M}(t)\right]^T \end{cases}$$

6.3.2 Modelling Electrical and Geometric Uncertainties

In the above section, the nature of the additional gain and phase modelled by the vector $\underline{g}_{i,j}$ were not examined in detail. This term is due to the gain and phase response inherent in each antenna element which in general is a function of the direction of arrival of the incoming signal wave (and will also be dependent on the polarisation of the incoming wave and the type and orientation of the antenna). Expressing $\underline{g}_{i,j}$ in terms of its gain and phase components gives:

$$\underline{g}_{i,j} = \underline{\gamma}_i(\theta_j, \varphi_j) \odot \exp\left(j\underline{\phi}_i(\theta_j, \varphi_j)\right) \in C^{N_L \times 1} \tag{6.45}$$

$$= \underline{\gamma}_i(\underline{u}_j) \odot \exp\left(j\underline{\phi}_i(\underline{u}_j)\right) \in C^{N_L \times 1} \tag{6.46}$$

where $\underline{\gamma}_i(\theta_j, \varphi_j) = \underline{\gamma}_i(\underline{u}_j) = \underline{\gamma}_{i,j}$ and $\underline{\phi}_i(\theta_j, \varphi_j) = \underline{\phi}_i(\underline{u}_j) = \underline{\phi}_{i,j}$ are $N_L \times 1$ real valued column vectors expressed in either polar or rectangular coordinates and collectively model what is known as the *electrical characteristics* of the array. In addition $\underline{u}_j$ is the unit norm direction vector of the j^{th} source, and defined as:

$$\underline{u}_j \triangleq \left[\cos\theta_j \cos\varphi_j \quad \sin\theta_j \cos\varphi_j \quad \sin\varphi_j\right]^T \in \mathcal{R}^{3\times 1} \tag{6.47}$$

Note that (θ_j, φ_j) and $\underline{u}_j$ could be expressed in any coordinate system, provided that the same one is used for each element of the array. Also, for the sake of notational convenience the gain and phase response of the i^{th} node's *Local Array* are assumed to be expressed in terms of a direction relative to the i^{th} node's coordinate system unless otherwise indicated.

6.3.2.1 Electrical Uncertainties

For a given type of antenna element the theoretical (or nominal) gain $\underline{\widehat{\gamma}}$ and phase $\underline{\widehat{\phi}}$ response can be calculated or estimated. However, in practice, any conducting object placed in the vicinity of the antenna or incorrect mathematical modelling of the antenna will result in a deviation $\underline{\widetilde{\gamma}}$,$\underline{\widetilde{\phi}}$ from this nominal response and will result in the actual or true array gain and phase being given by (where the i, j have been suppressed for notational brevity):

$$\underline{\gamma} = \underline{\widehat{\gamma}} + \underline{\widetilde{\gamma}} \tag{6.48}$$

$$\underline{\phi} = \underline{\widehat{\phi}} + \underline{\widetilde{\phi}} \tag{6.49}$$

Note that it is common to assume that the errors in the gain and phase response are independent of the direction of the incoming signals [78],[76],[79] although no such assumption has been made so far in this study.

The true array manifold vector can now be written as

$$\underline{S} = \underline{\gamma} \odot \exp\left(j\underline{\phi}\right) \odot \underline{a} \tag{6.50}$$

where $\underline{a}$ is the *bare manifold vector*, that is the part of the expressions given in Equations (6.30),(6.34) and (6.36) not dependent on the electrical characteristics of the array. Assuming that no error is made in estimating $\underline{a}$ (these errors/uncertainties will be examined shortly) and substituting Equations (6.48) and (6.49) into the above, then following a method similar to that used in [76] gives:

$$\begin{aligned}
\underline{S} &= \left(\underline{\widehat{\gamma}} + \underline{\widetilde{\gamma}}\right) \odot \exp\left(j\left(\underline{\widehat{\phi}} + \underline{\widetilde{\phi}}\right)\right) \odot \underline{a} \\
&= \underline{\widehat{\gamma}} \odot \exp\left(j\underline{\widehat{\phi}}\right) \odot \exp\left(j\underline{\widetilde{\phi}}\right) \odot \underline{a} + \underline{\widetilde{\gamma}} \odot \exp\left(j\underline{\widehat{\phi}}\right) \odot \exp\left(j\underline{\widetilde{\phi}}\right) \odot \underline{a} \\
&= \underline{\widehat{\gamma}} \odot \exp\left(j\underline{\widehat{\phi}}\right) \odot \underline{a} \odot \left(\exp\left(j\underline{\widetilde{\phi}}\right) + \underline{\widetilde{\gamma}} \oslash \underline{\widehat{\gamma}} \odot \exp\left(j\underline{\widetilde{\phi}}\right)\right) \\
&= \underline{\widehat{S}} \odot \left(\exp\left(j\underline{\widetilde{\phi}}\right) + \underline{\widetilde{\gamma}} \oslash \underline{\widehat{\gamma}} \odot \exp\left(j\underline{\widetilde{\phi}}\right)\right)
\end{aligned} \tag{6.51}$$

Hence the error in the manifold vector just due to electrical uncertainties is

$$\underline{\widetilde{S}} \triangleq \underline{S} - \underline{\widehat{S}} = \underline{\widehat{S}} \odot \left(\exp\left(j\underline{\widetilde{\phi}}\right) + \underline{\widetilde{\gamma}} \oslash \underline{\widehat{\gamma}} \odot \exp\left(j\underline{\widetilde{\phi}}\right) - \underline{1}_{N_L}\right) = \widetilde{\mathbf{\Delta}}_e \underline{\widehat{S}} \tag{6.52}$$

$$\text{where } \widetilde{\mathbf{\Delta}}_e = \text{diag}\left\{\left(\underline{\widehat{\gamma}} + \underline{\widetilde{\gamma}}\right) \oslash \underline{\widehat{\gamma}} \odot \exp\left(j\underline{\widetilde{\phi}}\right) - \underline{1}_{N_L}\right\}$$

Figure 6.2 shows the operation of a well known source direction of arrival estimation algorithm (MUSIC [80]) for an environment consisting of five uncorrelated signal sources with equal powers and with directions relative to a node $(\theta, \varphi)_j = (10\,°, 12\,°)_1$, $(76\,°, 40\,°)_2$, $(150\,°, -20\,°)_3$, $(158\,°, -20\,°)_4$, $(270\,°, -56\,°)_5$

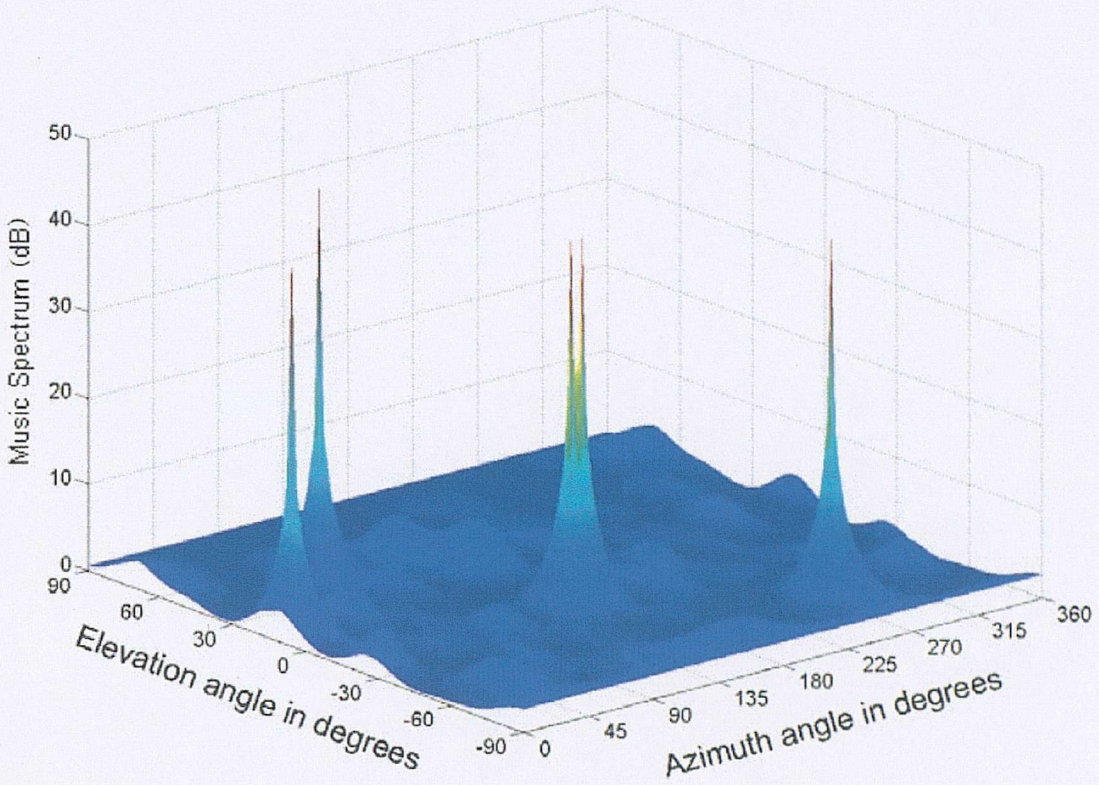


Figure 6.2: MUSIC spectrum using nodes local array with no uncertainties

in the presence of additive white Gaussian noise (10 dB below the power of each source). 500 snapshots were used to form the received covariance matrix and the node's *Local Array* was modelled as a 3D grid array with 24 elements without any uncertainties/errors. The peaks of the MUSIC spectrum shown in the figure correspond to the directions of arrival of the signals in the environment.

Figure 6.3 shows how the operation of this algorithm is affected by electrical uncertainties. It is clear from this figure that the MUSIC algorithm breaks down in the presence of such uncertainties. Fortunately, techniques for mitigating this and the other uncertainties presented here exist, one example being the technique proposed in [81].

6.3.2.2 Geometrical Uncertainties

As just indicated the above expressions assumed that no error/uncertainty exists in the nominal value of the *isotropic manifold vector* $\underline{\widehat{a}}$, i.e. $\underline{\widehat{a}} = \underline{a}$. However in practice errors/uncertainties in the locations of the array elements and (if calculating the source position vector - using an estimated source location), errors in the estimated source location can cause deviation of the nominal isotropic manifold vector from the true isotropic manifold vector. This subsection considers

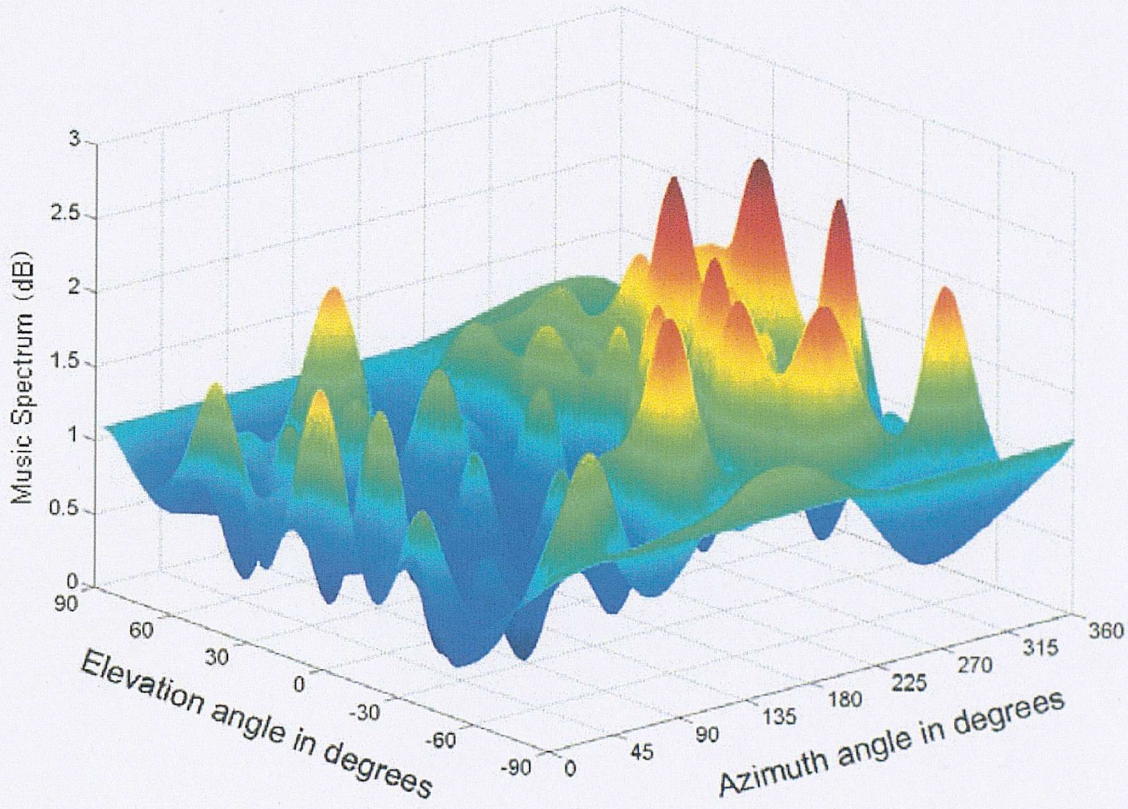


Figure 6.3: MUSIC spectrum using nodes local array in the presence of electrical uncertainties

the effect of the first of these two types of error, also known as Geometrical Errors or Uncertainties. (Note that the i, j have again been suppressed for notational brevity except for the matrix $\mathbf{r}_i$).

Starting from the true locations of the array elements expressed in the Node's Coordinate System $\mathbf{r}_i$, the relationship between the nominal locations $\widehat{\mathbf{r}}_i$ and the errors $\widetilde{\mathbf{r}}_i$ is defined by:

$$\widetilde{\mathbf{r}}_i \triangleq \mathbf{r}_i - \widehat{\mathbf{r}}_i \tag{6.53}$$

This suggests the following definition for the error in the isotropic manifold vector:

$$\widetilde{\underline{a}} \triangleq \underline{a} \oslash \widehat{\underline{a}} \tag{6.54}$$

This is because, for plane wave propagation, $\widetilde{\underline{a}}$ as defined above, is only a function of the error in the element positions and the source wavenumber vector. The following expressions show this to be the case:

$$\begin{aligned}
\widetilde{\underline{a}} &= \exp\left(-j\left(\widehat{\mathbf{r}}_i + \widetilde{\mathbf{r}}_i\right)^T \underline{k}(\theta,\varphi)\right) \oslash \exp\left(-j\widehat{\mathbf{r}}_i{}^T \underline{k}(\theta,\varphi)\right) \\
&= \exp\left(-j\widehat{\mathbf{r}}_i{}^T \underline{k}(\theta,\varphi)\right) \odot \exp\left(-j\widetilde{\mathbf{r}}_i{}^T \underline{k}(\theta,\varphi)\right) \oslash \exp\left(-j\widehat{\mathbf{r}}_i{}^T \underline{k}(\theta,\varphi)\right) \\
&= \exp\left(-j\widetilde{\mathbf{r}}_i{}^T \underline{k}(\theta,\varphi)\right)
\end{aligned} \tag{6.55}$$

However for spherical wave propagation this is not the case and both the true and the nominal isotropic manifold vectors need to be calculated to obtain $\widetilde{\underline{a}}$ by using Equation (6.54) and Equation (6.36) (without the $\underline{g}_{ij}$) using both $\mathbf{r}_i$ and $\widehat{\mathbf{r}}_i$. Incorporating Equation (6.54) into the expression for the true array manifold vector (including electrical uncertainties) gives:

$$\begin{aligned}
\underline{S} &= \left(\widehat{\underline{\gamma}} + \widetilde{\underline{\gamma}}\right) \odot \exp\left(j\left(\widehat{\underline{\phi}} + \widetilde{\underline{\phi}}\right)\right) \odot \widehat{\underline{a}} \odot \widetilde{\underline{a}} \\
&= \widehat{\underline{\gamma}} \odot \exp\left(j\widehat{\underline{\phi}}\right) \odot \exp\left(j\widetilde{\underline{\phi}}\right) \odot \widehat{\underline{a}} \odot \widetilde{\underline{a}} + \widetilde{\underline{\gamma}} \odot \exp\left(j\widehat{\underline{\phi}}\right) \odot \exp\left(j\widetilde{\underline{\phi}}\right) \odot \widehat{\underline{a}} \odot \widetilde{\underline{a}} \\
&= \widehat{\underline{\gamma}} \odot \exp\left(j\widehat{\underline{\phi}}\right) \odot \widehat{\underline{a}} \odot \left(\exp\left(j\widetilde{\underline{\phi}}\right) + \widetilde{\underline{\gamma}} \oslash \widehat{\underline{\gamma}} \odot \exp\left(j\widetilde{\underline{\phi}}\right)\right) \odot \widetilde{\underline{a}} \\
&= \widehat{\underline{S}} \odot \left(\exp\left(j\widetilde{\underline{\phi}}\right) + \widetilde{\underline{\gamma}} \oslash \widehat{\underline{\gamma}} \odot \exp\left(j\widetilde{\underline{\phi}}\right)\right) \odot \widetilde{\underline{a}}
\end{aligned} \tag{6.56}$$

Hence the error in the true manifold vector just due to both geometrical and electrical uncertainties is [76]:

$$\widetilde{\underline{S}} \triangleq \underline{S} - \widehat{\underline{S}} = \widehat{\underline{S}} \odot \left(\exp\left(j\widetilde{\underline{\phi}}\right) \odot \widetilde{\underline{a}} + \widetilde{\underline{\gamma}} \oslash \widehat{\underline{\gamma}} \odot \exp\left(j\widetilde{\underline{\phi}}\right) \odot \widetilde{\underline{a}} - \underline{1}_{N_L}\right) = \widetilde{\mathbf{\Delta}}\widehat{\underline{S}} \tag{6.57}$$

where $\widetilde{\mathbf{\Delta}} = \mathrm{diag}\left\{\left(\widehat{\underline{\gamma}} + \widetilde{\underline{\gamma}}\right) \oslash \widehat{\underline{\gamma}} \odot \exp\left(j\widetilde{\underline{\phi}}\right) \odot \widetilde{\underline{a}} - \underline{1}_{N_L}\right\}$

The effect of geometrical uncertainties due to errors in the positions of the antenna elements on the *Local Array* is expected to be negligible as the manufacturing tolerances are much smaller than the wavelength, however this type

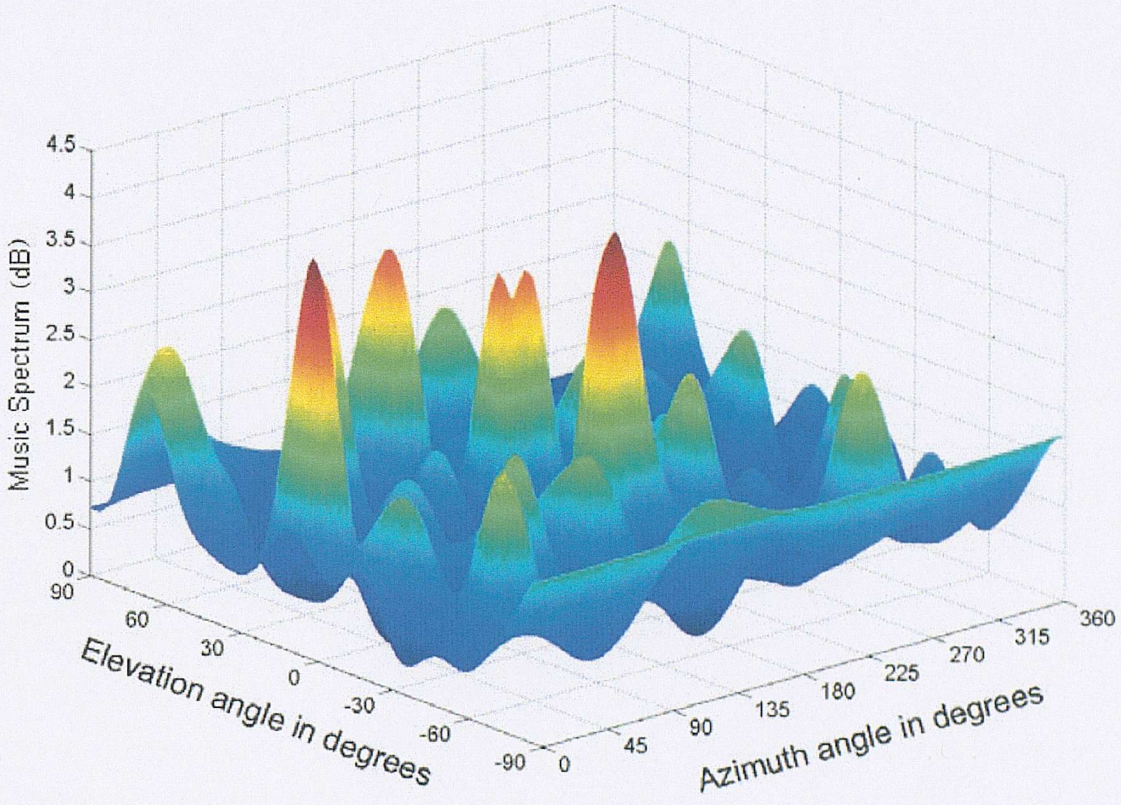


Figure 6.4: MUSIC spectrum using nodes local array in the presence of geometrical uncertainties

of uncertainty becomes dominant when considering *Wireless Arrays* (See Section 6.4).

The same environment as described for Figure 6.2 is used in Figure 6.4, which shows the effect of the presence of geometrical uncertainties (albeit larger than would be expected for the node's *Local Array*) on the MUSIC algorithm. As with the previous example, the MUSIC algorithm completely fails as the spectrum contains many false peaks and they are at a much lower level than in the unperturbed case. These examples illustrate the importance of modelling the system as accurately as possible, (e.g. by using calibration), and/or using techniques that are robust to uncertainties.

6.4 Uncertainties Relating to a *Wireless Array* of Nodes

A *Wireless Array* is formed from N nodes; $(N-1)$ of which are Element Nodes and the other is known as the Array Controller and is responsible for coordinating the *Wireless Array*. Each node in an Arrayed-WSN is assigned (prior to deployment) with a unique NodeID $\in \mathcal{N}$ denoted by i, and the Node IDs of the nodes constituting the u^{th} *Wireless Array* are the elements of the set $\mathcal{W}_u$, in addition the Controllers Node ID is denoted by c_u. Note that for notational brevity the subscript identifying the *Wireless Array* has been omitted in the following unless specific reference is made to a particular *Wireless Array*.

The number of antenna elements on a node used by the *inter-Wireless Array* link is denoted by N_{nw} and the positions of these elements for the i^{th} node relative to its own coordinate system are given by the columns of the matrix $\mathbf{r}_{\mathrm{nw},i}$, which can be written in terms of the positions of all the array elements on a node, given by the columns of $\mathbf{r}_{\mathrm{n}}$ as:

$$\mathbf{r}_{\mathrm{nw},i} = \mathbf{r}_{\mathrm{n}}\, \mathbb{Q}_{\mathrm{nw},i}, \forall i \in \mathcal{W} \tag{6.58}$$

where $\mathbb{Q}_{\mathrm{nw},i}$ is a N_{n} by N_{nw} selection matrix with each column containing a one in the row corresponding to a selected antenna element and zeros elsewhere. Similar to that defined in Equation (6.2). Note: for the case where the same antenna elements on a node are used for the *inter-Wireless Array* link as for the *initial* and *intra-Wireless Array* links the above selection matrix is equal to the selection matrix in Equation (6.1), i.e. $\mathbb{Q}_{\mathrm{nw},i} = \mathbb{Q}_i$ and $N_{\mathrm{nw}} = N_{\mathrm{L}}$.

The array reference point of the u^{th} *Wireless Array* is defined as the center of the controller node, with position $\underline{\tilde{p}}_{c_u}$. Also directions relative to this array

will be given in the Controllers Coordinate System i.e. in CCS_u (denoted using a $\smile$ above a symbol, as opposed to $\vee$ for the GCS). It is desirable to express the coordinates of the utilised array elements on the i^{th} node in the coordinate system of the controller node. Therefore applying Equation (6.6) to $\mathbf{r}_{\mathrm{nw},i}$ with $j = c_u$ and multiplying the position vectors by the row vector $\underline{1}_{N_{\mathrm{nw}}}^T$ so that each column of the $\mathbf{r}$ matrix is translated correctly gives the following expression for the positions of the utilised array elements:

$$\breve{\mathbf{r}}_{\mathrm{nw},i} = \mathbb{T}_{c_u}^{-1}\left(\mathbb{T}_i\mathbf{r}_{\mathrm{nw},i} + \left(\underline{\breve{p}}_i - \underline{\breve{p}}_{c_u}\right)\underline{1}_{N_{\mathrm{nw}}}^T\right), \forall i \in \mathcal{W}_u \tag{6.59}$$

$$= \breve{\mathbf{r}}_{\mathrm{W},i} + \underline{\breve{p}}_{ui}\underline{1}_{N_{\mathrm{nw}}}^T, \text{ where } \breve{\mathbf{r}}_{\mathrm{W},i} \triangleq \mathbb{T}_{c_u}^{-1}\mathbb{T}_i\mathbf{r}_{\mathrm{nw},i} \tag{6.60}$$

where $\breve{\mathbf{r}}_{\mathrm{W},i}$ is the result of rotating the locations of the selected antenna elements on the i^{th} node into the CCS_u but without translating.

In a *Wireless Array* each node processes the signals received at its own utilised antenna elements then passes a single signal to the array controller (via the *intra-Wireless Array* link) or in transmit mode a single signal is transmitted by the array controller and each element node processes it to obtain the signals to be transmitted on each of its utilised antenna elements. (Note that the array controller can pass parameters to control this processing to each of the element nodes using the *initial*-wireless communication link or as additional digital data interleaved with the signal data passed on the *intra-Wireless Array* link).

Therefore each node in *Wireless Array* acts like a directional antenna with its own gain and phase response (similar to that modelled by $\underline{g}_{ij}$ in Section 6.3.1). Hence the number of "information streams" provided by a single node in this approach is one, and the number of *effective Wireless Array* elements is $N_{\mathrm{wa}} = N$.

The positions of the effective elements of the u^{th} *Wireless Array* are therefore given by the positions of the nodes constituting the array. That is, the *Wireless Array* element positions (in the GCS) are given by the columns of the following matrix:

$$\breve{\mathbf{r}}_{\mathrm{I},u} = \left[\underline{\breve{p}}_{c_u},\ \underline{\breve{p}}_i,\ \cdots,\ \underline{\breve{p}}_k\right] \in \mathcal{R}^{3\times N}, \{c_u, i, k\} \subset \mathcal{W}_u \tag{6.61}$$

and in the coordinate system of the controller node as:

$$\breve{\mathbf{r}}_{\mathrm{I},u} = \mathbb{T}_{c_u}^{-1}\left(\breve{\mathbf{r}}_{\mathrm{I},u} - \underline{\breve{p}}_{c_u}\underline{1}_N^T\right) \in \mathcal{R}^{3\times N} \tag{6.62}$$

Note that the first column of this matrix will contain all zeros. The received signal vector at the utilised elements of the i^{th} node as a member of a *Wireless*

Array is given by:

$$\underline{x}_{\mathrm{W},i}(t) = \mathbb{S}_{\mathrm{W},i}\underline{m}_{\mathrm{W}}(t) + \underline{n}_i(t) \in \mathcal{C}^{N_{\mathrm{nw}}\times 1} \tag{6.63}$$

$$\text{where } \begin{cases} \mathbb{S}_{\mathrm{W},i} = \left[\underline{S}_{\mathrm{W},i,1}, \ \cdots, \ \underline{S}_{\mathrm{W},i,M}\right] \\ \underline{m}_{\mathrm{W}}(t) = \left[m_{\mathrm{W},1}(t), \ \cdots, \ m_{\mathrm{W},M}(t)\right]^T \end{cases}$$

which is exactly the same as for the *Local Array* as presented in Section 6.3.1, however $\underline{m}_{\mathrm{W}}(t)$ (subscript u omitted) represents the M message signals received at the center of the controller node, not the center of the i^{th} node. The plane wave manifold vector of the j^{th} source (located at $\breve{\underline{r}}_j$ in the GCS or $\breve{\underline{r}}_{uj}$ in CCS_u) as used by the above equation can be written as:

$$\underline{S}_{\mathrm{W},ij} = \underline{g}_{ij} \odot \exp\left(-j\breve{\mathbf{r}}_{\mathrm{W},i}{}^T\breve{\underline{k}}_{ij}\right)\left(\frac{\rho_{\mathrm{W}u,j}}{\rho_{ij}}\right)^{\eta}\exp\left(-j\varsigma_i\right) \in \mathcal{C}^{N_{\mathrm{nw}}\times 1} \tag{6.64}$$

$$\text{where } \begin{cases} \breve{\underline{k}}_{ij} = \frac{2\pi}{\lambda}\breve{\underline{r}}_{ij}/\left\|\breve{\underline{r}}_{ij}\right\| = \underline{k}\left(\breve{\theta}_{ij}, \breve{\varphi}_{ij}\right) \\ \breve{\underline{r}}_{ij} = \mathbb{T}_{c_u}^{-1}\left(\breve{\underline{r}}_j - \breve{\underline{p}}_i\right) = \breve{\underline{r}}_{uj} - \breve{\underline{p}}_{ui} \\ \rho_{\mathrm{W}u,j} = \left\|\breve{\underline{r}}_{uj}\right\|, \rho_{ij} = \left\|\breve{\underline{r}}_{ij}\right\| \end{cases}$$

and both the array element positions, the wavenumber vector and $\left(\breve{\theta}_{ij}, \breve{\varphi}_{ij}\right)$ are expressed in the coordinate system of the controller but relative to (or as measured at) the center of the i^{th} node (hence the use of $\breve{\mathbf{r}}_{\mathrm{W},i}$ instead of $\breve{\mathbf{r}}_{\mathrm{nw},i}$). The additional exponential scalar term in Equation (6.64) is needed in order for the reference point of the array to be at the center of the controller node and not the center of the i^{th} node. If the distance of the source from the *Wireless Array* is such that plane wave propagation can be assumed then ς_i is simply given by Equation (6.65) below, which can be derived by using Equation (6.60) and $\frac{\rho_{\mathrm{W}u,j}}{\rho_{ij}} \approx 1$. However if the distance to the source is small compared to the aperture of the *Wireless Array*, or if the source lies within the *Wireless Array* then the phase ς_i is determined by the difference in the distance from the source to the controller ($\rho_{\mathrm{W}u,j}$) and the source to the i^{th} node (ρ_{ij}) as expressed by Equation (6.67).

$$\varsigma_i = \breve{\underline{p}}_{ui}^T\breve{\underline{k}}_{ij}, \text{where } \forall i \in \mathcal{W}_u, \breve{\underline{k}}_{ij} = \breve{\underline{k}}_{uj} = \underline{k}\left(\breve{\theta}_{uj}, \breve{\varphi}_{uj}\right) \tag{6.65}$$

for the plane wave case (6.66)

$$\varsigma_i = \frac{2\pi}{\lambda}\left(\rho_{\mathrm{W}u,j} - \rho_{ij}\right), \forall i \in \mathcal{W}_u \tag{6.67}$$

for the spherical wave case (6.68)

The signals contained in $\underline{x}_{\mathrm{W},i}(t)$ are processed by the node using parameters sent by the controller to obtain a discrete (i.e. sampled) set of snapshots represented by the sequence $\{y_{\mathrm{W}u,i}(nT_s), n \in \mathcal{N}\}$, which is then source and channel

coded and sent via the *intra-Wireless Array* link to the controller node. The streams from all the element nodes can be reconstructed by the controller (which is not a trivial task as sample $y_i(nT_s)$ should correspond to the same chip or symbol in the message waveform as $y_k(nT_s)$ $i \neq k$, and this will be discussed in more detail shortly) and added to the controllers own processed signal giving the following discrete vector signal (where the subscript Wu has been omitted in the elements of the vector for notational brevity):

$$\underline{y}_{\mathrm{WA}u}[n] = \begin{bmatrix} y_{c_u}[n] \\ y_i[n] \\ \vdots \\ y_k[n] \end{bmatrix} \in \mathcal{C}^{N\times 1}, \{c_u, i, k\} \subset \mathcal{W}_u \tag{6.69}$$

Note that the time interval T_s between the n^{th} and the $(n+1)^{th}$ sample will be dependent on the chip rate of the message signal $\underline{m}_{\mathrm{W}}(t)$ and on the processing performed by each element node. If only spatial processing is performed then each element of the above vector can be written as

$$y_{\mathrm{W}u,i}(nT_s) = \underline{w}^H_{\mathrm{W}u,i}\underline{x}_{\mathrm{W}u,i}(nT_s) \tag{6.70}$$

where $\underline{w}_{\mathrm{W}u,i}$ is a complex weight vector determined by the spatial processor on each node or by the controller node.

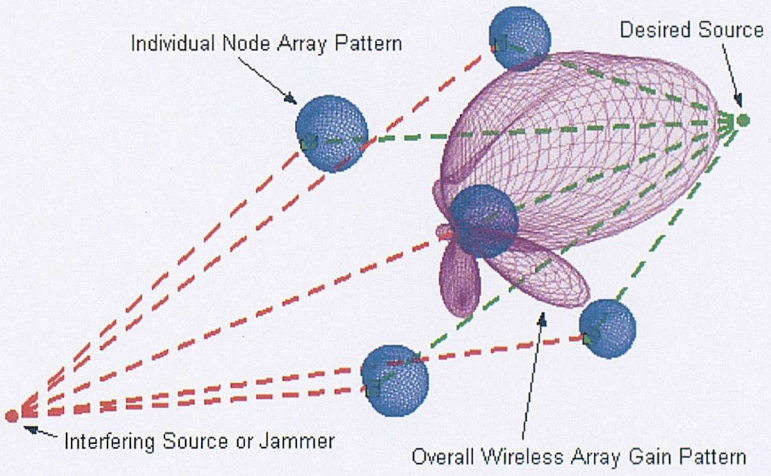


Figure 6.5: Wireless Array model showing both individual node and overall wireless array gain patterns

Figure 6.5 illustrates the operation of this *Wireless Array* model in the presence of an interfering source or jammer. The antenna elements on each node

are weighted and combined to provide a directional gain and phase response (individual node array pattern) shown in blue. The combined array pattern for the *Wireless Array* is shown in purple, and it is clear that the interference is completely cancelled whilst providing maximum gain for the desired signal (Note that the processing performed at the controller node can also be based on joint spatiotemporal techniques that provide much greater gain and signal cancellation capabilities - however it is difficult to show the response of such processing on a static 3D image).

Because each of the nodes in this model is an element in the *Wireless Array*, and assuming that each only performs spatial processing, the discrete received signal vector (due to just the j^{th} source) can be written using a sampled version of the familiar array response equation:

$$\underline{y}_{\mathrm{WA}u,(j)}\left(nT_s\right) = \underline{S}_{\mathrm{WA}u,(j)} m_{\mathrm{W}u,(j)}\left(nT_s\right) \tag{6.71}$$

where the *Wireless Array* source position vector $\underline{S}_{\mathrm{WA}u,(j)}$ is given by

$$\underline{S}_{\mathrm{WA}u,(j)} = \begin{bmatrix} \underline{w}^H_{\mathrm{W}u,c_u} \underline{S}_{\mathrm{W},c_u,j} \\ \underline{w}^H_{\mathrm{W}u,i} \underline{S}_{\mathrm{W},ij} \\ \vdots \\ \underline{w}^H_{\mathrm{W}u,k} \underline{S}_{\mathrm{W},kj} \end{bmatrix} \in \mathcal{C}^{N\times 1}, \{c_u, i, k\} \subset \mathcal{W}_u \tag{6.72}$$

Using Equation (6.64) for each node in the *Wireless Array*, the above can be written in terms of two interrelated source position vectors, the first using the matrix for the *Wireless Array* $\breve{\mathrm{r}}_{\mathrm{I},u}$ and corresponding to the scalar term in Equation (6.64) but repeated for all nodes in the *Wireless Array* to give an N by 1 vector, is given by

$$\underline{S}_{\mathrm{WA}u,j} = \underline{g}_{\mathrm{WA}u,j} \odot \exp\left(-j\breve{\mathrm{r}}_{\mathrm{I},u}{}^T \underline{\breve{k}}_{uj}\right) \in \mathcal{C}^{N\times 1} \tag{6.73}$$

for the plane wave case and

$$\underline{S}_{\mathrm{WA}u,(j)} = \underline{g}_{\mathrm{WA}u,j} \odot \left(\rho_{\mathrm{W}u,j}\underline{1}_N \oslash \underline{d}_{\mathrm{WA}u,j}\right)^{\eta} \exp\left(-j\frac{2\pi}{\lambda}\left(\rho_{\mathrm{W}u,j}\underline{1}_N - \underline{d}_{\mathrm{WA}u,j}\right)\right) \in \mathcal{C}^{N\times 1} \tag{6.74}$$

$$\text{where} \begin{cases} \mathrm{ele}_i\left\{\underline{d}_{\mathrm{WA}u,j}\right\} = \rho_{ij} = \sqrt{\left(\breve{\underline{r}}_{uj} - \mathrm{col}_i\left\{\breve{\mathrm{r}}_{\mathrm{I},u}\right\}\right)^T \left(\breve{\underline{r}}_{uj} - \mathrm{col}_i\left\{\breve{\mathrm{r}}_{\mathrm{I},u}\right\}\right)} \\ \text{or } \underline{d}_{\mathrm{WA}u,j} = \sqrt{\underline{1}_N \rho_{\mathrm{W}u,j} + \mathrm{diag}\left\{\breve{\mathrm{r}}_{\mathrm{I},u}{}^T \breve{\mathrm{r}}_{\mathrm{I},u}\right\} - 2\breve{\mathrm{r}}_{\mathrm{I},u}{}^T \breve{\underline{r}}_{uj}} \end{cases}$$

for the spherical wave case. Whereas the combination of the weight vectors in Equation (6.72) applied to the vector (left two) terms in Equation (6.64) for each

node forming the *Wireless Array* results in the following expression for the gain and phase response vector $\underline{g}_{\mathrm{WA}u,j}$ of the *Wireless Array* for the j^{th} source:

$$\mathrm{ele}_i\left\{\underline{g}_{\mathrm{WA}u,j}\right\} = \underline{w}^H_{\mathrm{W}u,i}\underline{S}_{ij} \tag{6.75}$$

in which $\underline{S}_{ij}$ is the second interrelated source position vector that is associated with the utilised elements on each node forming the *Wireless Array* and is given by the vector (left two) terms in Equation (6.72) which are repeated in the following expression:

$$\underline{S}_{ij} = \underline{g}_{ij} \odot \exp\left(-j\breve{\mathbf{r}}_{\mathrm{W},i}{}^T\underline{\breve{k}}_{ij}\right) \in \mathcal{C}^{N_{\mathrm{nw}}\times 1} \tag{6.76}$$

Note that the above modelling has assumed that the bandwidth B_m of the message signal $\underline{m}_{\mathrm{W}}(t)$ is small compared to the phase velocity ($v_{ph} = \frac{\lambda}{T}$) over the aperture D of the array, which for a *Wireless Array* spanning 6 half-wavelengths at $f_{\text{carrier-inter-wireless-link}} = 2.4\,\mathrm{GHz}$ implies that $B_m \ll 800$ MHz which is easily satisfied even for respectable processing gains and data rates. However such an array only spans roughly 37.5 cm which will require a very high node density to provide enough nodes to form the *Wireless Array* and increasing the aperture in half wavelengths past six will dramatically increase the number of ambiguities associated with the array. A possible solution to this problem is to consider a lower carrier frequency for the *inter*-wireless link, for example at $f_{\text{carrier-inter-wireless-link}} =$ 430 MHz (another ISM band) a *Wireless Array* spanning six half wavelengths will span roughly 2 m. Although the knock on effect of this is to require a lower bandwidth for the message signal ($B_m \ll 143\,\mathrm{MHz}$).

6.4.1 Reconstructing Streams from Element Nodes

In order to allow the sampled and processed data streams from each element node to be correctly re-constructed by the controller (or conversely for the controller to correctly synthesise the signals that should be sent to each element node) all the element node's clocks in the *Wireless Array* must be synchronised to the controller node's clock with an accuracy dependent on the chip period of the message waveform $\underline{m}_{\mathrm{W}}(t)$ used for the *inter- Wireless Array* link. Note that the uncertainty in the synchronisation for the i^{th} node ($\forall i \in \mathcal{W}_u, i \neq c_u$), as modelled in Section 6.2 by $\widetilde{T}_{SetTo,i}$ need not be smaller than the timing accuracy required in order to maintain a coherent *Wireless Array* (which for a 2 ° maximum acceptable phase drift in any of the node's clocks corresponds to a time error of 2.31×10^{-10} s) as once the nodes have been synchronised, the contribution that $\widetilde{T}_{SetTo,i}$ makes to the time error is constant (but different for each node). This constant timing

error is shown in Section 6.4.3 to manifest itself as an electrical uncertainty in the *Wireless Array* which is independent of the signal direction of arrival and can therefore be compensated for using array calibration techniques (although they will need to be adapted for *Wireless Arrays*).

The actual mechanism by which the controller then combines the streams is not critical for the modelling here, however one approach could be for the element nodes to form blocks of symbols from $\{y_{\mathrm{W}u,i}(nT_s), n \in \mathcal{N}\}$ and then between blocks encode a timestamp holding the value of the node's clock at the start of each block. The number of bits used to encode the timestamp needs only to be large enough to cover the duration of a single message at an accuracy of the same order of the chip period of $\underline{m}_{\mathrm{W}}(t)$.

6.4.2 Geometrical Uncertainties in *Wireless Arrays*

Unlike an individual node's *Local Array* where the locations of the antenna elements are known within well defined small manufacturing tolerances, the estimated positions and orientations of the nodes forming a *Wireless Array* are subject to small but nevertheless significant errors. These errors/uncertainties in the position and orientation of a node were examined briefly in Section 6.1.5 where the error in the estimation of the i^{th} node's position vector (in the GCS) was given as $\underset{\sim}{\tilde{p}}_i = \underset{\sim}{\hat{p}}_i - \underset{\sim}{p}_i$ and the error in the rotation matrix as $\tilde{\mathbb{T}}_i = \hat{\mathbb{T}}_i - \mathbb{T}_i$.

In a *Wireless Array* the errors/uncertainties in the estimation of the node's positions implies that within the controller node of the u^{th} *Wireless Array*, the following (incorrect - apart from the first column) matrix of the positions of the effective array elements is computed (where the estimates have been expressed in the CCS_u):

$$\hat{\breve{\mathrm{r}}}_{\mathrm{I},u} = \left[\underline{0}_3 \;\; \underset{\sim}{\hat{\breve{p}}}_{ui} \;\; \cdots \;\; \underset{\sim}{\hat{\breve{p}}}_{uk}\right] \in \mathcal{R}^{3\times N}, \{i,k\} \subset \mathcal{W}_u \tag{6.77}$$

Following the convention adopted in Section 6.3.2.2 the error in the above matrix is written as $\tilde{\breve{\mathrm{r}}}_{\mathrm{I},u} \triangleq \breve{\mathrm{r}}_{\mathrm{I},u} - \hat{\breve{\mathrm{r}}}_{\mathrm{I},u}$. As a consequence of this error, the terms of Equations (6.73) or (6.74) following the $\underline{g}_{\mathrm{WA}u,j}$ term (referred to as the isotropic manifold $\underline{a}_{\mathrm{WA}u,j}$) will be perturbed. Assuming plane wave propagation over the whole *Wireless Array*, the error in the isotropic manifold $\underline{\tilde{a}}_{\mathrm{WA}u,j} \triangleq \underline{a}_{\mathrm{WA}u,j} \oslash \underline{\hat{a}}_{\mathrm{WA}u,j}$ is given by:

$$\underline{\tilde{a}}_{\mathrm{WA}u,j} = \exp\left(-j\tilde{\breve{\mathrm{r}}}_{\mathrm{I},u}{}^T \breve{\underline{k}}_{uj}\right) \in \mathcal{C}^{N\times 1} \tag{6.78}$$

Whereas if the position of the j^{th} source is such that the spherical wave manifold expression holds, then the error $\underline{\tilde{a}}_{\mathrm{WA}u,j}$ must be computed according to

its definition from the true isotropic manifold using Equation (6.74) (without the $\underline{g}_{\mathrm{WA}u,j}$ term) and the estimated (or nominal) isotropic manifold $\widehat{\underline{a}}_{\mathrm{WA}u,j}$ using Equation (6.74) (again without the $\underline{g}_{\mathrm{WA}u,j}$ term but with $\widehat{\breve{\mathbf{r}}}_{\mathrm{I},u}$ in place of $\breve{\mathbf{r}}_{\mathrm{I},u}$).

Note that in the above it has been assumed that the controller has correctly estimated the direction of arrival or position of the j^{th} source, i.e. has knowledge of $\breve{\underline{k}}_{uj}$ or $\breve{\underline{r}}_{uj}$. Errors in these estimates are another type of geometrical uncertainty known as pointing errors but will not be examined here.

In addition to the above perturbation, errors in the estimates of position and orientation of the nodes can affect the calculation of the source position vectors associated with the utilised antenna elements for each node that forms the *Wireless Array* (Equation (6.76)). These errors can be completely eliminated if, instead of the controller estimating the j^{th} source location and using Equation (6.76) to calculate the array manifold for each node forming the *Wireless Array*, each element node (or i^{th} node,$\forall i \in \mathcal{W}_u, i \neq c_u$) were to perform the estimation independently and calculate the corresponding SPV using the following equation:

$$\underline{S}_{ij} = \underline{g}_{ij} \odot \exp\left(-j\mathbf{r}_{\mathrm{nw},i}{}^{T}\underline{k}_{ij}\right) \in \mathcal{C}^{N_{\mathrm{nw}}\times 1} \tag{6.79}$$

which is equivalent to Equation (6.76) except that both the array element positions and the wavenumber vector are both expressed in the coordinate system of the i^{th} node (hence removing the need for a coordinate transformation).

6.4.3 Electrical Uncertainties in *Wireless Arrays*

The expression for the signals received at a *Wireless Array* of antennas as given by Equation (6.63) is strictly the complex baseband representation of the received signals, that is, the complex exponential modelling the carrier has been removed. In order to understand the role of imperfect clocks and synchronisation uncertainties, consider the complex passband representation (complex pre-envelope) due to the j^{th} received signal at one of the nodes forming a *Wireless Array* (say the i^{th} node, $\forall i \in \mathcal{W}_u$):

$$\underline{z}_{\mathrm{W},ij}(t) = \underline{S}_{\mathrm{W},ij}\underline{m}_{\mathrm{W}}(t)\exp(j2\pi f_c t) \tag{6.80}$$

where$(F_c + F_k)$ corresponds to any subcarrier used by the *inter-Wireless Array* link and only one subcarrier has been considered. As the extension to multiple subcarriers is straightforward and simply involves summing over all the subcarriers with a different array manifold for each (unless the subcarrier separation over the center carrier frequency is small enough).

This signal is down converted to baseband by multiplication with another complex exponential as shown by

$$\underline{x}_{\mathrm{W},ij}(t) = \underline{z}_{\mathrm{W},ij}(t) \exp\left(-j2\pi\left(F_c + F_k\right) T_i(t)\right) \tag{6.81}$$

in which t has been replaced by the time function of the i^{th} node in order to take into account the non-ideal nature of the node's local oscillator. To simplify the analysis consider that all the nodes forming the *Wireless Array* were synchronised at $t = T_{Synch,i} = 0, \forall i \in \mathcal{W}_u$ and all the clocks were intended to be set to $\widehat{T}_{SetTo} = 0$, however because of synchronisation errors the i^{th} node was actually set to $T_{SetTo,i} = \widehat{T}_{SetTo} + \widetilde{T}_{SetTo,i} = \widetilde{T}_{SetTo,i}$. Using the clock model presented in Section 6.2, the baseband received signal can now be written as:

$$\underline{x}_{\mathrm{W},ij}(t) = \underline{S}_{\mathrm{W},ij}\underline{m}_{\mathrm{W}}(t) \exp\left(\begin{array}{c} j2\pi\left(F_c + F_k\right) \cdot \\ \left\{\alpha_{Clock,i}t + \beta_{Clock,i}t^2 + \widetilde{T}_{SetTo,i} + t_{Jitter,i}(t)\right\} \end{array}\right) \tag{6.82}$$

$$\tag{6.83}$$

Referring to the typical values for the parameters of the clock model presented in Section 6.2, it was found that the dominant terms in the above are $\alpha_{Clock,i}t$ and $\widetilde{T}_{SetTo,i}$, and in the following, the less important terms relating to aging effects and jitter are omitted - however they can easily be re-introduced. Incorporating the above into the expressions for the received signals for both *Wireless Array* models leads to the following modifications to the source position vector $\underline{S}_{\mathrm{WA}u,(j)}$

$$\underline{S}_{\mathrm{WA}u,(j)} = \underline{g}_{\mathrm{WA}u,j} \odot \exp\left(j\underline{\phi}_{\mathrm{W}u}\right) \odot \underline{a}_{\mathrm{WA}u,(j)} \tag{6.84}$$

where $\underline{a}_{\mathrm{WA}u,(j)}$ is the isotropic manifold vectors for the *Wireless Array* and $\underline{\phi}_{\mathrm{W}u}$ is given by

$$\underline{\phi}_{\mathrm{W}u} = \underline{\widehat{\phi}}_{\mathrm{W}u} + \underline{\widetilde{\phi}}_{\mathrm{W}u} \tag{6.85}$$

$$\underline{\widehat{\phi}}_{\mathrm{W}u} = 2\pi\left(F_c + F_k\right) \begin{bmatrix} \widehat{\alpha}_{Clock,c_u}t \\ \widehat{\alpha}_{Clock,i}t \\ \vdots \\ \widehat{\alpha}_{Clock,k}t \end{bmatrix}, \tag{6.86}$$

$$\underline{\widetilde{\phi}}_{\mathrm{W}u} = 2\pi\left(F_c + F_k\right) \begin{bmatrix} \widetilde{\alpha}_{Clock,c_u}t + \widetilde{T}_{SetTo,c_u} \\ \widetilde{\alpha}_{Clock,i}t + \widetilde{T}_{SetTo,i} \\ \vdots \\ \widetilde{\alpha}_{Clock,k}t + \widetilde{T}_{SetTo,k} \end{bmatrix} \in \mathcal{C}^{N\times 1}, \{c_u, i, k\} \subset \mathcal{W}_u \tag{6.87}$$

Comparing the above equations with the expressions in Section 6.3.2.1, it is easy to see that the uncertainty in the frequency offset of the node's clocks

$\widetilde{\alpha}_{Clock}$ and the synchronisation error $\widetilde{T}_{SetTo}$ of each node forming the *Wireless Array* manifest themselves as electrical uncertainties (although only the phase is effected).

The above has huge significance for the operation of a *Wireless Array*, as in order to operate correctly, phase coherence must be maintained between the nodes that form the array. The synchronisation error $\widetilde{T}_{SetTo,i}$ may cause significant phase decoherence between elements of the *Wireless Array*, however because it is constant it can be compensated for using array calibration techniques such as that presented in [79]. However, the uncertainty in the frequency offsets causes a phase difference in each node that linearly varies with time at an unknown rate and limits the time over which the *Wireless Array* can operate coherently following calibration. (In Section 6.2 an example was presented using a given typical set of parameters describing the node's clock which showed that after 1 ms, a phase error difference of 2.16 ° is observed for a carrier signal with a frequency of 2.4 GHz.)

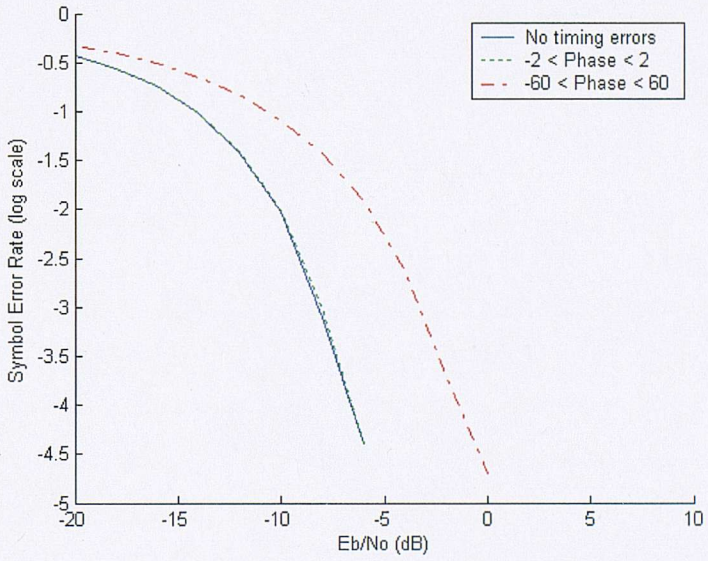


Figure 6.6: Affect of timing errors on the demodulation of QPSK using a wireless array

Figure 6.6 shows the effect of different phase offsets arising from timing errors on the Symbol Error Rate of a simple QPSK demodulator combined with a *Wireless Array* beamformer that completely cancels an interfering source with a power 20 dB above the desired signal in the presence of different levels of Additive White Gaussian Noise (AWGN). The degradation caused by decoherence of the *Wireless Array* is clear, whilst phase offsets of only 2 degrees (corresponding to

oscillator phase drift in the nodes over roughly 1 ms) have little impact on the performance.

6.5 Conclusion

In this study the following types of errors/uncertainties that are present in an Arrayed Wireless Sensor Network have been modelled:

- Timing uncertainties; relating to the stability of the node's clocks in addition to synchronisation errors.
- Errors in the estimation of a node's position and orientation.
- Electrical and geometric uncertainties in the context of the node's *Local Array*.
- Node *Local Array* element failure.
- Geometrical uncertainties present in two types of *Wireless Array* model.
- Electrical uncertainties in *Wireless Arrays* as a result of timing uncertainties.
- Node failure within a *Wireless Array*.

For almost all of the above representative examples have been presented that clearly show the importance of correctly modelling the Arrayed-WSN system, or have shown the need for techniques that are robust with respect to these effects.

A number of key observations and conclusions have arisen in this study and these are summarised below:

- In Section 6.2 it was observed that uncorrected deterministic effects are the dominant factors in the model of the node's clock (as opposed to stochastic variations, or jitter).
- Geometrical uncertainties are considered to be negligible for the node's *Local Array* due to the manufacturing tolerances of the microstrip array being much smaller than the wavelength used for all the wireless links. This leaves electrical uncertainties and mutual coupling as the dominant effects present for a node's *Local Array*.

- *Wireless Arrays* are sensitive to errors in the relative positions of the nodes that form the *Wireless Array*. However if nodes perform their own source DOA estimation, errors in the relative orientation of the nodes don't affect the *Wireless Array* response vector.

- Synchronisation errors between nodes forming a *Wireless Array* manifest themselves as electrical uncertainties that are constant, and can therefore be compensated relatively easily using array calibration techniques.

Chapter 7

Conclusions and Future work

The main objective of this study has been to seamlessly integrate the advanced wireless telecommunications techniques of antenna array processing with the emerging technology of Wireless Sensor Networks. The approach has been based on designing a novel type of WSN that uses antenna arrays on two levels and tackling some of the most important challenges that such a fusion entails. What follows is a summary of the technical work presented in this thesis, an outline of the main contributions of this study and a discussion on potential future research directions and objectives.

7.1 Thesis Summary

In Chapter 1 the motivation behind this study has been introduced. Furthermore, after a discussion of the main research challenges, we presented a literature review in the area of Wireless Sensor Networks and that of MIMO communications with special focus in the development of spatiotemporal array processing techniques.

In Chapter 2, a novel type of WSN, the Arrayed-WSN was introduced and its basic framework has been developed. To this aim, its two main building blocks, namely the wireless node and the wireless antenna array were discussed. We have proposed a scheme where each individual node is equipped with a block of environmental sensors for sensing the environment, an antenna array for wireless communications and the relevant underlying operational modules. Because the Arrayed-WSN is a randomly deployed network operating under the CDMA framework, a novel, decentralised network discovery and CDMA code allocation scheme, the CANDLA-DCSA, was also introduced in Chapter 2. The advantages of the scheme are the lack of need for synchronisation, the small overhead and the ability to be easily expanded to encompass different network scenarios.

As described throughout this thesis, a very important property of the Arrayed-WSN is the ability of individual nodes to group together and form self-contained modules called *Wireless Arrays*. The *Wireless Arrays* act as traditional antenna arrays where individual elements are replaced by network nodes and the traditionally wired links between the elements and the central array processing unit are replaced by wireless links. The brief discussion of the *Wireless Array* in Chapter 2 led to the identification of the need for the three separate wireless communication links involved in the Arrayed-WSN. In order to encompass the involvement of the *Wireless Arrays* and the general network operation we designed the different node roles and modes and unified them under a simple, easily implementable transitional framework.

In Chapter 3, the formation of *Wireless Arrays* in the Arrayed-WSN was discussed. This concerns the discrete problem of selecting a given number of nodes to form a *Wireless Array*. It is clear that such a selection will affect the geometry of the resulting array and thus its properties and capabilities. After an introduction to the geometrical aspects of array processing and a brief study of the important notion of the array manifold we introduced a collection of criteria which link the array geometry in 3D space to the performance of that array. By combining a number of distinct performance criteria we proposed a composite measure which takes into account the accuracy capabilities, the sensitivity to element location errors, the ambiguities and the consistent performance under different signal environments, of an array. Furthermore, we have proposed a distributed algorithm which can be used to incorporate such a measure in the framework of the Arrayed-WSN.

In Chapter 4, the design of appropriate communication links for the Arrayed-WSN was addressed. The need for different links for the individual node-to-individual node, *Wireless Array* node-to-*Wireless Array* node and *Wireless Array*-to-*Wireless Array* (*initial*, *intra*-wireless and *inter*-wireless links respectively) was established in Chapter 2. After a brief discussion on the possible applicable schemes and on the limitations imposed by the node size and energy efficiency and network specifications, we concluded on the general scheme of the three distinct communication links. In order to take full advantage of the array equipped nodes, and their capability to group together to form *Wireless Arrays*, we proposed the incorporation of a MIMO beamforming multicarrier DS-CDMA design. A common transceiver framework across all three links, simplifies the individual node construction without compromising network performance. However, the fact that a *Wireless Array* entity and an individual node face different signal environments

led to the introduction of two distinct novel channel modellings, one for each case. Furthermore, the detailed design of the transceivers were discussed and the performance was analysed by extensive simulation studies.

In Chapter 5, we introduce the reader to an important problem faced by all antenna array systems, namely the presence of ambiguous signal environments, or simply ambiguities. By reviewing some of the current research and modelling of the problem of ambiguities we analyse their significance in the case of the Arrayed-WSN. Since the Arrayed-WSN incorporates arrays that span three spatial dimensions, an extension of the analysis to the 3D space was needed. Indeed, such an analysis led to the classification of a novel type of ambiguities and their representation on the array manifold. Chapter 5 concludes with the presentation of a novel algorithm for resolving ambiguities. The algorithm is especially relevant to the Arrayed-WSN because it is a distributed, cooperative technique which aims at the minimisation of message exchange between nodes, and thus energy consumption. The effectiveness of the algorithm is confirmed via computer simulation studies.

Chapter 6 is dedicated to the modelling of uncertainties and the analysis of their effect on the operation of the Arrayed-WSN. The first part of the chapter introduces a framework for analysing uncertainties related to individual node orientation, self-position estimation and the lack of synchronisation between nodes. Such a study is crucial, since the design of the Arrayed-WSN presented here is based upon the assumption of a localisation scheme providing estimates of the node locations. Although the general network operation is not disrupted by small errors in such estimations, in the case of *Wireless Arrays,* estimation accuracy plays an important role. The same is true for node synchronisation, lack of which may be caused by the drift in the node clocks and may seriously affect the performance of a *Wireless Array.* The second part of Chapter 6 is dedicated to modelling the uncertainties relating to the node's *Local Array* and to those connected to the *Wireless Array* operation, while the use of computer simulation examples is used to validate our models and visualise the effect on performance. The analysis of this chapter is enlightening with respect to the dominant uncertainties in each area of the operation of the Arrayed-WSN. In effect, as far as the indivudual node and its *Local Array* is concerned, we conclude that the main source of synchronisation errors should be deterministic clock drifts as opposed to stochastic jitter. Furthermore, geometrical uncertainties are minimal, and overshadowed mainly by mutual coupling between the node's *Local Array* elements. The *Wireless Array* case is however different. Here, although position estimation

errors can have a dramatic effect, the overall array operation can be maintained by employing the node's own Direction of Arrival signal estimation. Furthermore, by showing that synchronisation errors between *Wireless Array* element nodes can be translated to (and hence are equivalent to) constant electrical uncertainties, we conclude that they can easily be eliminated by a suitable calibration method. It is clear from the analysis of this chapter that the Arrayed-WSN would greatly benefit from further development of array processing techniques, robust to the effects of the various uncertainties present.

7.2 List of contributions

It has to be noted that since the Arrayed-WSN is a novel type of network, most of the applications considered within this document appear for the first time, are specifically designed for application in the Arrayed-WSN and are tested by extensive computer simulation studies. Furthermore, most of the studies are easily extendable and applicable to any type of network that uses node collaboration for telecommunication purposes. The following list sumarises the contributions of this study in the order they appear in this thesis:

- Proposal of the Arrayed-WSN concept, network operational design and detailed description.
- Arrayed-WSN node design, conceptual outline and roles and modes unification.
- *Wireless Array* concept, operational design and description.
- Arrayed-WSN network discovery and efficient, collaborative code allocation scheme (CANDLA-DCSA).
- Compound criterion based on the differential geometry properties of the array manifold, specifically designed for the discrete array geometry selection problem, designed to be directly applicable to the *Wireless Array* formation procedure.
- *Wireless Array* formation procedure based on a distributed, efficient algorithm for node selection.
- Proposal and design of the three (*initial*, *intra* and *inter*-wireless) links. Simulation within the Arrayed-WSN framework of the contemporaneuos node-to-node and *Wireless Array*-to-*Wireless Array* communication.

- Novel channel modelling for the case of *Wireless Arrays*, applicable to any large aperture array system.
- Classification of ambiguities within the Arrayed-WSN.
- Classification of a new type of ambiguity in 3D signal environment.
- Distributed, communication efficient algorithm for the resolution of ambiguities occuring at an individual node or *Wireless Array* level.
- Introduction of a common framework for the modelling of node synchronisation and position estimation uncertainties.
- Use of the framework for the modelling of node synchronisation uncertainties and the study of their effect on the *Wireless Array* operation.
- Modelling of node's *Local Array* uncertainties.

7.3 Future work

The advances in hardware technology (and the passing from the MEMS era to the NEMS nano-scale era) indicate sensor nodes with the processing capabilities of today's portable computers and extensive communication capabilities. The research focus is thus expected to lie in finding ways to exploit such capabilities to the maximum, in order to achieve truly scalable networks that operate under hostile environments.

The introduction of the Arrayed-WSN is a very promising fusion of two important technologies in wireless communications, that of array processing systems and that of Wireless Sensor Networks. Within this thesis, the framework has been set for designing a self-contained, unattended, self-configurable network which can operate under extreme interference scenarios while providing high level services. Some of the research challenges associated with this type of network have been addressed by this study. However, the design of such a powerful network is very much an open research subject and there are a number of possible directions that research can be continued and extended. It has to be noted that the employment of arrays in a WSN not only introduces novel and interesting topics, but also redefines and alters the nature of existing well researched areas of both WSN and array communications engineering such as quality of service, reliable operation and network re-configurability.

Such An example in the area of WSN traditional research is node localisation. While this constitutes a well researched subject, it is reasonable to expect that the Arrayed-WSN can provide an improvement on current techniques. This is because self localisation in absence of external reference frames is mainly addressed by node-collaboration schemes. The Arrayed-WSN is an environment that favours node collaboration, and it is believed that research into node localisation under the Arrayed-WSN framework can yield promising novel techniques. The functionality provided by the node *Local Arrays* and the formed *Wireless Arrays* can be exploited to produce highly accurate localisation, by using high resolution space-time communications. This is essential to efficient and automated network organisation, particularly in the case of dynamically changing networks which also involves the selection of nodes for collaboration. Localisation is also very important when it comes to high quality sensing services. This is because information about sensed events need to be attached to information about the point in space where they occurred, in order to have any significant meaning in most applications. It is clear therefore, that in a static or moving network, the localisation of nodes and Events of Interest is important to both internal and external operations of a WSN. In view of the motion and dynamic topology of a moving network, the relative positions of nodes and targets changes continuously, and the estimation of these parameters becomes a hybrid between tracking and localisation. It is clear that such a scheme would be useful not only for providing localised services to network clients, but also to the smoother operation of the network itself in many areas such as code allocation, routing and *Wireless Array* formation.

Another very important issue that needs to be addressed is the modelling of communications in a real WSN. With scenarios inspired by the applications of a WSN, the respective "new", unconventional, communication channels may be modelled and new communication schemes can be devised to suit the specifications. Examples of such communication channels may be extreme due to the way a WSN is deployed and may involve sensors lying very close to the ground or on the canopy of a forest, situations where the channel is highly degraded by path loss and increasing number of multipath. The result of such a procedure can be highly exploitable in many applications such as commercial sensor networks (e.g. for noise, temperature and traffic monitoring) or even mobile phone networks. This is possible, because of the high capacity, interfering rejecting communication links that the employment of collaborating teams of nodes has to offer.

All communication systems based on multiple element transmissions require

a degree of calibration. This is especially applicable in the area of array communications where the accuracy of the spatial location of the elements is crucial. It is therefore evident that *Wireless Arrays* demand a high degree of calibration since they are formed under an uncertain environment based on estimates of node positions. Even after a highly precise localisation procedure, a very quick and efficient array calibration phase would be highly valuable to the actual effectiveness of the *Wireless Array* operation and its impact on the improved network capabilities.

Data fusion in the Arrayed-WSN is another promising area of research. Data fusion is a from of information pooling which can remove redundancy, improve quality and improve the rate of information transmission. In fact, array processing can be considered as a form of telecommunications data fusion. A collective of nodes operating as a group (such as the *Wireless Array*) forms a very good background on which data fusion can take place on data gathered by the environment. Data fusion is of importance to many applications of WSN and appropriate signal processing techniques and algorithms that utilise the Arrayed-WSN capabilities to the full will be of great use.

As discussed in Chapter 6, the uncertainties involved in an Arrayed-WSN can obstruct the operation of the network as a whole. Modelling and analysing the effects of the uncertainties laid the framework upon which further research can be based. The ultimate aim of such an endeavour would be to find methods to completely resolve or alleviate the effects of such uncertainties, or design more robust telecommunications and network operation techniques.

The future of WSNs is deemed to be based on node mobility and network re-configurability. Designing and implementing a fully mobile network is a very difficult task which is worth pursuing because of the numerous applications and uses that it entails. Self-configuration, efficiency and exploitation of redundancy in the abundance of available data for fault-tolerant, high-capability, advanced networks that can move through unfriendly terrains while operating is described as the future of situational awareness and is deemed to be the future of research in the field. It is clear that such a moving network creates new research problems, and further alters the specifications of many existing ones, that need to be tackled for the advancement of WSNs. Finally, advancing the technology of WSNs and providing higher-quality and more robust schemes ultimately leads to inventing and implementing useful high-level services. This is a "softer" but still demanding and useful research area that can be addressed by future studies.

The above research directions have the potential of extending the capabilities

of contemporary WSNs to a degree that a truly self-sustainable, self-configurable, scalable and flexible network that operates in hostile or otherwise unreachable environments will be made possible.

References

[1] I. F. Akyildiz, Su Weilian, Y. Sankarasubramaniam, and E. Cayirci, "A survey on sensor networks", *Communications Magazine, IEEE*, vol. 40, no. 8, pp. 102–114, 2002.

[2] Chong Chee-Yee and S. P. Kumar, "Sensor networks: evolution, opportunities, and challenges", *Proceedings of the IEEE*, vol. 91, no. 8, pp. 1247–1256, 2003.

[3] M. Tubaishat and S. Madria, "Sensor networks: an overview", *Potentials, IEEE*, vol. 22, no. 2, pp. 20–23, 2003.

[4] Xu Yongjun, Liu Lingyi, Shen Peifu, Lv Tao, and Li Xiaowei, "Low power processor design for wireless sensor network applications", in *Wireless Communications, Networking and Mobile Computing, 2005. Proceedings. 2005 International Conference on*, 2005, vol. 2, pp. 921–924.

[5] V. Handziski, J. Polastre, J. H. Hauer, C. Sharp, A. Wolisz, and D. Culler, "Flexible hardware abstraction for wireless sensor networks", in *Wireless Sensor Networks, 2005. Proceeedings of the Second European Workshop on*, 2005, pp. 145–157.

[6] Zhenyu Yin, Hai Zhao, Kai Lin, Peigang Sun, Yishan Gong, Yongqing Zhang, and Ye Xu, "Multi-sensor data fusion in wireless sensor networks", in *Computational Engineering in Systems Applications, IMACS Multiconference on*, 2006, pp. 1690–1694.

[7] Jiang Peng, Wen Yu, Wang Jianzhong, Shen Xingfa, and Xue Anke, "A study of routing protocols in wireless sensor networks", in *Intelligent Control and Automation, 2006. WCICA 2006. The Sixth World Congress on*, 2006, vol. 1, pp. 266–270.

[8] Zhou Yan, Xing Jianping, and Yu Qicai, "Overview of power-efficient mac and routing protocols for wireless sensor networks", in *Mechatronic and*

Embedded Systems and Applications, Proceedings of the 2nd IEEE/ASME International Conference on, 2006, pp. 1–6.

[9] N. Patwari, III A. O. Hero, M. Perkins, N. S. Correal, and R. J. O'Dea, "Relative location estimation in wireless sensor networks", *Signal Processing, IEEE Transactions on [see also Acoustics, Speech, and Signal Processing, IEEE Transactions on]*, vol. 51, no. 8, pp. 2137–2148, 2003.

[10] Ye Wei, J. Heidemann, and D. Estrin, "An energy-efficient mac protocol for wireless sensor networks", in *INFOCOM 2002. Twenty-First Annual Joint Conference of the IEEE Computer and Communications Societies. Proceedings. IEEE*, 2002, vol. 3, pp. 1567–1576.

[11] P. C. Nar and E. Cayirci, "Pcsmac: a power controlled sensor-mac protocol for wireless sensor networks", in *Wireless Sensor Networks, 2005. Proceeedings of the Second European Workshop on*, 2005, pp. 81–92.

[12] K. Sohrabi, J. Gao, V. Ailawadhi, and G. J. Pottie, "Protocols for self-organization of a wireless sensor network", *Personal Communications, IEEE [see also IEEE Wireless Communications]*, vol. 7, no. 5, pp. 16–27, 2000.

[13] L.F.W.van Hoesel and P.J.M.Havinga, "A lightweight medium access protocol (lmac) for wireless sensor networks: Reducing preamble transmissions and transceiver state switches", in *International Workshop on Networked Sensing Systems (INNS 2004), Tokyo, Japan,*, Jun 2004.

[14] W. B. Heinzelman, A. P. Chandrakasan, and H. Balakrishnan, "An application-specific protocol architecture for wireless microsensor networks", *Wireless Communications, IEEE Transactions on*, vol. 1, no. 4, pp. 660–670, 2002.

[15] C.Intanagonwiwat, R.Govindan, D.Estrin, J.Heidemann, and F.Silva, "Directed diffusion for wireless sensor networking", *Transactions on Networking*, 2003.

[16] Zenon Chaczko, Ryszard Klempous, Jan Nikodem, and Michal Nikodem, "Methods of sensors localization in wireless sensor networks", in *Engineering of Computer-Based Systems, 2007. ECBS '07. 14th Annual IEEE International Conference and Workshops on the*, 2007, pp. 145–152.

[17] I. Stojmenovic and Lin Xu, "Loop-free hybrid single-path/flooding routing algorithms with guaranteed delivery for wireless networks", *Parallel and*

Distributed Systems, IEEE Transactions on, vol. 12, no. 10, pp. 1023–1032, 2001.

[18] K. Seada and A. Helmy, "An overview of geographic protocols in ad hoc and sensor networks", in *Computer Systems and Applications, 2005. The 3rd ACS/IEEE International Conference on*, 2005, p. 62.

[19] D. Gesbert, M. Shafi, Shiu Da shan, P. J. Smith, and A. Naguib, "From theory to practice: an overview of mimo space-time coded wireless systems", *Selected Areas in Communications, IEEE Journal on*, vol. 21, no. 3, pp. 281–302, 2003.

[20] J. H. Winters and M. J. Gans, "The range increase of adaptive versus phased arrays in mobile radio systems", *Vehicular Technology, IEEE Transactions on*, vol. 48, no. 2, pp. 353–362, 1999.

[21] D.G. Brennan, "Linear diversity combining techniques", in *Proceedings of the IRE*, 1959, pp. 1075–1102.

[22] S. M. Alamouti, "A simple transmit diversity technique for wireless communications", *Selected Areas in Communications, IEEE Journal on*, vol. 16, no. 8, pp. 1451–1458, 1998.

[23] B. D. Van Veen and K. M. Buckley, "Beamforming: a versatile approach to spatial filtering", *ASSP Magazine, IEEE [see also IEEE Signal Processing Magazine]*, vol. 5, no. 2, pp. 4–24, 1988.

[24] P. D. Karaminas and A. Manikas, "Super-resolution broad null beamforming for cochannel interference cancellation in mobile radio networks", *Vehicular Technology, IEEE Transactions on*, vol. 49, no. 3, pp. 689–697, 2000.

[25] R. Price and P. E. Green, "A communication technique for multipath channels", *Proceedings of the IRE*, vol. 46, no. 3, pp. 555–570, 1958.

[26] B. H. Khalaj, A. Paulraj, and T. Kailath, "2d rake receivers for cdma cellular systems", in *Global Telecommunications Conference, 1994. GLOBECOM '94. 'Communications: The Global Bridge'. , IEEE*, 1994, pp. 400–404.

[27] Cui Shuguang, A. J. Goldsmith, and A. Bahai, "Energy-efficiency of mimo and cooperative mimo techniques in sensor networks", *Selected Areas in Communications, IEEE Journal on*, vol. 22, no. 6, pp. 1089–1098, 2004.

[28] A. M. Abbosh and D. Thiel, "Performance of mimo-based wireless sensor networks with cochannel interference", in *Intelligent Sensors, Sensor Networks and Information Processing Conference, 2005. Proceedings of the 2005 International Conference on*, 2005, pp. 115–119.

[29] S. Vakil and B. Liang, "Balancing cooperation and interference in wireless sensor networks", in *Sensor and Ad Hoc Communications and Networks, 2006. SECON '06. 2006 3rd Annual IEEE Communications Society on*, 2006, vol. 1, pp. 198–206.

[30] Li Xiaohua, Chen Mo, and Liu Wenyu, "Application of stbc-encoded cooperative transmissions in wireless sensor networks", *Signal Processing Letters, IEEE*, vol. 12, no. 2, pp. 134–137, 2005.

[31] L. Liu and H. Ge, "Space-time coding for wireless sensor networks with cooperative routing diversity", in *Signals, Systems and Computers, 2004. Conference Record of the Thirty-Eighth Asilomar Conference on*, 2004, vol. 1, pp. 1271–1275.

[32] S. K. Jayaweera, "An energy-efficient virtual mimo architecture based on v-blast processing for distributed wireless sensor networks", in *Sensor and Ad Hoc Communications and Networks, 2004. IEEE SECON 2004. 2004 First Annual IEEE Communications Society Conference on*, 2004, pp. 299–308.

[33] J. Burdin and J. Dunyak, "Enhancing the performance of wireless sensor networks with mimo communications", in *Military Communications Conference, 2005. MILCOM 2005. IEEE*, 2005, pp. 2321–2326.

[34] J. Burdin and J. Dunyak, "Cohesion of wireless sensor networks with mimo communications", in *SoutheastCon, 2005. Proceedings. IEEE*, 2005, pp. 547–551.

[35] H. Ochiai, P. Mitran, H. V. Poor, and V. Tarokh, "Collaborative beamforming for distributed wireless ad hoc sensor networks", *Signal Processing, IEEE Transactions on [see also Acoustics, Speech, and Signal Processing, IEEE Transactions on]*, vol. 53, no. 11, pp. 4110–4124, 2005.

[36] Liang Quanquan, Yuan Dongfeng, Wang Yong, and Zhang Ruihua, "A new sensor antenna-array selecting method in wireless sensor networks", in *Communications, Circuits and Systems Proceedings, 2006 International Conference on*, 2006, vol. 3, pp. 1523–1526.

[37] Li Xiaohua, Chen Mo, and E. P. Ratazzi, "Array-transmission based physical-layer security techniques for wireless sensor networks", in *Mechatronics and Automation, 2005 IEEE International Conference*, 2005, vol. 3, pp. 1618–1623.

[38] M. S. Sharawi, "Use of low-cost patch antennas in modern wireless technology", *Potentials, IEEE*, vol. 25, no. 4, pp. 35–47, 2006.

[39] A. Manikas and L. K. Huang, "Star channel estimation in ds-cdma communication systems", *Communications, IEE Proceedings-*, vol. 151, no. 4, pp. 387–393, 2004.

[40] A. Sabban, "Ka band microstrip antenna arrays with high efficiency", in *Antennas and Propagation Society International Symposium, 1999. IEEE*, 1999, vol. 4, pp. 2740–2743.

[41] A.Manikas, *Differential Geometry in Array Processing*, Imperial College Press, 2004.

[42] Guo Chunlong, Charlie Z. Lizhi, and J. M. Rabaey, "Low power distributed mac for ad hoc sensor radio networks", in *Global Telecommunications Conference, 2001. GLOBECOM '01. IEEE*, 2001, vol. 5, pp. 2944–2948.

[43] A. Manikas and M. Sethi, "A space-time channel estimator and single-user receiver for code-reuse ds-cdma systems", *Signal Processing, IEEE Transactions on [see also Acoustics, Speech, and Signal Processing, IEEE Transactions on]*, vol. 51, no. 1, pp. 39–51, 2003.

[44] A. Y. Wang, Cho SeongHwan, C. G. Sodini, and A. P. Chandrakasan, "Energy efficient modulation and mac for asymmetric rf microsensor systems", in *Low Power Electronics and Design, International Symposium on, 2001.*, 2001, pp. 106–111.

[45] H. R. Karimi and A. Manikas, "Manifold of a planar array and its effects on the accuracy of direction-finding systems", *Radar, Sonar and Navigation, IEE Proceedings* -, vol. 143, no. 6, pp. 349–357, 1996.

[46] A. Manikas, A. Alexiou, and H. R. Karimi, "Comparison of the ultimate direction-finding capabilities of a number of planar array geometries", *Radar, Sonar and Navigation, IEE Proceedings* -, vol. 144, no. 6, pp. 321–329, 1997.

[47] A. Sleiman and A. Manikas, "The impact of sensor positioning on the array manifold", *Antennas and Propagation, IEEE Transactions on*, vol. 51, no. 9, pp. 2227–2237, 2003.

[48] A. Alexiou and A. Manikas, "Array robustness to sensor failure", in *Phased Array Systems and Technology, 2000. Proceedings. 2000 IEEE International Conference on*, 2000, pp. 177–180.

[49] Bandyopadhyay Seema and E. J. Coyle, "An energy efficient hierarchical clustering algorithm for wireless sensor networks", in *INFOCOM 2003. Twenty-Second Annual Joint Conference of the IEEE Computer and Communications Societies. IEEE*, 2003, vol. 3, pp. 1713–1723.

[50] W. R. Heinzelman, A. Chandrakasan, and H. Balakrishnan, "Energy-efficient communication protocol for wireless microsensor networks", in *System Sciences, 2000. Proceedings of the 33rd Annual Hawaii International Conference on*, 2000, p. 10.

[51] A. Molnar, B. Lu, S. Lanzisera, B. W. Cook, and K. S. J. Pister, "An ultra-low power 900 mhz rf transceiver for wireless sensor networks", in *Proceedings of the IEEE Custom Integrated Circuits Conference*, Oct 2004, pp. 401–404.

[52] B. P. Otis, Y. H. Chee, R. Lu, N. M. Pletcher, and J. M. Rabaey, "An ultra-low power mems-based two-channel transceiver for wireless sensor networks", in *Symposium on VLSI Circuits, Digest of Technical Papers*, Jun 2004, pp. 20–23.

[53] Eugene Shih, Seong-Hwan Cho, Nathan Ickes, Rex Min, Amit Sinha, Alice Wang, and Anantha Chandrakasan, "Physical layer driven protocol and algorithm design for energy-efficient wireless sensor networks", in *Proc. of the Seventh Annual ACM/IEEE International Conference on Mobile Computing and Networking*, Jul 2001.

[54] D. J. Sadler and A. Manikas, "Blind reception of multicarrier ds-cdma using antenna arrays", *Wireless Communications, IEEE Transactions on*, vol. 2, no. 6, pp. 1231–1239, 2003.

[55] Callaway E.H, *Wireless Sensor Networks - Architectures and Protocols*, Auerbach (CRC Press), 2003.

[56] R.C.Crane, *Propagation Handbook for Wireless Communication System Design*, CRC Press, 2003.

[57] Liang Ying-Chang and F. Chin, "Transmit antenna array techniques for cellular cdma systems", in *Personal, Indoor and Mobile Radio Communications, 1998. The Ninth IEEE International Symposium on*, 1998, vol. 3, pp. 1396–1400.

[58] T. Salzer and D. Mottier, "Transmit beamforming for sdma in multi-carrier cdma downlink on a per subcarrier basis", in *Telecommunications, 2003. ICT 2003. 10th International Conference on*, 2003, vol. 1, pp. 793–798.

[59] D. J. Sadler and Manikas A., "Mmse multiuser detection for array multicarrier ds-cdma in fading channels", *IEEE Transactions on Signal Processing*, 2005.

[60] Xu Weiping and L. B. Milstein, "On the performance of multicarrier rake systems", *Communications, IEEE Transactions on*, vol. 49, no. 10, pp. 1812–1823, 2001.

[61] A. Klein, G. K. Kaleh, and P. W. Baier, "Zero forcing and minimum mean-square-error equalization for multiuser detection in code-division multiple-access channels", *Vehicular Technology, IEEE Transactions on*, vol. 45, no. 2, pp. 276–287, 1996.

[62] M. Wax and I. Ziskind, "On unique localization of multiple sources by passive sensor arrays", *Acoustics, Speech, and Signal Processing [see also IEEE Transactions on Signal Processing], IEEE Transactions on*, vol. 37, no. 7, pp. 996–1000, 1989.

[63] A.Manikas and C.Proukakis, "Modeling and estimation of ambiguities in linear arrays", *IEEE Transactions on Signal Processing*, vol. 46, pp. 2166–2179, 1998.

[64] B.Baygun and Y.Tanik, "Performance analysis of the music algorithm in directionding systems", in *International Conference on Acoustics, Speech, and Signal Processing, 1989 (ICASSP-89)*, 1989, pp. 2298–2301.

[65] T.Kah-Chye and Z.Goh, "A detailed derivation of arrays free of higher rank ambiguities", *IEEE Transactions on Signal Processing*, vol. 44, pp. 351–359, 1996.

[66] T.Kah-Chye, S.G.Say, and T.Eng-Chye, "A study of the rank-ambiguity issues in direction-of-arrival estimation", *IEEE Transactions on Signal Processing*, vol. 44, pp. 880–887, 1996.

[67] A.Manikas, C.Proukakis, and V.Lefkaditis, "Investigative study of planar array ambiguities based on hyperhelical parameterization", *IEEE Transactions on Signal Processing*, vol. 47, pp. 1532–1541, 1999.

[68] Y. I. Abramovich, N. K. Spencer, and A. Y. Gorokhov, "Resolving manifold ambiguities in direction-of-arrival estimation for nonuniform linear antenna arrays", *Signal Processing, IEEE Transactions on [see also Acoustics, Speech, and Signal Processing, IEEE Transactions on]*, vol. 47, no. 10, pp. 2629–2643, 1999.

[69] Y.I.Abramovich, A.Y.Gorokhov, and N.K.Spencer, "Asymptotic efficiency of manifold ambiguity resolution for doa estimation in nonuniform linear antenna arrays", in *First IEEE Signal Processing Workshop on Signal Processing Advances in Wireless Communications*, 1997, pp. 173–176.

[70] S.Pillai and F.Haber, "Statistical analysis of a high resolution spectrum estimator utilizing an augmented covariance matrix", *IEEE Trans. Acoust. , Speech, Signal Processing*, vol. ASSP-35, pp. 1517–1523, 1987.

[71] Y. I. Abramovich, N. K. Spencer, and A. Y. Gorokhov, "Identifiability and manifold ambiguity in doa estimation for nonuniform linear antenna arrays", in *Acoustics, Speech, and Signal Processing, 1999. ICASSP '99. Proceedings. , 1999 IEEE International Conference on*, 1999, vol. 5, pp. 2845–2848.

[72] K. T. Wong and M. D. Zoltowski, "High accuracy 2d angle estimation with extended aperture vector sensor arrays", in *Acoustics, Speech, and Signal Processing, 1996. ICASSP-96. Conference Proceedings. , 1996 IEEE International Conference on*, 1996, vol. 5, pp. 2789–2792.

[73] David L. Hall and James Llinas, *Handbook of Multisensor Data Fusion*, CRC Press LLC, 2001.

[74] L. D. Cosart, L. Peregrino, and A. Tambe, "Time domain analysis and its practical application to the measurement of phase noise and jitter", *IEEE Transactions on Instrumentation and Measurement*, vol. 46, no. 4, pp. 1016–1019, 1997.

[75] M. Carbonelli, D. De Seta, and D. Perucchini, "Clock stability measures for the assessment of synchronization network performance", in *Proceedings of IEEE Singapore International Conference on Networks*, Sep 1993, vol. 1, pp. 188–192.

[76] N. Fistas, *Eliminating array manifold and mutual coupling uncertainties*, Thesis/dissertation, Imperial College, 1994.

[77] P Karaminas, *Array Processing in Mobile Radio Networks*, Thesis/dissertation, Imperial College, 2001.

[78] K. Stavropoulos and A. Manikas, "Array calibration in the presence of unknown sensor characteristics and mutual coupling", in *EUSIPCO Proceedings*, 2000, vol. 3, pp. 1417–1420.

[79] N. Fistas and A. Manikas, "A new general global array calibration method", in *IEEE International Conference on Acoustics, Speech, and Signal Processing, (ICASSP)*, Apr 1994, vol. iv, pp. IV/73–IV/76.

[80] R. Schmidt, "Multiple emitter location and signal parameter estimation", *IEEE Transactions on Antennas and Propagation*, vol. 34, no. 3, pp. 276–280, 1986.

[81] T. Ratnarajah and A. Manikas, "An h^∞ approach to mitigate the effects of array uncertainties on the music algorithm", *IEEE Signal Processing Letters*, vol. 5, no. 7, pp. 185–188, 1998.